THE DEVELOPMENT AND UTILIZATION OF INELASTIC ELECTRON TUNNELING SPECTROSCOPY AS A TOOL FOR INVESTIGATING FUNDAMENTAL CATALYTIC PROCESSES

Thesis by
Howard E. Evans

In Partial Fulfillment of the Requirements
for the Degree of

Doctor of Philosophy

California Institute of Technology
Pasadena, California

1980

(Submitted August 1, 1979)

ACKNOWLEDGMENTS

I would like to express appreciation to my research advisor, W. Henry Weinberg , for his association as well as for his generous assistance and advice throughout the course of this research.

I have also benefitted greatly from a number of other special people here at Caltech. William M. Bowser in particular has contributed a great deal throughout the course of my graduate career, as have many other fellow students that I have come to know both within and outside of our research group.

Amoung the more permanent residents of the chemical engineering department, I would like to especially thank Henry Smith, Ray Reed, Chic Nakawatase, George Griffith, and Kathy Lewis. There are numerous others I appreciate as well.

The National Science Foundation and Caltech have both contributed generously to my support during the course of this work.

I am very grateful for the continuing support and influence of my parents, Edwin and Mildred Evans, and my parents-in-law, Edward and Lola Murdock.

Most of all, I would like to thank Jeannie (my wife), and Ryan, Joel and Laurie (our three children) for their tremendous support and encouragement, and for making my life very happy.

ABSTRACT

A diverse number of reactant/catalyst systems have been investigated utilizing inelastic electron tunneling spectroscopy (IETS) to probe the vibrational structures of the various surface species. Catalytic systems studied were selected for their relevance to important industrial reactions, as well as to demonstrate the versatily of IETS and to expand the range of its known applications. These studies include observation of an ethoxide-to-acetate transformation above 470K for ethanol on alumina, demonstrating that IETS can effectively monitor surface reactions. Unique characterization of surface acetates formed on alumina by ethanol, acetic acid and acetaldehyde is obtained via analysis of IET spectra, as is information on the initial adsorption mechanism for each of the three species. Results obtained for ethanol adsorption on alumina-supported silver particles extend the use of IETS into new areas of supported metal catalysis. Characterization of the silver particles was accomplished utilizing transmission electron microscopy. Most significant, perhaps, are the studies of $Zr(BH_4)_4$ supported on aluminum oxide. This is the first reported instance of IETS being utilized to characterize the structure of a supported complex; and, indeed, represents one of the few structural studies performed thus far for this increasingly important class of catalysts. Interactions of ethylene,

acetylene and propylene with the $Zr(BH_4)_4/Al_2O_3$ (a known polymerization catalyst under certain conditions) were examined with the resultant observation of polyacetylene formation. The alumina films utilized in IETS studies were characterized by X-ray photoelectron spectroscopy to facilitate comparisons to actual commercial aluminas.

TABLE OF CONTENTS

Chapter I

Introduction

Catalysis has proved to be economically indispensible since the pioneering discoveries of Davey and Faraday with heterogeneous catalysts early in the nineteenth century. Recently, there has been a significant expansion in catalysis research, paralleling an increased awareness of the limited nature of raw materials, the detrimental effects of pollution, and the rapidly inflating cost (as well as scarcity) of energy (1). The correlation between increased research effort and growing concern over energy and natural resources is based on the ability of catalysts to improve the efficiency of many industrial processes: catalysts can reduce energy requirements by lowering the activation energy required for a reaction, and can contribute to resource conservation by increasing yields through selectively promoting the desired reaction pathways. The ultimate goal of catalytic research is to establish a set of fundamental principles from which specific catalysts and catalytic reactors can be designed *a priori*. Carberry and Butt (2) note,

> The creation of such bases (principles) assumes an ultimate command of all fundamental disciplines related to heterogeneous catalysis. In light of present knowledge we recognize the difficulty of achieving this...*a priori* design from first principles seems not to be possible at this moment.

Ashmore (3) also observes that although the fundamentals of catalysis have proved fascinating as well as important, improvements in utilizing catalysts have thus far come mainly from empirical experimentation rather than from the application of chemical theory.

Traditionally, catalysis research has focused on observing the effects of macroscopic properties (such as temperature, pressure, reactant concentration, catalyst composition and preparation procedure, etc.) on the overall product yields and reaction rates of catalytic systems; then attempting to interpret these macroscopic observations in terms of the microscopic (i.e., molecular) fundamental processes occurring on catalyst surfaces. This type of research has thus far provided for rather consistent step-wise developments in improved catalysts and catalytic reactions and can reasonably be expected to continue producing such step-wise improvements in the future. Unfortunately, however, due largely to the inhomogeneous and complex nature of many catalytic systems as well as the inability (using traditional research techniques) to probe directly processes on catalyst surfaces at the molecular level, the fundamental principles underlying the steps of catalytic processes at the molecular level are not yet generally well understood. Such an understanding of basic molecular processes is essential for the rational design of new catalysts and novel catalytic systems; and (as noted above) the need for this knowledge of catalytic fundamentals is being heightened dramatically by the energy and raw materials supply problems now confronting us.

Recently, advances in vacuum technology and the development of a number of surface sensitive experimental techniques have coupled with new theoretical insights to enable researchers to probe directly many aspects of processes on surfaces at the molecular level. Particular successes are being achieved, for

example, in identifying (and, to a lesser extent, determining the concentrations of) distinct chemical elements present on catalytic surfaces (4), determining the geometrical arrangement of ordered arrays of molecules or atoms adsorbed on solid surfaces (5), and characterizing the electronic structure of surfaces and surface species (6). The goal of the research presented in this thesis has been to provide a significant contribution toward understanding the fundamental molecular level processes of catalytic reactions through successfully accomplishing the following two primary objectives:

(1) Develop an experimental technique not yet widely utilized in catalytic research into a valuable tool for examining fundamental catalytic processes, demonstrating implicitly its value and versatility; and

(2) Provide new experimental information on a number of industrially (as well as fundamentally) important catalytic systems.

Research projects were thus designed specifically to fulfill the dual purpose of assisting in the development of a valuable experimental technique while concurrently providing new information on systems of considerable interest and importance. The experimental technique selected for primary use in this study is inelastic electron tunneling spectroscopy, more commonly denoted by the acronym IETS, which is capable of probing the vibrational structure of model catalytic surfaces.

The phenomenon of electron tunneling has been known for some time, and its observation was, in fact, one of the early successes of quantum (wave) mechanics. Basically, it involves transport of electrons through (not over) a potential barrier. Of particular concern here are metal-insulator-metal junctions as illustrated in Fig. 1, where a thin insulating layer provides a barrier through which electrons can "tunnel" from filled states in one electrode to empty states in the other. Elastic tunneling, i.e., tunneling where no energy is lost by electrons in traversing the barrier, has been well studied experimentally and theoretically both prior to and after 1966 (see, for example, Ref. 7 and references therein). In 1966, Jaklevic and Lambe (8) identified a newly observed phenomenum: inelastic tunneling (i.e., tunneling where electrons lose energy upon passage through the barrier) due to the interaction of tunneling electrons with vibrational modes of molecules at, or near, the surface of the insulator. This inelastic mechanism for electron tunneling causes increases in the conductance of a tunnel junction at voltages determined by the characteristic vibrational frequencies (ω_i) of molecular species near the barrier region. This is illustrated schematically in Fig. 1, where the vertical and horizontal axes represent energy and distance, respectively. When a bias voltage (eV) is placed across the barrier, it causes the Fermi levels of the two electrodes (initially at the same energy level when no bias voltage is applied) to become offset from one another by an amount equal to the magnitude

of the bias voltage, as shown in the diagram. The shift in Fermi levels produces empty electronic states in metal 2 which are at equal or lower energies than occupied levels in metal 1. This is the condition required for electron tunneling. Elastic transitions are represented by the horizontal dashed line, while the oblique dashed line is illustrative of inelastic transitions. As shown in Fig. 1, the inelastically tunneling electron loses an amount of energy $|E_1-E_2|$ which is equal to $\hbar\omega_o$, the energy required for a particular vibrational transition. Inelastic processes related to vibrational excitations can occur only when $eV \geq \hbar\omega$, and open up new channels for electron transport through the barrier in addition to those already existing for elastic tunneling. If the bias voltage is increased continuously, these additional tunneling channels that become accessible as a vibrational excitation threshold is reached are manifest as a slight "kink" in the current-voltage (I-V) functional at $eV=h\omega_i$. This kink becomes a step in the first derivative spectrum (dI/dV-V) and a peak in the second derivative spectrum (d^2I/dV^2-V), where the peak positions correspond to vibrational excitation energies (see Fig. 2). Such representations of the second derivative of tunneling current as a function of the applied voltage have been shown experimentally and theoretically to be analogous to optical absorption spectra, both infrared and Raman active modes appearing in tunneling spectra (9, 10).

As noted, the basic structure of a tunnel junction consists of a thin insulating layer sandwiched between two metal electrodes.

Since the electrodes are formed via thermal evaporation (and in order to minimize contamination), samples in this study were prepared in an oil diffusion pumped vacuum system with a base pressure on the order of 10^{-7} torr. Initially, the first metal electrode is evaporated onto a glass substrate through a suitable mask, producing a main strip approximately 1mm in width and 2cm in length, along with four smaller strips which serve as electrical connections for sample heating and temperature measurement. [A resistive heating technique devised by Bowser and Weinberg (11) is employed throughout this study.] This geometry is shown in Fig. 3b, the indium pads representing the locations of electrical leads preconnected to the glass substrate with In solder (Fig. 3a). The top few atomic layers (approximately 20Å) of this metal film are then oxidized, forming the insulating barrier required for the tunneling experiment. In our applications, oxide layers are grown in a plasma discharge of pure O_2. Other studies have reported oxidations via water vapor discharges (12), or by removing samples from the vacuum system and immersing briefly in water (13) or heating in air (14) [In addition to oxide layers, insulating barriers of aluminum nitride (15) and thin films of Formvar (16) have been used, and the use of biological membranes has been proposed (17).] The oxide layer additionally serves as a model catalytic surface, and reactants can be introduced into the system and allowed to interact on the surface at predetermined temperatures and pressures. Following exposure to reactants, samples are completed

by evaporation of top metal electrodes in the form of cross strips (typically 1mm in width) as shown in Fig. 3c. Various materials have been incorporated in junction construction. Base electrodes of Mg, Ag, Pb, Sn, In, Cr, Al, Y, Zn and Cd have been studied (their oxides being used to form the insulating barrier), as have top electrodes of Al, Ag, Sn, Au, Pb, Mg, Ni and In (18-20). Research presented here has utilized exclusively Al-Al_2O_3-Pb tunnel junctions. Al was chosen due to the catalytic importance of its oxide, while Pb was selected since it apparently causes fewer distortions in the spectra (e.g., peak shifts) due to top electrode effects than do other metals (21). This is postulated to be a result of the relative inertness and large atomic size of Pb, which, respectively, inhibit bonding with surface species and penetration into the oxide layer.

Following fabrication, samples are mounted on a measurement probe which can be inserted directly into a liquid He dewar. Measurements are performed at liquid He temperatures (4.2K) to ensure that all molecular species will be in their ground vibrational states, and also to reduce thermal broadening of observed spectral features. For metal electrodes in a normal (as opposed to superconducting) state, the thermal broadening contribution to peak widths can be expected to be on the order of 5.44kT, where T is temperature and k is Boltzmann's constant (22). Superconducting electrodes substantially reduce the magnitude of thermal broadening over what would be predicted

for a normal metal at corresponding temperatures. For example, there is an increase in the resolution by a factor of five when the superconducting transition is made in Sn-SnO_2-Sn junctions. This effect is due to a sharp peak in the density of states immediately above the superconducting band gap. At liquid He temperature, the Pb is superconducting, while the Al remains in a normal state. This is the situation depicted in Fig. 1. The superconducting gap in this figure is denoted 2Δ, and for lead at this temperature is on the order of 2.6meV.

Electronics utilized in the tunneling measurement are shown schematically in Fig. 4. Measurements are controlled by a PDP 11/10 computer. The computer is utilized to generate a d.c. bias voltage, ramping it (in specified increments) through the spectral range of interest, typically 30 to 500meV (240 to 4000 cm^{-1}). Second derivative spectra are obtained directly via a harmonic detection scheme. A small a.c. modulation voltage is superimposed upon the d.c. bias voltage, V, generated by the computer. Modulation at frequency ω_o is supplied by a signal generator, the output of this oscillator being split into two parts. One line is fed through a frequency double and becomes the reference signal for a lock-in amplifier (now at frequency $2\omega_o$). The other is superimposed on the bias voltage to the sample. Output from the sample is then sent also to the lock-in amplifier, which detects only those com-

ponents with frequency $2\omega_o$ (the second harmonic of the original signal). The second harmonic is proportional to the second derivative, d^2I/dV^2. The magnitude of this harmonic signal is then stored back in the computer, a spectrum being completed when a predetermined number of d^2I/dV^2:V pairs have been measured over the desired spectral range.

Theoretical and experimental details of IETS have been the subject of several reviews, including articles by Weinberg (23) and by Hansma (24), and information more extensive than that presented here can be found in these reviews and the references contained therein. A more thorough description of our particular experimental equipment and techniques is presented in Appendix A.

At the time this thesis research was being initiated, IETS had been demonstrated to have applications in a number of diverse areas, including studies in biochemistry (25) and water pollution (13). More recently, its range of applications has been extended to areas such as adhesion (26) and damage due to electron beam irradiation (27). Outside of vibrational spectroscopy, IETS techniques have been utilized to study rotational (28) and electronic levels of chemisorbed species (29-31), as well as to produce a broad band tunable light source (32,33). Tunneling spectroscopy had additionally been utilized in a few limited cases to probe catalysis-related phenomena. These included a study of the dissociative adsorption of benzoyl

chloride (34); determination of the orientation of chemisorbed phenol, catechol, resorcinol and hydroquinone (35); and examination of the surface structures of adsorbed formic and acetic acids, and determination of the sticking coefficient for formic acid on the surface (36). All of these studies utilized aluminum oxide surfaces. Further studies on the orientation of sulfonic acids (37), and the nature of various organic acids (38, 39) and phenolic derivatives (40), adsorbed primarily on aluminas, have been subsequently reported. Additional important studies reported recently relate closely to the present work, and are accordingly discussed in conjunction with this work below. Although even the earliest IETS studies of catalytic phenomena were quite successful, the lack of greater widespread development in this area has been somewhat surprising.

At the beginning of this work, the following projects were outlined in order to accomplish the primary goal and objectives as presented previously:

(1) Contribute to the characterization of IETS thin aluminum oxide films relative to commercial aluminas;

(2) Demonstrate that experimental features, such as top electrodes and liquid He measurement temperatures, do not prevent the use of IETS to follow surface reactions;

(3) Show that IETS can distinguish between even very similar surface species, which is important for determining correctly the structure of reaction

intermediates; and

(4) Extend the use of IETS to industrially important types of catalysts besides metal oxides, such as supported metal catalysts and homogeneous catalytic compounds anchored onto supports.

In each of these areas, the catalytic systems selected for study were chosen particularly for their relevance to industrial problems and processes. They are discussed individually below.

(1) There is a wide range of industrial aluminum oxides and hydroxides, varying slightly one from another in crystal structure and, more particularly, in degree of hydration. Some forms exhibit high catalytic activity, while others are essentially inactive. In order that the results of IETS experiments on "model" catalytic surfaces can be properly applied to understand industrial reactions, it is important to characterize the thin film model alumina catalysts relative to commercial (bulk) aluminas. Since IETS oxide layers can be prepared in various ways (as mentioned above), the oxides formed via different techniques need to be related also to one another so that results obtained in different laboratories can be compared accurately. X-ray photoelectron spectroscopy (XPS) was applied to study a number of variously prepared oxide films

XPS can provide information on the chemical states of individual elements near the surface, and the nature of their environments. Analysis of peak widths and peak intensities in the photoelectron spectra can yield qualitative information on the distribution of chemical states and relative concentrations of the various chemical elements, respectively. XPS can be expected to be sensitive to slight differences amoung the various possible types of aluminum oxides and hydroxides. Results for thin oxide films might be profitably compared to corresponding information for bulk aluminas. Some difficulties arise in XPS studies of bulk oxides due to surface charging effects, and few of the studies performed on bulk aluminas thus far have adequately compensated for surface charging (41). Further reliable data for bulk aluminas are required before extensive comparisons to the results obtained here for thin films can be accomplished. The required data might be anticipated shortly, as additional XPS studies of oxides seem to appear regularly in the literature (42, 43).

(2) If IETS is to be a useful tool for investigating catalytic phenomena, it must be capable of following the course of surface chemical reactions. Specifically, this implies that IET spectra must reflect the nature (i.e., structure) of the surface species

as they exist at the temperatures and pressures utilized in sample preparation, with no significant perturbations being introduced by the presence of top electrodes or the extreme cooling (to 4.2K) during measurement. One pertinent study in this area has recently appeared. McBride and Hall (44) used IETS to observe the controlled hydrogenation of muconic acid chemisorbed on aluminum oxide. They observed that the reaction depended on the amount of hydrogen available from surface hydroxyl groups at a given temperature; additional hydroxyl groups participating at higher temperatures. Earlier, Shklyarevskii, et al., (45) observed (via IETS) the transformation of acetic acid on alumina from a physically adsorbed to a chemisorbed state as the temperature is raised from 77K to room temperature. These preliminary studies complement the work reported here. In this research, significant attention has been centered on catalytic systems with industrial applications. Reactions for which aluminas are extensively utilized as catalysts include the dehydration of alcohols. IR studies have shown that ethanol reacts with alumina in an interesting manner as a function of temperature. Adsorption below approximately 470K produces surface species similar to

aluminum ethoxide, while above this temperature acetate-like structures are formed (46, 47). The use of IETS to study ethanol adsorption on alumina would demonstrate further the validity of its application to catalytic research. Any effects due to top electrodes and low measurement temperatures can be determined by comparing IETS results with those observed via infrared spectroscopy. Additionally, as IETS has a wider spectral range for metal oxide systems than IR (due to strong absorption of photons by the substrate below approximately 1100 cm^{-1}), new details should be contributed by the IETS work.

(3) The most important contribution that can be made to catalytic research by vibrational spectroscopy is to elucidate the structure of reaction intermediates on the surface. In order to do so, it is necessary that a technique be capable of distinguishing clearly between different species with very similar structures. It was noted above that alumina is an effective catalyst for the dehydration of alcohols to aldehydes. Alumina has also been utilized as a condensation catalyst for aldehydes. Important comparisons might readily be made (via vibrational spectroscopy) between surface species formed from adsorbed alcohols and those formed by adsorption of the corresponding aldehydes. In conjunction with previous work, IETS

was applied to compare ethanol and acetaldehyde adsorption on aluminum oxide as a function of temperature. Since ethanol adsorption was found to form acetate structures at higher temperatures, adsorption of acetic acid was also studied and compared to results for ethanol and acetaldhyde. Since surface species formed from these three hydrocarbons are definitely interrelated, study by IETS should demonstrate the degree of discrimination that can be expected from this technique, as well as contribute to an understanding of the reaction pathways followed by the three species.

(4) Even though aluminum oxides alone are catalysts for some industrial processes, there are other types of heterogeneous catalysts which are employed more extensively, offer more flexibility, and have greater economic value than plain aluminas. Specifically, these include supported metal catalysts and supported complexes. The application of IETS to these additional types of catalysts would demonstrate decisively its versatility and greatly enhance its value to catalytic research. During the course of the current study, it was reported by Hansma, et al., (48) and Klein, et al., (49) that IETS could be utilized to monitor CO adsorption on alumina-supported Rh particles. Of particular interest was the observation of metal-carbon stretching and carbon-oxygen

bending modes, since these are not generally observed in infrared studies due to strong absorption by the support at lower frequencies. This present work was undertaken to expand further the range of supported metal systems which might profitably be examined via IETS. Specifically, we applied IETS to study ethanol adsorption on Ag particles supported on alumina. Supported silver catalysts are also employed in alcohol-to-aldehyde conversions, and these results might therefore prove to be a valuable complement to those obtained for ethanol on plain alumina. Silver particles were characterized by means of electron microscopy. Based on the results of an electron energy loss spectroscopy study of methanol and ethanol on copper single crystals (50), we can expect the formation of surface ethoxides on silver similar to those observed on plain alumina. Slight differences in the nature of the hydrocarbon-surface bond between silver and aluminum ethoxide species should appear due to differences in the electronegativities of Al and Ag (51). Since the aluminum surface is not entirely covered by silver particles, some ethanol will also adsorb on the alumina. This will be a further test of the ability of IETS to distinguish between similar species, as features from

both silver and alumina species will appear in the spectra. In addition to traditional supported metal catalysts, new types of supported systems are proving to be valuable in a number of important applications. These new catalysts are supported complexes, formed by grafting known homogeneous catalytic complexes onto support materials. Supported complexes combine the stability and ease of separation from products characteristic of heterogeneous systems, with the selectivity and ability to be tailored to fit specific reactions characteristic of homogeneous systems. Such catalysts have already proved useful in a number of important applications (e.g., polymerization reactions of olefins), and are generally considered to be the most promising type of catalyst known from an applied point of view (52). Unfortunately, progress in the important area of catalysis by supported complexes has been hindered by a lack of structural information of the surface species. One group researching this area has concluded that "significant progress is impossible unless new techniques are exploited" (53). IETS is a new technique which might profitably be exploited in research on catalysis by supported complexes. Various zirconium complexes are known polymerization catalysts for olefins. In this study,

IETS is utilized to probe the vibrational structure of $Zr(BH_4)_4$ adsorbed on alumina. Particular attention is given to understanding the nature of Zr-surface and Zr-BH_4 bonds, as well as the possible migration of ligands onto the support. Characterization of the surface species is benefitted by studying the effects of temperature and interactions with H_2O, D_2O and D_2. After characterizing the $Zr(BH_4)_4/Al_2O_3$ system, the reactions of ethylene, propylene and acetylene over the catalyst are also examined in this study. This is the first reported attempt to study a supported complex utilizing IETS. In view of the importance of such systems and the lack of information currently available, the current study can offer a significant contribution to the field.

The results of these investigations are reported in subsequent chapters. Since many chapters represent manuscripts which have been submitted for publication, the references, tables, and figures are self-contained within each chapter. Results of the XPS characterization studies are reported in Chapter 2. Chapter 3 presents the results for ethanol adsorption on alumina, while the comparison of adsorbed ethanol, acetic acid and acetaldehyde is discussed in Chapter 4. Results for ethanol adsorption on supported silver are contained in Chapter 5. Chapters 6-8 discuss the nature of $Zr(BH_4)_4$ adsorption on alumina and its

interactions with deuterium, deuterium oxide, water vapor, ethylene, propylene and acetylene. The accomplishments and contributions of this work are summarized in Chapter 9. As mentioned previously, Appendix A presents a detailed outline of the experimental equipment and techniques utilized in this study. A method developed for extracting data stored on floppy discs (by our laboratory computer) for manipulation with the IBM 370/3032 system is outlined in Appendix B.

REFERENCES

1. Mosaic 7, 22 (1976).
2. J.J. Carberry and J.B. Butt, Catal. Rev. 10, 221 (1975).
3. P.G. Ashmore, Catalysis and Inhibition of Chemical Reactions, Butterworths, London (1963).
4. W.N. Delgass, T.R. Hughes and C.S. Fadley, Catal. Rev. 4, 179 (1970).
5. M.A. Van Hove, Surface Sci. 81, 1 (1979).
6. D.E. Eastman and M.I. Nathan, Physics Today, April (1975), p.44.
7. C.B. Duke, Tunneling in Solids, Academic Press, New York (1969).
8. R.C. Jaklevic and J. Lambe, Phys. Rev. Letters 17, 1139 (1966)
9. J. Lambe and R.C. Jaklevic, Phys. Rev. 165, 821 (1968).
10. D.J. Scalapino and S.M. Marcus, Phys. Rev. Letters 18, 459 (1967).
11. W.M. Bowser and W.H. Weinberg, Rev. Sci. Instrum. 47, 583 (1976).
12. W.M. Bowser and W.H. Weinberg, Surface Sci. 64, 377 (1977).
13. Y. Scarlatos, R.C. Barker and G.L. Haller, Surface Sci. 43, 353 (1974).
14. J.T. Hall and P.K. Hansma, Surface Sci. 77, 61 (1978).
15. O.I. Shklyarevskii, I.K. Yanson and V.D. Zaporozhskii, Solid State Communications 14, 327 (1974).

16. G. Burrafato, G. Faraci, G. Giaquinta and N.A. Moncini, J. Phys. C: Solid State Phys. 5, 2179 (1972).

17. R.G. Keil, T.P. Graham and K.P. Roenker, manuscript.

18. T.T. Chen and J.G. Adler, Solid State Communications 8, 1965 (1970).

19. J.M. Rowell, W.L. McMillan and W.L. Feldman, Phys. Rev. 180, 658 (1969).

20. G.I. Rochlin and P.K. Hansma, Phys. Rev. B 2, 1460 (1970).

21. J.R. Kirtley and P.K. Hansma, Phys. Rev. B 12, 531 (1975).

22. J. Klein, A. Leger, M. Belin, D. Defourneau and M.J.L. Sangster, Phys. Rev. B 7, 2336 (1973).

23. W.H. Weinberg, Ann. Rev. Phys. Chem. 29, 115 (1978).

24. P.K. Hansma, Phys. Rep. 30C, 145 (1977).

25. M.G. Simonson, R.V. Coleman and P.K. Hansma, J. Chem. Phys. 61, 3789 (1974).

26. H.W. White, L.M. Goodwin and T.Wolfram, Inelastic Electron Tunneling Spectroscopy (T. Wolfram, ed.), Springer-Verlag, N.Y., 1978, p. 70.

27. J.T. Hall, P.K. Hansma and M. Parikh, Surface Sci. 65, 522 (1977).

28. J. Klein and A. Leger, Phys. Letters 30A, 96 (1969).

29. S. de Cheveigne, J. Klein, A. Leger, M. Belin and D. Defourneau, Phys. Rev. B 15, 750 (1977).

30. Y. Maruyama, A. Yamada, N. Hakamata and H. Anzai, Solid State Communications 23, 755 (1977).

31. U. Roll, S. Ewert and H. Luth, Chem. Phys. Letters 58, 91 (1978).

32. J. Lambe and S.L. McCarthy, Phys. Rev. Letters 37, 923 (1976).

33. S.L. McCarthy and J. Lambe, Applied Phys. Letters 30, 427 (1977).

34. D.G. Walmsley, I.W.N. McMorris and N.M.D. Brown, Solid State Communications 16, 663 (1975).

35. W.H. Weinberg, W.M. Bowser and B.F. Lewis, Jap. J. Appl. Phys., Supplement 2, Part 2 (1974).

36. B.F. Lewis, M. Mosesman and W.H. Weinberg, Surface Sci. 41, 142 (1974).

37. J.T. Hall and P.K. Hansma, Surface Sci. 71, 1 (1978).

38. R. Magno and J.G. Adler, J. Appl. Phys. 49, 4465 (1978).

39. N.M.D. Brown, W.J. Nelson and D.G. Walmsley, J. Chem. Soc. Faraday Trans. II 75, 32 (1979).

40. I.W.N. McMorris, N.M.D. Brown and D.G. Walmsley, J.Chem. Phys. 66, 3952 (1977).

41. T.E. Madey, C.D. Wagner and A. Joshi, J. Elec. Spec. 10, 359 (1977).

42. Y. Boudeville, F. Figueras, M. Forissier, J.L. Portefaix and J. Vedrine, J. Catal. 58, 52 (1979).

43. F.J. Grunthaner, P.J. Grunthaner, R.P. Vasquez, B.F. Lewis, J. Maserjian and A. Madhukar, submitted to J. Vac. Sci. Technol. (1979).

44. D.E. McBride and J.T. Hall, J. Catal. 58, 320 (1979).

45. O.I. Shklyarevskii, A.A. Lysykh and I.K. Yanson, Sov. J. Low. Temp. Phys. 2, 328 (1976).

46. R.G. Greenler, J. Chem. Phys. 37, 2094 (1962).

47. H. Arai, Y. Saito and Y. Yoneda, Bull. Chem. Soc. Jap. 40, 731 (1967).

48. P.K. Hansma, W.C. Kaska and R.M. Laine, J.Am. Chem. Soc. 98, 6064 (1976).

49. J. Klein, A. Leger, S. de Cheveigne, C. Guinet, M. Belin and D. Defourneau, Surface Sci. 82, L288 (1979).

50. B.A. Sexton, submitted to Surface Sci. (1979).

51. N. Takezawa and H. Kobayashi, J. Catal. 25, 179 (1972); 28, 335 (1973).

52. D.G.H. Ballard, J. Polymer Sci. 13, 2191 (1975).

53. J.M. Bassett and J. Norton, Fundamental Research in Homogeneous Catalysis (M. Tsutsui and R. Ugo, eds.), Plenum Press, N.Y. (1977), pp 69-98.

Figure Captions

Fig. 1: Schematic energy diagram for both elastic (horizontal dashed line) and inelastic (oblique dashed line) electron tunneling through a barrier of width ℓ. E_1 is the initial energy and E_2 the final energy, separated by $\hbar\omega_o$ (a vibrational excitation energy). E_{F1} and E_{F2} are the respective Fermi levels in the two metals, $2\Delta_2$ represents the superconducting gap in metal 2, and eV is the bias voltage.

Fig. 2: Schematic representation showing the effect of a vibrational excitation at energy eV_o on the tunneling current and its first (dI/dV) and second (d^2I/dV^2) derivatives as a function of voltage (V).

Fig. 3: Representation of IET sample preparation procedure showing (a) clean glass substrate with attached electrical leads, (b) evaporation of aluminum strip, followed by oxidation, exposure to reactants, and (c) deposition of top metal electrodes. Electrical connections are not shown in part (c) for sake of clarity.

Fig. 4: Schematic of IETS computer-controlled measurement electronics.

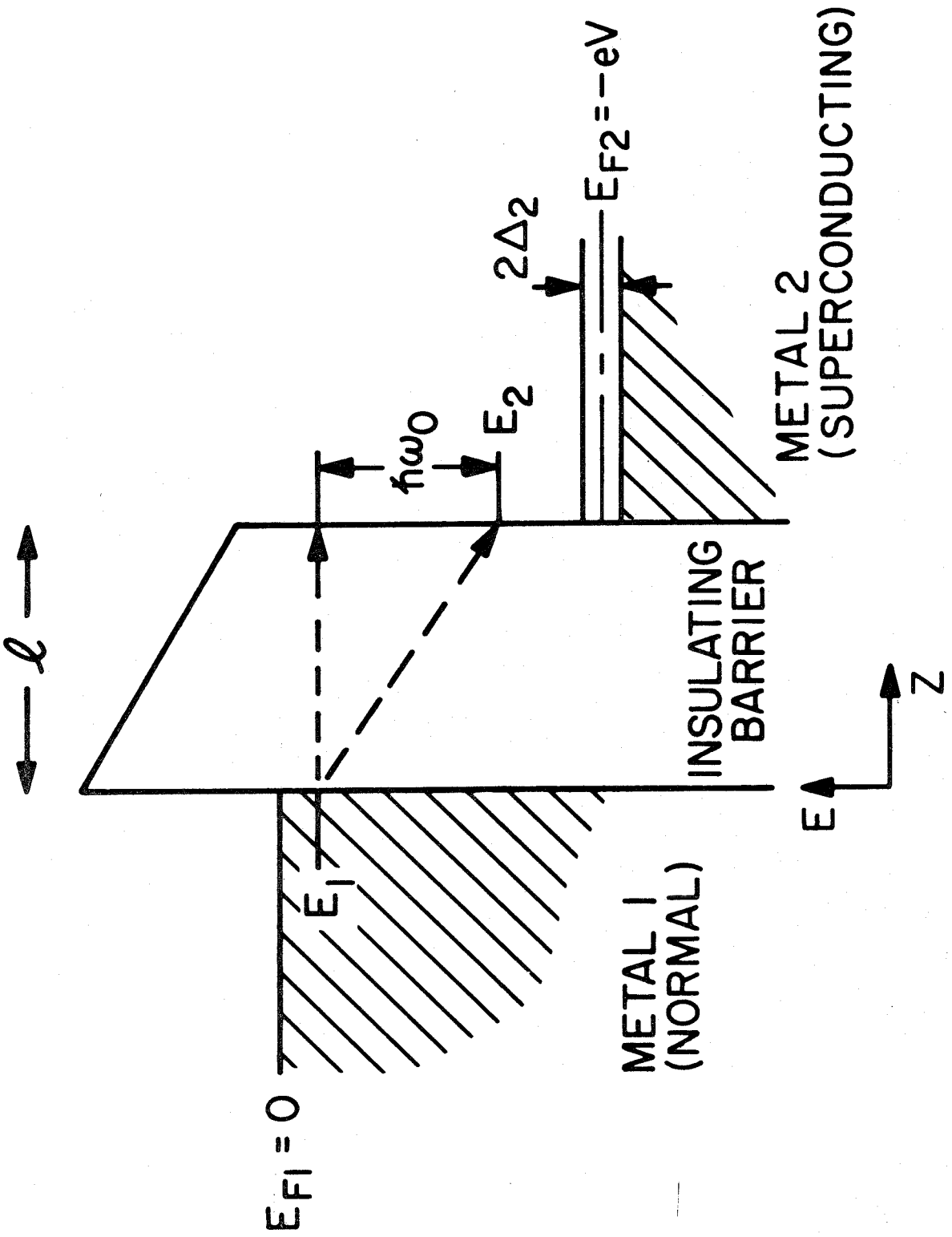
$E_{F2}=-eV$
$2\Delta_2$
E_2
$\hbar\omega_0$
METAL 2
(SUPERCONDUCTING)
INSULATING
BARRIER
E_1
METAL 1
(NORMAL)
$E_{F1}=0$
ℓ
E
Z

Figure 1

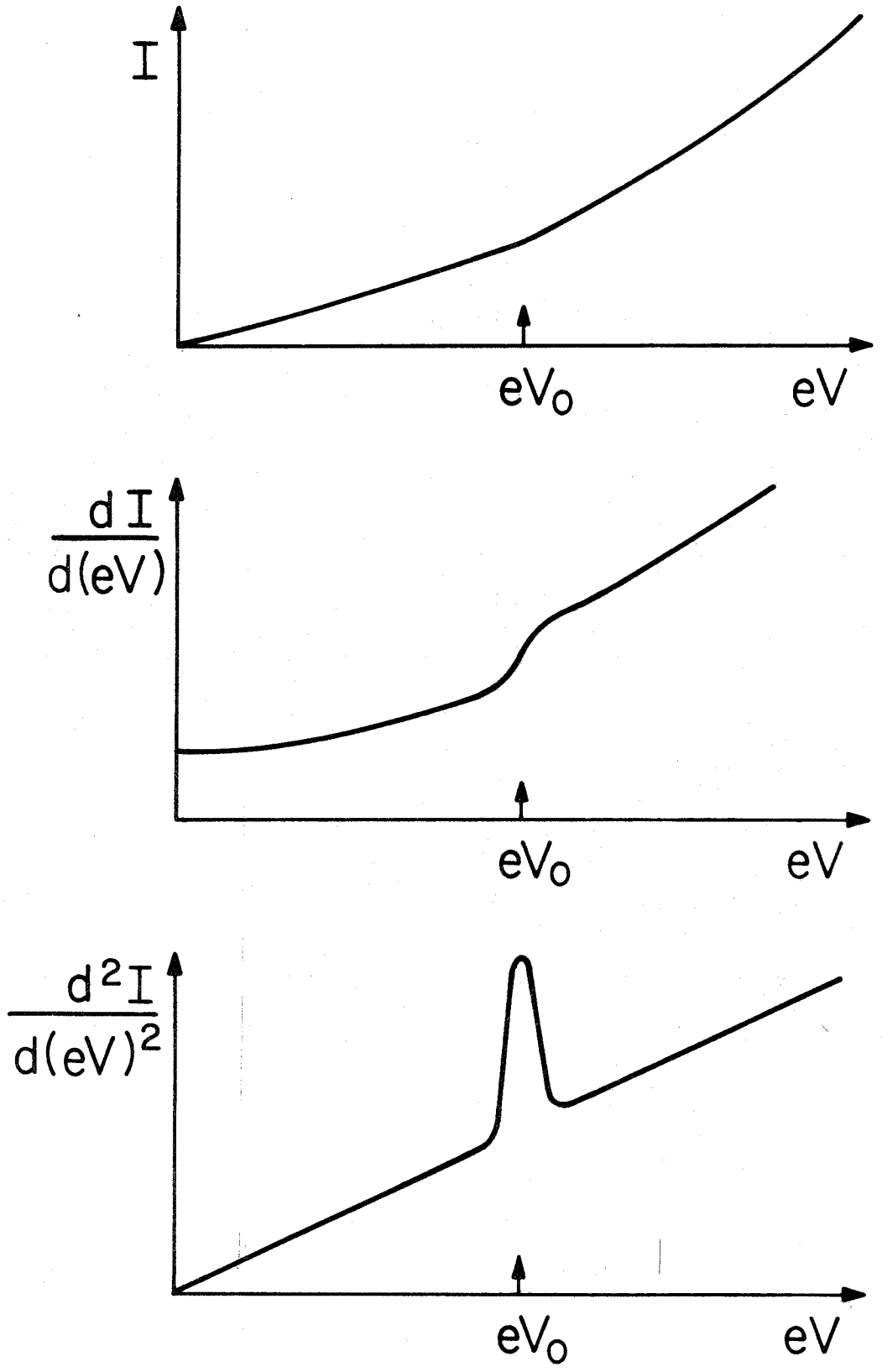

Figure 2

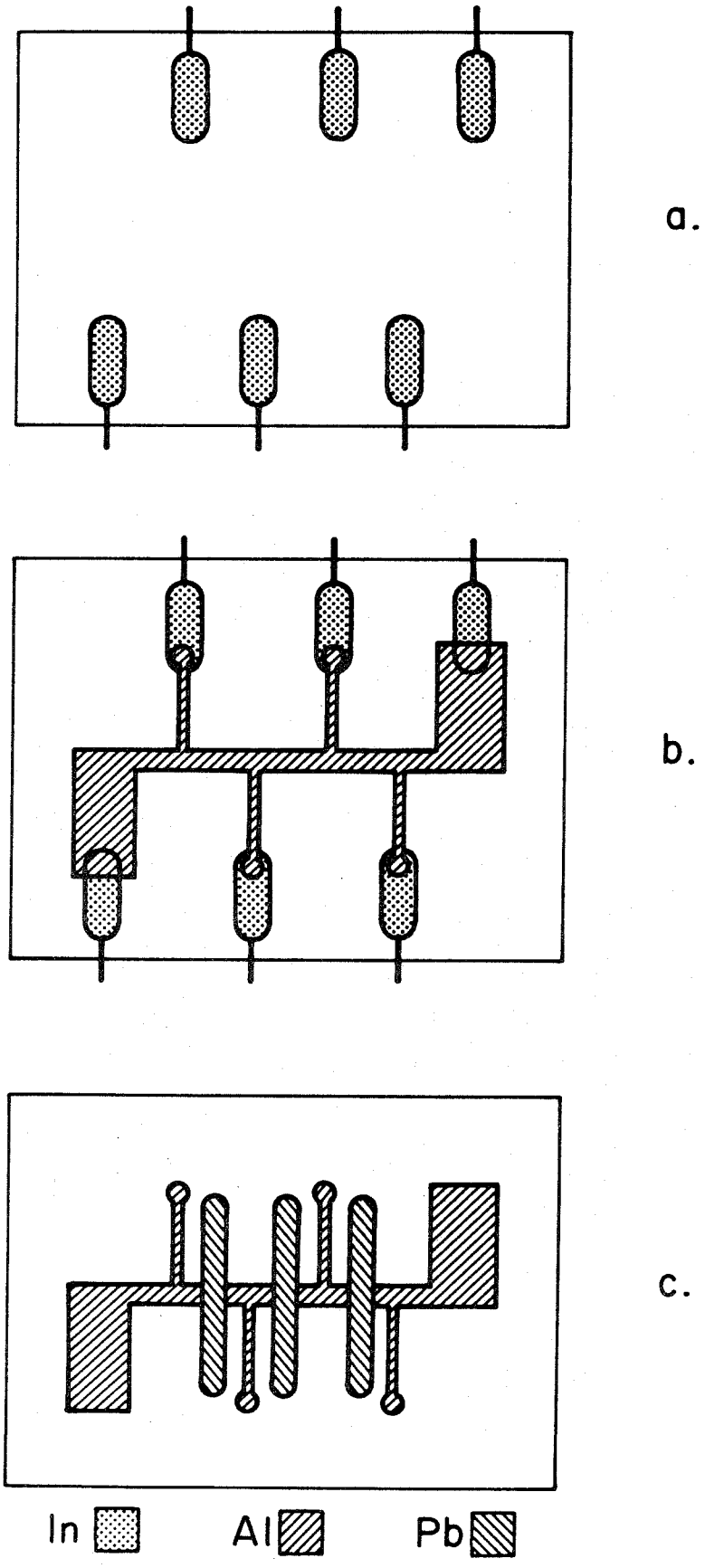

Figure 3

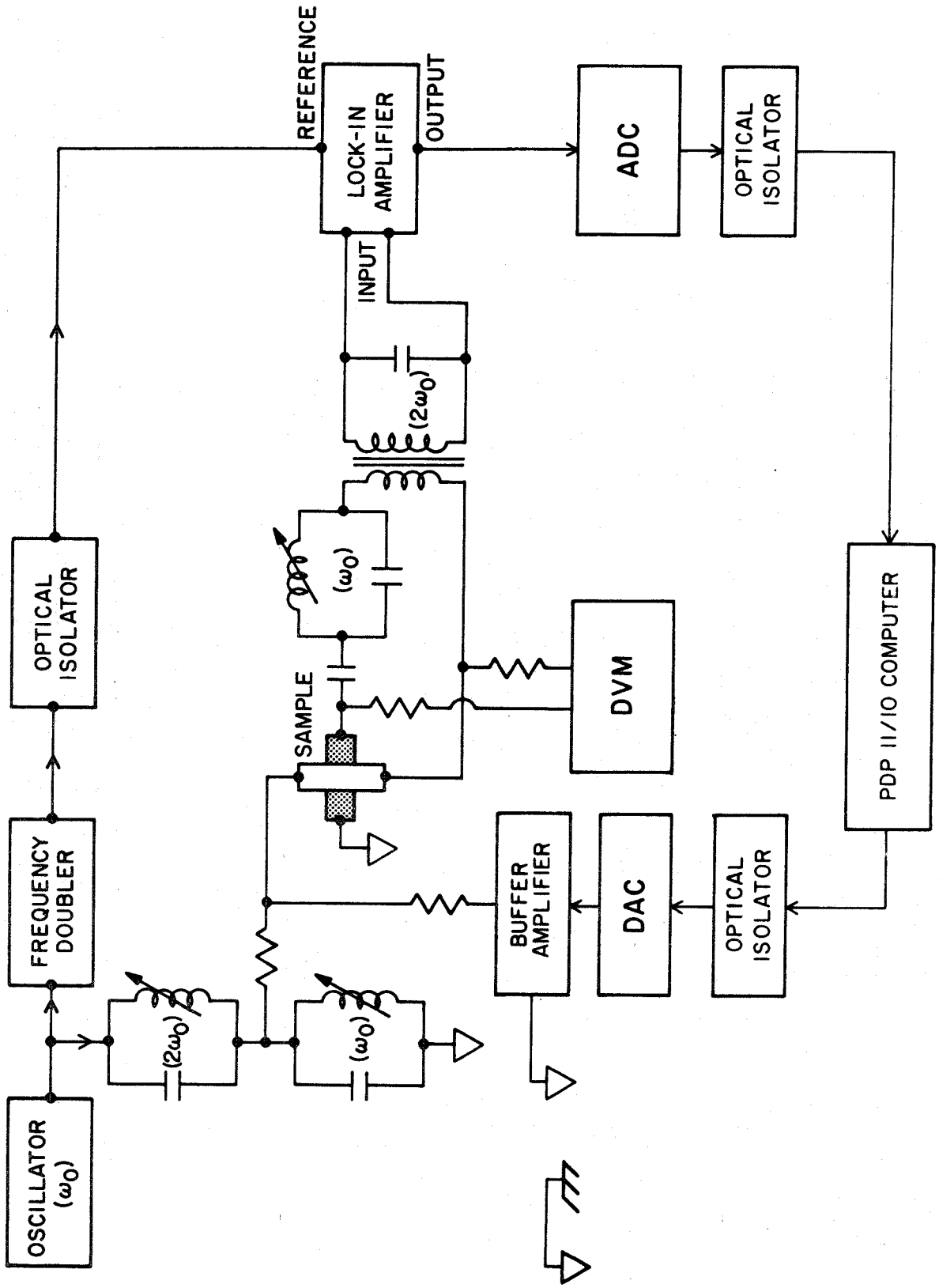
REFERENCE
LOCK-IN AMPLIFIER
OUTPUT
ADC
OPTICAL ISOLATOR
INPUT
$(2\omega_0)$
(ω_0)
OPTICAL ISOLATOR
SAMPLE
DVM
PDP 11/10 COMPUTER
FREQUENCY DOUBLER
BUFFER AMPLIFIER
DAC
OPTICAL ISOLATOR
$(2\omega_0)$
(ω_0)
OSCILLATOR (ω_0)

Figure 4

Chapter II

An XPS Investigation of Alumina Thin Films Utilized in IETS

Abstract

X-ray photoelectron spectroscopy (XPS) has been applied to characterize a number of different aluminum oxide (alumina) thin films utilized in inelastic electron tunneling spectroscopy (IETS). Since IETS has been found to be an effective means for obtaining vibrational information on catalytic systems, reliable means of clarifying the exact relationship between the IET thin film "model" catalysts and high surface area commercial aluminas are of considerable importance. XPS data might profitably provide such a means of comparison, although sufficiently reliable XPS data for commercial samples are not currently available. The various thin film aluminas are characterized as to their chemical nature, chemical state distributions, and relative oxygen-to-alumina concentration ratios by analysis of peak positions, peak widths and peak intensities, respectively. Moreover, effects due to heating and halogenating the surface have been investigated independently, since these are commonly utilized to enhance the catalytic behavior of commercial aluminas.

1. Introduction

Inelastic electron tunneling spectroscopy (IETS) is a valuable experimental technique for probing the vibrational structure of molecules near insulating (metal oxide) surfaces (1). In particular, IETS has shown significant promise as a means of monitoring structural changes characteristic of catalytic reactions. This has been demonstrated for systems involving both alumina films and alumina-supported metal catalyst surfaces. Specific examples of work in this area include studies of CO chemisorption on alumina-supported Rh particles (2), the adsorption of ethanol on Ag particles supported on alumina (3), and the formation of surface ethoxide and acetate structures during ethanol adsorption on alumina (4), with comparisons to corresponding acetate structures observed for adsorbed acetaldehyde and acetic acid (5). Important results have also been obtained recently for metal cluster compounds adsorbed on alumina. The structure of adsorbed chlorodicarbonylrhodium dimer, $[RhCl(CO)_2]_2$, has been observed and compared with the previous results of CO adsorption on supported Rh particles (6); and the polymerization reaction of ethylene has been studied over $Zr(BH_4)_4$ complexes supported on alumina surfaces (7).

Widely used industrially as catalysts and catalyst support materials, there are a number of different forms of alumina. Some of the known, distinct types of alumina are listed in Table 1, and additional forms are continuing to be discovered or synthesized. These various forms can differ slightly from one another in crystal structure. Variations exist also in the relative amounts of bulk hydration, ranging from extremely "dry" α-alumina (Al_2O_3) to forms such as tucanite ($Al_2O_3 \cdot 3.5\ H_2O$) which can

contain significant amounts of interlamellar water. Most of the more catalytically active aluminas have been found to contain from a few tenths to several percent H_2O, being characterized by the formula $Al_2O_3 \cdot nH_2O$, where $0 < n \lesssim 0.6$. A number of excellent references are available detailing the physical as well as the catalytic properties of aluminas (8, 9). An important point is that the catalytic properties are determined by the exact form of alumina being utilized, which, in turn, depends markedly on the origin and preparation of the alumina. This dependence of catalytic properties on preparation technique has often led to disagreements between catalytic results obtained in different laboratories. Indeed, it has been noticed that results obtained with the same catalyst can vary with time as subtle changes occur in the nature of the catalyst, particularly when even a small amount of hydration or dehydration takes place (10).

The alumina surfaces utilized in IETS studies to model commercial aluminas are formed by oxidizing the first 20 - 30 $\mathring{A}$ of an aluminum electrode which has been evaporated in the form of a thin strip onto a clean ceramic substrate. After the desired reactants are allowed to adsorb and interact on the surface of this thin oxide layer, IET samples are completed by the evaporation of top metal electrodes. Electrons tunnel through the oxide barrier when a voltage is applied across the sample, and they can lose energy during the tunneling process by exciting vibrational modes of molecules in, or near, the barrier region. Such excitations can occur only when the applied bias voltage is greater than, or equal to, an energy equivalent to a vibrational excitation. These excitations lead to small increases in the tunneling current which become peaks when d^2V/dI^2

(proportional to the second derivative of tunneling current with respect to voltage, d^2I/dV^2) is plotted against the applied voltage, V. Peak positions in this representation are indicative of vibrational excitation energies and have been shown to yield analogous information to that obtained by optical techniques such as infrared and Raman spectroscopies. Complete experimental and theoretical details of IETS are available in the literature (11).

Formation of the thin oxide films on the aluminum underlayer in IETS studies has been accomplished in a number of ways, including (1) exposure to a plasma discharge of pure O_2, H_2O or a mixture of the two (12), (2) immersing briefly in liquid H_2O external to the vacuum system (13), and (3) heating in air (14). In view of the complexities associated with the commercial aluminas outlined above, we can expect that each of these oxidation procedures might possibly produce an alumina film with unique structure, degree of hydration and catalytic activity. The limited experimental evidence available on thin alumina films indicates that this is indeed the case. These results will be discussed together with those of the current study in Sec. 3. It is important, therefore, to characterize IET aluminas prepared by different methods in order to make valid comparisons between results obtained on the various surfaces. Also, it is clear that IETS studies of these model alumina catalysts will be of maximum value if correlations can be made with commercial aluminas. Only one study has been attempted in this area heretofore (50).

The current study was performed in order to characterize alumina films prepared by the various oxidation procedures utilized in IETS experiments not only to facilitate comparisons among them, but to provide

characteristic information which might be related also to commercial aluminas. X-ray photoelectron spectroscopy (XPS) was utilized in this investigation. It is capable of providing information concerning the environment of separate chemical elements near the surface. Various amounts of bulk hydration, or even different crystal structures, produce shifts in the binding energies of core level electrons which are revealed in XPS. Details of XPS experiments are available elsewhere (15). This technique has been applied here to characterize the thin oxide layers formed on clean, evaporated Al films by some of the oxidation techniques employed in IETS studies reported in the literature. Also, since halogen atoms are often added to aluminas as "promoters" of greater catalytic activity, we have studied the effects of fluorination of some of the separate oxide surfaces, and on one particular surface have examined perturbations due to varying degrees of fluorination. The adsorption of chlorine on one surface was studied also. Details of experimental procedures and results are presented and discussed in the following two sections. Our conclusions are presented in Sec. 4.

2. Experimental Details

Samples were prepared in an oil diffusion pumped bell jar with a base pressure of 10^{-7} torr. Aluminum (Balzers 99.99%) was evaporated to a thickness of 1000 Å onto clean 10 mm x 12 mm glass substrates cut from #2 thickness (0.2 mm) glass cover slips. The top few atomic layers of the aluminum were then oxidized by one of the methods reportedly used to form alumina surfaces in IETS studies of model catalyst systems. The

various oxidation procedures are listed in Table 2. After oxidation, the samples were transported in a dessicator under nitrogen to the XPS spectrometer.

XPS measurements were accomplished in a modified HP-5950A ESCA spectrometer with a base pressure below 10^{-9} torr. A more complete description of the particular instrument utilized in this study is presented elsewhere (16). A sample preparation chamber is connected directly to the spectrometer and consists of a stainless steel dry box with an introduction lock. A positive pressure of five psi of nitrogen dried over LN_2 is maintained at all times inside the sample preparation box. Inside this chamber, samples were removed from the dessicator and mounted between a gold backing platen and a gold window placed on the top surface of the sample, then attached to a probe and inserted through an interlock into the spectrometer. The gold platen and window are utilized routinely in these procedures to minimize undesirable charging of insulator and semiconductor surfaces, although this is not expected to be relevant in the current study. Further comments and a discussion of charging effects are presented below.

Some samples prepared by the same oxidation techniques listed in Table 2 were exposed to vapors of HF and HCl. This was accomplished by opening a container of one of the acids inside the sample preparation chamber. For heavy (saturation) exposures, samples were placed alongside the open container for up to one minute. Lower exposures could be obtained by first removing the acid container before placing samples inside the chamber. Both high and low exposures of HF were studied on O_2 discharge (type 1) samples. A high exposure of HCl to this type of

surface was also studied. Low exposures of HF on types 3 and 5 of oxidized aluminum, as well as on O_2 discharge samples exposed first to HCl, were similarly investigated.

XPS measurements were made at room temperature utilizing a monochromatized beam of X-radiation from an aluminum (Kα = 1486.6 eV) source. Channel sampling densities ranged from 0.03 to 0.04 eV/channel. Typical signal-to-noise characteristics are illustrated in Fig. 1, which shows representative spectra of an O1s line and an Al2p line, these being two of the most important spectral features monitored in this study. A number of samples were measured for one specific set of preparation conditions to check reproducibility and establish error limits. Each sample was first observed with a wide scan from a binding energy of zero to 1280 eV to determine basic elemental composition. A typical wide scan is shown in Fig. 2a, which is a spectrum for a low exposure of HF on alumina prepared in an O_2 discharge. This was followed by a closer examination of particular peaks of interest, such as the Al2p, Al2s, O1s, O2s, C1s, F1s, Cl2p and/or Cl2s lines. On some samples the oxygen KLL Auger transition near 980 eV was studied also.

3. Results and Discussion

The XPS technique has been utilized previously to distinguish various oxidation states of metals such as Ni (17), Mg (10), Pb (18), Cu (19) and Pt (20). In another recent detailed study, Grunthaner et al. (21) have observed a number of Si oxidation states within a thin oxide film grown on Si. Thus, we expect XPS spectra to reveal differences in structure and stoichiometry among the variously oxidized alumina films if differences

are actually present. There is significant experimental evidence which indicates that such differences will indeed be present. Fundamental studies of the initial oxidation of Al single crystals (22,23), as well as of polycrystalline (evaporated) Al films (24), have demonstrated that aluminum can exist over a range of oxidation states within the oxide layers. Using XPS, oxide formation on evaporated films was noted, the exact nature of which depended entirely on the extent of oxygen exposure. This variation in the nature of the oxide was determined by observing a continuous shift in the oxide Al2p peak position from a binding energy of 75.4 eV to 75.7 eV as a function of oxygen exposure. On the (111), (110) and (100) surfaces of Al single crystals, three separate initial interaction mechanisms between oxygen and aluminum were reported. On the (110) surface, it was found that oxygen adsorption causes a surface reconstruction, and that oxygen atoms are bound to more than the first layer of Al atoms. For the (111) plane, no reconstruction or bonding to lower substrate levels of Al atoms was observed. Initial stages of oxygen adsorption on Al(100) left a surface layer of clean Al, all the oxygen atoms being incorporated into the bulk below the surface. These results illustrate that a variety of Al-O compounds and interactions can occur in surface oxide layers.

Structural variations might cause, or result from, different aluminum-oxygen coordinations. Although oxide films such as those used in IETS experiments are generally considered to be amorphous, this is not necessarily the case. Herfert (25) has observed structural variations in anodic films on Al depending on preparation conditions. Both crystal-

line and amorphous films, as well as mixtures of the two, were observed. Other results have confirmed this observation (26 - 28). Even though XPS is not necessarily capable of determining structural parameters, it does reflect the distinct chemical environments created by different structures. Herfert (25) found also that anodic films could be hydrated to a greater or lesser extent as a function of the precise conditions during formation. This parallels the work of Bowser and Weinberg (12), who, in an extensive IETS study, have shown that it is possible to vary the degree of bulk hydration in alumina films by varying the substrate temperature while oxidizing in a plasma discharge of H_2O vapor. Hydration would not only result in peak position shifts in the XPS spectra, but also in changes in the ratio of aluminum to oxygen concentrations. Relative concentrations can be determined approximately by monitoring XPS peak intensities. Finally, observed variations in catalytic activity indicate also differing types of aluminas among the alumina films utilized in IETS. For example, significant differences in the number of active sites for acetaldehyde adsorption at room temperature can be seen when comparing IETS results of Evans and Weinberg (5) with those of Brown et al. (29), even though oxide films in the two studies were formed in relatively similar manners.

In agreement with our anticipations, oxide layers grown on evaporated Al films via procedures outlined in Table 2 are each characterized by unique XP spectra. Peak positions for the various alumina films are presented in Table 3 (numerical form) and in Fig. 3a (graphical representation). In both cases, peak positions are tabulated relative to the Al 2p line from bulk aluminum underlying the thin oxide layer, which is detectable since the oxide thickness is less than the escape depth for these photoelectrons of high kinetic energy. This difference could be determined

much more precisely (deviations less than ± 0.05 eV) than could absolute peak positions due to the difficulty of accurately determining the exact onset of the Fermi level. Absolute peak positions can be determined by adding the binding energy of Al 2p electrons for bulk aluminum to the values of Table 3. Various studies report this value as lying between 72.6 (30,31) and 75.0 eV (32), although the most reliable value for this binding energy is perhaps 73.0 eV (24). The first five samples listed in Table 3 and Fig. 3 correspond to alumina layers formed by the various oxidation procedures listed in Table 2. In much of the following, other samples will be related to the O_2 discharge-oxidized alumina since that is the procedure utilized in our IETS experiments. Aluminum and oxygen electronic levels for the thermally oxidized alumina appear at energies 0.15 to 0.3 eV lower than corresponding levels for O_2 discharge samples. In the case of H_2O discharge-formed alumina, aluminum levels are approximately 0.15 eV higher and oxygen levels approximately 0.15 eV lower than for the O_2 discharge. Aluminas formed by direct contact with liquid water show larger shifts to higher binding energies relative to the positions of O_2 discharge peaks, being on the order of 0.25 eV for Al 2p and 2s levels, and approximately 0.3 and 0.6 eV for the O1s and 2s levels, respectively. Heating oxide layers formed in an O_2 discharge above 850 K causes a rather uniform shift of from 0.3 eV to 0.6 eV to higher binding energies for both the aluminum and oxygen peaks. Shifts to higher energies for both aluminum and oxygen levels with heating has been noted earlier in studies of thin aluminum oxide films (33).

Few, if any, general trends are evident in examining the data. Thermally oxidized alumina appears to be more similar to O_2 discharge

samples than to samples heated after plasma oxidation. Likewise, alumina formed in a discharge of H_2O is more similar to O_2 discharge-formed alumina than to that formed in liquid H_2O. Since immersion of aluminum in water is known to yield a product similar to boehmite, containing 18 to 45% by weight of H_2O (34,35), this seems to indicate that the range of aluminas that can be prepared with an H_2O discharge (as discussed above) is more closely related to catalytically "active" aluminas (containing significantly less H_2O) than to less active alumina mono- or trihydrates. Relative peak intensity data, presented in Table 4, indicates H_2O or OH concentrations for the various aluminas in the order liquid H_2O > H_2O discharge > O_2 discharge > thermal O_2 > heated in argon. There is no obvious correlation between peak positions and O/Al concentration ratios. Although Pitton, et al. (36) proposed that oxide peak positions decrease with progressive loss of water, more thorough studies have shown that this is actually opposite to the behavior exhibited by magnesium oxide and hydroxide (10), and by commercial γ- and α-aluminas (37). It appears, therefore, that no generally applicable correlation can be made between water content of oxides and XPS peak positions. In connection with discussions concerning extents of hydration, it should be noted also that pumping in vacuum can affect chemical structures, especially by dehydration reactions, an effect which has been observed previously (38). The possibility exists also that this is not necessarily a uniform effect, i.e., dehydration and/or structural rearrangements in vacuum may occur more readily with some types of samples than with others. Even beyond these possible changes in oxygen and aluminum concentrations during measurements in vacuum, a determination of absolute concentrations from XPS peak intensity measurements is approximate at best.

XPS line intensities can be affected by a number of factors, such as contamination, analyzer and detector efficiencies, X-ray source photon flux, etc. (39). These can vary signficantly from instrument to instrument, sample to sample, or even as a function of time. Based on previous studies in the literature, it appears that even the most precise absolute intensity measurements can only be repeated within approximately 30% (40). Madey et al. (38) have reported that although absolute intensity measurements are unreliable, consistent trends can be reproduced by measuring relative peak areas. Using this approach to present the intensity data in this study (see Table 4) has indicated that repeated measurements of relative intensities are consistent to within approximately ± 3%. Finally, a determination of even concentration ratios is complicated by an incomplete understanding of exact photo-ionization cross-sections for the various elements and electronic levels (as indicated in Table 4). Therefore, we believe that the information presented in Table 4 for relative oxygen and aluminum concentrations accurately represents general trends among the various aluminas, although it may not be an accurate indication of absolute concentrations of the individual chemical elements.

Data for aluminas exposed to HF and HCl are presented also in Fig. 3 and Table 3. Lower exposures to HF on O_2 discharge, H_2O discharge, or the heated (in Ar) samples had little effect on the oxygen or aluminum peaks. Absolute determination of the fluorine concentrations is uncertain, as discussed above. Our best estimates indicate a coverage of from 0.1 to 0.33 monolayer. Relative intensity measurements indicate the same fluorine coverage in each case. Preheating can be seen to have a definite effect on the F1s binding energy, shifting it to approximately 0.75 eV

higher binding energy than for the unheated O_2 discharge alumina. Extensive exposure of samples oxidized in an O_2 discharge to HF more than doubles the surface fluorine concentration. O_2 discharge oxidized samples first exposed to the lower amounts of HF and then to more extensive amounts of HCl have approximately equivalent F and Cl concentrations on the surface. These two types of samples are listed as "Exposed to HF" and "Exposed to HCl", respectively. Higher halogen concentrations also shift peaks to higher binding energies, but this has less effect on the F1s peak than does preheating. Also, increasing halogen concentration has the same effect on the nature of the F1s level regardless of whether fluorine or chlorine is being added to the surface.

One unexpected feature of this study resulted in an increased awareness of the possible introduction of impurities into samples with few obvious means of detecting them. Even low levels of impurities can greatly affect catalytic properties. For example, Rubinshtein, et al. (41) found that previously reported observations of apparent H_2 adsorption on Al_2O_3 were actually due to reduction of Fe_2O_3 impurities. The XPS samples used in this study were prepared over the course of a number of months. At one particular time, XPS samples were prepared within a few days after the vacuum system had been utilized to prepare IETS samples with ferrocene adsorbed on the alumina. While the base pressure of the vacuum system remained at a constant level over the time elapsed in making these junctions, the XPS samples made later showed a great deal of Fe contamination, as shown in Fig. 2b. Although the incorporation of Fe impurities into the IETS alumina films could significantly alter their catalytic properties, the possibility exists that such impurity-induced

perturbations might mistakenly be attributed only to alumina-adsorbate interactions. Additional pumping with intermittant oxygen discharges removed the source of Fe impurities from our sample fabrication system. Based on our experience in this case, we feel that care needs to be taken to insure against unwanted (and, worse yet, unknown) impurities which might alter the nature of an experiment and lead to misinterpretations of the data.

Widths of XPS peaks, although functions of several variables, are indicative of the distribution of chemical states for a particular element. Data for the full-width at half-maximum (FWHM) of the Al 2p, Al 2s and O 1s levels of the various alumina samples are shown in Table 5. With the exception of the sample containing the Fe impurity, little variation is seen in widths of the Al 2p and 2s levels. The width of the O 1s level appears to be more sensitive. In particular, it is interesting to note that the presence of halogens broadens the peak by approximately 0.4 eV. Heating tends to cause a significant sharpening of the O 1s chemical state distributions, since the peak widths for samples heated in argon after oxidation and samples oxidized thermally are at least 0.3 to 0.4 eV less than corresponding peak widths for any of the other samples. Also, the O 1s peak widths for the heated and thermally oxidized samples are extremely similar, even though peak positions indicated very little similarity between these two types of samples. Again, although Pitton, et al. (36) claim a correlation between peak position and peak width (the peak width having an inverse relationship to shifts in the binding energy), no general correlation is apparent in our data.

In principle, the XPS data offer an excellent means of comparison

between thin films of oxidized aluminum and samples of commercial aluminas since the results include information on chemical composition, chemical environments of each of the separate elements, relative concentrations, and distributions of distinct chemical states. In actuality, however, attempts to relate the alumina films to commercial bulk aluminas are complicated by the absence of sufficient, reliable data on the bulk samples. Difficulties arise in attempting to obtain data on bulk aluminas due to charging effects, a common problem for photoemission from semiconducting and insulating surfaces. The presence of positive or negative charge trapped at the surface or in the bulk of an insulator such as alumina causes variations in potential within the substrate, which in turn lead to apparent shifts in binding energies and some line broadening. Charging is not a problem for our oxidized films due to their thickness (on the order of 20 Å) and their intimate contact with the underlying bulk aluminum (conducting) layer. As static charging may easily vary with measurement time, measurements should be accomplished by multiple rapid sweeps through the entire energy range so that any charging will affect all spectral features uniformly. Various methods of compensating for charging of bulk oxide samples have been attempted. These include gold decoration (42,43), simultaneous flooding of the surface with low-energy electrons (44), and referencing to contaminant carbon (36,45), the Al 2p (oxide) line (37), or a convenient Auger feature such as the oxygen KLL transition (31).

Gold decoration, which involves gold vapor deposition on top of all but a small window area of the sample, has in certain cases been found to alter the chemical nature of the surface of the sample (39). Grunthaner

et al. (21) have found the use of electron "flood guns" to be inferior to operating under normal conditions with only the low background of secondary electrons present. An extensive survey of some referencing techniques by Madey et al. (38) agrees with these conclusions, indicating that both gold vapor deposition and electron flooding are inferior as means of compensating for static charging to the method of referencing to the C 1s level, which itself was found to be reliable only to within a standard deviation of 0.41 eV.

Siegbahn et al. (46) were the first to suggest that residual carbon could be used as an internal standard for binding energy measurements. This practice has been rather widespread, although the method is being met with increasing dissatisfaction (47). The most precise and extensive data available on aluminas indicate that the major problem encountered in referencing to the C 1s level of contaminant carbon is the lack of knowledge of its chemical state (37,38). Such contamination might, for example, come from the atmosphere, from pump oil or grease on vacuum seals, or from the support used for mounting since many alumina powders are examined by dusting onto two-sided adhesive tape and mounted in this manner in the spectrometer (10). The intensity, lineshape and even the number of observed C 1s peaks vary considerably from sample to sample. Madey et al. (38) illustrate this point in their work. Jørgensen and Berthou (48) have utilized C 1s referencing in a number of studies. Examining a range of aluminas along with Pitton (36), they reported unsystematic C 1s peak variations over a range of 3 eV. On some samples, two peaks were visible, while on others, only one was present. Variations in Al 2p and O 1s peak poistions, referenced to C 1s peaks, among the different aluminas were in

general less than the standard deviation of approximately 0.4 eV that can be expected for C 1s referenced data. Comparisons of our data with their results for commercial samples only indicate that films oxidized in liquid H_2O are more like AlO(OH) or aluminum trihydrate than are films oxidized in O_2 or H_2O discharges, or thermally. Their results for O/Al atomic ratios offer little means of comparison since these were obtained by a semi-quantitative analysis of signal amplitudes, a method which appears to be unreliable for even indicating general trends (38).

Ogilvie and Wolberg (37) have proposed using the Al 2p line as an internal standard when working with bulk aluminum oxides, and similar methods of referencing have proven effective with other oxide studies (21). They showed that while standard deviations for absolute positions of the Al 2p, C 1s and O 1s lines are as much as 1.2 eV for measurements on a number of γ-alumina samples, the Al 2p-O 1s difference had a standard deviation of only 0.12 eV for the same measurements. Similar precision was obtained for Zn/Al_2O_3 catalysts. Unfortunately, this type of data is not available for a range of different commercial aluminas which might be compared profitably with our results on alumina films. Fig. 3b illustrates our data using the Al 2p (oxide) peak as the internal reference. This is in a form which may be compared directly to additional data on commercial aluminas. One possible problem of using data in this form to distinguish among various types of aluminas is the lack of uniqueness exhibited from sample to sample. Referencing to the Al 2p (oxide) line tends to obscure peak position variations, as can be seen by comparison with Fig. 3a which represents absolute peak positions. Thus, although

referencing to the Al 2p level for commercial (bulk) aluminas yields precise results, it may reduce peak position variations between samples to the point where closely related aluminas cannot be identified uniquely. Pitton, et al. (36) believe that changes in the chemical nature of aluminum oxides shift the Al and O peaks in the same direction, often by approximately equivalent amounts. This indicates also that absolute differences may be hidden by this type of referencing.

Wagner (31) has suggested a different type of internal reference when working with oxides that would not result in obscuring important peak position differences. He proposes the use of an "Auger parameter", this being the difference in positions between an XPS peak of interest and a convenient Auger transition. Auger lines frequently exhibit far larger chemical shifts than photoelectron lines, mainly because they are more strongly affected by extra-atomic relaxation energies. Chemical shifts over a range of 6.8 eV have been observed for the Al(KLL) Auger peak as the aluminum oxidation state varies from zero to +3 (49). Fig. 4 shows data for the Al 2p, O 1s and O 2s levels referenced to the O(KLL) Auger transition for films oxidized in an O_2 discharge, thermally in O_2-enriched air, and in liquid H_2O. In order that data for the various electronic levels can be presented using a common energy axis, the relevant peak position difference for the O_2 discharge sample is placed at zero and differences for the other samples related to it. This figure indicates that referencing to an Auger transition might be an effective means of interpreting XPS results of metal oxides (such as aluminas). Again, however, such data are not yet available to allow comparisons.

4. Conclusions

In summary, we have presented results for XPS investigations of thin alumina layers made by oxidizing the top few atomic layers of evaporated aluminum films. Oxidation was carried out via a number of methods which have been utilized previously in IETS studies, and these variously oxidized samples compared by means of analyzing peak positions, peak widths, and relative O/Al concentration ratios. As anticipated, distinct spectral differences were apparent between the various types of alumina films. The effects of adding halogens to the surface were observed also. Heating was shown to cause similar, significant sharpening of chemical state distributions for oxygen in both thermally oxidized samples and samples heated in an inert atmosphere after oxidation in an O_2 discharge. No generalized correlations could be made, however, between peak positions and either chemical state distributions (peak widths) or extents of hydration (O/Al ratios). No comparisons can be made with XPS results for commercial aluminas as yet due to the lack of reliable data on bulk samples. Internal referencing to an Auger transition appears to be the most promising means of producing precise, accurate results for bulk aluminas, but more work needs to be done before this can be determined. As reliable XPS results on commercial samples become available, comparisons may then be readily made with the data for thin alumina films presented here. One important comparison can be made immediatedly, however. Our results indicate that the chemical nature of thermally oxidized films is similar to that of alumina films prepared in an O_2 or H_2O discharge. Thus, IETS studies utilizing discharge-grown oxides might be

compared directly to studies with thermally grown oxides. This is important since thermal oxide films have been related to commercial γ-alumina by catalytic studies (50).

The current study reveals important information on the chemical nature of various thin alumina films, which can be added to information already available on many of the physical properties of similar films. Similarities and differences resulting from different oxidation procedures are now apparent, allowing more accurate comparisons among IETS studies done on various alumina surfaces. Finally, although further studies are certainly necessary, the current study provides significant information which should allow comparisons among IETS studies done on alumina films and studies on commercial bulk aluminas when additional reliable XPS data are available for commercial samples.

Acknowledgment

We appreciate the very valuable advice and assistance of Dr. B. F. Lewis. Financial support by the National Science Foundation under Grant Number ENG78-16927 is gratefully acknowledged.

References

1. E.g., J. Lambe and R. C. Jaklevic, Phys. Rev. 165, 821 (1968). Inelastic Electron Tunneling Spectroscopy, T. Wolfram, ed., Springer-Verlag, N.Y., 1978.
2. P. K. Hansma, W. C. Kaska and R. M. Laine, J. Am. Chem. Soc. 98, 6064 (1976).
3. H. E. Evans, W. M. Bowser and W. H. Weinberg, Surface Sci. (in press).
4. H. E. Evans and W. H. Weinberg, J. Chem. Phys., Aug. 15, 1979.
5. H. E. Evans and W. H. Weinberg, J. Chem. Phys. (submitted).
6. W. M. Bowser and W. H. Weinberg, in preparation.
7. H. E. Evans and W. H. Weinberg, in preparation.
8. B. C. Lippens and J. J. Steggerda, Physical and Chemical Aspects of Adsorbents and Catalysts, B. G. Linsen, ed., p. 171, Academic Press, N.Y., 1970.
9. K. Wefers and G. M. Bell, Technical Paper # 19, Alcoa Research Laboratories, 1972.
10. H. Vinek, J. Latzel, H. Noller and M. Ebel, J. Chem. Soc. Faraday Trans. I 74, 2092 (1978).
11. W. H. Weinberg, Ann. Rev. Phys. Chem. 29, 115 (1978).
12. W. M. Bowser and W. H. Weinberg, Surface Sci. 64, 377 (1977).
13. Y. Scarlatos, R. C. Barker and G. L. Haller, Surface Sci. 43, 353 (1974).
14. J. T. Hall and P. K. Hansma, Surface Sci. 77, 61 (1978).
15. E.g., M. Cardona and L. Ley, Topics in Applied Phys. 26, (1978).
16. F. J. Grunthamer, NBS Special Publication 400-23, p. 151, March, 1979.
17. K. S. Kim and N. Winograd, Surface Sci. 43, 625 (1974).
18. K. S. Kim, J. J. O'Leary and N. Winograd, Anal. Chem. 45, 2214 (1973).

19. S. Evans, J. Chem. Soc. Faraday Trans. II 71, 1044 (1975).

20. K. S. Kim, N. Winograd and R. E. Davis, J. Am. Chem. Soc. 93, 6296 (1971).

21. F. J. Grunthaner, P. J. Grunthaner, R. P. Vasquez, B. F. Lewis, J. Maserjian and A. Madhukar, J. Vac. Sci. Technol. (submitted).

22. C. W. B. Martinson, L. G. Petersson, S. A. Flodström and S. B. M. Hagström, Proceedings of the 7th International Vacuum Congress and Proceedings of the 3rd International Conference on Solid Surfaces, Vienna, 1977, p. 869, F. Berger and Söhne, Vienna, 1977.

23. S. A. Flodström, C. W. B. Martinsson, R. Z. Bachrach, S. B. M. Hagström and R. S. Bauer, Phys. Rev. Letters 40, 907 (1978).

24. S. A. Flodström, R. Z. Bachrach, R. S. Bauer and S. B. M. Hagström, Phys. Rev. Letters 37, 1282 (1976).

25. R. E. Herfert, Technical Report AFML-TR-76-142, Northrup Corporation, August, 1976.

26. D. J. Stirland and R. W. Bicknell, J. Electrochem. Soc. 106, 481 (1959).

27. P. Bodson, F. Bouillon and M. Jardinier-Offergeld, Metallurgie 6, 47 (1966).

28. L. Harris, J. Opt. Soc. Am. 45, 27 (1955).

29. N. M. D. Brown, R. B. Floyd and D. G. Walmsley, J. Chem. Soc. Faraday Trans. II 75, 17 (1979).

30. A. Barrie, Chem. Phys. Letters 19, 109 (1973).

31. C. D. Wagner, J. Chem. Soc. Faraday Discussions 60, 291 (1976).

32. P. Lorenz, J. Finster, G. Wendt, J. V. Salyn, E. K. Zumadilov and V. I. Nefedov, J. Elec. Spec. 16, 267 (1979).

33. K. Hirokawa, F. Honda and M. Oku, J. Elec. Spec. 6, 333 (1975).

34. W. J. Bernard and J. J. Randall, J. Electrochem. Soc. 107, 483 (1960).

35. W. Vedder and D. A. Vermilyea, Trans. Faraday Soc. 65, 561 (1969).

36. O. Pitton, C. K. Jørgensen and H. Berthou, Chimia 30, 540 (1976).

37. J. L. Ogilvie and A. Wolberg, Appl. Spec. 26, 401 (1972).

38. T. E. Madey, C. D. Wagner and A. Joshi, J. Elec. Spec. 10, 359 (1977).

39. C. Defossé, P. Canesson, P. G. Rouxhet and B. Delmon, J. Catal. 51, 269 (1978).

40. C. K. Jørgensen and H. Berthou, J. Chem. Soc. Faraday Discussions 54, 269 (1972).

41. A. M. Rubinshtein, K. I. Slovetskaya, T. R. Brueva and E. A. Federovskaya, Dokl. Akad. Nauk. SSSR. 167, 1308 (1966).

42. C. R. Ginnard and W. M. Riggs, Anal. Chem. 46, 1306 (1974).

43. D. S. Urch and M. Webber, J. Elec. Spec. 5, 791 (1974).

44. D. A. Stephenson and N. J. Binkowski, J. Non-Cryst. Solids 22, 399 (1976).

45. W. P. Dianis and J. E. Lester, Anal. Chem. 45, 1416 (1973).

46. K. Siegbahn, C. Nordling, A. Fahlman, R. Nordberg, K. Hedman, G. Johansson, T. Borgmark, S. Karlsson and B. Lindberg, ESCA, Almquist and Wiksells, Uppsala, 1967.

47. C. R. Brundle, Appl. Spec. 25, 8 (1971).

48. C. K. Jørgensen and H. Berthou, Chem. Phys. Letters 31, 416 (1975).

49. J. E. Castle, L. B. Hazell and R. Whitehead, J. Elec. Spec. 9, 247 (1976).

50. P. K. Hansma, D. A. Hickson and J. A. Schwarz, J. Catal. 48, 237 (1977).

51. J. H. Scofield, J. Elec. Spec. 8, 129 (1976).

52. V. I. Nefedov, N. P. Sergushin, I. M. Bond and M. B. Trzhaskovskaya, J. Elec. Spec. 2, 383 (1973).

53. C. D. Wagner, Anal. Chem. 44, 1050 (1972).

Table 1

Some Aluminum Oxides and Hydroxides

Preferred Names	Form
Gibbsite or α-alumina trihydrate	$Al(OH)_3$
Bayerite or β-alumina trihydrate	$Al(OH)_3$
Nordstrandite	$Al(OH)_3$
Boehmite or α-alumina monohydrate	AlO(OH)
Diaspore or β-alumina monohydrate	AlO(OH)
ρ-alumina, χ-alumina, η-alumina, γ-alumina	$Al_2O_3 \cdot nH_2O$, $0 < n < 0.6$ (dehydrated below 600 C)
κ-alumina, θ-alumina, δ-alumina	"nearly" anhydrous Al_2O_3 (dehydrated between 900 - 1000 C)
Corundum or α-alumina	Al_2O_3

Table 2

Alumina Film Preparation

Sample Type	Oxidation Procedure	Reference to Use in IETS
1. O_2 Discharge	Exposed to plasma discharge of O_2 (Matheson Research Grade, 99.99%) for 15 minutes.	Ref. (12)
2. Thermal O_2	Heated in O_2 enriched air at 600 K for 10 minutes.	Ref. (14)
3. H_2O Discharge	Exposed to plasma discharge of tripley distilled H_2O for 20 minutes.	Ref. (12)
4. Liquid H_2O	Immersed in liquid H_2O for a few seconds, then dried immediately in a stream of N_2.	Ref. (13)
5. Heated	Oxidized as type 1, then heated in Ar (Matheson Prepurified Grade, 99.998%) at 850 K for 10 minutes.	

Table 3

Binding Energy Differences Compared to Bulk Al 2p in eV

Sample	Al 2p (oxide)	Al 2s	O 1s	O 2s	O (Auger)	C 1s	F 1s
O_2 Discharge	2.54	47.36	459.87	-48.40	906.72	213.10	613.83
Thermal O_2	2.42	47.21	459.56	-48.57	906.87	-	-
H_2O Discharge	2.66	-	459.87	-48.53	-	213.4-	613.94
Liquid H_2O	2.77	47.62	460.49	-47.42	907.08	-	-
Heated in Ar	3.10	-	460.13	-47.81	-	213.88	614.57
Exposed to HF	2.67	-	-	-	-	-	614.16
Exposed to HCl	2.89	47.70	460.39	-47.99	-	213.46	614.16
Fe Impurity	2.06	47.01	459.45	-48.00	904.13	-	-

Table 4

Oxygen-to-Aluminum Concentration Ratios

Sample	(Intensity O 1s/Intensity Al 2p)* $\frac{1}{5.4^a}$
O_2 Discharge	1.56 ± 0.04
Thermal O_2	1.52
H_2O Discharge	1.60
Liquid H_2O	1.85
Heated in Ar	1.41

[a]This factor takes into account photo-ionization cross-section differences between the O 1s and Al 2p levels. This value was taken from Ref. (51). Other authors have reported values of 5.6 (39), 4.6 (52), 3.7 (53) and 3.3 (40).

Table 5

Peak Widths (FWHM), eV

Sample	Al 2p	Al 2s	O 1s
O_2 Discharge	1.65	2.2	2.6
Thermal O_2	1.7	2.3	2.25
H_2O discharge	1.7	-	2.5
Liquid H_2O	1.65	2.2	2.55
Heated in Ar	1.6	-	2.2
Exposed to HF	1.7	-	-
Exposed to HCl	1.7	2.2	3.0
Fe Impurity	1.9	2.2	1.7

Figure Captions

Fig. 1: Representative spectra for the O 1s and Al 2p levels for a sample oxidized in a plasma discharge of O_2.

Fig. 2: Wide spectral scans for (a) a sample oxidized in an O_2 discharge and exposed to HF, and (b) a sample with significant amounts of Fe contamination due to residual ferrocene in the system.

Fig. 3: Peak positions for the Al 2p (oxide), Al 2s (oxide), O 1s, O 2s, O (Auger), C 1s and F 1s levels referenced to the Al 2p (bulk) line for the various samples.

Fig. 4: As in Fig. 3, except all peak positions are referenced to the Al 2p (oxide) line.

Fig. 5: Use of the Auger parameter to distinguish between various types of aluminas: positions of the Al 2p, O 1s and O 2s peaks relative to an oxygen Auger line for samples prepared in an O_2 discharge (■), thermally in O_2-enriched air (◇) and in liquid H_2O (▽).

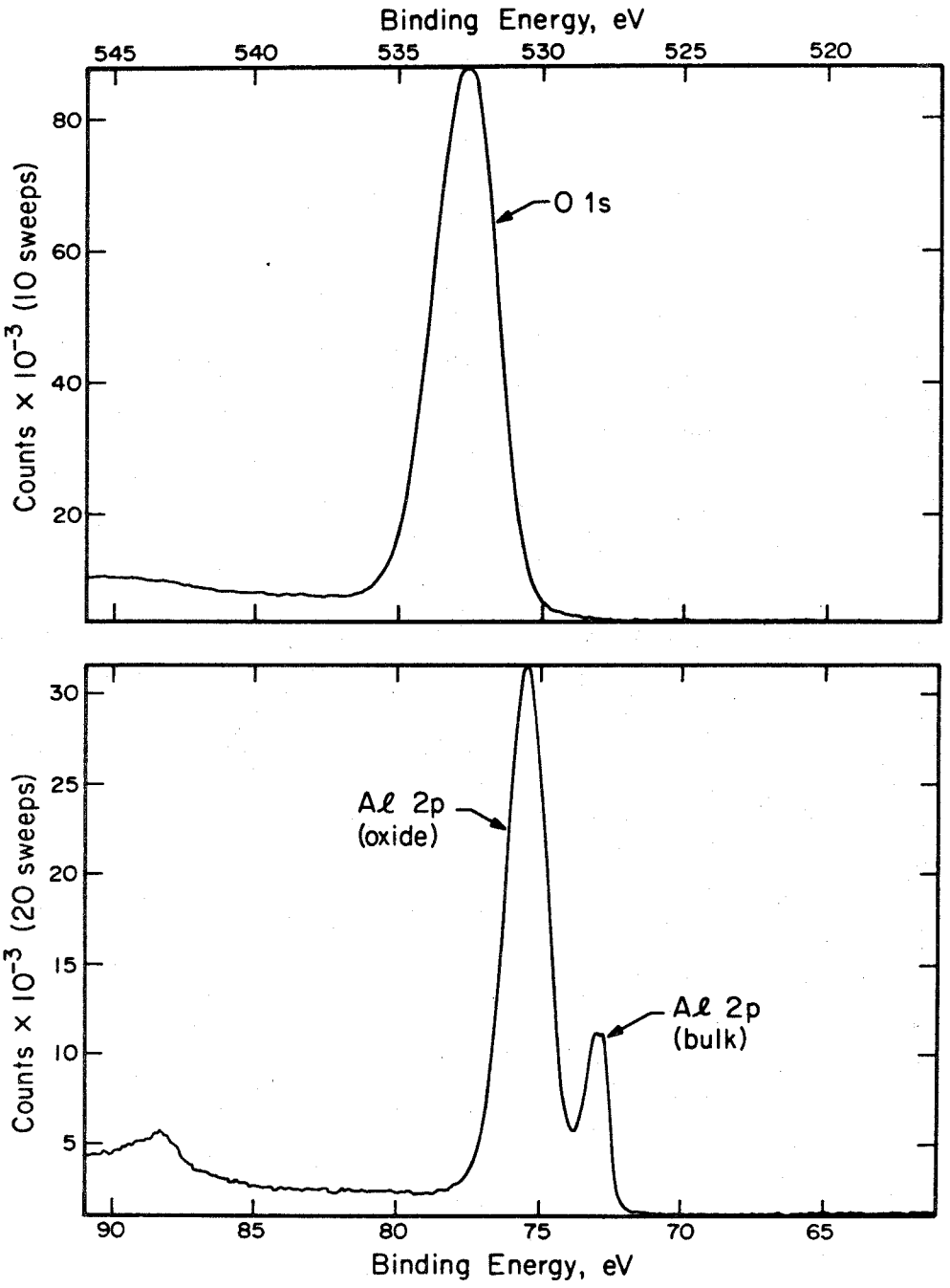
Binding Energy, eV
545
540
535
530
525
520
80
60
40
20
Counts x 10⁻³ (10 sweeps)
O 1s
30
25
20
15
10
5
Counts x 10⁻³ (20 sweeps)
Aℓ 2p
(oxide)
Aℓ 2p
(bulk)
90
85
80
75
70
65
Binding Energy, eV

Fig. 1

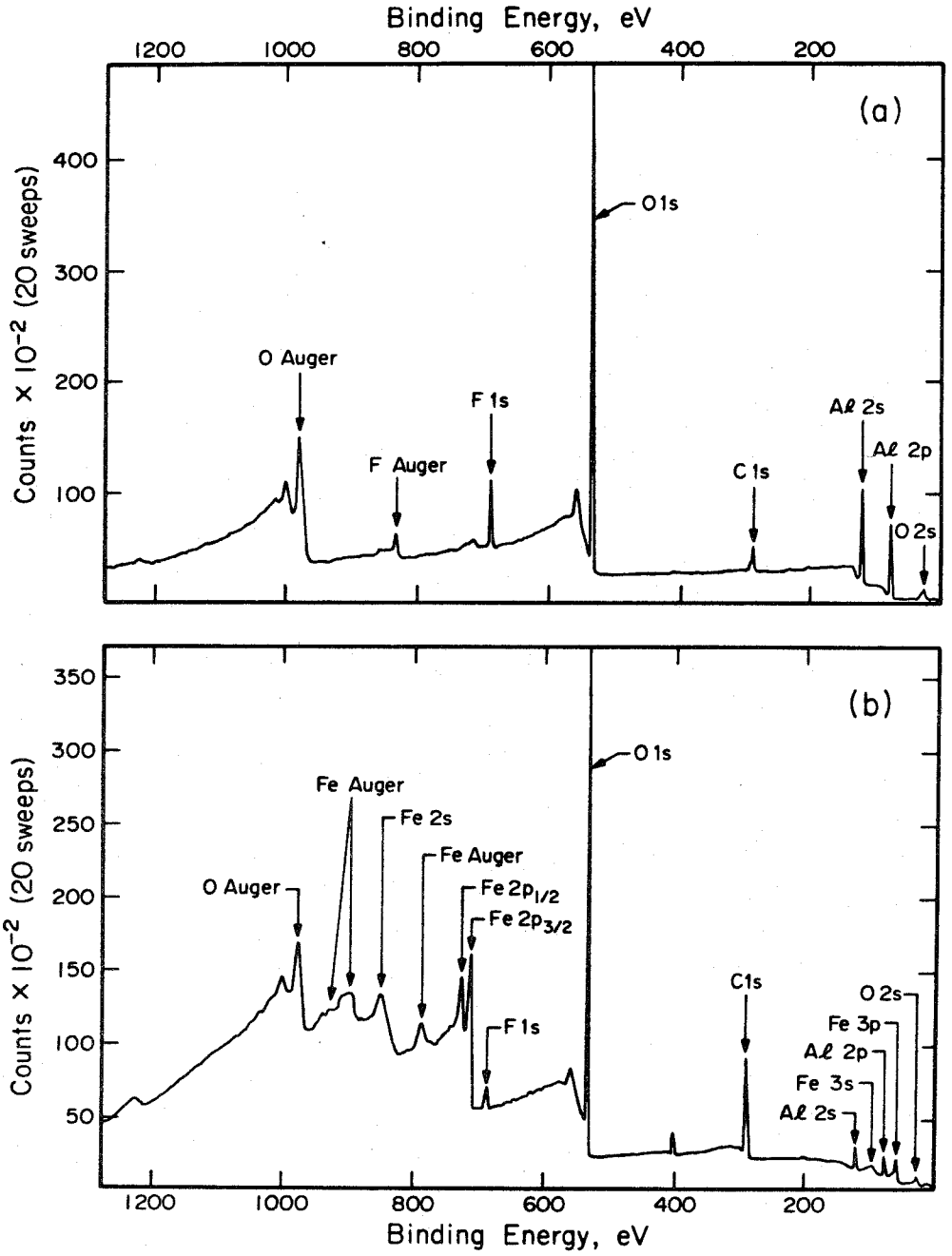
Binding Energy, eV
1200
1000
800
600
400
200
(a)
Counts X 10⁻² (20 sweeps)
400
300
200
100
O 1s
O Auger
F 1s
F Auger
C 1s
Aℓ 2s
Aℓ 2p
O 2s
(b)
350
300
250
200
150
100
50
O 1s
Fe Auger
Fe 2s
Fe Auger
O Auger
Fe 2p1/2
Fe 2p3/2
F 1s
C1s
O 2s
Fe 3p
Aℓ 2p
Fe 3s
Aℓ 2s
1200
1000
800
600
400
200
Binding Energy, eV

Fig. 2

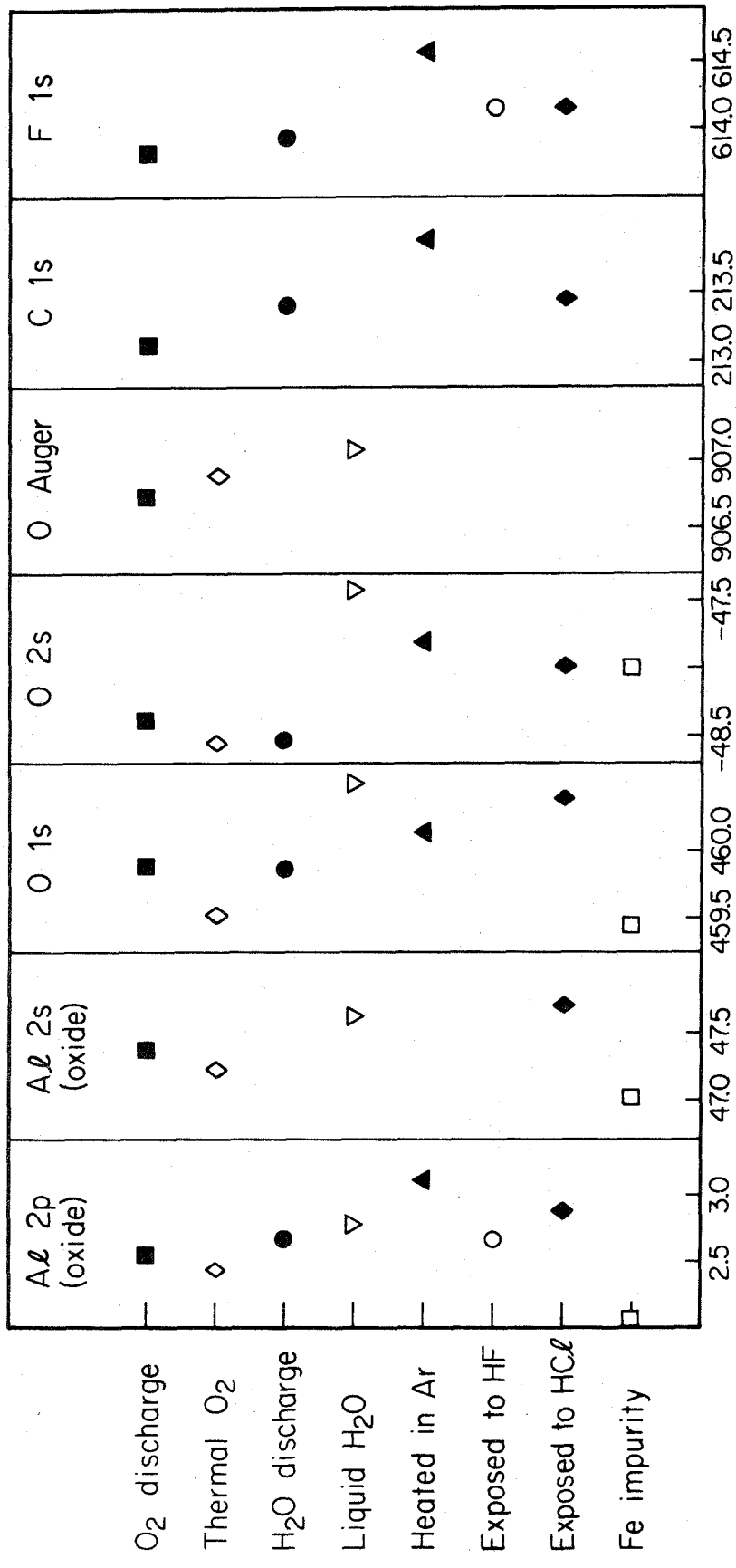
Aℓ 2p (oxide)
Aℓ 2s (oxide)
O 1s
O 2s
O Auger
C 1s
F 1s
O2 discharge
Thermal O2
H2O discharge
Liquid H2O
Heated in Ar
Exposed to HF
Exposed to HCℓ
Fe impurity
2.5
3.0
47.0
47.5
459.5
460.0
-48.5
-47.5
906.5
907.0
213.0
213.5
614.0
614.5
Differences From Aℓ 2p Bulk Peak, eV

Fig. 3

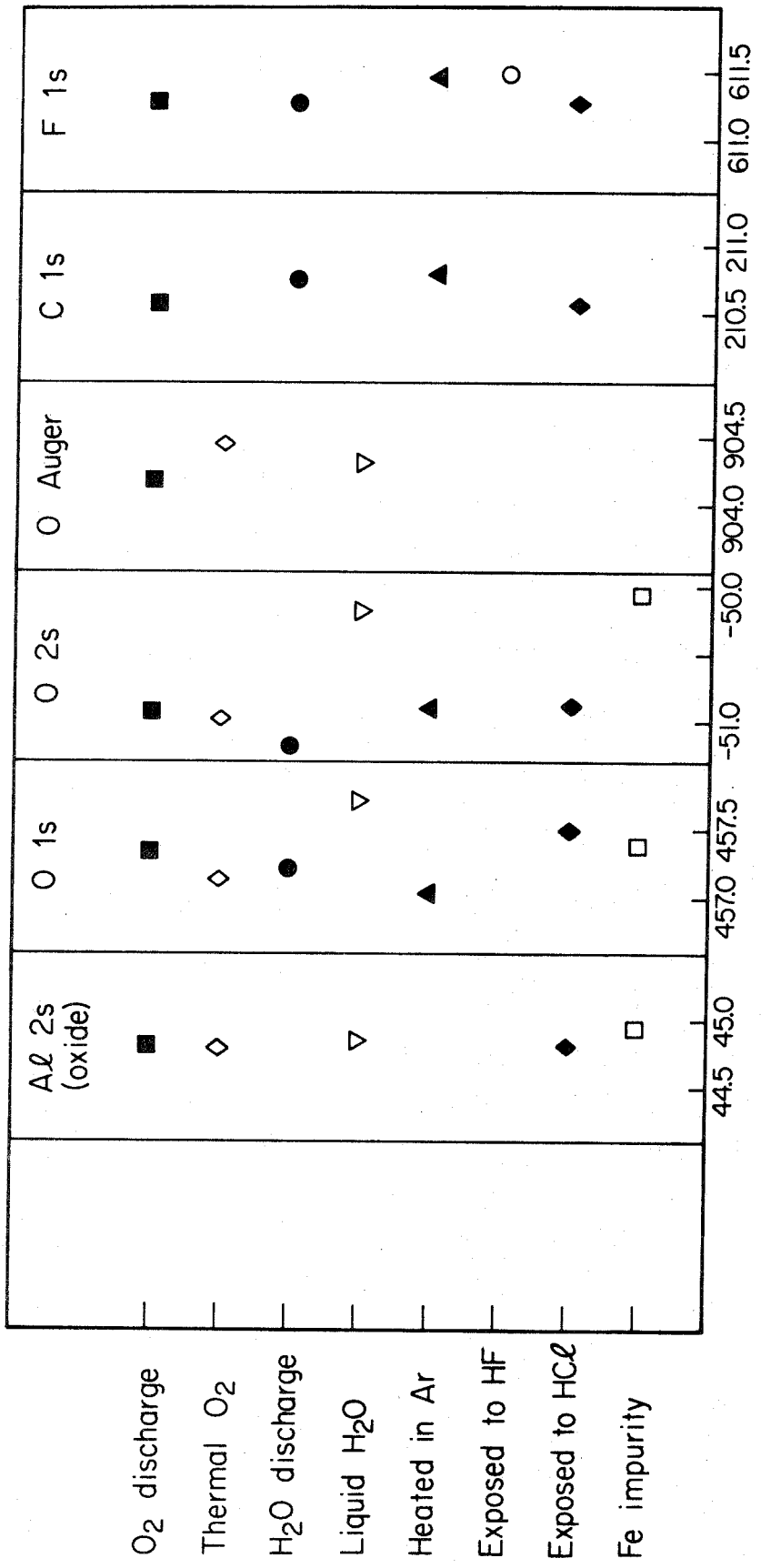
Aℓ 2s (oxide)
O 1s
O 2s
O Auger
C 1s
F 1s
O2 discharge
Thermal O2
H2O discharge
Liquid H2O
Heated in Ar
Exposed to HF
Exposed to HCℓ
Fe impurity
44.5 45.0
457.0 457.5
-51.0 -50.0
904.0 904.5
210.5 211.0
611.0 611.5
Differences From Aℓ 2p Oxide Peak, eV

Fig. 4

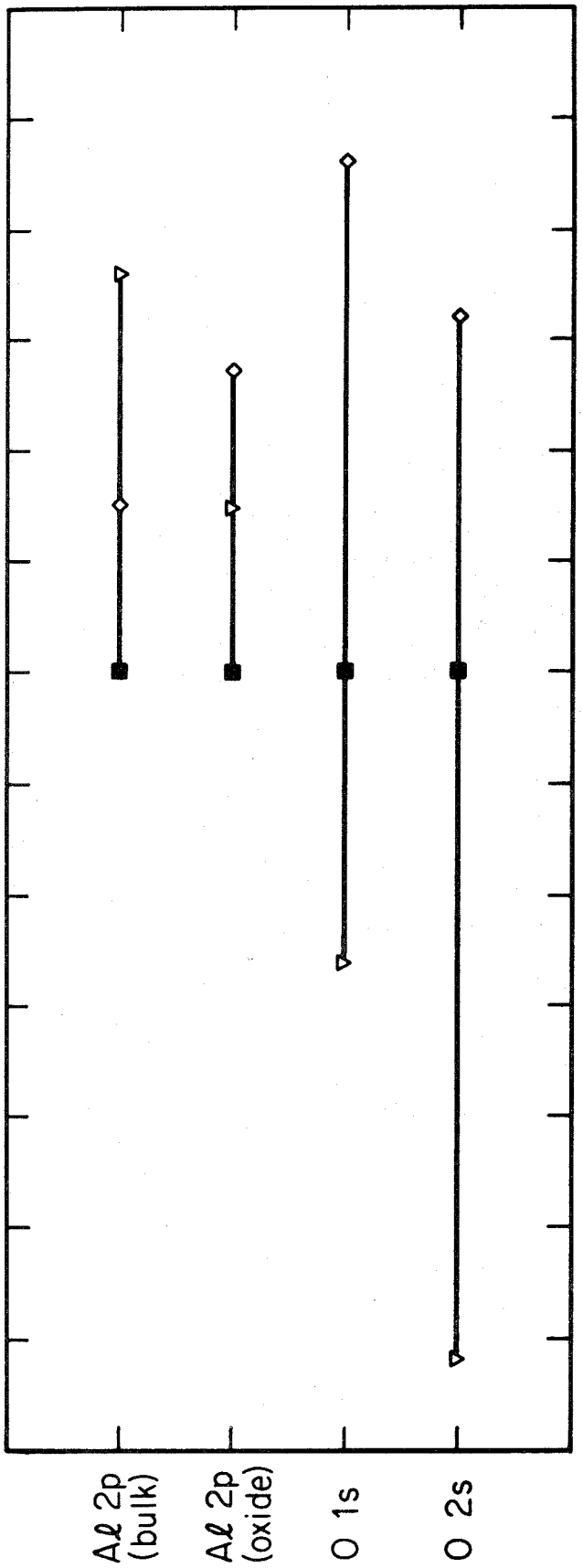
Al 2p (bulk)
Al 2p (oxide)
O 1s
O 2s
-0.5
0
+0.5
Differences From Oxygen Auger Line, eV
(relative to O2 discharge sample)

Fig. 5

Chapter III

The Reaction of Ethanol with an Aluminum Oxide Surface Studied by IETS

Abstract

Inelastic Electron Tunneling Spectroscopy (IETS) has been employed to study the vibrational structure of ethanol reacting with a clean alumina surface as a function of temperature from 295 K to 575 K. The spectra for the surface species up to approximately 450 K correspond to infrared spectra of aluminum ethoxide, $Al(OC_2H_5)_3$. Between 450 K and 475 K the structure changes from an ethoxide to an acetate, the most obvious spectral change being the appearance of a new peak at approximately 1585 cm^{-1} (197 meV) which is characteristic of the asymmetric OCO stretching mode of various inorganic acetates. No further changes are observed above 475 K. Above 370 K, there is also a significant increase in the total concentration of adsorbed species. This is due to a partial dehydration or dehydroxylation of the surface, thus freeing active sites which had previously been blocked by water or hydroxyl groups formed during the initial stages of ethanol adsorption. This dehydration or dehydroxylation of the surface is simultaneously accompanied by a transformation of the bulk aluminum oxide to aluminum hydroxide. While IETS has been applied successfully in the past to study a wide variety of adsorbate-adsorbent systems, here tunneling spectroscopy is demonstrated explicitly to be effective in monitoring quantitatively the structural changes occurring in a reacting system at low pressures as a function of temperature.

1. INTRODUCTION

Since its discovery by Jaklevic and Lambe (1), IETS has been shown to be an effective probe of vibrational structure. Its utility has been demonstrated for a number of diverse problems, including studies in adhesion (2), biochemistry (3), water pollution (4) and damage due to electron beam irradiation (5). In addition, IETS has shown particular promise in the areas of surface chemistry and catalysis, where it has been used to investigate a number of chemisorption phenomena, primarily on aluminum oxide catalytic surfaces. These investigations include structural determinations for a number of organic molecule-alumina complexes (6); the nature and composition of "model" alumina catalysts (7); the sticking probability of formic acid as a function of coverage (8); and the orientation of chemisorbed benzoic acid (9), dihydroxy-substituted phenols (10), and sulfonic acids (11). IETS applications have recently been expanded to include also the study of model supported-metal catalytic systems, such as the adsorption of CO on alumina-supported Rh (12) and C_2H_5OH on supported Ag (13). The value of IETS as an experimental tool for the catalytic scientist would be enhanced further if its routine use could be extended beyond studying the "static" features of chemisorption systems as outlined above, to include also monitoring the dynamic structural changes occurring in catalytic systems as a function of such variables as time, pressure, temperature and surface coverage.

Some initial efforts have been made in this direction. Shklyarevskii et al. (14), in a study of CH_3COOH adsorption on alumina, reported the observation of spectral changes corresponding to the transition from a

physically adsorbed to a chemisorbed state as the substrate is heated from 77 K to room temperature. Kroeker et al. (15) observed hydrocarbon formation as CO molecules chemisorbed on alumina-supported Rh particles reacted with hydroxyl groups present on the surface of the oxide. Also, McBride and Hall (16) have recently noted the catalytically induced hydrogenation of muconic acid, chemisorbed on alumina as a muconate ion, by surface hydroxyl groups between 293 K and 673 K. While IETS has proved to be an effective tool for probing some details of "dynamic" catalytic phenomena in these few simple cases, the lack of greater utilization in this direction is somewhat surprising considering the current importance of fundamental research in catalysis and the success of initial IETS studies.

The primary purposes of this work are to demonstrate further the utility of IETS for investigating dynamic catalytic processes, while at the same time to provide additional information on a catalytic system of considerable interest and importance. The system chosen for this study is ethanol adsorption on aluminum oxide as a function of both exposure and temperature. Alumina has been utilized extensively as an effective catalyst for the dehydration of alcohols, and this has prompted numerous investigations into the catalytic behavior of alcohol-alumina systems (17). The vibrational structure of ethanol reacting with an alumina surface has previously been studied via infrared spectroscopy by Babushkin and Uvarov (18), Naito (19), Uvarov (20), Greenler (21), Treibmann and Simon (22), Kagel (23), and Arai et al. (24). Their collective results indicate that ethanol chemisorbs dissociatively on alumina at room temperature, yielding a structure similar to that of aluminum ethoxide. Around 450 K, however,

spectral changes indicate a shift from an ethoxide-type structure to one more characteristic of aluminum acetate. By performing further experiments on this system, we have demonstrated the capability of IETS for monitoring quantitatively structural changes which occur in catalytic reactions and have contributed additional and more detailed spectroscopic information on this system.

2. EXPERIMENTAL DETAILS

Both the experimental and theoretical aspects of tunneling spectroscopy have been discussed in detail elsewhere (25), and only the general features and procedures will be outlined briefly here.

Our applications of the IETS technique employ tunnel junctions consisting of a metal film, a thin oxide barrier, and a top metal film arranged in a planar or diode geometry. The vibrational structure of molecules at or near the insulating barrier can be measured by monitoring the current-voltage characteristics of the junction as a voltage is applied between the two metal film electrodes.

In practice, a thin aluminum strip, approximately 1000 Å in thickness and 2 mm in width, is evaporated onto a clean glass slide in a vacuum chamber with base pressure on the order of 10^{-7} torr. The top 20 - 30 Å of this film is then oxidized in a plasma discharge of pure O_2, thus forming the oxide barrier required for the tunneling experiment. Aluminum oxide surfaces prepared in this manner were then allowed to interact with ethanol vapor at predetermined exposures and temperatures, and the samples were completed by the evaporation of top lead electrodes in the form of cross strips approximately 3000 Å in thickness.

Balzers 99.9999% Pb and 99.99% Al were used for the metal evaporations, Matheson Research Grade (99.99%) O_2 for the plasma oxidation, and U.S. Industrial Chemicals Co. reagent quality pure ethyl alcohol for the ethanol adsorption. Sample heating was accomplished via a technique devised by Bowser and Weinberg (26), where a four-point-probe geometry is used to heat the aluminum strip and oxide film resistively while simultaneously measuring the temperature. Accuracy in temperature measurements utilizing this method is ± 8%, and the temperature during exposure to ethanol was stable to within ± 2 - 3 K.

After evaporation of the top Pb electrode, samples are removed from the vacuum system and mounted on a probe which can be inserted directly into a liquid He dewar for measurement. Only those junctions whose room temperature resistance fell in the range 30 - 200 Ω were measured, as these exhibit the most favorable signal-to-noise characteristics utilizing our electronics.

Spectral measurements were accomplished by means of PDP 11/10 computer-controlled electronics, where a harmonic detection scheme is utilized to monitor directly the second harmonic signal due to a small modulation voltage (1 meV rms in this case) as a function of bias voltage across the junction. Plots obtained in this manner relating the second derivative d^2V/dI^2 (proportional to d^2I/dV^2) to the applied voltage, V, have been shown to be analogous to optical absorption experiments, such as infra-red or Raman spectroscopy (27). Spectra were recorded over the range 240 to 3950 cm^{-1} (30 to 490 meV). The resolution of the measurement allowed the determination of peak positions for sharp peaks to within ± 4 cm^{-1} (0.5 meV).

3. RESULTS

Measurements were made with samples exposed to varying amounts of ethanol vapor, from 0.01 torr-sec exposure (where hydrocarbon adsorption on the alumina first became apparent at room temperature) to exposures greater than 100 torr-sec. An exposure of 100 torr-sec corresponds to saturation coverage under our conditions, as judged by the lack of increases in intensity for any spectral features as exposure is continued beyond this point. Neither peak positions nor peak shapes exhibited any significant variations with coverage. Therefore, all the spectra illustrated below are at saturation coverage.

The temperature was varied from 295 K to 575 K. Samples which were first preheated in vacuum at 575 K for several minutes, then cooled and exposed to ethanol at a lower temperature, showed no variations from samples where no preheating at 575 K was done. Since this indicates that any spectral changes observed upon heating are due primarily to activated processes involving the ethanol and its adsorption products, rather than changes in the alumina upon heating, the preheating step was omitted for most of the samples. Spectra obtained at a few of the temperatures studied are shown in Fig. 1 (240 cm^{-1} to 2250 cm^{-1}) and Fig. 2 (2000 cm^{-1} to 3950 cm^{-1}). A list of peak positions for these spectra is presented in Table 1. The top Pb electrode has been reported to cause slight shifts to lower energies in observed IETS peak positions relative to optically observed frequencies. Shifts of up to 1.6 cm^{-1} (0.2 meV) for C-C

stretching and deformation modes, 4 cm^{-1} (0.5 meV) for C-H deformations, and 73 cm^{-1} (9 meV) for surface O-H stretching vibrations have been reported for benzoic acid chemisorbed on alumina (28). Shifts for the C-H stretching modes were not presented. Peak shifts of this magnitude have a negligible effect in the interpretation of our results.

Overall, there is little change in the appearance or intensity of any spectral features up to approximately 370 K. Above this point, the intensity of the hydrocarbon peaks begins to increase continuously with temperature, although their peak shapes and relative intensities remain constant. This growth in hydrocarbon peak intensity is accompanied by a similar increase in the broad feature centered at approximately 1863 cm^{-1} (231 meV) and the long shoulder on its low-energy side, as well as in the low-energy shoulder on the prominent feature at 910-935 cm^{-1} (113-115 meV). Also, the peak which had remained stable at 3637 cm^{-1} (451 meV) up to 370 K began to shift slowly but continuously down in energy with further increases in temperature, being centered at 3605 cm^{-1} (447 meV) at the highest temperature studied. Similar, but less pronounced behavior was noted for the 935 cm^{-1} (116 meV) peak, which shifted slightly to 927 cm^{-1} (115 meV) with increasing temperature, and for the 1863 cm^{-1} (231 meV) peak, which experienced a shift to 1847 cm^{-1} (229 meV).

These increases in the hydrocarbon peak intensity continued, with peak shapes and positions generally remaining constant, until changes began to occur in the spectral appearance above approximately

450 K. By 475 K a new structure was developed fully. This new structure is characterized by several distinct features, most prominent of which is the appearance of a new rather broad peak at approximately 1589 cm^{-1} (197 meV). In addition, features appearing at 710 cm^{-1} (88 meV) and 806 cm^{-1} (100 meV) in the low temperature species have been replaced by new features at 621 cm^{-1} (77meV), 669 cm^{-1} (83 meV), and 879 cm^{-1} (109 meV). The broad, rounded peak at 1036 cm^{-1} (131 meV) is considerably sharper and shifted slightly (to approximately 1048 cm^{-1}) in the high temperature species. Also, peaks occurring at 1379 cm^{-1} (171 meV) and 1472 cm^{-1} (182.5 meV) for the low temperature species are missing at higher temperatures. No further variations in appearance or major changes in intensity were noted above 475 K.

4. DISCUSSION

Assignments for the various peaks shown in Figs. 1 and 2 are given in Table 1. Although some uncertainty and contradictory identifications are present in the literature, they do not involve any of the spectral features crucial to the interpretations presented here and accordingly will not be discussed in detail. Further clarifications based on

ethanol, actetic acid and acetaldehyde adsorbed on alumina will be reported elsewhere.

Each of the spectra has certain features which are independent of the adsorbed hydrocarbon. These include the peak at 282 cm^{-1} (35 meV) due to phonons in the underlying Al film , and the OH stretching vibration of surface hydroxyl groups near 3630 cm^{-1} (450 meV) (27). Bending vibrations of these surface OH groups are partly responsible for the prominent low-energy shoulder on the large feature at 911 - 935 cm^{-1} (113 - 116 meV). The peak near 935 cm^{-1} (116 meV) has been identified as the Al-O stretching vibration of aluminum oxide, although an AlOH bending vibration of bulk aluminum hydroxide can also appear at this energy (7). More will be said below concerning the nature of this peak, and of its harmonic at approximately 1860 cm^{-1} (231 meV).

Other features which remain relatively unchanged during the course of the experiments, and thus figure only peripherally in the interpretations of the data, include apparent structures on both the low- and high-energy sides of the 282 cm^{-1} (35 meV) peak which possibly result from adsorbate-surface bending and stretching vibrations; the peak near 430 cm^{-1} (53 - 54 meV) which has previously been ascribed to C-C or C-O torsional modes (29), or possibly to an OCO or CCO mode (8,14); a C-C stretching peak at 911 cm^{-1} (113 meV) (30,31); C-C-O skeletal vibrations near 1105 cm^{-1} (137 meV) and 1165 cm^{-1} (145 meV) (32); and a small peak near 2718 cm^{-1} (337 meV) apparently resulting from the harmonic of the 1360 cm^{-1} (169 meV) peak or other possible combination bands. The

asymmetric and symmetric C-H stretching vibrations between 2860 cm^{-1} (354.5 meV) and 2950 cm^{-1} (366 meV) (33) also enter only slightly into further interpretations, except as their intensity increases with temperature.

The low temperature species exhibit a number of bands associated with the symmetric and asymmetric deformations of CH_3 and CH_2 groups. These appear at 1472 cm^{-1} (182.5 meV), 1440 cm^{-1} (178.5 meV), 1380 cm^{-1} (171 meV), 1360 cm^{-1} (168.5 meV), and (probably) 1285 cm^{-1} (159.5 meV) (4,15,24,29,34). Additionally, there is structure near 710 cm^{-1} (88 meV), a region where CH_2 bending vibrations would appear (15). The Al-O stretching vibrations for aluminum alkoxides are expected to add also to the intensity of structure in this area (36). Aluminum ethoxide should have a peak at approximately 1057 cm^{-1} (131 meV) arising from an Al-O-C stretching vibration (32). This peak should almost coincide with a CH bending mode near this same energy (8,14). Examination of the spectra below 345 K shows a feature at this energy. Its broadness and rounded top suggest that it is probably a combination of two overlapping (but not exactly identical) bands as suggested above.

These assignments are consistent with the identification of the low temperature species as being similar to aluminum ethoxide. Comparison with published spectra for aluminum ethoxide (21,24,32) and the infrared spectroscopy studies of ethanol on alumina mentioned earlier support this

identification. Ethoxide formation has been observed also in similar studies of ethanol adsorption on magnesia (36) and silica (37), and for a variety of other alcohols on alumina (38).

As the temperature is raised past 450 K, the surface species undergo a considerable change in structure. All the bands associated with CH_2 and Al-O-C vibrations disappear. In particular, the band at 1057 cm^{-1} (131 meV) sharpens significantly and shifts by approximately 8 cm^{-1} (1 meV) to 1049 cm^{-1} (130 meV). This lends further credence to our identification of overlapping Al-O-C stretching and CH bending modes in the low-temperature case. Definite new peaks and features for the high temperature species appear at 1589 cm^{-1} (197 meV), 879 cm^{-1} (109 meV), 669 cm^{-1} (83 meV), and 621 cm^{-1} (77 meV). Comparison with results from other IETS (4,8,14,39) and infrared (40) studies of CH_3COOH adsorption on alumina, as well as with spectra for acetic acid and the free acetate ion (29,30, 31,34,41,42), and a number of inorganic acetates (31,43-46) permits the assignments for these new peaks as well as a straightforward identification of the new surface species as aluminum acetate. The 1589 cm^{-1} (197 meV) peak arises from an asymmetric OCO stretching mode, while the others have been attributed to the various OCO deformations. Thus, the structural changes associated with the reaction of ethanol and an alumina surface may be represented schematically in the following manner [after Greenler (21)]:

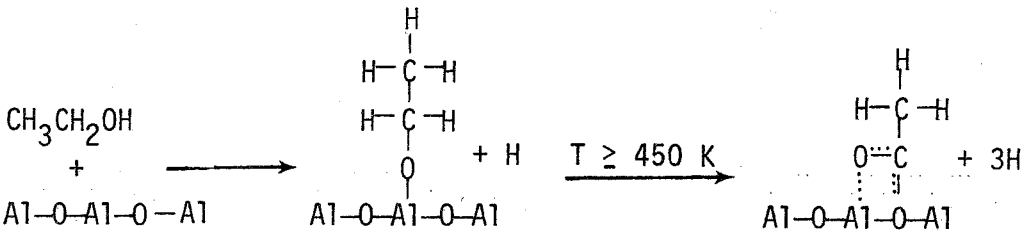

It is a distinct possibility that not all of the adsorbed ethanol molecules are converted from an ethoxide form to that of an acetate. Parrott, et al. (36) found, for example, that with ethanol on magnesia at 637 K only 75% of the surface species have been converted to acetate, with the remainder maintaining the ethoxide structure. Thus, although similar results are not apparent in our data on alumina, care still needs to be exercised in making peak assignments for the high temperature spectra since there may be some minor contributions from ethoxide species still on the surface.

Finally, there are two other related observations that warrant discussion here: the increase in concentration of the adsorbed species with temperature (as noted from the increasing intensity of relevant spectral features); and the changing nature of both the bulk and surface properties of the alumina, reflected by changes in the Al–O stretching peak, particularly its harmonic, and the OH stretching peak of surface hydroxyls. As noted previously, the peak shapes, positions, and intensities remain relatively constant up to approximately 370 K. Above this temperature, the total intensities of the hydrocarbon features showed a gradual but continuous increase, while their relative intensities and shapes remained constant up to approximately 450 K. Above 475 K, at which point the structural conversion to acetate had been completed, no further intensity increases were noted. Correspondingly, temperatures above 370 K produced also significant growth of the harmonic of the Al–O bulk stretching mode at 1863 cm^{-1} (231 meV). The fundamental peak (at 935 cm^{-1}), its overtone, and the OH stretching mode began to shift slightly downward in energy as the temperature was raised, with final changes of 8 cm^{-1} (1 meV), 16 cm^{-1}

(2 meV) and 32 cm^{-1} (4 meV), respectively.

These observations can be explained in the following manner. Below 370 K, ethanol adsorption produces H_2O and/or OH groups which block other adsorption sites. Above this temperature, the H_2O and OH groups are removed, thus increasing the surface concentration of hydrocarbons by opening up additional sites for ethanol adsorption. This is consistent with the work of Parrott, et al. (36), who noted similar effects on magnesia. At the same time, rather than being desorbed, the H_2O or OH groups participate in the activated transformation of aluminum oxide to aluminum hydroxide. This is most apparent in the growth of the 1863 cm^{-1} (231 meV) overtone band. As observed by Bowser and Weinberg (7) in a detailed tunneling spectroscopy study of a number of aluminum oxides and hydroxides, overtones for bulk AlOH bending modes are significantly more intense than those of bulk AlO stretching modes due to the greater anharmonicity of bonds involving hydrogen (47). Comparison with their results indicates clearly the formation of some bulk hydroxide in our spectra, induced above 370 K by ethanol adsorption. The small shifts noted in the bulk bands and surface OH modes are indicative also of the changing nature of the substrate.

5. CONCLUSIONS

A detailed investigation of the adsorption of ethanol on aluminum oxide has been carried out utilizing IETS. The advantages of IETS are its high sensitivity and especially its wide spectral range while maintaining typical optical resolution.

In agreement with previous results (18 - 24), we have observed the

catalytic dehydrogenation first to a surface ethoxide and then to a surface acetate as a function of temperature, the ethoxide-acetate transformation occurring above 450 K. Spectral details have been presented over the entire energy range from 240 cm^{-1} (30 meV) to 3950 cm^{-1} (490 meV). In particular, low-energy vibrations are observed clearly in areas often inaccessible to infrared studies on oxide catalysts. In addition, we have identified a bulk aluminum oxide-to-aluminum hydroxide transformation above 370 K in the presence of adsorbed ethanol, the most prominent indication of this transformation being the perturbation in the 1863 cm^{-1} (231 meV) overtone band. These observations demonstrate explicitly the utility of IETS for monitoring accurately changes in the structure of surface species during the course of catalytic reactions.

References

1. R. C. Jaklevic and J. Lambe, Phys. Rev. Letters 17, 1139 (1966).
2. H. W. White, L. M. Goodwin and T. Wolfram in Inelastic Electron Tunneling Spectroscopy, T. Wolfram, Ed., Springer-Verlag, N.Y. 1978, p. 70.
3. M. G. Simonsen, R. V. Coleman and P. K. Hansma, J. Chem. Phys. 61, 3789 (1974).
4. Y. Scarlatos, R. C. Barker and G. L. Haller, Surface Sci. 43, 353 (1974).
5. J. T. Hall, P. K. Hansma and M. Parikh, Surface Sci. 65, 552 (1977).
6. C. S. Korman and R. V. Coleman, Phys. Rev. B 15, 1877 (1977).
I. W. N. McMorris, N. D. M. Brown and D. G. Walmsley, J. Chem. Phys. 66, 3952 (1977).
7. W. M. Bowser and W. H. Weinberg, Surface Sci. 64, 377 (1977).
8. B. F. Lewis, M. Mosesman and W. H. Weinberg, Surface Sci. 41, 142 (1974).
9. P. K. Hansma, Proc. 14th Internal. Conf. Low Temp. Phys., Otaniemi, Finland, 5, 264 (1975).
10. W. H. Weinberg, W. M. Bowser and B. F. Lewis, Japan J. Appl. Phys. Suppl. 2, Pt. 2, 863 (1974).
11. J. T. Hall and P. K. Hansma, Surface Sci. 71, 1 (1978).
12. P. K. Hansma, W. C. Kaska and R. M. Laine, J. Am. Chem. Soc. 98, 6064 (1976).
13. H. E. Evans, W. M. Bowser and W. H. Weinberg, in preparation.
14. O. I. Shklyarevskii, A. A. Lyskh and I. K. Yanson, Sov. J. Low Temp. Phys. 2, 328 (1976).

15. R. M. Kroeker, W. C. Kaska and P. K. Hansma, to be published.

16. D. E. McBride and J. T. Hall, to be published.

17. H. Knözinger and R. Köhne, J. Catal. 5, 264 (1966).
J. M. Parera and N. S. Figoli, J. Catal. 14, 303 (1969).
H. Knözinger and B. Stübner, J. Phys. Chem. 82, 1526 (1978).

18. A. A. Babushkin and A. V. Uvarov, Dokl. Akad. Nauk. SSSR 110, 581 (1956).

19. K. Naito, Bull. Osaka Industr. Res. Inst. (Japan) 10, 160 (1959).

20. A. V. Uvarov, Zh. Fiz. Khim. (USSR) 37, 1186 (1963).

21. R. G. Greenler, J. Chem. Phys. 37, 2094 (1962).

22. D. Treibmann and A. Simon, Ber. Bunsenges. Phys. Chem. 70, 526 (1966).

23. R. O. Kagel, J. Phys. Chem 71, 844 (1967).

24. H. Arai, Y. Saito and Y. Yoneda, Bull. Chem. Soc. Jap. 40, 731 (1967).

25. W. H. Weinberg, Ann. Rev. Phys. Chem. 29, 115 (1978).
J. Klein, A. Léger, M. Berlin, D. Défourneau and M. J. L. Sangster, Phys. Rev. B 7, 2336 (1973).

26. W. M. Bowser and W. H. Weinberg, Rev. Sci. Instrum. 47, 583 (1976).

27. J. Lambe and R. C. Jaklevic, Phys. Rev. 165, 821 (1968).

28. J. Kirtley and P. K. Hansma, Phys. Rev. B 13, 2910 (1976).

29. J. K. Wilmhurst, J. Chem. Phys. 25, 1171 (1956).

30. K. Ito and H. J. Bernstein, Can. J. Chem. 34, 170 (1956),

31. K. Nakamoto, Infrared and Raman Spectra of Inorganic and Coordination Compounds, Wiley, N.Y., 1978.

32. R. C. Wilhoit, J. R. Burton, Fu-tien Kuo, Sui-rong Huang and A. Viquesnel, J. Inorg. Nucl. Chem. 24, 851 (1962).

33. A. Metcalfe and S. U. Shankar, J. C. S. Faraday I 74, 1945 (1978).

34. K. Fukushima and B. J. Zwolinski, J. Chem. Phys. 50, 737 (1969).

35. D. C. Bradley and A. H. Westlake, Proc. Conf. Symp. Coord. Chem., Tihany, Hungary, 1964.

36. S. L. Parrott, J. W. Rogers, Jr. and J. M. White, Appl. Surface Sci. 1, 443 (1978).

37. H. Jeziorowoski, H. Knözinger, W. Meye and H. D. Muller, J. C. S. Faraday I 10, 1744 (1973).

B. A. Morrow, L. W. Thompson and R. W. Witmore, J. Catal 28, 332 (1973).

E. Borello, A. Zecchina and C. Morterra, J. Phys. Chem. 71, 2938 (1967).

38. E. I. Heiba and P. S. Landis, J. Catal. 3, 471 (1964).

39. J. T. Hall and P. K. Hansma, Surface Sci. 77, 61 (1978).

40. A. V. Kiselev and A. V. Uvarov, Surface Sci. 6, 399 (1967).

41. K. Nakamoto and S. Kishida, J. Chem. Phys. 41, 1554 (1964).

42. R. C. Herman and R. Hofstadter, J. Chem. Phys. 7, 460 (1939).

43. V. N. Maksimov and A. I. Grigor'ev, Russ. J. Inorg. Chem. 9, 559 (1964).

A. I. Grigor'ev and V. N. Maksimov, Russ. J. Inorg. Chem. 9, 580 (1964).

44. K. J. Wilmhurst, J. Chem. Phys. 23, 2463 (1955).

45. B. Orel and D. Hadzi, Spectrochimica Acta 32A, 1731 (1976).

46. G. B. Deacon and J. H. S. Green, Spectrochimica Acta 24A, 885 (1968).

47. G. Herzberg, Molecular Spectra and Molecular Structure. II. Infrared and Raman Spectra of Polyatomic Molecules (Van Nostrand, N.Y., 1945).

Table 1. Peak Positions (in cm^{-1}) and Assignments for CH_3CH_2OH on Alumina.

295 K	365 K	373 K	473 K	575 K	Assignment
282	282	282	278	278	Al phonon
426	426	426	430	430	C-C or C-O torsion
			621	621	OCO deformations[a]
			669	669	
710	710	710			CH_2 bend or Al-O ethoxide stretch[e]
806	806	806	806	806	C-C stretch?
			879	879	OCO mode[a]
911	911	911	911	911	C-C stretch
935	935	935	927	927	Bulk Al-O stretch
1057	1057	1057	1049	1049	Al-O-C stretch[e] and CH bend
1105	1105	1105	~1090	~1105	C-C-O skeletal
1161	1161	1161	1165	1161	
1285	1285	1285	1285	1293	CH_3 and CH_2[e] deformations for
1356	1356	1356	1364	1360	low temperature species
1380	1380	1380			CH_3 deformations and OCO symmetric
1440	1440	1440	1444	1440	stretch for high temperature species
1472	1472	1472			
			1589	1589	OCO asymmetric stretch[a]
1863	1863	1863	1847	1847	935 cm^{-1} overtone
2718	2718	2718	2710	2710	Overtone or combinations
2859	2859	2859	2863	2863	
2915	2915	2915	2915	2911	C-H stretch
2952	2952	2952	2952	2952	
3633	3633	3633	3621	3605	OH stretch

a = features characteristic of acetate structure.

e = features characteristic of ethoxide structure.

Figure Captions

Fig. 1. IET spectra of CH_3CH_2OH on alumina, 240 - 2250 cm^{-1}.
(a) 293 K; (b) 366 K; (c) 373 K; (d) 473 K; (e) 573 K.

Fig. 2. IET spectra of CH_3CH_2OH on alumina, 2000 - 3950 cm^{-1}.
(a) 293 K; (b) 366 K; (c) 373 K; (d) 473 K; (e) 573 K.

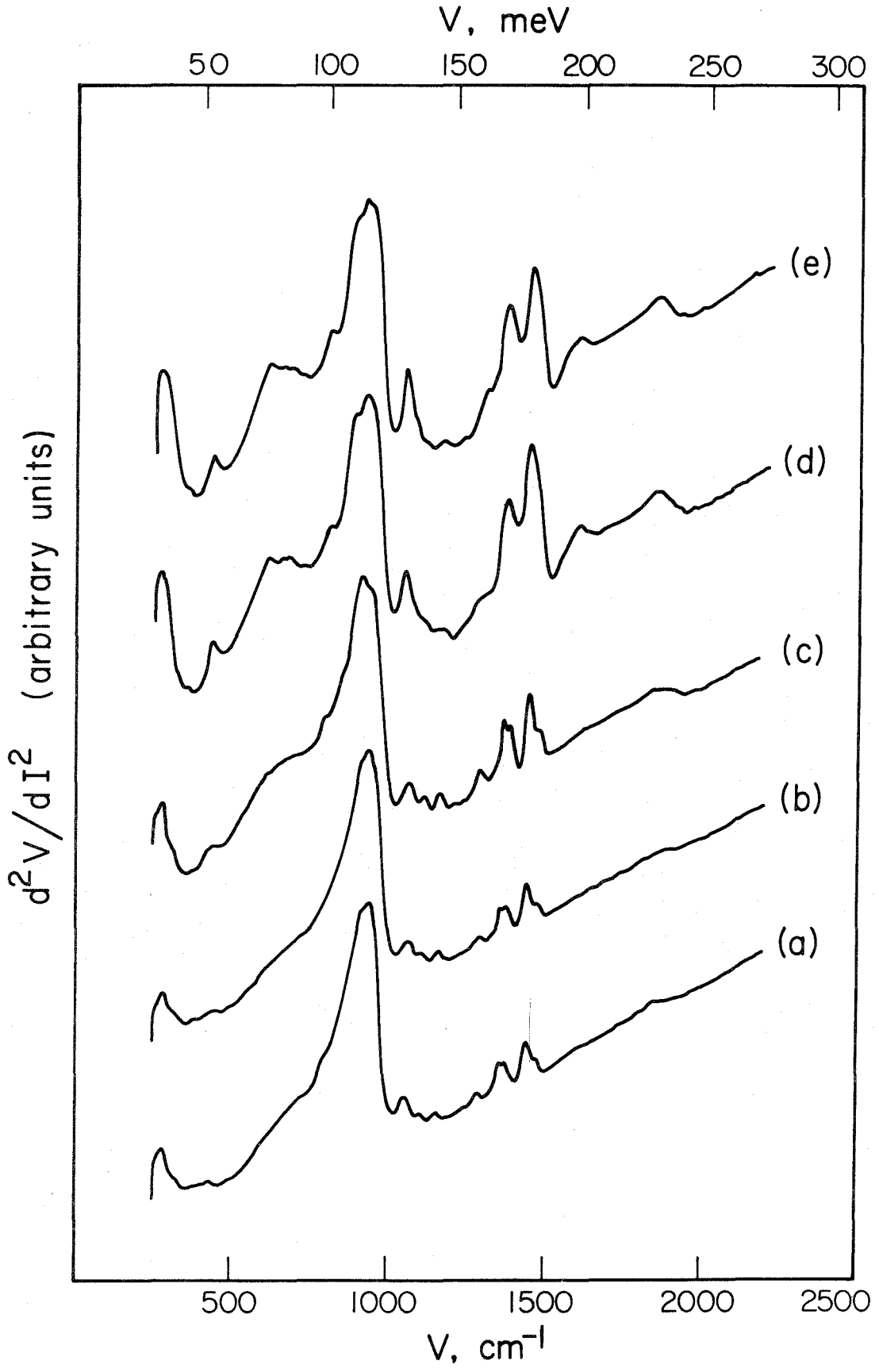
V, meV
50
100
150
200
250
300
(e)
(d)
(c)
(b)
(a)
d^2V/dI^2 (arbitrary units)
500
1000
1500
2000
2500
V, cm^{-1}

Fig. 1

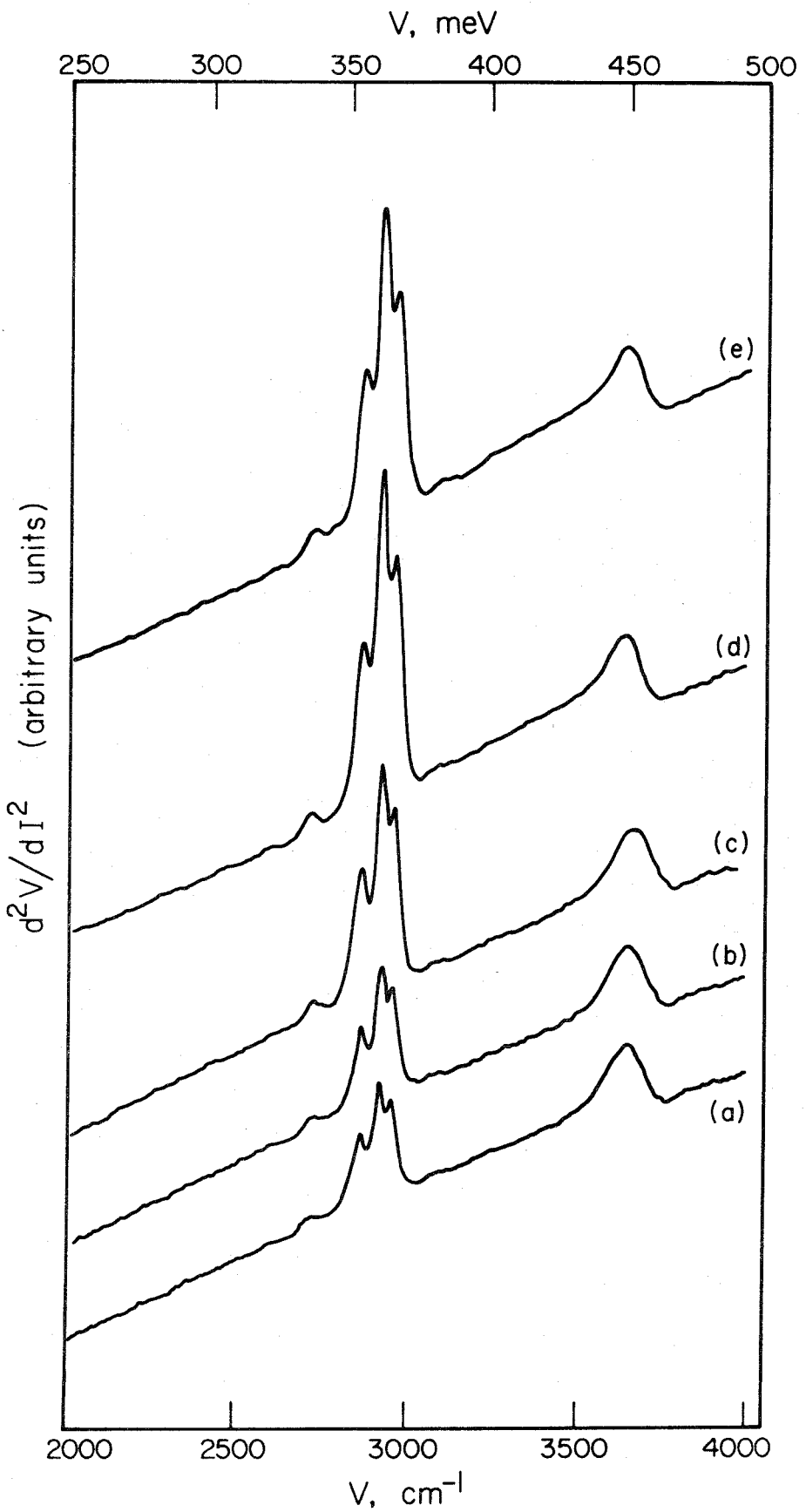
V, meV
250
300
350
400
450
500
(e)
(d)
(c)
(b)
(a)
d^2V/dI^2 (arbitrary units)
2000
2500
3000
3500
4000
V, cm^{-1}

Fig. 2

Chapter IV

A Comparison of the Vibrational Structures of Ethanol, Acetic Acid and Acetaldehyde Adsorbed on Alumina

Abstract

The adsorption on aluminum oxide of acetaldehyde (CH_3CHO) and acetic acid (CH_3COOH) has been studied by utilizing inelastic electron tunneling spectroscopy (IETS) to probe the vibrational structures of the surface species over the spectral range between 240 and 4000 cm^{-1}. Results for temperatures between 295 and 475 K are compared with our previous IETS results for ethanol (CH_3CH_2OH) adsorption on alumina up to 575 K. Although all three hydrocarbons form acetate complexes with the surface under certain conditions, slight differences in bonding and structure are evident in the IET spectra. The formation of some bulk aluminum hydroxide is observed also in certain cases. Observed variations in surface concentrations, bulk hydration and the nature of surface hydroxyl groups are related to previous experimental results. Mechanisms are substantiated for the initial adsorption and subsequent reaction of each hydrocarbon with the surface.

1. Introduction

Previously, we have reported results monitoring structural changes which occur as ethanol is adsorbed on aluminum oxide at temperatures between 300 and 575 K (1). Structural information was obtained utilizing inelastic electron tunneling spectroscopy (IETS) to probe the vibrational spectrum of the surface-adsorbate complex. In agreement with infrared spectroscopic studies of the adsorption of ethanol on alumina (2,3), we observed the transformation of ethoxide-like surface species formed during adsorption below approximately 475 K to acetate-like structures at higher temperatures. Other work, including the observation by Shklyarevskii et al. (4) of a transformation from a physically adsorbed state to a chemisorbed state for acetic acid adsorbed between 77 and 300 K on alumina, a study by McBride and Hall (5) of the catalytically induced hydrogenation of muconic acid chemisorbed on alumina between 293 and 673 K, and the reported formation of hydrocarbon from reactions between CO on alumina-supported Rh particles and surface OH groups by Kroeker, et al. (6), together with our own results for ethanol on alumina, offer strong evidence as to the value of IETS for monitoring the dynamic structural changes which occur in catalytic systems. Since the development and application of IETS to catalytic studies have occurred relatively recently, however, its capabilities as an experimental probe have not as yet been explored and utilized fully.

This study was undertaken in order to demonstrate fully the utility of IETS as a valuable tool for the catalytic scientist. Specifically, we have characterized and compared the surface structures formed by three

chemically similar hydrocarbon molecules as they have reacted with an alumina surface as a function of temperature, and we have demonstrated that IETS is indeed capable of distinguishing small structural differences between surface species. This capability of IETS for observing even subtle differences and changes in surface structures might be utilized effectively to provide significant insight into the fundamental nature of catalytic processes, e.g., in determining the composition and form of reaction intermediates, and the direction of reaction pathways.

Alumina has been extensively utilized as a catalyst both for the dehydration of alcohols and the conversion of alcohols to aldehydes, as well as for condensation reactions of aldehydes. This study compares the structures of surface species formed by adsorption of acetaldehyde on alumina between 300 and 500 K with our previous results for ethanol adsorption. Since ethanol formed an acetate-type complex above approximately 475 K, we have investigated also the adsorption of acetic acid as a function of temperature up to approximately 475 K. Thus, the selection of ethanol, acetaldehyde and acetic acid was based both upon the economic importance of industrial reactions involving these molecules, as well as the interrelationships of their structures during alumina-catalyzed reactions. The results presented here thereby accomplish the dual purpose of demonstrating the utility and versatility of IETS while at the same time providing further information on industrially important reaction systems.

2. Experimental Procedures

Tunneling samples were prepared in an oil diffusion pumped vacuum

system with a base pressure of 10^{-7} torr. Aluminum (Balzers 99.99%) was evaporated through a mask onto a clean glass slide to form a strip approximately 1000 Å in thickness and 2 mm in width. The top few atomic layers of this strip were then oxidized in a plasma discharge of pure oxygen (Matheson Research Grade, 99.99%) to form a thin aluminum oxide layer 20 to 30 Å in thickness. This oxide is the catalytic surface utilized in these tunneling spectroscopy experiments. Aluminum oxide surfaces prepared in this manner were exposed to hydrocarbon vapors of ethanol (U.S. Industrial Chemicals Co. reagent quality pure ethyl alcohol), acetic acid (Baker Chemical Co. reagent grade glacial acetic acid) and acetaldehyde (Eastman Kodak Co.) for various times at predetermined pressures and substrate temperatures.

Bowser and Weinberg (7) have developed a useful technique for heating tunneling samples. Their method involves a four point probe geometry to heat the aluminum strip resistively while simultaneously monitoring changes in the resistance of the strip. Changes in resistance can then be related directly to changes in temperature. Their method was utilized in this study to heat the aluminum strip and oxide layer during exposure to hydrocarbon vapors. Temperature measurements which utilize this technique are accurate to within ± 8%. Temperature stability during exposure was ± 2 to 3 K.

Following exposure to the hydrocarbons, the tunneling samples were completed by the evaporation of Pb (Balzers 99.9999%) cross strips approximately 3000 Å in thickness and 1 mm in width. The Pb and Al strips are used as electrodes for the tunneling measurements. These top Pb electrodes interact minimally with the oxide-adsorbate system and introduce few, if

any, noticeable perturbations (8). Further discussion on this point is presented below.

Completed samples were removed from the vacuum system and mounted on a probe which can be inserted directly into a liquid He dewar for measurement. Tunneling measurements were performed at 4.2 K in order to maximize resolution (by minimizing thermal broadening). Part of the significance of our previous study of ethanol adsorption was the demonstration that the extreme cooling of the samples for measurement produced no significant alterations in the surface-adsorbate structure following exposure. Samples the room temperature resistance of which fell outside the range 30 to 200 Ω were not measured, since previous experience has shown that these generally have poor signal-to-noise characteristics.

Spectral measurements are accomplished by applying a voltage between the Al and Pb electrodes. Small currents result from the tunneling of electrons through the thin oxide (insulating) layer. Slight increases (approximately 1%) in this tunneling current occur at voltages which are equal to the vibrational frequencies of molecules in the barrier region. This results from new channels for tunneling being opened for electrons which lose energy while crossing the barrier by exciting these vibrational modes. These slight increases in slope of the I-V functional become peaks in the second derivative d^2V/dI^2 (proportional to d^2I/dV^2) when represented as a function of the applied voltage, V. In our laboratory, PDP 11/10 computer-controlled electronics are utilized to monitor directly, via a harmonic detection scheme, the second harmonic signal (proportional to d^2V/dI^2) due to a small modulation voltage (1 meV rms) superimposed upon the dc bias voltage, as a function of the bias voltage across the junction.

Results of IETS experiments have been shown to be analogous to those obtained in optical absorption experiments, such as infrared or Raman spectroscopy (9). Spectra were recorded over the range 240 to 4000 cm^{-1} (30 to 500 meV) with a resolution on the order of ± 4 cm^{-1} (±0.5 meV). A more detailed description of our experimental procedures, as well as the basic theoretical aspects of tunneling spectroscopy, have been presented elsewhere (10).

3. Results

Measurements were carried out for each of the hydrocarbon species as a function of both exposure (i.e., the pressure-time product) and temperature. For ethanol exposures, the temperature was varied from 295 to 575 K. For both acetic acid and acetaldehyde, the temperature range studied was 295 to 475 K. A maximum in hydrocarbon peak intensity is observed at high exposures, and this is taken as corresponding to saturation coverage on the alumina surface. An exposure of 100 torr-sec was found to produce the maximum intensity in all the cases studied, independent of the adsorbate or the temperature. All the results presented here represent saturation coverage, since neither the peak positions nor the relative peak intensities exhibited any significant variations as the exposure and coverage were varied.

Figure 1 (240 cm^{-1} to 2250 cm^{-1}) and Fig. 2 (2000 cm^{-1} to 4000 cm^{-1}) show spectra obtained for ethanol adsorbed at 475 K, acetic acid at 295 and 475 K, and acetaldehyde at 295 K. Spectra for ethanol adsorbed at 295, 366, 375 and 575 K have been presented previously (1). Spectra for

acetaldehyde adsorbed at temperatures up to 475 K exhibited no variations in either peak positions or intensities compared to the room temperature spectrum. Peak positions for the spectra shown in Figs. 1 and 2 are given in Table 1. A list of the peak positions for ethanol adsorbed on alumina at room temperature is presented in Table 2.

Since our results for ethanol adsorption have been detailed previously (1), only those features pertinent to a comparison with the other hydrocarbon species will be presented here. Two distinct types of adsorbed ethanol were observed: a low-temperature species which formed below approximately 470 K, and a high-temperature species which formed above this temperature. The low-temperature form was characterized uniquely by peaks (identified as arising from the adsorbate) at 710, 1057, 1380, 1440 and 1472 cm^{-1}. In the high-temperature form, the peak at 1057 cm^{-1} was sharpened considerably and shifted slightly to 1049 cm^{-1}, and the peaks at 1440 and 1472 were replaced by one strong peak at approximately 1444 cm^{-1}. Peaks at 710 and 1380 cm^{-1} disappeared, and new features arose at 621, 669 and 1589 cm^{-1}. The intensity of the adsorbate peaks (i.e., the surface concentration of adsorbed species) exhibited a significant increase between 370 and 475 K, the intensity of ethanol adsorbed at room temperature being comparable to that of adsorbed acetaldehyde as shown in Fig. 1. This change was accompanied by gradual shifts in features identified with the substrate from 935 to 927 cm^{-1}, from 1863 to 1847 cm^{-1} and from 3633 to 3605 cm^{-1}, as well as with a growth in intensity of the 1863 cm^{-1} peak. There are also three distinct, intense peaks at 2863, 2915 and 2952 cm^{-1} which exhibit intensity increases with temperature, although their positions and

relative intensities remain constant.

Adsorbed acetic acid exhibits many features similar to ethanol at 475 K, as can be seen in Table 1. These features include a broad peak at approximately 1593 cm^{-1} and sharper peaks at 1468, 1415, 1335, 1041, 677 and 610 cm^{-1}. A weak, rounded feature at approximately 475 cm^{-1} is also apparent, but the exact position is unclear due to variations of the background between samples in this region. In comparison with adsorbed ethanol, the prominent feature near 900 cm^{-1} is less broad for acetic acid and less structure is apparent. In particular, only one peak at 939 cm^{-1} with an unresolved low-energy shoulder is observed for acetic acid, compared to features at 927, 911, 879 and 806 cm^{-1} which can be resolved for ethanol. At higher energies, there are two strong peaks located at 2919 and 2972 cm^{-1}, with poorly resolved shoulders appearing near 2835 and 3000 cm^{-1}. The intensities of adsorbate peaks for acetic acid at 295 K are comparable to those for adsorbed ethanol at 475 K. No significant changes in either adsorbate peak positions or intensities are noted for the adsorption of acetic acid as the temperature is increased to 475 K. The apparent shift of the 475 cm^{-1} peak to 448 cm^{-1} probably results from the difficulty in locating accurately its position (as mentioned above), rather than from an actual change in molecular structure. Only minimal shifts are observed also for the substrate features at 475 K, from 939 cm^{-1} and 1855 cm^{-1} to 935 cm^{-1} and 1843 cm^{-1}, respectively. There is, however, a definite increase in the intensity of the 1855 cm^{-1} feature at 475 K compared to at room temperature.

Spectra for acetaldehyde adsorbed on the aluminum oxide surface exhibited no apparent variations with temperature over the range studied. The peak

positions varied little from those in spectra of adsorbed acetic acid, with the exception of a rather prominent shoulder on the 1423 cm^{-1} peak at approximately 1395 cm^{-1}. Acetaldehyde, however, adsorbs on alumina less readily than either acetic acid at any of the temperatures studied, or ethanol at temperatures above approximately 370 K. Again, intensities for adsorbed acetaldehyde are most similar to peak intensities observed previously for ethanol adsorbed below 370 K.

4. Discussion

In agreement with infrared spectroscopy studies of ethanol adsorption on aluminum oxide (2,3), we have identified previously the low- and high-temperature species of adsorbed ethanol as corresponding to ethoxide- and acetate-like structures, respectively. This change in surface structure can be represented schematically [after Greenler (3)] as

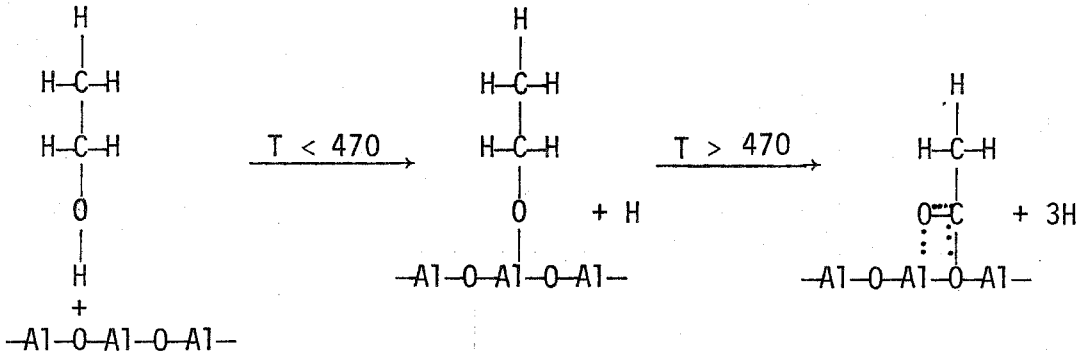

Identification of the low-temperature species as a type of aluminum ethoxide can be accomplished readily by comparing the IET spectra with the infrared results cited above and with vibrational spectra of pure aluminum ethoxide, as is done in Table 2. Over the range in energy which these studies have in common, it can be seen that there is an excellent correlation

between the low-temperature form of adsorbed ethanol and aluminum ethoxide. Evolution of the acetate structure involves, among other changes, the loss of the 710 cm^{-1} peak (identified as a methylene rocking mode and/or an Al-O ethoxide stretching mode) and the appearance of OCO asymmetric and symmetric deformation bands at 669 and 621 cm^{-1}. The most prominent spectral change is a new peak at 1589 cm^{-1} due to the OCO asymmetric stretching vibration. Changes in the 1300 to 1500 cm^{-1} region reflect the loss of CH_2 deformation bands and the addition of the OCO symmetric stretching mode. In addition, the changing shape and position of the 1057 cm^{-1} feature has been interpreted as revealing the loss of the Al-O-C ethoxide stretching mode from a position nearly coincident with a CH_3 mode (1).

Peaks in the C-H stretching region do not enter into these surface structural determinations for adsorbed ethanol since their positions (at 2863, 2915 and 2952 cm^{-1}) and relative intensities appear generally insensitive to changes from ethoxide to acetate. This might have been anticipated, since even in pure ethanol CH_2 stretching vibrations are weak compared to the CH_3 modes. Moreover, the additional constraint of being fixed in a particular configuration on the surface might introduce orientation effects favoring the excitation of CH_3 stretching modes relative to the corresponding CH_2 vibrations.

The increase with temperature in the surface concentration of adsorbed species (as judged from the corresponding increase in hydrocarbon peak intensities) is interpreted as being due to an increase in the number of adsorption sites available. Ethanol adsorption creates initially OH or H_2O groups which can block other active sites. At higher temperatures

(i.e., greater than 370 K) these groups are displaced, thus opening additional adsorption sites for ethanol molecules. Similar observations have led to this conclusion for other systems (12). Not all of the hydrogen being displaced from the surface is desorbed as H_2O, however. Our previous study showed that some of the hydrogen migrates into the alumina, forming some bulk aluminum hydroxide. The most distinctive feature of this hydroxide formation is the growth in intensity of the 1847 cm^{-1} peak. This is the first harmonic of the bulk band at approximately 930 cm^{-1}, which corresponds to either (or both) a bulk AlO stretch or an AlOH bend. In a detailed study, Bowser and Weinberg (13) have shown that it is possible to distinguish between bulk oxide and hydroxide by observing the size of the harmonic band: the greater anharmonicity of bonds involving hydrogen leading to larger harmonics for bulk hydroxides (14). Moreover, our previous results indicated that the positions of these bulk features, as well as that of the stretching mode of surface hydroxyl groups (near 3600 cm^{-1}), are also characteristic of an oxide-hydroxide transformation. Further discussion concerning this hydroxide formation will be presented below.

Since ethanol was found to form a surface acetate when chemisorbed on alumina above 475 K, separate measurements were performed for adsorbed acetic acid. While CH_3COOH adsorption on alumina has been the subject of previous IETS studies (4,9,15 - 17), it has not been investigated heretofore as a function of temperature in the range presented here. Our results are compared with those of the previous IETS studies in Table 3. The overall agreement between these studies is relatively good, both in reported peak positions and in proposed peak identifications. Peak assignments in most cases are based upon comparisons with infrared and Raman studies of acetic

acid and free acetate ions (18 - 23), as well as various inorganic acetates (18,24 - 27). There is a consensus that the peaks near 680, 610 and 475 cm^{-1} are due to OCO deformations and an OCO rocking mode, respectively. In one study, separate peaks were resolved for the C-C (948 cm^{-1}) and bulk Al-O (940 cm^{-1}) stretching modes, whereas other investigators have observed only one band near 940 - 955 cm^{-1}. The identification of peaks near 1040 and 1590 cm^{-1} as being the CH_3 rocking and OCO asymmetric stretching modes, respectively, also enjoysa consensus of opinion. Disagreement, however, arises over assignments for three intermediate peaks, generally positioned near 1340, 1410 and 1470 cm^{-1}, the contradictory assignments being indicated in Table 3. Infrared results for CH_3COO^- (18,20,25), CD_3COO^- (20), CH_3COONa (18,25) and $CH_3COOLi \cdot 2H_2O$ (28) seem to indicate that the three peaks in question should be assigned to the CH_3 symmetric deformation, the OCO symmetric stretch and the CH_3 asymmetric deformation, respectively. Initial IETS spectra of Lambe and Jaklevic (9) for adsorbed CD_3COOD indicate, however, that the 1470 cm^{-1} peak may actually be the OCO symmetric stretching mode. Brown et al. (15) have examined CD_3COOD adsorption in addition to their recent work with CH_3COOH. They reported peak shifts from 1463, 1411 and 1338 cm^{-1} to 1448, 1093 and 1023 cm^{-1} in going from the hydrogenated to the deuterated surface species. Spectra of the deuterated species exhibited also an unresolved shoulder at 1466 cm^{-1}. They identified the 1411 cm^{-1} peak as the OCO symmetric stretch, yet offered no explanation for its being shifted to higher energy (1448 cm^{-1}) upon deuteration. On the other hand, we interpret their observations as evidence that the 1463 cm^{-1} peak in the hydrogenated species is actually the OCO symmetric stretching vibration. The shift to 1448 cm^{-1} upon deuteration is in

excellent agreement with work by Greenler (3) and by Ito and Bernstein (20), which show shifts to lower energies on the order of 10 to 15 cm^{-1} in the asymmetric and symmetric OCO stretching bands due to deuteration. (The shoulder at 1466 cm^{-1} in the deuterated species probably results from residual hydrogenated molecules in the background.) Supporting evidence for this assignment comes from the study of CH_3COOH, physically adsorbed as well as chemisorbed on alumina, by Shklyarevskii et al. (4). They noted a peak near 1470 cm^{-1} for the chemisorbed species only, lending further credence to its assignment as an OCO mode. Finally, this assignment is consistent with investigations in which the OCO stretching modes of aluminum acetate were observed by Alcock et al. (29) at 1590 and 1465 cm^{-1}, and by Maksimov and Brigor'ev (24) at 1595 and 1472 cm^{-1}. Thus, we feel confident in assigning the 1468 cm^{-1} peak in our spectra as the symmetric OCO stretching mode, and the 1415 and 1335 cm^{-1} peaks, respectively, as the asymmetric and symmetric CH_3 deformation modes.

Assignments for the asymmetric and symmetric OCO stretching vibrations are of considerable importance in attempting to understand the nature of the surface species, particularly in identifying the metal environment. Following the classifications used by Alcock et al. (29), acetates and acetato-complexes can be divided into various groups according to the type of metal $-O_2CCH_3$ interaction. These include uncoordinated (ionic) species; unidentate species, one of the oxygen atoms being bound to one metal atom

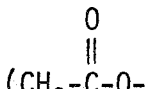

(CH_3-C-O-M); bidentate chelating species, where both oxygen atoms are bound to the same metal atom

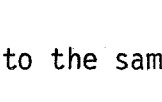

(CH_3-C M); and bidentate bridging species,

the oxygen atoms being bound to separate metal atoms ($CH_3-C\begin{smallmatrix}O-M\\O-M\end{smallmatrix}$). Moreover, the bidentate structures can be either symmetrical or unsymmetrical, i.e., both oxygen-metal bonds can be equivalent, or one might possess more double-bond character than the other. Studies of a number of complexes [see, for example, Ref. (29) and references therein] have shown that the positions of the asymmetric and symmetric OCO stretching bands, in addition to the difference between their peak positions, $\Delta\nu$, are indicative of the bonding structure. Comparing previous IETS results with numerous complexes of known structure, Hall and Hansma (30) have concluded that acetic acid is bound in a bidentate, symmetrical structure when adsorbed on alumina. They also tentatively suggest that it is probably of the bridging, rather than of the chelating type. We concur with this evaluation, particularly in view of the close correlation between our results and results for aluminum acetate (24,29) (discussed briefly above), which is believed to have the bidentate, symmetrical bridging structure.

Temperature seems to have little effect upon either the structure or the concentration of adsorbed CH_3COOH. The most noticeable difference between spectra for adsorption at room temperature and 475 K is the growth of the harmonic feature, and a shift in its position from 1855 to 1843 cm^{-1}. Similar to our observations for adsorbed ethanol (1), we again conclude that higher temperatures enable some of the surface hydrogen to migrate into the bulk, thereby effecting the transformation of some of the bulk oxide into bulk hydroxide. With ethanol adsorption, the possibility existed that the growth of the harmonic feature was actually related to

increases in hydrocarbon concentration on the surface. Since the C-C stretch is very nearly coincident with the bulk mode near 930 cm^{-1}, we might have been observing the C-C harmonic rather than that of the bulk AlO or AlOH modes. This possibility is excluded by the results for CH_3COOH adsorption; there is no increase in hydrocarbon peak intensities attendant to increases in the harmonic feature. Judging from the spectra (Fig. 1), it appears qualitatively that the bulk is hydrated to a lesser extent during acetic acid adsorption than during ethanol adsorption. Observed peak shifts for the bulk band and its harmonic confirm this conclusion, being smaller for the acetic acid samples than for the ethanol ones.

Unlike ethanol or acetic acid, adsorption of acetaldehyde on the alumina surface does not lead to any apparent bulk hydroxide formation in the temperature range examined. Also, there are no apparent variations in peak positions or intensities up to 475 K, the highest temperature studied. Thus, although the spectra for adsorbed acetaldehyde shown in Figs. 1 and 2 correspond to adsorption at 295 K, they are also equivalent to spectra for any of the other temperatures studied. Examination of peak positions over the entire spectral range reveals the absence of the C=O stretching mode (1715 to 1740 cm^{-1}) and the C-H wagging mode (1111 to 1121 cm^{-1}), as well as a close correlation between adsorbed acetaldehyde and adsorbed acetic acid. This suggests that acetaldehyde forms a surface acetate when adsorbed on alumina the structure of which is essentially equivalent to that of acetate formed by acetic acid. This conclusion agrees with recent IETS work by Brown, et al. (15), who also observed no apparent structural differences between

acetaldehyde and acetic acid adsorbed on alumina at room temperature. Our results differ from theirs, however, in the amount of acetaldehyde which can be chemisorbed on the surface. They reported equivalent peak intensities, or surface concentrations, for both acetaldehyde and acetic acid at room temperature. Although no quantitative results for surface concentrations can be drawn from our data, it is qualitatively obvious that we observe only a small amount of acetaldehyde adsorption relative to acetic acid even up to 475 K. This is much more in keeping with recent studies of acetaldehyde adsorption on commercial alumina catalysts, where it has been observed that temperatures in excess of 475 K are required to produce any surface acetate from the adsorption of acetaldehyde (31,32). The fact that we observe even small amounts of acetate formation below this temperature might result from either a greater sensitivity of IETS than available in the experiments involving commercial alumina, or slight differences in the number of available sites between our plasma-grown oxides and the commercial alumina. Since Brown et al. (15) also employed plasma-grown oxides in their IETS study of acetaldehyde adsorption, the reason for the discrepancy in the observed surface concentrations is not obvious. Perhaps their larger intensities are due to adsorption of CH_3COOH present in the background as a contaminant, or else slight differences in background pressures and oxidation procedures have led to significant differences in oxide surface structures.

As stated above, an evaluation of the peak positions for acetaldehyde and acetic acid, particularly for the asymmetric and symmetric OCO stretching peaks, indicates that both form surface acetates with symmetric bidentate structures, probably bridging between two aluminum atoms. The

acetate formed by ethanol, however, has a slightly different structure. Separation between the two OCO stretching modes, $\Delta\nu$, is greater for ethanol than the differences exhibited by the other species. This is indicative of a lesser degree of equivalence between the two C-O bonds in adsorbed ethanol than is the case in adsorbed acetic acid or acetaldehyde. Since C-C bonds of inorganic acetates are known to be sensitive to even small variations in the OCO bond structure (29), structural differences between the surface acetate formed by ethanol and acetates formed by either acetic acid or acetaldehyde are probably responsible for the slight spectral variations noted in the 800 to 950 cm^{-1} region, where C-C stretching modes and, possibly, some OCO and CCO modes appear. Positions of the CH_3 deformation modes reveal further differences between adsorbed ethanol and the other two species, both the asymmetric and symmetric deformation bands for ethanol being shifted approximately 50 cm^{-1} lower in energy than corresponding bands for acetaldehyde and acetic acid. Other differences are manifested in the appearance of peaks in the CH stretching region. Spectra for adsorbed ethanol show three distinct peaks, whereas spectra for both acetic acid and acetaldehyde show only two distinct peaks with a low energy shoulder on the lower peak and a high energy shoulder on the higher energy peak. How these observations correlate with differences between the OCO bonds is as yet not well understood. It should be pointed out that some of these variations might be due to the hydrated nature of the alumina on which the acetate-like structure formed from ethanol is observed. This seems unlikely, however, since varying stages of bulk hydration appear to have little effect on surface structure in the case of acetic acid.

The observed variations in surface concentrations (i.e., peak intensities) of adsorbed species can be related to differences in adsorption

sites and mechanisms. Ethanol is present on the surface only at low concentrations below approximately 370 K. Above this temperature the concentration increases until a much higher, apparent maximum concentration is reached at about 476 K. Acetic acid adsorbs with a similar high concentration at all temperatures between 295 and 475 K. Acetaldehyde only adsorbs with low concentrations on the surface in this same temperature range.

Again, these variations in concentration for ethanol are related to the production, during adsorption, of OH (or possibly H_2O) groups which remain on the surface blocking other active sites (12). They are displaced only above 370 K. Acetic acid adsorption proceeds by the acid hydrogen from the hydrocarbon combining with a surface hydroxyl group to produce H_2O, which is then desorbed and replaced on the surface by the acetate ion. This mechanism is supported by studies which have observed H_2O in the gas phase as a product of acetic acid adsorption, and an accompanying decrease in the concentration of surface OH groups (15, 33 - 35). The production of surface hydroxyls is ruled out also by studies of CH_3COOD adsorption, which reveal no OD or CD bonds remaining on the surface (15,30). Acetic acid either produces H_2O which is desorbed immediately, or else it is capable of displacing H_2O from active sites even at room temperature.

There are fewer active sites on the surface for acetaldehyde adsorption than for acetic acid or high temperature ethanol adsorption. Acetaldehyde adsorption on alumina has been observed to produce only H_2 (31,32), as opposed to OH or H_2O produced by the other species. It has been postulated that acetaldehyde, similar to acetyl chloride, requires

a site consisting of a surface cation adjacent to a particular type of surface OH group (15). As noted above, these types of sites occur only at temperatures higher than 475 K on commercial aluminas and in small concentrations at lower temperatures on our plasma grown alumina films. That acetaldehyde adsorption was not observed to produce any bulk hydroxide in this study is related undoubtedly to the fact that, unlike ethanol or acetic acid, it produces H-H rather than any O-H type bonds on the surface during adsorption.

Additional evidence supporting many of these views comes from comparing the positions of the surface OH stretching peaks among the various samples. No quantitative evaluation of OH peak intensities is possible as the spectral ordinate has not been calibrated absolutely and might vary considerably from sample to sample. In particular, even though the OH intensity in Fig. 2 appears much greater for acetaldehyde than for any of the other samples, this might only be due to differences in calibration rather than to differences in absolute concentration. The peak positions, however, reveal significant information. The acetic acid and ethanol samples for 475 K both show similar surface acetate (and perhaps OH) concentrations, and both show also the presence of some bulk hydroxide. Since the surface concentration and bulk composition can each be expected to affect the nature of surface OH groups, we expect similar OH groups to be found for both the ethanol and acetic acid samples at 475 K. This is in excellent agreement with what is observed, since the surface OH stretching frequency in both of these cases appears at 3621 cm^{-1}.

In contrast to ethanol and acetic acid adsorption at 475 K, the bulk alumina remains unhydrated for ethanol and acetic acid adsorption at

room temperature, and for acetaldehyde adsorption at all temperatures. Since the bulk structure is identical in each of the last three cases, a comparison of the nature of their surface hydroxyl groups (as indicated by the observed frequencies of the surface OH stretching vibrations) might be expected to reveal variations in hydroxyl-adsorbed hydrocarbon interactions and, particularly, adsorption mechanisms. Ethanol near room temperature can be expected to produce additional hydroxyl groups, (perhaps) loosely held on the surface. The observed OH peak position is at 3633 cm^{-1}. Acetic acid, however, can be expected to remove the most loosely held surface OH groups. The remaining, more strongly bound OH groups would have a weaker OH bond, which agrees with the observed peak position of 3613 cm^{-1}. Acetaldehyde adsorption, on the other hand, should have a tendency to remove the most weakly bound hydrogens, i.e., from the OH groups bound most strongly to the surface, in contrast to what is expected of acetic acid. Again, this agrees well with the observed hydroxyl peak position at 3637 cm^{-1}.

One final point of discussion relates to the IETS technique rather than the surface chemistry of the hydrocarbon-alumina systems studied here. Kirtley and Hansma (8) have examined the effect of the top metal electrode utilized in IET measurements by comparing observed IETS peak positions for benzoic acid adsorbed on alumina with corresponding optical results for a similar system. IET spectra were obtained for Ag, Sn and Pb top electrodes. Their results indicate that C-C stretching, bending and deformation modes are all unperturbed (within the resolution of the experiment) by the presence of a top Pb electrode. It was reported also that IET samples with Ag top electrodes showed slightly larger discrepancies

from the optical data than did those with Pb electrodes. Shifts from the optical data of up to 4 cm^{-1} (0.5 meV) were reported for CH deformation modes in IET measurements utilizing Pb electrodes. (Unfortunately, no results were presented for C-H stretching modes.) The most significant perturbation due to top Pb electrodes was reported as occurring with surface OH groups, the stretching frequency appearing at 3596 cm^{-1} (446 meV) compared to the optically observed value of 3669 cm^{-1} (455 meV). Although the possibility exists that this variation results solely from interactions with the top electrode, the fact that the surface hydroxyl stretching frequency can vary significantly depending upon the nature of the bulk alumina involved indicates that at least a part of the observed frequency difference might be attributed to differences in the nature of the aluminas used in the IETS and optical studies. It should be noted also that the optical result listed for the OH stretching frequency was obtained in a different study than were optical results for the C-C and C-H modes, which showed relatively insignificant variations from IETS data. In our current study, Table 2 allows a comparison of the C-H stretching modes of adsorbed ethanol between IET spectra which utilized Pb electrodes and infrared results. Peaks at 2859, 2915 and 2952 cm^{-1} in the IET spectra are shifted slightly from the optically observed positions of 2865, 2930 and 2963 cm^{-1}. Slight shifts are also observed between our results for acetaldehyde adsorbed on alumina (with C-H stretching features at 2874, 2919, 2975 and 3008 cm^{-1}) and optical results for acetaldehyde adsorbed on porous glass [where C-H stretching vibrations appear at 2878, 2939, 2981 and 3008 cm^{-1} (36)]. These observed variations are not necessarily significant when compared to experimental resolution and/or the differing nature of the surfaces involved in the IETS and

optical studies. Thus, we feel that there is no definite evidence that Pb electrodes interact with the surface or adsorbed species to produce a noticeable shift of the vibrational frequencies to lower energies. Therefore, frequencies observed in IETS studies are actually characteristic of the nature of the adsorbate-substrate system, no significant perturbations being introduced by the measurement technique.

5. Conclusions

We have compared the vibrational spectra of ethanol, acetaldehyde and acetic acid adsorbed on aluminum oxide as a function of temperature between 295 and 475 K for acetic acid and acetaldehyde, and between 295 and 575 K for ethanol. Ethanol above approximately 475 K forms a surface acetate, its spectra revealing slight structural differences from acetates formed on alumina by either acetic acid or acetaldehyde at any of the temperatures studies. By accurately assigning the spectral features which correspond to asymmetric and symmetric OCO stretching vibrations in the surface acetates, structural determinations have been made by comparison with the observed frequencies of equivalent vibrational modes in a number of inorganic acetates and acetato-complexes of known structure. In agreement with other, preliminary work, we conclude that acetic acid chemisorbs as a bidentate symmetrical bridging acetate. Acetaldehyde forms an almost equivalent structure on the surface. The acetate formed from ethanol also forms a bidentate bridging species, but with a more unsymmetrical OCO bonding geometry than acetaldehyde or acetic acid, as judged by a greater difference between the two OCO stretching peaks.

Other similarities between adsorbed acetaldehyde and acetic acid, and differences from ethanol, are seen in the positions and appearance of the CH_3 bending and stretching modes. Lower frequencies are observed in the case of adsorbed ethanol, and three distinct peaks in its stretching region are observed, as compared with two for either acetic acid or acetaldehyde.

At the higher temperatures studied, we have observed the formation of some bulk aluminum hydroxide during ethanol and acetic acid adsorption. No bulk oxide-hydroxide transformation was observed for exposures to acetaldehyde. Coupled with the observed surface concentration variations with temperature among the three hydrocarbon systems, as well as with the peak positions of surface hydroxyl groups, these observations have been related to differences in adsorption mechanisms among the different hydrocarbon species. Specifically, good agreement has been shown with previous experimental results and proposed mechanisms which indicate that ethanol and acetic acid form surface O-H bonds during adsorption, while acetaldehyde forms H-H bonds.

Finally, good agreement in absolute peak positions with infrared studies of adsorbed species and analysis of a previous study of top electrode effects (8) indicate that few, if any, perturbations are introduced into the adsorbent-adsorbate systems by the presence of top Pb electrodes utilized in the tunneling measurements. Thus, in addition to providing detailed additional information on industrially important catalytic systems, we have demonstrated the worth of IETS for characterizing and differentiating among very similar surface structures without significant perturbations being introduced by the measurement technique itself.

References

1. H. E. Evans and W. H. Weinberg, submitted for publication.
2. H. Arai, Y. Saito and Y. Yoneda, Bull. Chem. Soc. Japan 40, 731 (1967); J. Catal. 10, 128 (1968).
3. R. G. Greenler, J. Chem. Phys. 37, 2094 (1962).
4. O. I. Shklyarevskii, A. A. Lyskh and I. K. Yanson, Sov. J. Low Temp. Phys. 2, 328 (1976).
5. D. E. McBride and J. T. Hall, to be published.
6. R. M. Kroeker, W. C. Kaska and P. K. Hansma, to be published.
7. W. M. Bowser and W. H. Weinberg, Rev. Sci. Instrum. 47, 583 (1976).
8. J. R. Kirtley and P. K. Hansma, Phys. Rev. B 13, 2910 (1976).
9. J. Lambe and R. C. Jaklevic, Phys. Rev. 165, 821 (1968).
10. W. H. Weinberg, Ann. Rev. Phys. Chem. 29, 115 (1978).
11. R. C. Wilhoit, J. R. Burton, Fu-tien Kuo, Sui-rong Huang and A. Viquesnel, J. Inorg. Nucl. Chem. 24, 851 (1962).
12. S. L. Parrott, J. W. Rogers, Jr. and J. M. White, Appl. Surface Sci. 1, 443 (1978).
13. W. M. Bowser and W. H. Weinberg, Surface Sci. 64, 377 (1977).
14. G. Herzberg, Molecular Spectra and Molecular Structure. II. Infrared and Raman Spectra of Polyatomic Molecules (Van Nostrand, N.Y., 1945).
15. N. M. D. Brown, R. B. Floyd and D. G. Walmsley, J. Chem. Soc. Faraday Trans. II 75, 17 (1979).
16. Y. Skarlatos, R. C. Barker and G. L. Haller, Surface Sci. 43, 353 (1974).
17. B. F. Lewis, M. Mosesman and W. H. Weinberg, Surface Sci. 41, 142 (1974).

18. K. Nakamoto, Infrared and Raman Spectra of Inorganic and Coordination Compounds (Wiley, N.Y., 1978).

19. J. K. Wilmhurst, J. Chem. Phys. 25, 1171 (1956).

20. K. Ito and H. J. Bernstein, Can. J. Chem. 34, 170 (1956).

21. K. Fukushima and B. J. Zwolinski, J. Chem. Phys. 50, 737 (1969).

22. K. Nakamoto and S. Kishida, J. Chem. Phys. 41, 1554 (1964).

23. R. C. Herman and R. Hofstadter, J. Chem. Phys. 7, 460 (1939).

24. V. N. Maksimov and A. I. Grigor'ev, Russ. J. Inorg. Chem. 9, 559 (1964).

A. I. Grigor'ev and V. N. Maksimov, Russ. J. Inorg. Chem. 9, 580 (1964).

25. J. K. Wilmhurst, J. Chem. Phys. 23, 2463 (1955).

26. B. Orel and D. Hadzi, Spectrochimica Acta 32A, 1731 (1976).

27. G. B. Deacon and J. H. S. Green, Spectrochimica Acta 24A, 885 (1968).

28. M. Cadene and A. M. Vergnoux, Spectrochimica Acta 28A, 1663 (1972).

29. N. W. Alcock, V. M. Tracy and T. C. Waddington, J. C. S. Dalton, 2243 (1976).

30. J. T. Hall and P. K. Hansma, Surface Sci. 77, 61 (1978).

31. P. Fink, Rev. Roumaine Chim. 14, 811 (1968).

32. D. V. Sokolskii, V. F. Vozdvizhenskii, A. Sh. Kuanyshev and A. V. Kobets, Reaction Kinetics Catalysis Letters 5, 163 (1976).

33. A. V. Kiselev and A. V. Uvarov, Surface Sci. 6, 399 (1967).

34. Y. Noto, K. Fukada, T. Onishi and K. Tamaru, Trans. Faraday Soc. 63, 2300 (1967).

35. S. Hayashi, T. Takenaka and R. Goton, J. Chem. Soc. Japan 88, 133 (1967).

36. R. P. Young and N. Sheppard, J. Catal. 7, 223 (1967).

Table 1. Peak Positions (in cm^{-1}) and Assignments for CH_3CH_2OH, CH_3COOH and CH_3CHO on Alumina.

CH_3CH_2OH 475 K	CH_3COOH 295 K	CH_3COOH 475 K	CH_3CHO	Assignment
430	475	448	426	OCO rock
621	610	610	613	OCO deformations
669	677	681	687	
806				C-C stretch?
879				
911				C-C stretch
927				Bulk Al-O stretch
	939	935	939	C-C and bulk Al-O stretch
1049	1041	1033	1049	CH_3 rock
1090				C-C-O skeletal
1165				
1285	1335	1335	1343	CH_3 symmetric deformation
			1395	
1364	1415	1411	1423	CH_3 asymmetric deformation
1444	1468	1464	1472	OCO symmetric stretch
1589	1593	1589	1605	OCO asymmetric stretch
1847	1855	1843	1855	Harmonic of bulk Al-O
2863	2835	2859	2874	CH_3 stretch
2915	2919	2915	2919	
2952	2972	2972	2975	
	3000	3004	3008	
3621	3613	3621	3637	O-H stretch

Table 2. Comparison of Peak Positions (in cm^{-1}) of Ethanol Adsorbed on Alumina with Aluminum Ethoxide.

Ethanol on Al_2O_3 below 475 K (Ref. 1)	Ethanol on Al_2O_3 345 K (Ref. 2)	Aluminum Ethoxide (Ref. 3)	Aluminum Ethoxide (Ref. 11)	Assignment (Ref. 11)
426	I*	I		
			515	
			650	
710			707	
806				
911			896	
935			935	Al-O stretch
1057		1050	1059	Al-O-C stretch
	1070	1070		
1105	1115	1120	1105	skeletal vibrations
1161	1172	1170	1178	
1285	1287	I	I	
1356			1350	
1380	1387	1385	1382	CH_3 deformation
1440	1445	1450	1460	CH_2 deformation
1472	1490	1480	I	
I	I	I		
2859	2865	2860		
2915	2930			
2952	2963	2970		
3633	3640	I		

*I, indicates region of spectrum not listed.

Table 3. Combined Results for IETS Studies of CH_3COOH on Al_2O_3 at 300 K (peak positions in cm^{-1}).

This Study[a]	Lewis et al.[b] (Ref. 17)	Brown et al.[c] (Ref. 15)	Shklyarevskii et al.[d] (Ref. 4)	Skarlatos et al.[e] (Ref. 16)	Assignment
290		294			Al phonon
475	484	466	484	476	OCO rock
610	613	613	610	629	OCO deformation
677	685	689	685	701	
				725	
	831		895	870	C-C stretch (b) OCO or CCO mode (d)
939	956	940		955	Bulk Al-O stretch
		948	948		C-C stretch
1041	1024	1024	1048	1056	CH_3 rock (a,b,c) CH deformation (e) CH out-of-plane bend (d)
		1044	1070		
1335	1331	1338	1365	1273	CH_3 symmetric deformation (a,b,c,e) OCO mode (d)
1415	1403	1411	1425	1435	CH_3 asymmetric deformation (a,b,d) OCO mode (c,e)
1468	1452	1463	1472		OCO symmetric deformation (a,b,d) CH_3 deformation (c,e)
1593	1589	1583	1585	1596	OCO asymmetric deformation
2835	2806	2866	2855		CH_3 stretch
2919	2895	2910	2922	2910	
2972	2944	2964	2976	2966	
3000		3000	3005	3039	
3613	3629	3600	3620	3627	O-H stretch

Figure Captions

Fig. 1.: IET spectra of (a) CH_3COOH, 295 K; (b) CH_3COOH, 475 K; (c) CH_3CHO; and (d) CH_3CH_2OH, 475 K, adsorbed on alumina. The spectral range is between 240 and 2250 cm^{-1}.

Fig. 2: As in Fig. 1, except the spectral range is between 2000 and 4000 cm^{-1}.

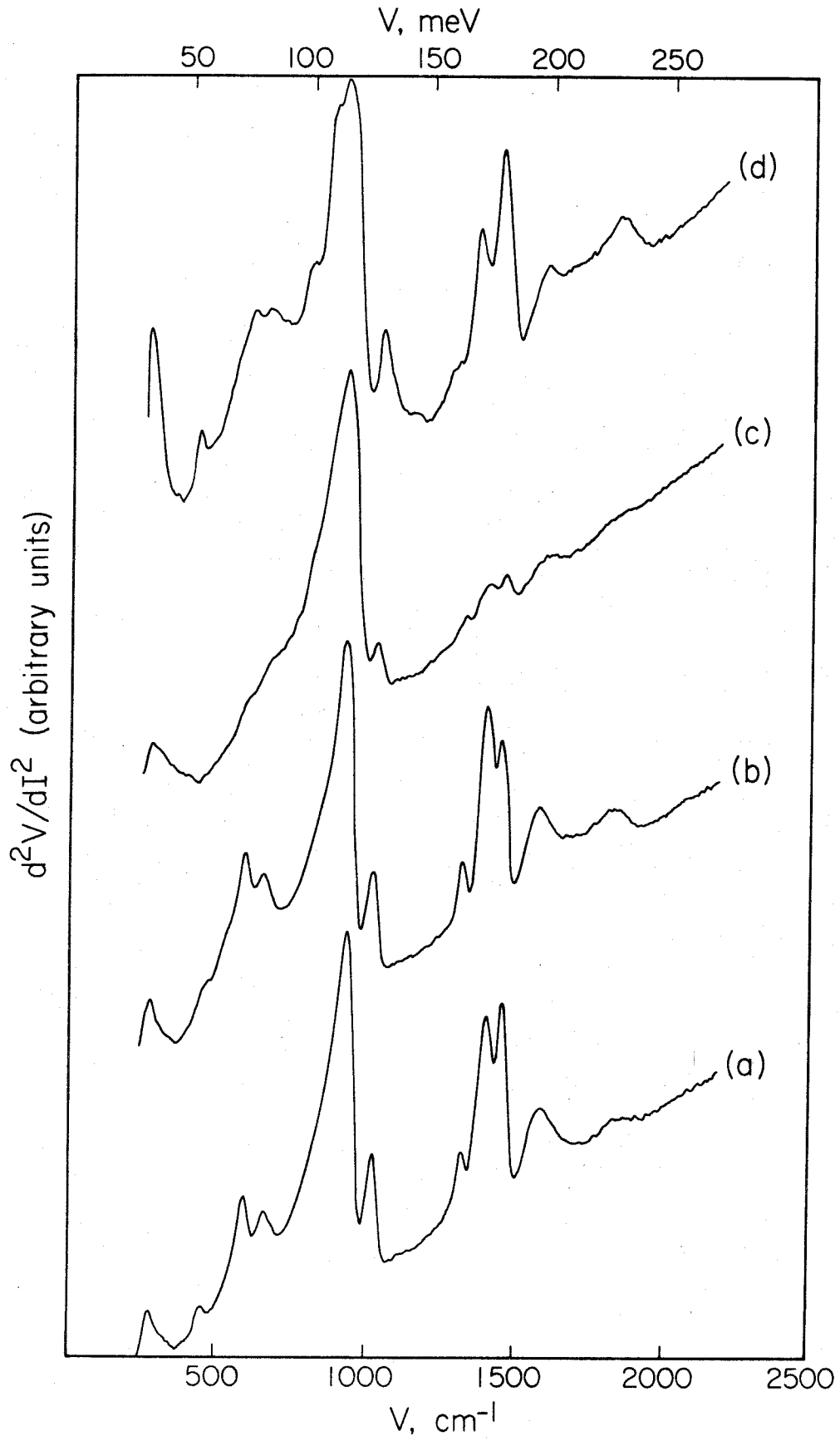
V, meV
50
100
150
200
250
(d)
(c)
(b)
(a)
d^2V/dI^2 (arbitrary units)
500
1000
1500
2000
2500
V, cm^{-1}

Fig. 1

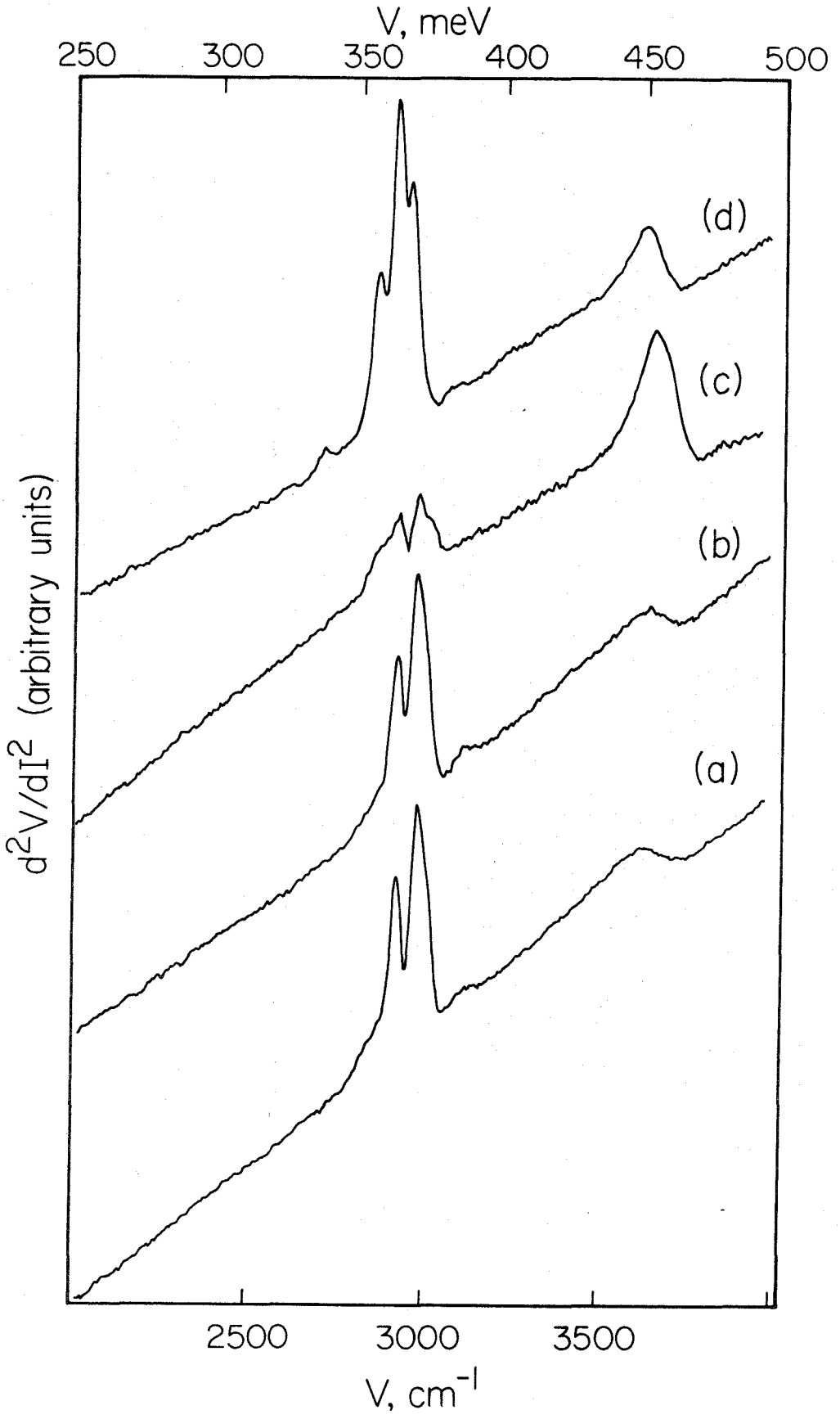
V, meV
250
300
350
400
450
500
(d)
(c)
(b)
(a)
d^2V/dI^2 (arbitrary units)
2500
3000
3500
V, cm^{-1}

Fig. 2

Chapter V

The Adsorption of Ethanol on Silver Clusters Supported on Alumina

Abstract

The adsorption of ethanol on islands of Ag supported on a surface of Al_2O_3 has been investigated utilizing both inelastic electron tunneling spectroscopy (IETS) to probe the vibrational structure of the adsorbed species, and transmission electron microscopy to characterize some of the physical properties of the solid surface. Results are reported for the number and average size of Ag clusters on the surface as the amount of Ag is varied up to a statistically-averaged coverage of approximately 10 Å. Vibrational spectra are shown for saturation coverage of ethanol as a function of Ag coverage. Peak shifts expected to arise due to the difference in electronegativities between Al and Ag are observed for the surface ethoxide species which form upon adsorption.

Inelastic electron tunneling spectroscopy (IETS) has been shown previously to be an effective tool for probing the vibrational structure of a number of reactants and reaction intermediates on metal oxide catalytic surfaces (1). Hansma and his co-workers (2) have reported recently the application of IETS to the study of CO chemisorbed onto alumina supported Rh particles. These results, together with unpublished work in our own laboratory for CO chemisorption on supported Ni, have enhanced the worth of IETS as an experimental tool significantly by increasing its potential applications to include at least some types of catalytic reactions which occur over supported metal catalysts. Due to the widespread industrial use and economic importance of supported metal catalysts, the present work was undertaken to expand further the range of supported metal catalytic systems which might be examined profitably utilizing IET spectroscopy. Specifically, we report here an IETS study of ethanol adsorbed on alumina supported Ag. This system represents one step in the oxidation reaction of alcohols to aldehydes over silver catalysts and is fundamentally different from the CO reactions on the Group VIII metals that have been examined previously.

Our experimental techniques, as well as the phenomenological and theoretical aspects of tunneling spectroscopy, have been reported in detail previously (3). Our model catalyst surfaces were prepared by oxidizing the top 20 to 30 Å of a freshly evaporated Al film in a plasma discharge of O_2, followed by the evaporation of small amounts of Ag onto the thin oxide film. The amount of Ag deposited was monitored with a quartz crystal oscillator located approximately one-third of the distance to the sample

from the evaporation source. This geometry permitted the oscillator, which is sensitive to changes on the order of approximately 0.5 Å in statistical coverage of Ag, to reflect accurately amounts of Ag at the sample surface with approximately ten times this sensitivity. Measurements were made on samples where the statistical coverage of Ag was varied up to approximately 10 Å.

The structure of Ag on the aluminum oxide was determined via transmission electron microscopy (TEM). The electron microscopy samples were prepared in our bell jar using carbon films supported on 400 mesh Cu grids as substrates. The Al and Ag evaporations and the plasma oxidation steps were identical to those for the tunneling samples, and TEM measurements were made over the same range of Ag coverage. The beam currents and voltages which were employed, 2 - 3 μA and 60 - 80 keV, respectively, were substantially below the levels that might be expected to stimulate Ag agglomeration or migration as judged from other studies (4). Typical results are illustrated in Fig. 1. The experimentally determined relationship between the number of Ag clusters and their average diameter and the statistical Ag coverage is shown in Fig. 2. The solid lines in Fig. 2 indicate only a "best fit" to the available data points; the line showing average particle diameter was drawn to include also a point approximately representing the atomic diameter of Ag near zero Ag coverage.

At room temperature, ethanol chemisorbs dissociatively on alumina to form aluminum ethoxide (5). Similar results have been noted on other surfaces (6), and the same type of structure can be expected to form on Ag also. Even though ethoxide formation occurs on both Ag and alumina, slight differences between the two species are expected to be manifest in their vibrational spectra. Takezawa and Kobayashi (7) have studied alcohol

adsorption on a number of surfaces and have established that hydrocarbon vibrational frequencies of surface ethoxides can be expected to increase with increasing electronegativity of the surface metal ion. The electronegativities of Ag and Al are 1.93 and 1.61, respectively, on the Pauling scale (8), and thus we expect slight shifts upward in frequency for the CH vibrations of silver ethoxide relative to the corresponding vibrational frequencies of the ethoxide formed on Al ions. Since even at the highest Ag coverages studied, much of the alumina surface is still available for ethanol adsorption, we anticipate spectra resulting from the superposition of vibrations from both Ag and Al ethoxide.

Spectra at room temperature for saturation coverage of ethanol over a range of Ag coverages are shown in Figs. 3 and 4. The low intensities of the hydrocarbon peaks even at saturation coverage result from the blockage of additional adsorption sites below 400 to 500 K by H_2O or OH formed during ethanol adsorption (5,6). Few noticeable changes occur in the spectra up to a statistical Ag coverage of 2.5 Å, probably due to the extremely large ratio of Al to Ag adsorption sites at these low coverages. As Ag coverage is increased beyond this point, however, features due to the Ag ethoxide species become more prominent. In Fig. 3, which shows the CH_2 and CH_3 deformation bands (at 1472, 1440, 1380 and 1360 cm^{-1} on alumina) (5,9), we can observe the decreasing intensity of the 1360 cm^{-1} band as well as the growth of new structure between 1380 and 1440 cm^{-1}, and at approximately 1470 cm^{-1} and above. Similar effects are evident in Fig. 4, which shows the CH stretching bands. These bands appear at approximately 2863, 2915 and 2952 cm^{-1} for the Al ethoxide structure. Again, as Ag coverage is increased, we can observe the growth

of new structure between 2865 and 2900 cm^{-1}, 2920 and 2950 cm^{-1}, and at approximately 2998 cm^{-1}.

Although not shown in Figs. 3 and 4, there are two other spectral features that should be mentioned. In previous work concerning ethanol adsorption on alumina, we have reported the observation of a C-C stretching peak near 911 cm^{-1}; the bulk Al-O stretching band at 935 cm^{-1}; and a broad, rounded peak at approximately 1055 cm^{-1} arising from the overlapping of an out-of-plane C-H bending mode (lower energy) and an Al-O-C stretching vibration (slightly higher energy). As the Ag coverage is increased, the C-C band shifts upward in energy until it is nearly coincident with the bulk Al-O mode. Also, the 1055 cm^{-1} feature becomes significantly sharper. We attribute this to a slight increase in the C-H bending frequency coupled with a decrease in frequency for the Al-O-C mode for molecules adsorbed on Ag relative to those on Al. These results are also consistent with our expectations based on the work of Takezawa and Kobayashi (8).

As expected due to the realtive electronegativities of Ag and Al, ethanol adsorption on supported Ag produces an ethoxide the CH vibrational frequencies of which appear at slightly higher energies than the corresponding modes of ethoxide formed on the alumina support. The IET technique has been shown to be capable of distinguishing between these two very similar ethoxide species. More significantly, the observation of ethanol adsorption on alumina supported Ag opens up an entirely new class of important supported metal catalytic systems which can be studied utilizing IETS, thus demonstrating the increasing versatility and value of this spectroscopic technique.

ACKNOWLEDGMENTS

We wish to express our appreciation to Mr. Patrick F. Koen for his valuable technical assistance in obtaining the transmission electron micrographs.

References

1. J. Lambe and R. C. Jaklevic, Phys. Rev. 165, 821 (1968); B. F. Lewis, M. Mosesman and W. H. Weinberg, Surface Sci. 41, 142 (1974).

2. P. K. Hansma, in Inelastic Electron Tunneling Spectroscopy, p. 186 (T. Wolfram, Ed.), Springer-Verlag, N.Y., 1978;
P. K. Hansma, W. C. Kaska and R. M. Laine, J. Am. Chem. Soc. 98, 6064 (1976).

3. W. H. Weinberg, Ann. Rev. Phys. Chem. 29, 115 (1978).

4. J. W. Sprys and Z. Mencik, J. Catal. 40, 290 (1975).

5. H. E. Evans and W. H. Weinberg, submitted for publication;
R. G. Greenler, J. Chem. Phys. 37, 2094 (1962);
H. Arai, Y. Saito and Y. Yoneda, Bull. Chem. Soc. Jap. 40, 731 (1967).

6. S. L. Parrott, J. W. Rogers, Jr. and J. M. White, Appl. Surface Sci. 1, 443 (1978);
B. A. Morrow, L. W. Thompson and R. W. Witmore, J. Catal. 28, 332 (1973).

7. N. Takezawa and H. Kobayashi, J. Catal. 25, 179 (1972); 28, 335 (1973).

8. A. L. Allred, J. Inorg. Nucl. Chem. 17, 215 (1961).

9. R. C. Wilhoit, J. R. Burton, Fu-Tien Kuo, Sui-rong Huang and A. Viquesnel, J. Inorg. Nucl. Chem. 24, 851 (1962).

Figure Captions

Fig. 1: Transmission electron micrographs of Ag particles on alumina films for statistically averaged Ag coverages of (a) 2.5 Å, and (b) 10.0 Å.

Fig. 2: Number of Ag particles and their average diameters as a function of Ag coverage on the alumina surface.

Fig. 3: IET spectra in the range 1200 to 1600 cm^{-1} of ethanol adsorbed on Ag/Al_2O for statistical Ag coverages of (a) 0 Å, (b) 2.5 Å, (c) 5.0 Å, and (d) 10.0 Å.

Fig. 4: IET spectra in the range 2700 to 3100 cm^{-1} of ethanol adsorbed on Ag/Al_2O_3 for statistical Ag coverages of (a) 0 Å, (b) 2.5 Å, (c) 5.0 Å, and (d) 10.0 Å.

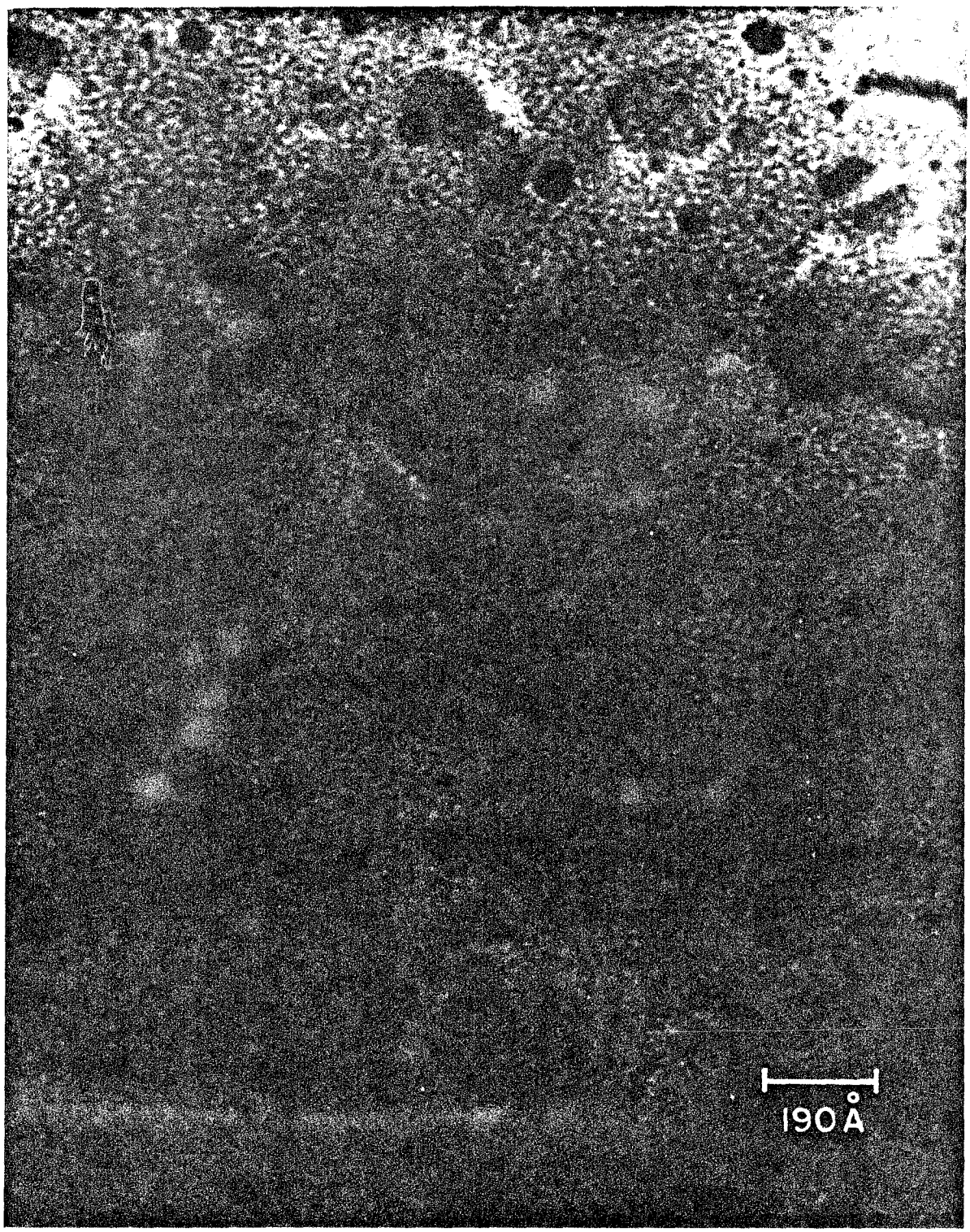

Fig. 1a

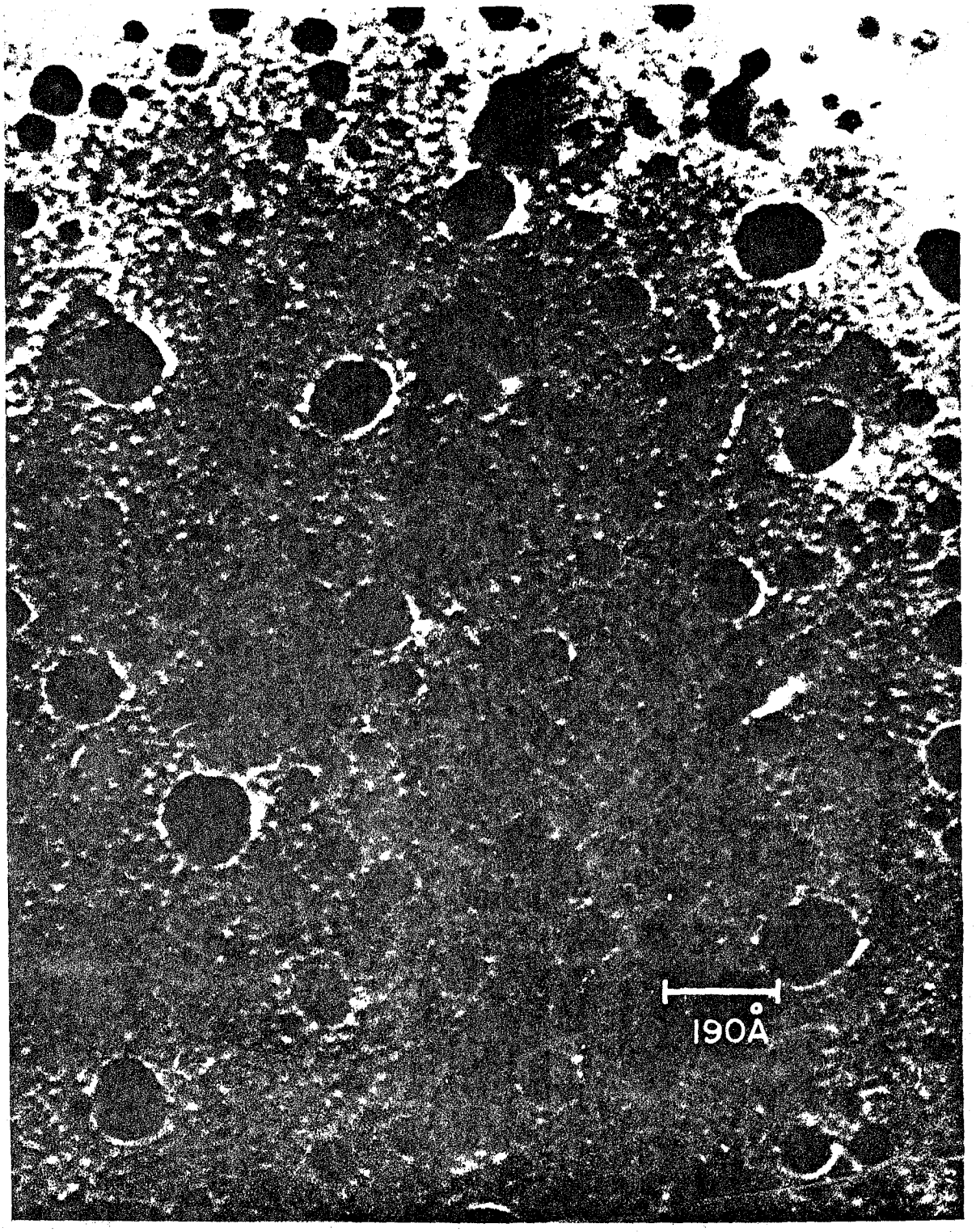

Fig. 1b

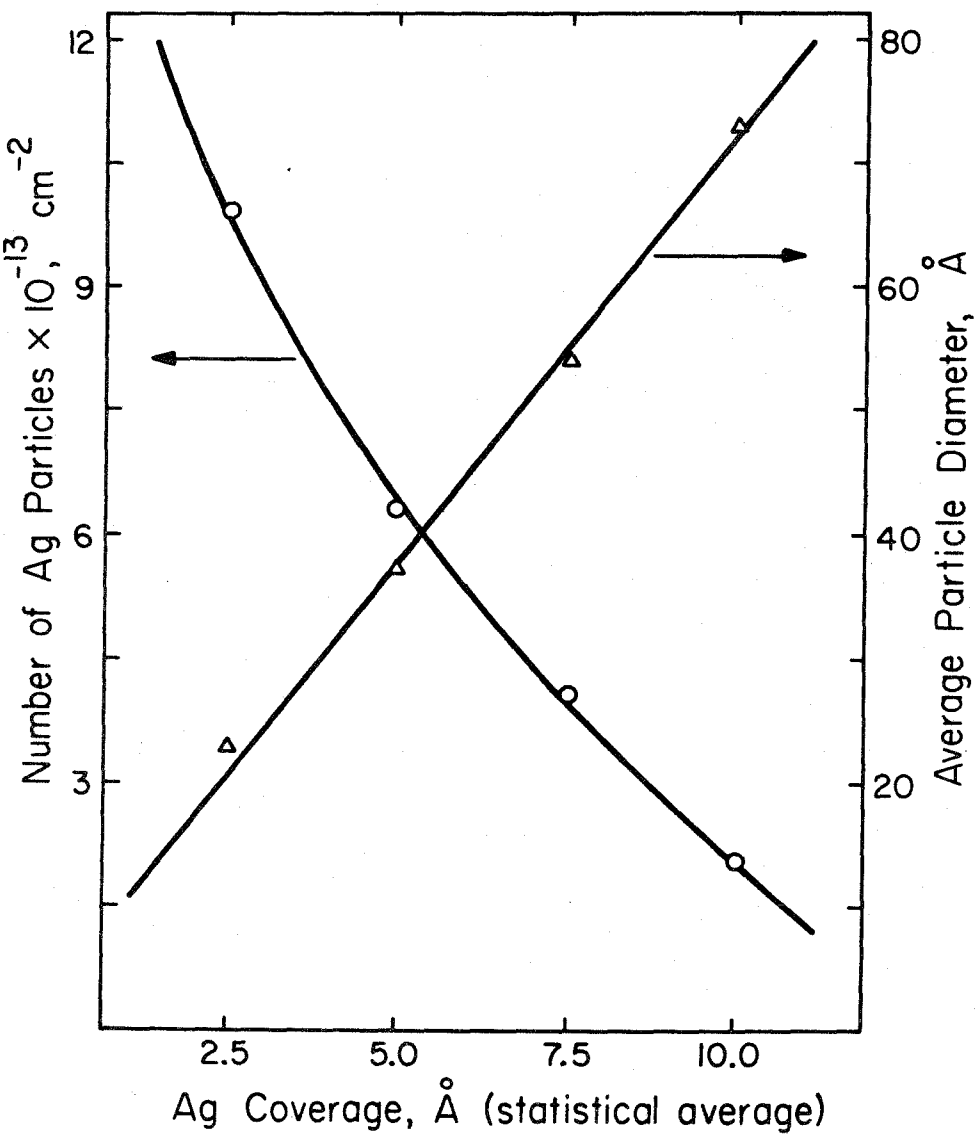
12
9
6
3
80
60
40
20
Number of Ag Particles × 10^-13, cm^-2
Average Particle Diameter, Å
2.5
5.0
7.5
10.0
Ag Coverage, Å (statistical average)

Fig. 2

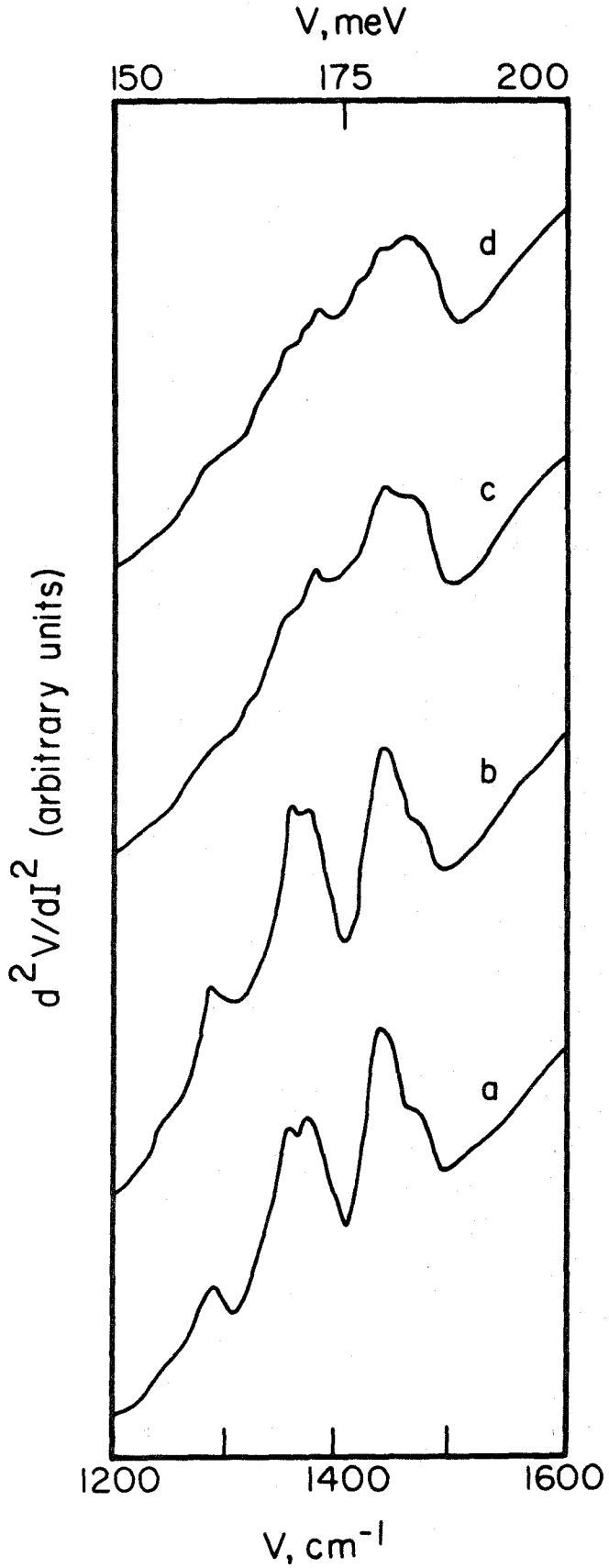
V, meV
150
175
200
d
c
b
a
d^2V/dI^2 (arbitrary units)
1200
1400
1600
V, cm^{-1}

Fig. 3

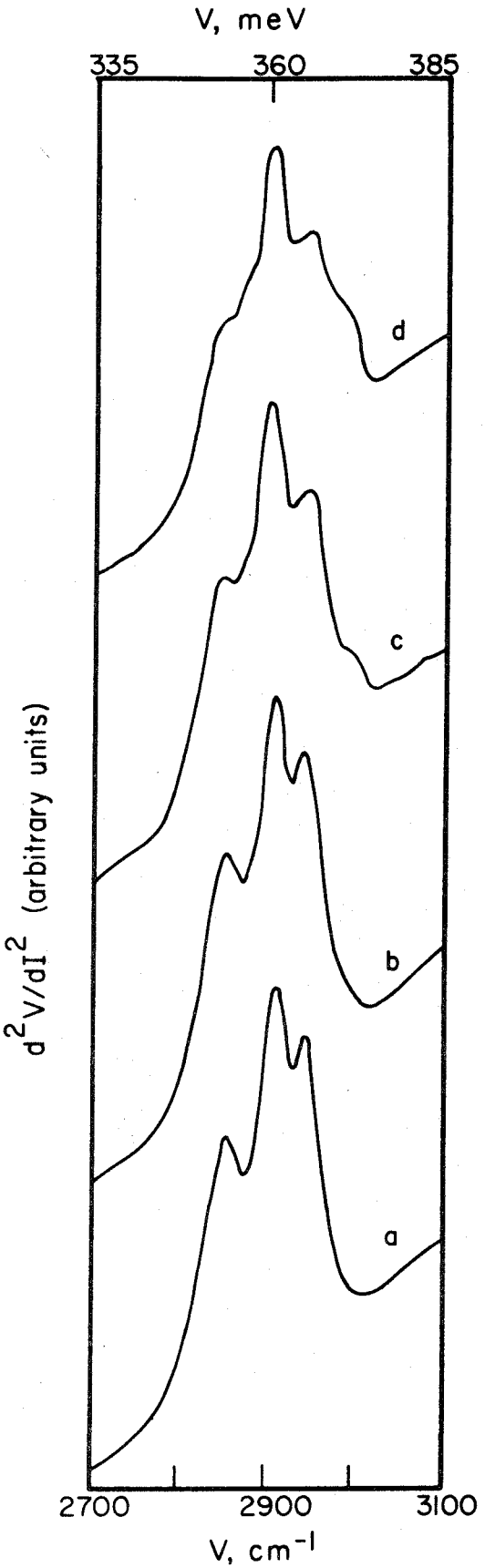
V, meV
335
360
385
d
c
b
a
d^2V/dI^2 (arbitrary units)
2700
2900
3100
V, cm^{-1}

Fig. 4

Chapter VI

IET Spectroscopy of Zirconium Tetraborohydride Supported on Aluminum Oxide

Sir:

Currently, there is significant interest in newly developed supported-complex catalysts, which are formed by anchoring or grafting a homogeneous catalyst (a cluster compound) onto a high surface area support.[1] Such catalysts can combine the activity and selectivity found in homogeneous systems with the stability and ease of separation characteristic of heterogeneous catalysts, and they frequently exhibit activities an order of magnitude or more greater than the corresponding unsupported systems.[2] Progress in this area, however, has been hampered by a lack of detailed structural information for supported complexes. Characterization of supported complexes has been poor, plagued by many of the same problems that arise in attempting to characterize traditional heterogeneous catalysts; and, as yet, there are not reported cases where the structure of a supported complex has been definitely determined. We report here the vibrational spectrum of the supported complex formed by the interaction of zirconium tetraborohydride, $Zr(BH_4)_4$, a known homogeneous polymerization catalyst for olefins, with an alumina surface. This vibrational information was obtained utilizing inelastic electron tunneling spectroscopy (IETS).

IETS involves monitoring the current due to electrons tunneling inelastically through a thin insulating barrier between two metal electrodes. Although most of this tunneling current is elastic, some electrons can tunnel inelastically by exciting vibrational modes of molecules at, or near, the surface of the insulating barrier. Such inelastic transitions can occur only when the bias voltage across the barrier is greater than, or equal to, a vibrational excitation energy, and lead to increases in conductance across the barrier by providing additional channels for electron

tunneling. These conductance increases become peaks when the second derivative of voltage with respect to current, d^2V/dI^2 (proportional to d^2I/dV^2), is plotted as a function of the bias voltage, V. Peak positions correspond to vibrational excitation energies, and yield information analogous to that obtained by optical absorption spectroscopies. Both IR and Raman active modes are observed in the IET spectra. Further theoretical and experimental details are available elsewhere.[3]

In our experiments, the top few atomic layers of a freshly evaporated Al film were oxidized to form the thin insulating barrier. The $Zr(BH_4)_4$ was then allowed to adsorb on the resultant aluminum oxide surface. Saturation coverage was obtained by exposure to 5×10^{-2} torr of $Zr(BH_4)_4$ for 15 minutes. The samples were completed by evaporation of top metal (Pb) electrode. Measurements were made over the entire spectral range from 240 to 4000 cm^{-1}, with a resolution on the order of 4 cm^{-1} and a sample surface area of approximately 1 mm^2. An IET spectrum for a saturation coverage of $Zr(BH_4)_4$ on aluminum oxide at 300 K is shown in Fig. 1. Peak positions are also indicated in the figure.

Comparisons with IETS studies of "clean" Al_2O_3 indicate that the spectral features at 299, 945 and 1863 cm^{-1} can be assigned to a phonon in the underlying Al film, a bulk Al-O stretching mode and its harmonic overtone, respectively.[4] The 3675 cm^{-1} peak is the O-H stretching vibration of surface hydroxyl groups, while the peak near 2930 cm^{-1} arises from the C-H stretching vibration of a small amount of adsorbed hydrocarbon contamination.[4] Contamination might also contribute to the intensity of features at 1030 cm^{-1} and in the 1300 - 1500 cm^{-1} region.

The boron atoms in $Zr(BH_4)_4$ are arranged tetrahedrally, each being bound to the central Zr atom in a tridentate manner with three bridging

hydrogens.[5] During adsorption, one or more of the BH_4 ligands are lost as the Zr becomes either singly or multiply coordinated to oxygen atoms on the surface.[2] Since the surface becomes a virtual ligand, it might well affect bonding in the remaining BH_4 groups. For example, $(C_5H_5)_2Zr(BH_4)_2$ and $(C_5H_5)_2Zr(H)BH_4$ are both known to have bidentate bridging structures,[6] and the surface could be expected to have a similar affect. Information concerning bonding can be obtained by examining the stretching vibrations of both terminal (H_t) and bridging (H_b) hydrogens. The B-H_t region shows at least three peaks near 2407, 2437 and 2490 cm^{-1}. For the tridentate structure, only one peak at 2560 - 2580 cm^{-1} is to be expected.[7] The observed frequencies are more closely related to those reported for bidentate species (between 2375 and 2550 cm^{-1}),[6] yet the presence of more than two peaks, as well as the observation of four features in the B-H_b stretching region (at 2142, 2177, 2230 and 2252 cm^{-1}), indicate that there is more than one type of surface species. This is consistent with the assignments of features at 693 and 910 cm^{-1} to Zr-O stretching modes of multiply (bulk-like) and singly (or, at least, less highly) coordinated Zr atoms.[8,9] Additionally, some of the BH_4 ligands displaced during adsorption might remain on the surface, forming

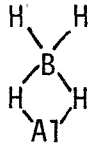

and

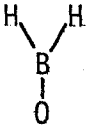

complexes. Similar surface species have been observed for diborane (B_2H_6) adsorption on Al_2O_3[10] and could also be expected to produce additional structure in the B-H stretching regions. Modes appearing at 1106, 1130, 1173, 1220 and 1260 cm^{-1} (and possibly 1030 cm^{-1}) can be assigned to deformations of the metal-BH_4

structure.[7] An AlH_2BH_2 deformation might also contribute to structure near 1457 cm^{-1}.[10] The 1378 cm^{-1} peak has been previously assigned to a B-O stretch, and a B-O vibration might also contribute to the intensity of the 1260 cm^{-1} peak.[10] Unresolved structure between 480 and 600 cm^{-1} can be assigned to Zr-B skeletal stretching modes,[11] with possible contributions from additional Zr-O vibrations.[8] Low energy features near 264 and 323 cm^{-1} probably arise from BH_4-Zr-BH_4 bending and Zr-BH_4 torsional modes.[7]

Although this is by no means a complete characterization of alumina-supported $Zr(BH_4)_4$ (the details of more extensive results characterizing the supported complex as a function of temperature, as well as its interaction with D_2, D_2O, H_2O, C_2H_4, C_3H_6 and C_2H_2 will be reported later), this preliminary communication does indicate the versatility of IETS and clearly demonstrates the value of information that can be obtained by applying IETS to the study of supported complexes.

Acknowledgment. We wish to thank Dr. F. N. Tebbe and Dr. L. E. Firment both for useful correspondence as well as for supplying the $Zr(BH_4)_4$. This research was supported by the National Science Foundation under Grant No. ENG78-16927. Additional support from the Camille and Henry Dreyfus Foundation in the form of a Teacher-Scholar award to WHW is also greatly appreciated.

References

1. Basset, J. M.; Smith, A. K. in "Fundamental Research in Homogeneous Catalysis" (M. Tsutsui and R. Ugo, ed.); Plenum Press: New York, N.Y., 1977; pp. 69 - 98.
2. Zakharov, V. A.; Yermakov, Yu. I. Catal. Rev.-Sci. Eng. 1979, 19, 67 - 103.
3. Weinberg, W. H. Ann. Rev. Phys. Chem. 1978, 29, 115 - 139.
4. Bowser, W. M.; Weinberg, W. H. Surface Sci. 1977, 64, 377 - 392.
5. Bird, P. H.; Churchill, M. R. Chem. Comm. 1967, 403.
6. Marks, T. J.; Kennelly, W. J.; Kolb, J. R.; Shimp, L. A. Inorg. Chem. 1972, 11, 2540 - 2546.
7. Davies, N.; Wallbridge, M. G. H.; Smith, B. E.; James, B. D. J. Chem. Soc. Dalton Trans. 1973, 162 - 165.
8. Maekawa, T.; Terada, M. Trans. Japan. Inst. Metals 1963, 4, 57 - 59.
9. Ozin, G. A. in "Vibrational Spectroscopy of Trapped Species" (H. E. Hallum, ed.); John Wiley and Sons: London, 1973; pp. 237 - 244.
10. Matsuda, T.; Kawashima, H. J. Catal. 1977, 49, 141 - 149.
11. James, B. D.; Smith, B. E.; Shurwell, H. F. J. Mol. Struc. 1976, 33, 91 - 95.

Figure Caption

Fig. 1: IET spectrum for $Zr(BH_4)_4$ supported on Al_2O_3 at 300 K over the energy range (a) 240 - 2000 cm^{-1}, and (b) 2000 - 4000 cm^{-1}.

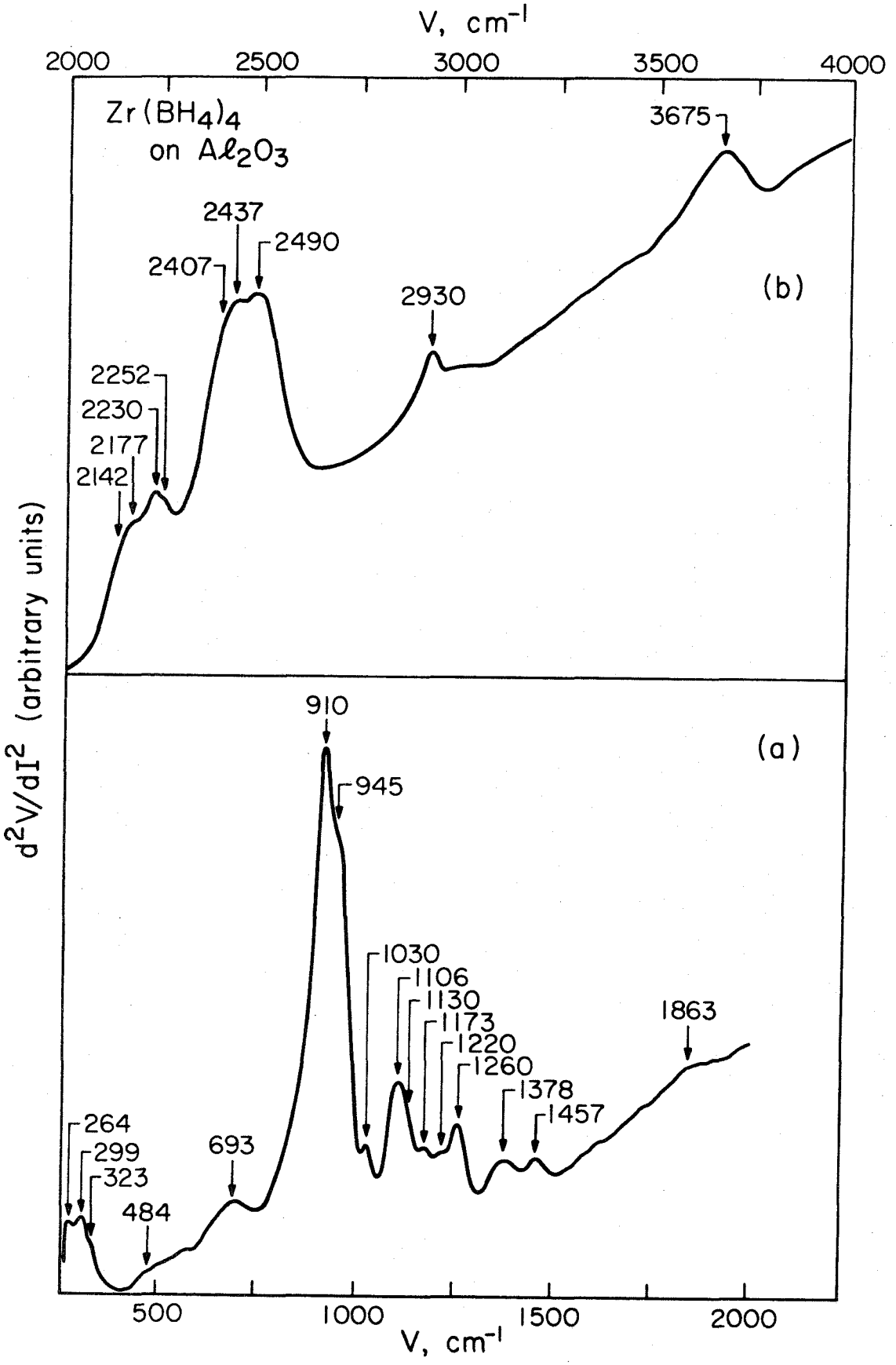
V, cm⁻¹
2000
2500
3000
3500
4000
Zr(BH4)4
on Aℓ2O3
3675
2437
2490
2407
2930
(b)
2252
2230
2177
2142
d²V/dI² (arbitrary units)
910
(a)
945
1030
1106
1130
1173
1220
1260
1378
1457
1863
264
299
323
484
693
500
1000
1500
2000
V, cm⁻¹

Fig. 1

Chapter VII

Interactions of Deuterium, Deuterium Oxide and Water Vapor with Zirconium Tetraborohydride Supported on Alumina

Abstract

Supported complexes, formed by grafting known homogeneous catalytic compounds onto support materials, are currently of significant interest and have great potential value in industrial applications. Progress in this field, however, has been hampered by a lack of information about the structure of the supported complexes. In the current study, inelastic electron tunneling spectroscopy (IETS) has been used to probe the vibrational structure of $Zr(BH_4)_4$ supported on Al_2O_3 as a function of temperature between 300 and 475 K. A number of surface species have been identified. Interactions of the supported zirconium complex with H_2O, D_2O and D_2 have been observed also over the same temperature range. Vibrational transitions throughout the entire spectral range from 240 to 4000 cm^{-1} are clearly observed, and peak assignments are presented based on vibrational results available for a number of related compounds and systems. This study demonstrates the utility of IETS while at the same time provides significant new insight on a system of considerable interest and importance.

Introduction

Since 1970, there has been increasing interest in attempts to form new types of catalysts combining the desirable features of both homogeneous and heterogeneous catalytic systems (1). Traditionally, heterogeneous systems have provided for easy separation of catalyst from products, good catalyst stability and high activity. Homogeneous catalysts, while being often expensive, fragile compounds easily lost due to separation problems, can typically provide greater selectivity, and can be tailored and adapted to fit a specific process in a more logical and easy fashion than their heterogeneous counterparts. Efforts to combine the advantages from both areas into a new class of catalysts have centered on attempts to graft or anchor homogeneous catalytic compounds onto high surface area supports (see, for example, Ref. 1 and references therein). These supported complexes have formed a new class, or "third generation", of catalysts which span both the homogeneous and heterogeneous areas, and already are of considerable industrial importance. An additional important feature of many of the supported complexes observed thus far has been a significant increase in catalytic activity relative to the homogeneous analogs (1,2). Increases in activity of up to four orders of magnitude resulting from grafting a complex onto a support have been reported (3). Interactions between homogeneous catalytic compounds and supports evidently ensure and/or increase the number of complexes existing in a form required to produce catalytically active sites or centers.

There are, however, difficulties and inconveniences associated with grafting complexes onto supports, the most serious apparently being an

accompanying loss of knowledge concerning the structure of the complex. To date, there is very little detailed structural information available for any supported complexes. (No definite proof of any structure for such a complex has yet been reported.) In general, the number and nature of any ligands which remain associated with a complex on the surface are not known. Also, the support itself, in addition to insolubilizing and dispersing the catalytic compounds, might provide a cooperative effect and function as a co-catalyst or activating agent. Little is known or understood about such possible effects. This lack of understanding concerning the nature and structure of supported complexes is hindering progress in the field. One working group, formed to examine the status of catalysis by supported complexes, has reported that the deficiency of detailed structural information is holding up advances in this area and that "significant progress is impossible unless new techniques are exploited" (4).

Recently, we have reported preliminary results of the vibrational structure of $Zr(BH_4)_4$ supported on aluminum oxide at 300 K (5). Vibrational data were obtained by utilizing inelastic electron tunneling spectroscopy (IETS), a relatively new technique which has been shown to be an effective means of probing the vibrational structure of molecules adsorbed on insulating surfaces. $Zr(BH_4)_4$ is one of several metal tetraborohydrides which have proved effective in catalyzing polymerization reactions of olefins (6,7). While the rate of polymerization in solution is rather low, greatly enhanced activity has been obtained by interacting $Zr(BH_4)_4$ with various supports. Grafting $Zr(BH_4)_4$ onto Al_2O_3 has produced more active catalysts than have been obtained using other supports (3). Although

$Zr(BH_4)_4/Al_2O_3$ is an effective olefin polymerization catalyst, the exact nature and behavior of even the unsupported complex, particularly the nature of the metal-BH_4 interaction, during reaction is not known.

This study represents part of a continuing effort to understand the behavior of Al_2O_3-supported $Zr(BH_4)_4$ catalytic systems. In the following sections, we will outline our experimental procedures, and report and discuss vibrational spectra obtained with IETS for $Zr(BH_4)_4$ on Al_2O_3 as a function of temperature, as well as for its reactions with H_2O, D_2O and D_2. The final section is a summary of the major findings of this study. The following paper deals with the interactions of $Zr(BH_4)_4/Al_2O_3$ with ethylene, propylene and acetylene.

Experimental Details

IETS involves monitoring the current produced by electrons tunneling through a thin insulating barrier between two metal electrodes when a bias voltage is placed across the barrier. The conductance of such a metal-insulator-metal tunnel junction exhibits increases in magnitude at values of the bias voltage which correspond to vibrational excitation energies of molecules in the barrier region. These conductance increases arise from additional channels becoming available for tunneling electrons which traverse the insulating barrier inelastically (i.e., with a net energy loss) by exciting vibrational modes of molecules in or near the barrier. A derivative spectrum presenting d^2V/dI^2 (proportional to the second derivative of the current, d^2I/dV^2) as a function of the applied voltage, V, yields a series of peaks the positions of which correspond to vibrational excitation energies for molecules in the barrier region. Spectra obtained in this manner have been shown to be analogous to those obtained by optical absorption spectroscopies such as IR or Raman (both IR- and Raman-active modes being observed in the tunneling spectra)(8).

In our application of the IETS technique, samples are prepared in an oil diffusion pumped bell jar with a base pressure of 10^{-7} torr. A thin aluminum strip is evaporated onto a clean glass substrate; then the top few atomic layers of the strip are oxidized in a plasma discharge of pure O_2. This thin (20 - 30 Å) layer of Al_2O_3 forms the insulating barrier required for IET experiments, and additionally serves as the aluminum oxide substrate used for supporting the $Zr(BH_4)_4$. Loading of the zirconium complex onto the support was accomplished by exposing the Al_2O_3 films to 5×10^{-2} torr of $Zr(BH_4)_4$ for 15 minutes (a surface area of approximately

1 mm^2 being probed during measurement). This exposure was sufficient to produce a saturation coverage of adsorbate on the surface as judged by the lack of any observed changes in the vibrational spectra for higher exposures. Unused $Zr(BH_4)_4$ vapor was collected in a LN_2-cooled trap and transferred under vacuum to a collection cylinder, since exposure to air can result in fire and/or explosion. Samples were then heated to various temperatures between 300 K and 475 K for up to 30 minutes in either vacuum, 5 torr of D_2, or 1 torr of N_2, H_2O or D_2O. (Samples which were exposed to $Zr(BH_4)_4$ and then heated showed no differences in this temperature range from samples where the substrate was heated during exposure to the complex.) Sample heating was accomplished via a resistive heating technique developed by Bowser and Weinberg (9). Lastly, a Pb cross-strip was evaporated on top of the sample, the Pb and underlying Al layers serving as the two metal electrodes required for the tunneling measurements. Measurements were carried out over the entire spectral range from 240 to 4000 cm^{-1} via standard techniques. Measurements for several samples at each set of conditions were made to ensure reproducibility. Spectral features can typically be resolved to within ± 4 cm^{-1}. Further details of both experimental and theoretical aspects of IETS are available elsewhere (10).

Results

The spectrum for $Zr(BH_4)_4$ on aluminum oxide at 300 K, reported earlier in a preliminary communication (5), is presented in Fig. 1. Peak positions are also identified in this figure. The spectrum for this system is presented again for comparative purposes in Fig. 2 along with spectra for $Zr(BH_4)_4/Al_2O_3$ exposed to D_2 or D_2O at both 300 K and 475 K, and to vacuum and H_2O at 475 K. No discernable differences were evident between samples heated in vacuum and those heated in N_2. It should be noted that the 1000 - 1500 cm^{-1} and 1500 - 4000 cm^{-1} regions of the spectra in Fig. 2 have been enhanced by factors of 3 and 1.5, respectively, relative to the region below 1000 cm^{-1}. Peak positions for each of the spectra shown are listed in Table 1. Spectra measured for samples at intermediate temperatures are not shown since they contribute little additional information. Temperature had little, if any, noticeable affect on samples exposed to either H_2O or D_2O.

At 300 K (see especially Fig. 1), the supported complex showed low-energy bands at 264 and 299 cm^{-1}, a shoulder near 323 cm^{-1}, and unresolved low-intensity structure between approximately 480 and 580 cm^{-1}. A stronger, broad peak appears near 693 cm^{-1}. The most intense spectral feature consists of a rather sharp peak at 910 cm^{-1} with a strong high-energy shoulder at 945 cm^{-1}. Between 1000 and 1500 cm^{-1} there are two relatively strong, rather sharp peaks at 1106 and 1260 cm^{-1} (the former with an unresolved shoulder near 1130 cm^{-1}); two broad, rounded peaks of lower intensity at 1378 and 1457 cm^{-1}; and weak features near 1030, 1173 and 1220 cm^{-1}. An extremely broad feature of varying intensity appears in all the spectra near 1863 cm^{-1}. Structure in the 2100 - 2300 cm^{-1} region can be resolved

into at least four features (at 2142, 2177, 2230 and 2252 cm^{-1}), while at least three rather intense features can be discerned between 2400 and 2500 cm^{-1} (approximately at 2407, 2437 and 2490 cm^{-1}). Although more individual peaks may exist in these areas, they cannot be resolved adequately due to overlap with other closely spaced features. Broad features also appear near 2930 and 3675 cm^{-1}.

Heating the $Zr(BH_4)_4/Al_2O_3$ system to 475 K produced a slight decrease in intensity for features in the 1000 - 1300 cm^{-1} region and for the unresolved structure between 480 and 580 cm^{-1}, with a concomitant enhancement of the 1378 and, especially, 1457 cm^{-1} peaks. This apparent enhancement might be due only to the changing shape of the background resulting from intensity decreases below 1300 cm^{-1}. Only a slightly raised background remains between 2140 and 2160 cm^{-1}. Features near 2407, 2437 and, particularly, 2490 cm^{-1} have decreased in intensity and appear only as a single very broad rounded feature, the highest point being near 2455 cm^{-1}.

Similar changes occur also when the supported complex is exposed to D_2 at 300 K, although both the increases and the decreases in intensity are more pronounced. Additionally, the 264 cm^{-1} peak is significantly reduced in intensity as is the peak at 910 cm^{-1}. Heating in D_2 to 475 K further reduces the intensity of the 910 cm^{-1} peak to a point where it is approximately equal in intensity to the 945 cm^{-1} feature. No structure above the normal background remains in the 480 - 580 cm^{-1} and 2140 - 2260 cm^{-1} regions. Intensity in the 2400 - 2500 cm^{-1} region is further reduced as are the intensities of peaks between 1000 and 1300 cm^{-1}, except for the 1260 cm^{-1} peak which has apparently experienced no additional intensity decrease.

Samples exposed to either H_2O or D_2O are characterized by a complete loss of structure in the 480 - 580 cm^{-1}, 1100 - 1250 cm^{-1} and 2100 - 2500 cm^{-1} regions. The 1260 cm^{-1} peak is reduced in intensity but is still present. The 910 cm^{-1} peak has been reduced to only a shoulder on the 945 cm^{-1} feature. The 264 cm^{-1} peak is greatly reduced. Enhancement of the 1450 cm^{-1} and, to a lesser extent, the 1380 cm^{-1} features might result only from the changing nature of the background (as mentioned earlier) rather than from an actual net increase in intensity. A new, broad, low-intensity feature might be present near 1300 cm^{-1} in both H_2O and D_2O samples. A broad peak near 2670 cm^{-1} appears in samples exposed to D_2O.

Discussion

As a first step in interpreting the spectra shown in Figs. 1 and 2, it is possible to identify those features not associated with the supported zirconium complex itself via comparisons with published spectra of "clean" aluminum oxide surfaces. On this basis, the following assignments can be made: the peak at 299 cm^{-1} is due to a phonon in the underlying Al film; the strong shoulder at 945 cm^{-1} is a bulk Al-O stretch, the weak feature near 1870 being the harmonic overtone of this peak; and features near 2930 and 3675 cm^{-1} can be assigned to the C-H stretch of contaminant hydrocarbons and the O-H stretch of surface hydroxyl groups, respectively (11). Additionally, various modes of hydrocarbon contaminants may also be contributing some intensity to features at 1030, 1378 and 1475 cm^{-1}, although other species also have characteristic transitions in these areas.

As a pure component, $Zr(BH_4)_4$ has been studied extensively by a variety of techniques, including X-ray (12) and electron (13) diffraction, and NMR (14,15), IR (15 - 19), Raman (16 - 20) and photoelectron (21) spectroscopies. An analysis of these results indicates that the boron atoms are arranged tetrahedrally around the central zirconium atom, each boron being bonded to the zirconium through three bridging hydrogen atoms (designated H_b), leaving a single terminal hydrogen (H_t). Among zirconium complexes, this type of tridentate bond appears to be restricted only to species with four BH_4 ligands. In related complexes such as $(C_5H_5)_2Zr(BH_4)_2$ and $(C_5H_5)_2Zr(H)BH_4$, the bonding between the zirconium and boron atoms is interpreted as being bidentate, i.e., occurring through only two bridging hydrogens (6,7,16). Bidentate hydrogen bridges are also formed in complex

anions such as $Li^{+}[Zr(BH_4)_5^{-}]$(7). No evidence for monodentate bonding has yet been presented.

During $Zr(BH_4)_4$ adsorption, one or more of the BH_4 ligands are displaced in order to accommodate zirconium-surface bonds (1). For supported complexes the surface becomes a virtual ligand, and can be expected to contribute both electronic and steric effects exerting an influence on the rest of the complex. Thus, we would not necessarily expect bonds between zirconium and the remaining BH_4 ligands to retain their unperturbed tridentate form; in fact, a bidentate structure would appear to be more probable. The nature of this bonding can be determined by examining the B-H stretching region of the spectrum, particularly vibrations involving the terminal hydrogens (H_t). For a tridentate bond, there is a single H_t atom, which has been shown to result in one peak between 2560 and 2580 cm^{-1} (15,17,19,20). The two H_t atoms in bidentate bonds produce two peaks, both a symmetric and an asymmetric stretch, which appear at lower energies (6,7,16). Figure 1 shows that at least three distinct features appear in the B-H_t stretching region, at 2407, 2437 and 2490 cm^{-1}. This observed energy range is compared in Fig. 3 with observed transitions for the tridentate $Zr(BH_4)_4$, as well as for a number of complexes with known bidentate structure. The observed transition energies indicate a bidentate structure. At the same time, the observation of more than two B-H_t stretching modes, as well as more than two modes for B-H_b stretching (at least four, at 2142, 2177, 2230 and 2252 cm^{-1}) suggests the presence of more than one type of complex on the surface. The most likely mode of adsorption of $Zr(BH_4)_4$ is by interacting with surface hydroxyl groups. Since the molecular nature of hydroxyl groups on the surface is not uniform, we might expect some

nonuniformity among adsorbed complexes (3). If we assume that the surface complexes have the same compositions (i.e., the same number and type of ligands, as well as identical bonding to the surface), however, then the nonuniformity of adsorption sites would generally result in a broadening of features in the vibrational spectrum rather than in the creation of additional features. It is probable, therefore, that the surface complexes do not have identical compositions.

Differences in composition can occur due to the possibility of zirconium atoms becoming either singly or multiply coordinated to surface oxygen atoms. On silica, adsorption of zirconium complexes with hydrocarbon and halogen ligands have been shown to produce both of the following surface species (2,3):

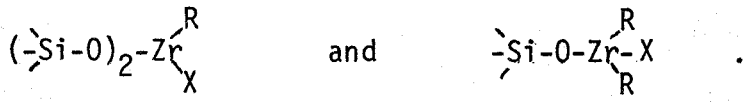

Similar results have been obtained on aluminum oxides (2). It has been reported also that the oxidation state of zirconium can change upon adsorption to yield species containing Zr(III) and, perhaps, even Zr(II) in addition to the more prevalent Zr(IV) (3,22). (The amount of Zr in the +3 oxidation state has been estimated to be several percent of the total Zr: see Ref. 3 and references therein.) Titration with H_2 of organozirconium compounds adsorbed on silica indicates that each zirconium atom on the average retains only 1.8 of its original four ligands (3). The presence of surface complexes with zirconium atoms both singly and multiply coordinated to surface oxygens, as well as both Zr(III) and Zr(IV) complexes, would undoubtedly result in multiple types of BH_4 ligands, corresponding

to the multiple bonds observed for both terminal and bridging boron-hydrogen stretching vibrations. These differences in zirconium-oxygen coordinations should be revealed in the vibrational spectra. Multiply coordinated species might be expected to have vibrational transitions similar to those in bulk zirconium oxides or in thin zirconium oxide films. Such transitions would produce a peak near 700 cm^{-1}, and possibly weaker features near 350 and 500 - 570 cm^{-1} (23). Alternately, complexes where the zirconium-oxygen bonds are not bulk-like, i.e., where there is only one Zr-O bond or where one of the Zr-O bonds possesses slightly more double bond character than any others in the same complex, vibrational frequencies would appear between 800 and 1000 cm^{-1} (24,25). [This same frequency range has been shown to apply also to similar types of bonds for Ti, Si, Mo, V and Cr oxide species (25,26).] Referring again to Fig. 1, peaks at 693 and 910 cm^{-1} can be assigned to these two types of zirconium-oxygen coordinations. (These peak positions also do not coincide with modes for any other proposed surface species.)

Although additional peaks in the B-H stretching region can be accounted for by surface complexes with different types of Zr-O coordination (and perhaps even different Zr oxidation states), there are other possible surface species which require consideration. During adsorption of $Zr(BH_4)_4$, displaced ligands might remain on the surface, becoming associated with either Al or O atoms. [$Al(BH_4)_3$ is well known and quite stable when not exposed to air, and also has bidentate hydrogen bridging (6).] Studies of diborane (B_2H_6) adsorption on Al_2O_3 have shown that adsorption is dissociative, resulting in formation of the following surface complexes (27):

(I) 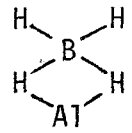 and (II) 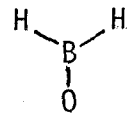 .

Similar complexes might be formed by displaced BH_4 ligands during $Zr(BH_4)_4$ adsorption. [The known slow decomposition of the zirconium complex at room temperature producing B_2H_6 presents another possible source for the above surface species (28).] The B-H vibrations in these species would not produce unique features in the spectra (see Fig. 3). Species II, however, might produce unique features due to B-O vibrations. Comparison with IR studies of B_2H_6 adsorption on Al_2O_3 (27) and with vibrational studies for a number of compounds containing B-O bonds (29 - 33) indicates that B-O vibrations would appear in the 1200 - 1450 cm^{-1} range. The peaks appearing near 1378 and 1457 cm^{-1} might therefore be assigned to B-O vibrations. A B-O vibration might also be contributing to the peak at 1260 cm^{-1}, although this peak also falls in the range where B-H deformations are expected to appear (1000 - 1300 cm^{-1}). One report has alternately assigned the 1457 cm^{-1} peak to a BH_4 deformation mode. The remaining peak in the spectrum for adsorbed $Zr(BH_4)_4$ at 300 K appears at 264 cm^{-1}, and can be assigned to BH_4-Zr-BH_4 bending and/or Zr-BH_4 torsional modes. Features at 323 and 480 - 580 cm^{-1}, regions where various weak Zr-O modes could possibly be expected, might also reflect Zr-BH_4 torsional and stretching modes, respectively (18).

Decomposition of zirconium borohydrides, which occurs only slowly at 300 K, proceeds rapidly above approximately 450 K evolving mainly H_2 (28).

Adsorption on Al_2O_3 apparently stabilizes the complex somewhat. Examination of the spectrum for supported $Zr(BH_4)_4$ heated to 475 K (see Fig. 2) indicates that although B-H deformation and stretching modes are all reduced in intensity, some of the B-H bonds remain intact. This is in agreement with other studies which indicate enhanced thermal stability for complexes grafted onto supports (3). Only very low intensity, unresolved structure remains in the $B\text{-}H_b$ stretching region. The change in shape of the $B\text{-}H_t$ stretching features indicates that surface species characterized by modes in the 2470 - 2500 cm^{-1} region are more sensitive to heat than are species with the lower energy $B\text{-}H_t$ stretching vibrations.

Zirconium and aluminum borohydrides, as well as diborane and other BH compounds, are easily hydrolyzed even at room temperature (6). Spectra for the supported zirconium complex exposed to D_2O at both 300 K and 475 K (see Fig. 2) are devoid of any B-H stretching features; neither are there any new features which might be attributed to B-D modes. The absence of any possible exchange features is confirmed by comparison to the spectrum shown for H_2O exposure at 475 K, which is identical to the D_2O spectra except for a new peak near 2670 cm^{-1} in the case of D_2O. This feature can readily be assigned to the O-D stretch of surface deuteroxyl groups (11), but since D_2O readily exchanges with hydroxyls on Al_2O_3 it is indeterminant whether the observed OD groups are attached to Zr or Al. It is important to note that the 910 cm^{-1} peak has been reduced to only a very weak shoulder on the 945 cm^{-1} feature (assigned to the bulk Al-O stretch). This is in agreement with our previous assignment of the 910 cm^{-1} feature to a Zr-O stretch for a singly coordinated (or similar type) Zr

atom, the band disappearing as further oxidation of Zr occurs during exposure to water vapor. Features at 1106, 1130, 1173 and 1220 cm^{-1}, attributed to BH_4 deformation modes, are also missing in the samples exposed to water vapor, as is the peak at 264 ($Zr-BH_4$ bending and/or torsional modes). The peak at 1260 cm^{-1} is significantly reduced, but a weak feature still remains at this energy. This supports the assignment of this peak as a combination of B-O stretching and BH_4 deformation modes. Peaks at 1378 and 1457 cm^{-1} which were additionally ascribed to B-O modes remain also after hydrolysis, supporting their previous assignments. These peaks, especially the one at 1457 cm^{-1}, show apparent intensity increases upon exposure to water vapor, although (as discussed earlier) this might be in large part only due to the change in slope of the background in this region. There is a possible increase in intensity near 1300 cm^{-1}, although this is indefinite due to the other overlapping features near this energy. It could arise from new types of B-O vibrations. A less likely assignment would be a Zr-H-Zr mode for incompletely oxidized zirconium atoms. These modes occur between 1240 and 1520 cm^{-1}, and have been observed to form in solutions of a number of complexes containing both Zr and H, as well as during the partial thermolysis of some zirconium borohydrides (19,22).

Exposure to D_2 fails to produce any exchange with BH groups. Although BH_4 groups are being displaced as evidenced by intensity decreases in all regions of the spectrum where B-H or $Zr-BH_4$ modes appear, there is no firm evidence for a new Zr-D or Zr-H stretching peak [expected near 1150 (34) or 1625 (3,16,19) cm^{-1}, respectively]. This might be due either to the formation of Zr-H-Zr (or Zr-D-Zr) species as mentioned above, or to

oxidation by slight traces of O_2 or H_2O contamination. The decreasing intensity of the 910 cm^{-1} peak tends to indicate further oxidation, although the formation of Zr-H-Zr species might also be affecting this type of Zr-O bond. It is important to note that, especially for D_2 exposure at 475 K, some B-H_t bonds remain even though there are no B-H_b bonds left. This tends to confirm the presence of O-BH_2 species on the surface. That these groups are more stable with respect to both heating and reaction than other BH species on the surface is in agreement with previous reports (27).

Conclusions

Examination of vibrational spectra obtained via IETS for Al_2O_3-supported $Zr(BH_4)_4$ reveals that during the initial adsorption a variety of surface species are formed. BH_4 ligands remaining attached to zirconium atoms, as well as any which migrate onto the support and bond to surface aluminum, change from a tridentate to a bidentate bonding geometry. Additional peaks in both the B-H_b and B-H_t stretching regions as well as two types of Zr-O stretching features indicate the nonuniformity of the surface species. The presence of O-BH_2 groups is confirmed both by the appearance of B-O vibrational modes and by the existence of B-H_t stretching modes without accompanying B-H_b vibrations. Hydrolysis occurs readily, even at 300 K. Its effects on the existing Zr-O bonds are observed in the decrease of a peak ascribed to Zr atoms singly coordinated to surface oxygen. No exchange was observed between the supported complex and either D_2 or D_2O. Vibrational modes throughout the 240 - 4000 cm^{-1} range were clearly observed. The successful application of IETS in this study not only demonstrates the versatility of the technique, but more importantly provides useful structural information on a type of system (i.e., a supported complex) which is becoming increasingly important in industrial catalytic processes.

Acknowledgments

We express our appreciation to Drs. F. N. Tebbe and L. E. Firment for supplying the $Zr(BH_4)_4$, as well as for providing much information concerning the handling and many useful suggestions. We also wish to thank Professor

R. H. Grubbs for fruitful discussions. This research was supported by the National Science Foundation under Grant No. ENG78-16927. Additional support from the Camille and Henry Dreyfus Foundation in the form of a Teacher-Scholar Award to WHW is also greatly appreciated.

References

1. Basset, J. M.; Smith, A. K. in "Fundamental Research in Homogeneous Catalysis" (M. Tsutsui and R. Ugo, ed.); Plenum Press: New York, N.Y., 1977; pp. 69-98.
2. Ballard, D. G. H. J. Polymer Sci. 1975, 13, 2191-2212.
3. Zakharov, V. A.; Yermakov, Yu. I. Catal. Rev.-Sci. Eng. 1979, 19, 67-103.
4. Basset, J. M.; Norton, J. in "Fundamental Research in Homogeneous Catalysis" (M. Tsutsui and R. Ugo, ed.); Plenum Press: New York, N. Y., 1977; pp. 215-224.
5. Evans, H. E.; Weinberg, W. H., submitted to J. Am. Chem. Soc.
6. James, B. D.; Wallbridge, M. G. H. Prog. Inorg. Chem. 1970, 11, 99-231.
7. Marks, T. J.; Kolb, J. R. Chem. Rev. 1977, 77, 263-293.
8. Lambe, J.; Jaklevic, R. C. Phys. Rev. 1968, 165, 821-832.
9. Bowser, W. M.; Weinberg, W. H. Rev. Sci. Instrum. 1976, 47, 583-586.
10. Weinberg, W. H. Ann. Rev. Phys. Chem. 1978, 29, 115-139.
11. Bowser, W. M.; Weinberg, W. H. Surface Sci. 1977, 64, 377-392.
12. Bird, P. H.; Churchill, M. R. Chem. Commun. 1967, 403.
13. Plato, V.; Hedberg, K. Inorg. Chem. 1971, 10, 590-594.
14. Marks, T. J.; Shimp, L. A. J. Am. Chem. Soc. 1972, 94, 1542-1550.
15. James, B. D.; Nanda, R. K.; Wallbridge, M. G. H. J. Chem. Soc. (A) 1966, 182-184.
16. Marks, T. J.; Kennelly, W. J.; Kolb, J. R.; Shimp, L. A. Inorg. Chem. 1972, 11, 2540-2546.
17. Davies, N.; Wallbridge, M. G. H; Smith, B. E.; James, B. D. J. Chem. Soc. Dalton Trans. 1973, 162-165.

18. James, B. D.; Smith, B. E.; Shurwell, H. F. J. Mol. Struc. 1976, 33, 91-95.

19. Smith, B. E.; Shurwell, H. F.; James, B. D. J. Chem. Soc. Dalton Trans. 1978, 710-722.

20. Smith, B. E.; James, B. D. Inorg. Nucl. Chem. Letters 1971, 7, 857-859.

21. Downs, A. J.; Egdell, R. G.; Orchard, A. F.; Thomas, P. D. P. J. Chem. Soc. Dalton Trans. 1978, 1755-1761.

22. Marks, T. J.; Kolb, J. R. J. Am. Chem. Soc. 1975, 97, 3397-3401.

23. Maekawa, T.; Tereda, M. Trans. Japan Inst. Metals 1963, 4, 57-59.

24. Ozin, G. A. in "Vibrational Spectroscopy of Trapped Species" (H. E. Hallum, ed.); Wiley and Sons: London, 1973; pp. 237-244.

25. Barraclough, C. G.; Lewis, J.; Nyholm, R. S. J. Chem. Soc. 1959, 3552-3555.

26. Zeitler, V. A.; Brown, C. A. J. Phys. Chem. 1957, 61, 1174-1177.

27. Matsuda, T.; Kawashima, H. J. Catal. 1977, 49, 141-149.

28. Smith, B. E.; James, B. D.; Dilts, J. A. J. Inorg. Nucl. Chem. 1976, 38, 1973-1978.

29. Lehmann, W. J.; Onak, T. P.; Shapiro, I. J. Chem. Phys. 1959, 30, 1215-1218, 1219-1222.

30. Lehmann, W. J.; Weiss, H. G.; Shapiro, I. J. Chem. Phys. 1959, 30, 1222-1226, 1226-1231.

31. Brame, E. G., Jr.; Margrave, J. L.; Meloche, V. W. J. Inorg. Nucl. Chem. 1957, 5, 48-52.

32. Bellamy, L. J.; Gerrard, W.; Lappert, M. F; Williams, R. L. J. Chem. Soc. 1958, 2412-2415.

33. Lehmann, W. J.; Shapiro, I. Spectrochimica Acta 1961, 17, 396-411.

34. Flotow, H. E.; Osborne, D. W. J. Chem. Phys. 1961, 34, 1418-1425.

Table 1: Peak Positions in cm^{-1} for $Zr(BH_4)_4$ Supported on Al_2O_3.

In Vacuum		Exposed to D_2		Exposed to D_2O or H_2O		Assignments
300 K	475 K	300 K	475 K	300 K	475 K	
264	264	264	264			BH_4-Zr-BH_4 bend or Zr-BH_4 torsion
299	299	299	299	299	299	Al phonon
323	323	323	323	323	323	Metal-oxide or Zr-BH_4 torsion
480-580	480-580					Zr-BH_4 stretch or Zr-O modes
693	685	705	693	693	695	Zr-O stretch
910	910	910	910	possible sh near 910		Zr-O stretch
945	945	945	945	942	942	Bulk Al-O stretch
1027		1056	1056	1048	1048	CH bend (contamination)
1106	1106	1114	1114			BH deformation
1130	1121					
1173	1165	1165	1170			
1220	1214					
1260	1252	1257 (possible weak feature near 1300)	1260	1258	1258	BH deformation and B-O stretch
1378	1378	1378	1385	1374	1380	B-O modes
1457	1457	1457	1457	1450	1450	
1870	1873	1868	1870	1870	1870	Harmonic of 945 cm^{-1}
2142						Bridging B-H stretch
2177	2137-2258 (weak-broad)					
2230						
2252						
2407						Terminal B-H stretch
2437	2455 (broad)	2455 (broad)	2455 (broad)			
2490						
				2670	2670 (D_2O only)	O-D stretch
2930	2930	2930	2930	2930	2930	CH stretch (contamination)
				3615	3615 (D_2O)	O-H stretch for D_2O exposure only
3675	3675	3669	3669	3640	3640 (H_2O)	O-H stretch for all other samples

Figure Captions

Fig. 1: IET spectrum for $Zr(BH_4)_4$ adsorbed on Al_2O_3 at 300 K over the spectral ranges (a) 240 to 2000 cm^{-1}, and (b) 2000 to 4000 cm^{-1}.

Fig. 2: IET spectra over the range 240 to 4000 cm^{-1} for $Zr(BH_4)_4$, designated "ZBH", adsorbed on Al_2O_3 at 300 K and 475 K, and for the supported complex after exposure to D_2, D_2O and H_2O at the same temperatures.

Fig. 3: Comparison of both terminal (H_t) and bridging (H_b) B-H stretching frequencies for $Zr(BH_4)_4$ supported on Al_2O_3 with the corresponding vibrations for $Zr(BH_4)_4$ (Ref. 17); $Al(BH_4)_3 \cdot L$, where L is a coordination ligand (Ref. 6); $Al(BH_4)_3$ (Ref. 6); AlH_2BH_2, resulting from diborane adsorption on Al_2O_3 (Ref. 27); and $(C_5H_5)_2Zr(BH_4)_4$ (Ref. 28).

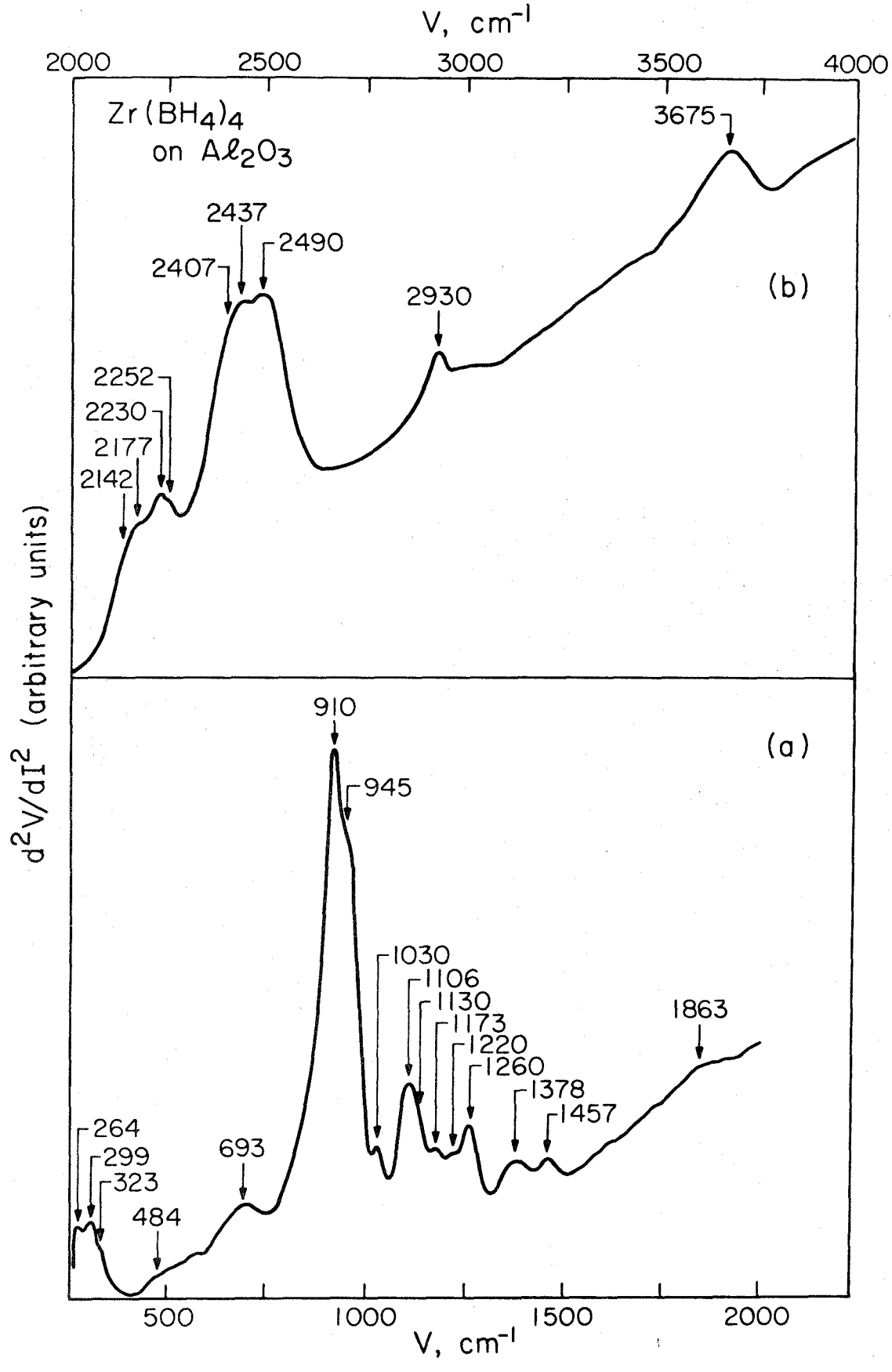
V, cm-1
2000
2500
3000
3500
4000
Zr(BH4)4
on Aℓ2O3
3675
2437
2490
2407
2930
(b)
2252
2230
2177
2142
d2V/dI2 (arbitrary units)
910
(a)
945
1030
1106
1130
1173
1220
1260
1378
1457
1863
264
299
323
484
693
500
1000
1500
2000
V, cm-1

Figure 1

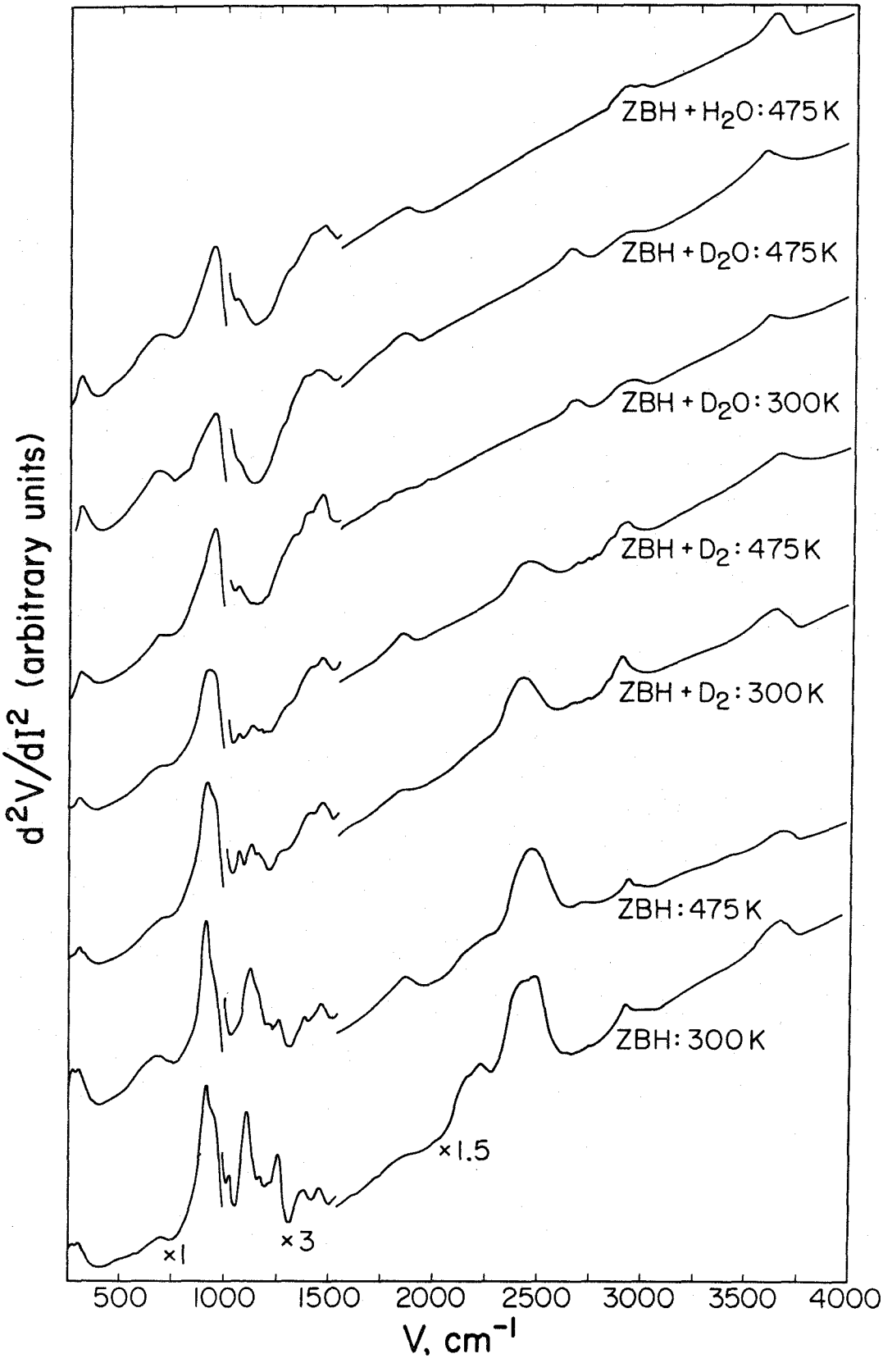
ZBH + H2O: 475 K
ZBH + D2O: 475 K
ZBH + D2O: 300 K
ZBH + D2: 475 K
ZBH + D2: 300 K
ZBH: 475 K
ZBH: 300 K
×1
×3
×1.5
d²V/dI² (arbitrary units)
500
1000
1500
2000
2500
3000
3500
4000
V, cm⁻¹

Figure 2

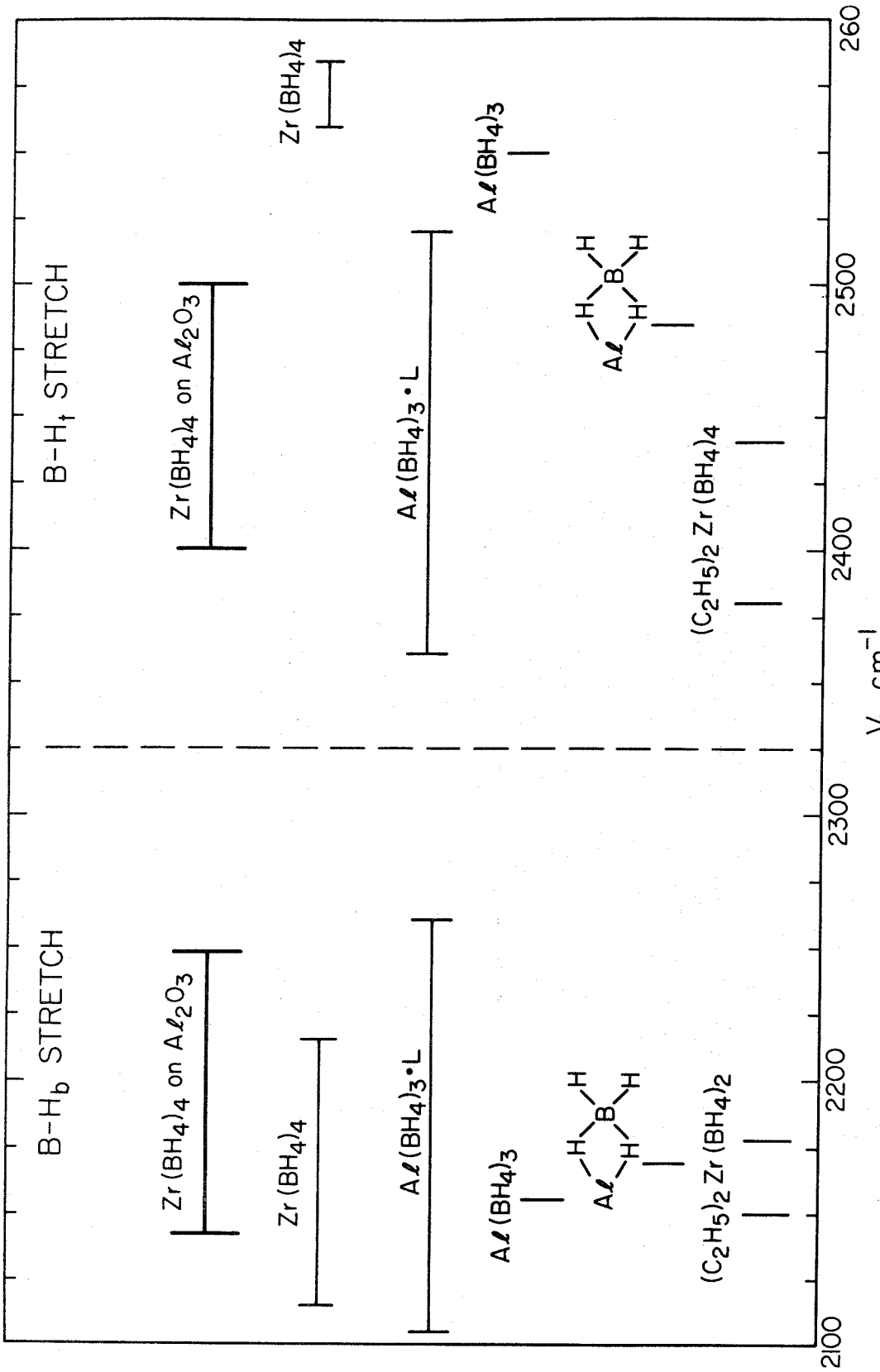
B-H$_b$ STRETCH
B-H$_t$ STRETCH
Zr(BH$_4$)$_4$ on Aℓ$_2$O$_3$
Zr(BH$_4$)$_4$
Aℓ(BH$_4$)$_3$·L
Aℓ(BH$_4$)$_3$
(C$_2$H$_5$)$_2$Zr(BH$_4$)$_2$
Zr(BH$_4$)$_4$ on Aℓ$_2$O$_3$
Zr(BH$_4$)$_4$
Aℓ(BH$_4$)$_3$·L
Aℓ(BH$_4$)$_3$
(C$_2$H$_5$)$_2$Zr(BH$_4$)$_4$
2100
2200
2300
2400
2500
2600
V, cm^{-1}

Figure 3

Chapter VIII

Interactions of Ethylene, Propylene and Acetylene with Zirconium Tetraborohydride Supported on Alumina

Abstract

Supported complexes, formed by grafting homogeneous catalysts onto support materials, are becoming increasingly important in industrial applications as well as in fundamental studies. Little information is available, however, about the structures of supported complexes and the nature of their interactions with reactants. Inelastic electron tunneling spectroscopy (IETS) has here been applied to obtain vibrational spectra of $Zr(BH_4)_4/Al_2O_3$, a known polymerization catalyst for olefins, exposed to ethylene, propylene and acetylene. These gas-surface interactions have been investigated for hydrocarbon exposures up to 6×10^3 torr-sec and for temperatures between 300 and 575 K. The IET spectra (observed over the entire range from 240 to 4000 cm^{-1}) provide information regarding the types of C-C and C-H bonds present in the various surface species. Polymer formation is also revealed in the vibrational spectra. The versatility of IETS is demonstrated explicitly by providing valuable new information on a unique catalytic system of significant importance.

Introduction

In the preceeding paper (1), and in an earlier communication (2), inelastic electron tunneling spectroscopy (IETS) has been utilized to probe the vibrational structure of $Zr(BH_4)_4$ (zirconium tetraborohydride) adsorbed on aluminum oxide. The behavior of the supported zirconium complex was observed also as a function of temperature, and for exposures to D_2, D_2O and H_2O. Metal borohydride compounds have been of considerable interest due both to the unique types of M-H-B bonds existing in such molecules and, more importantly, due to their ability to catalyze polymerization reactions of olefins (3). The rate of olefin polymerization by any individual complex, however, is relatively low compared to traditional Ziegler-Natta type catalysts (4). Over the past several years, there has been a rapidly growing interest in the field of "supported homogeneous catalysts", catalysts formed by grafting homogeneous catalytic compounds onto support materials. These supported complexes exhibit many of the desirable features of both homogeneous and heterogeneous catalysts: they combine the greater stability and ease of separation from products characteristic of heterogeneous systems with the ability of homogeneous catalysts to be tailored selectively to fit specific reactions in a more logical and easier fashion. Research in this area has received significant impetus by the observation that grafting onto a support can increase the catalytic activity of a complex by several orders of magnitude (4). In addition, supported complexes have been noted to produce higher degrees of crystallinity than obtained in homogeneous polymerization reactions, as the presence of the surface limits access to central metal centers and

thereby establishes an orientation preference. Partial control of the degree of crystallinity can be obtained by varying the surface concentration of supported complexes, as crowding metal centers together on the surface can limit access even further (5). (This does, however, reduce activity somewhat.) Supported complexes are already being utilized in a number of important industrial processes and, as a group, offer more promise from an applied point of view than other currently known types of catalysts (6). Progress in the area of catalysis by supported complexes, however, has unfortunately been hindered by the lack of structural information available for the surface species (6,7). Structural characterization of supported complexes has been very poor, plagued by many problems similar to those encountered in attempting to characterize the surfaces of traditional heterogeneous systems (8).

The current study represents part of an ongoing effort to provide new structural information concerning supported-complex catalytic systems by utilizing an experimental probe not previously exploited in this area of research. Specifically, we have applied inelastic electron tunneling spectroscopy to obtain vibrational spectra for acetylene (C_2H_2), ethylene (C_2H_4) and propylene (C_3H_6) on alumina-supported $Zr(BH_4)_4$. Aspects of our experimental procedures unique to the current study are presented in the next section, which will be followed by presentation and, then, discussion of the results. This report will be concluded by a brief summary of some of the important results and conclusions presented herein.

Experimental Details

Inelastic electron tunneling spectroscopy (IETS) has been shown to be

an effective means of monitoring the vibrational structure of molecules on or near insulating surfaces (9). In our application of the IETS technique, aluminum oxide surfaces were prepared in a vacuum system with a base pressure on the order of 10^{-7} torr by oxidizing the top few atomic layers of freshly evaporated aluminum films. The resultant oxide surfaces were then exposed to 5 x 10^{-2} torr of $Zr(BH_4)_4$ for 15 minutes at 300 K. [These exposure conditions were sufficient to produce a saturation coverage of the zirconium complex on the surface as discussed previously (1).] The supported zirconium complex was then allowed to interact with C_2H_2, C_2H_4 or C_3H_6. The effects of exposure (i.e., the pressure-time product) and temperature were examined for each of the hydrocarbon species. Heating was accomplished by means of a technique devised by Bowser and Weinberg (10) specifically for the resistive heating and simultaneous temperature measurement of thin films. IET spectra are typically presented in the form of a plot of d^2V/dI^2 (proportional to d^2I/dV^2) as a function of V, where I is the current due to electrons tunneling through the thin aluminum oxide layer from the underlying Al film to a Pb electrode placed on top of the sample, and V is the value of the bias voltage across the aluminum oxide barrier between the Al and Pb electrodes. As electrons tunnel through the insulating barrier, a few lose energy (i.e., tunnel "inelastically") by exciting vibrational modes of molecules in or near the barrier region. These inelastic tunneling electrons cause changes in the conductance of the Al-Al_2O_3-Pb junction which appear as peaks in the d^2V/dI^2 - V plots. The positions of these peaks correspond to vibrational excitation energies of molecules adsorbed on the oxide surface, as well as to vibrational modes of the

oxide layer itself. Spectra obtained in this manner have been shown to be analogous to vibrational spectra obtained via infrared and Raman spectroscopies (9). Spectral measurements were performed over the range 240 - 4000 cm^{-1}, with a resolution of approximately 4 cm^{-1}. A thorough description of both the theoretical and experimental aspects of our IETS experiments is available elsewhere (11).

Results

Spectral measurements were performed for samples of supported $Zr(BH_4)_4$ exposed to ethylene at exposures from 15 torr-sec (5×10^{-2} torr of C_2H_4 for 300 sec) to greater than 6×10^3 torr-sec (5 torr for 1200 sec), and at various temperatures between 300 and 575 K. Very little adsorption, with no resolvable structure above background contamination, was noted for lower exposures. Furthermore, no C_2H_4 adsorbs on the base Al_2O_3 under these experimental conditions. This is also true for both C_3H_6 and C_2H_2. Saturation coverage was obtained at all temperatures with exposures of 3×10^3 torr-sec, as judged by the lack of any further spectral changes at higher exposures. No reproducible shifts in peak positions were observed as a function of coverage. Spectra obtained for saturation coverages of C_2H_4 at 300, 400, 450 and 575 K are shown in Fig. 1. Peak positions are listed in Table 1. Increasing temperatures are accompanied by increases in intensity for spectral features between 2850 and 3000 cm^{-1}, at 1380 and 1455 cm^{-1}, and the appearance of a new feature near 1300 cm^{-1}. Apparent (small) shifts seen for peaks between 2850 - 3000 cm^{-1} are probably only due to the difficulty of accurately locating positions for several overlapping, closely spaced features. A feature at approximately 1870 cm^{-1}

also grows slightly with temperature. Alternately, modes appearing near 1106, 1130, 1169 and 1218 cm^{-1} decrease as the temperature is raised, the 1169 and 1218 features not being apparent at 575 K. The intensity of features between 2100 and 2300 cm^{-1} shows corresponding decreases, no structure in this spectral region being observed above 450 K. Distinct features near 2406, 2435 and 2486 cm^{-1} at 300 K also decrease with temperature, the peak at 2486 more rapidly than the others. Above 450 K, separate peaks can no longer be resolved in this spectral region; remaining structure appears only as a broad, rounded feature centered near 2440 cm^{-1}. The feature at 3672 cm^{-1} at 300 K shifts approximately 30 cm^{-1} to 3641 cm^{-1} at 575 K.

Results for saturation exposures of propylene to the supported $Zr(BH_4)_4$ at 300, 400 and 575 K are illustrated in Fig. 2, peak positions being recorded also in Table 1. As is the case with ethylene, increases in intensity for features at 2850 - 3000, 1378 and 1449 cm^{-1} accompany increasing temperature. Also, analogous to ethylene adsorption, there are intensity decreases observed for features near 1100 - 1250, 2100 - 2300 and 2400 - 2500 cm^{-1} with increasing temperature; however, loss of intensity in these regions is perhaps not so great as with ethylene. Of particular interest is the observation of a peak at 2501 cm^{-1}, which is more intense than others in the 2400 - 2500 cm^{-1} region. (If a similar feature is present in the ethylene spectra, it is only a shoulder and not such a prominent peak as in the case of propylene.) Also of interest is the appearance of a feature near 1342 cm^{-1}, and a shift similar to that observed in the ethylene spectra of the feature at 3669 cm^{-1} (at 300 K) to 3625 cm^{-1} (575 K).

Acetylene adsorption exhibited different behavior than either ethylene or propylene. Spectra for 3×10^2 torr-sec exposure of acetylene at 300 and 400 K are shown in Fig. 3. At higher temperatures, the concentration of hydrocarbon species on the surface increased rapidly with no apparent saturation limit. Hydrocarbon concentration can be monitored approximately by measuring the resistance of the aluminum oxide-plus-adsorbed species insulating layer between the Al and Pb electrodes. Samples producing usable spectra typically fall in the 30 - 200 Ω range (for an area of approximately 1 mm^2), since these exhibit the best signal/noise ratios utilizing our electronics. The thickness of the oxide layer can be controlled by varying the O_2 plasma discharge parameters (principally time), and the resistance of samples with various adsorbate concentrations can thus be adjusted to fall within this range. No samples with acetylene exposures above 400 K could be prepared with resistance below several kilohms. (Exposures, unfortunately, could not be reduced below 5 torr-sec using our current pressure monitoring system.) The intensity of the features in the 2850 - 3000 cm^{-1} region for acetylene is comparable to that observed for propylene and significantly greater than that observed for ethylene. Intensity decreases in the 1100 - 1250, 2150 - 2300 and 2400 - 2500 cm^{-1} regions are not so great for acetylene exposures as for the other two hydrocarbons. Structure in the 2400 - 2500 cm^{-1} region is similar in appearance to that observed for propylene, the most prominent feature being a peak at 2505 cm^{-1} (at 300 K). A peak at 2978 cm^{-1} is approximately 20 cm^{-1} higher in energy than corresponding features for ethylene and propylene. There is a small feature appearing near 1351 cm^{-1}, which possibly corresponds to features near 1302 and 1342 cm^{-1} for

ethylene and propylene, respectively. Two well-resolved peaks can be seen at 485 and 573 cm^{-1}. Although there is weak structure in the 480 - 580 cm^{-1} region for both ethylene and propylene, it is weaker than for acetylene and cannot be resolved clearly. A weak feature is present near 1613 cm^{-1}. No shift of the 3677 cm^{-1} peak with temperature is observed, although this is to be expected since shifts observed for this peak in the spectra of adsorbed ethylene and propylene were not continuous and appeared only at higher temperatures.

It should be reiterated that hydrocarbon adsorption was not observed for exposures of acetylene, ethylene or propylene to aluminum oxide surfaces with no pre-adsorbed $Zr(BH_4)_4$. This is in agreement with a previous IR study which also failed to observe ethylene or propylene adsorption on alumina (12). No hydrocarbon contamination is observed for "clean" Al_2O_3 surfaces. The amount of contamination observed on the supported complex without deliberate exposure to hydrocarbons can be observed in previously published spectra (1) and in Fig. 4 (which is discussed in the following section).

Discussion

Figure 4 shows the spectrum of $Zr(BH_4)_4$ supported on Al_2O_3 at 300 K, together with a listing of observed peak positions. This spectrum has been analyzed in detail in the preceding paper (1). Spectral details were interpreted in terms of a number of distinct surface species, the presence of more than one type of surface species being confirmed particularly by multiple peaks appearing in the B-H stretching region beyond the number that could be assigned to a single, uniform type of surface

complex. When the zirconium complex adsorbs on the surfaces, one or more BH_4 ligands are displaced as the zirconium atom becomes coordinated to one or more surface oxygens (4,5). The number of ligands displaced can be greater than the number of Zr-O bonds formed, since the oxidation state of zirconium can change upon adsorption, for example in going from Zr(IV) to Zr(III) . Such phenomena have been observed previously for similar complexes (4,13). Features appearing at 693 and 910 cm^{-1} have been assigned, respectively, to a bulk-like Zr-O stretch and the corresponding mode for Zr less highly coordinated (e.g., singly coordinated) with oxygen atoms. Since the surface becomes a virtual ligand for the adsorbed complex, the nature of Zr-O bonding can be expected to affect bond properties in the other ligands as well (8), producing multiple surface BH species, as observed. An additional effect of the surface becoming a ligand relates to the mode of bonding between remaining BH_4 groups and the central zirconium atom. Bonding between the metal and boron atoms in metal borohydrides has been found to occur through bridging hydrogen atoms (3). The energies at which both bridging (H_b) and terminal (H_t) hydrogen stretching modes appear in the supported zirconium complex are indicative of bidenate bonds (i.e., two bridging and two terminal hydrogens), as opposed to the tridentate bonds (three bridging and one terminal hydrogen) occurring in pure $Zr(BH_4)_4$. This behavior is not unexpected for cases where BH_4 is replaced by a new ligand (1). When attempting to account for the variety of surface species, the effects of possible ligand migration onto the support must also be considered (8). Rather than merely desorbing, displaced BH_4 groups might remain on the surface as

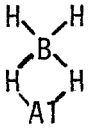

and/or

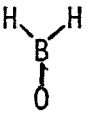

.

These surface species have been reported to occur during adsorption of diborane (B_2H_6) on alumina (12). Although unique characterization of the AlH_2BH_2 species is restricted by overlap with features of adsorbed $Zr(BH_4)_4$, the presence of the OBH_2 species has been determined by the peak at 1378 cm^{-1} which has been assigned to a B-O vibration (12). At least part of the intensity at 1260 cm^{-1} (some intensity also being contributed from BH modes) and (possibly) at 1457 cm^{-1} can also be related to B-O vibrations (1,12). Remaining spectral features are assigned to BH deformations (1100 - 1300 cm^{-1}); Zr-BH_4 stretching (480 - 580 cm^{-1}), bending and torsional modes (264 and 323 cm^{-1}); phonons in the underlying Al film (299 cm^{-1}); bulk Al-O stretching vibrations (945 cm^{-1}) and harmonic overtones (1863 cm^{-1}); the O-H stretch of surface hydroxyl groups (3675 cm^{-1}); possible, weak contributions from contaminant hydrocarbon bending and deformation modes near 1030 and 1300 - 1500 cm^{-1}, and the stronger contaminant C-H stretching peak near 2930 cm^{-1}. [See Ref. (1), and references therein.]

Unsaturated hydrocarbons can be expected to interact with many, if not all, of the various types of surface species formed during $Zr(BH_4)_4$ adsorption. This has been confirmed for the AlH_2BH_2 and OBH_2 species in a study of olefins interacting with adsorbed diborane (12). Supported zirconium complexes, particularly those supported on Al_2O_3, are known to be active for the polymerization of olefins. Group VIII transition metals,

on the other hand, readily form complexes with olefins but make poor polymerization catalysts. This difference in polymerization activity between zirconium and group VIII metals is attributed to the weaker interaction of olefins with zirconium (5). Zirconium has few, if any (depending on the oxidation state), d-electrons for back donation to olefins. Therefore, only a relatively weak Lewis acid-Lewis base type interaction occurs. [Zr^{4+} has been observed in other studies to function as a strong Lewis acid (3).] This type of interaction allows for the formation of nonlinear π-complexes as olefins become coordinated to zirconium atoms. This coordination, without displacing additional ligands from the supported complex, is generally considered to be the first step in the polymerization process. The next step is insertion of the hydrocarbon between the zirconium atom and one of its remaining ligands. Repeated coordination and insertion of other olefin molecules creates a polymer chain. It has been postulated that only hydrogen ligands form active centers for polymerization (5). BH_4 groups could also have several functions in such a reaction scheme, e.g., providing a source of hydrogen (forming Zr-H active centers), providng a variable coordination sphere for the zirconium, or exerting some activating influence on other ligands.

The observed behavior of acetylene exposed to $Zr(BH_4)_4/Al_2O_3$ can be explained consistently by the formation of polyacetylene on the surface. There are no corresponding definite indications of polymer formation resulting from ethylene and propylene exposures. These conclusions are based partly on the observed adsorption characteristics and also on comparisons of the vibrational spectra observed here to published results for saturated and unsaturated hydrocarbons (14,15), polyethylene (16 - 19), polypropylene

(19 - 21) and polyacetylene (22).

The polymerization of acetylene is of significant interest and importance due to the recently discovered electrical conductivity properties of doped polyacetylenes [see, for example, Refs. (23,24), and references therein]. Perhaps the most obvious indication of polymer formation in the case of acetylene is its continuous adsorption without reaching saturation coverage under the exposure/temperature conditions studied here. On the other hand, the observed rapid attainment of saturation coverages for ethylene and propylene indicates no extensive formation of polymers on the surface. It is possible that conditions are such as to foster only the growth of short chains, which undergo frequent separation from the surface via hydrogenolysis. More likely is a lack of polymerization centers which are sufficiently active to promote continued reaction under the conditions which we employed. High surface concentrations of zirconium complexes might be a factor (as discussed above), with coordination of even a limited number of olefins creating steric barriers preventing further olefin coordination at the active centers. The observed slight increase in hydrocarbon concentration with temperature would then occur as a few new active centers (Zr-H) are formed, or as some olefin molecules become energetic enough to displace BH ligands or overcome steric effects which previously blocked active sites.

Analysis of the hydrocarbon stretching and deformation modes can be expected to yield information about the nature of the various surface species. The fact that many different types of CH groups can produce peaks in similar spectral areas definitely complicates interpretation of the spectra. As noted above, the interpretations and conclusions presented

here are those which appear to reflect all of the observed data in the most consistent manner, although other interpretations might be possible. A more detailed view than is available in the other figures of the spectral region between 2000 and 3300 cm^{-1} is shown in Fig. 5. This includes the C-H stretching region (2850 - 3000 cm^{-1}), and compares spectra of ethylene, acetylene and propylene exposed to the supported complex at 300 K. Although more than one type of surface species might be expected due to the inhomogeneity of the $Zr(BH_4)_4/Al_2O_3$ surface, the number of observed C-H stretching modes (four each for ethylene and propylene, two plus a possible, weak shoulder for acetylene) is inconclusive in determining the number of possible surface hydrocarbon species. For example, up to four distinct modes can be observed for a single type of saturated hydrocarbon containing both CH_2 and CH_3 groups; while, alternately, degeneracies and loss of distinct structure due to inadequate resolution of closely spaced features can lead to fewer observed peaks for other molecules which also contain CH_2 and CH_3 functional groups (14). More definite information can be expected from examining the peak positions. Surface species formed from ethylene and propylene are saturated hydrocarbons as judged from the absence of a C=C stretch near 1600 cm^{-1}. This is also expected based on the postulated adsorption mechanism of insertion as discussed above. (Insertion reactions can occur with the aluminum borohydride and OBH_2 species, as well as with zirconium complexes.) C-H stretching features (a combination of both CH_3 and CH_2) would thus be anticipated between approximately 2860 and 2960 cm^{-1}, with corresponding deformation modes near 1450, 1375 and 1350 - 1150 cm^{-1} (14). This correlates well with features observed at 2879 - 2960, 1455, 1383 and 1302 cm^{-1} for ethylene; and at 2863 - 2952, 1449,

1378 and 1342 cm^{-1} for propylene.

Polyacetylene has a conjugated double bond skeletal structure as shown:

$$-C=C-C=C-C=C-\ ,$$

each carbon atom along the chain being attached to a single hydrogen (22). Polymer formed here by acetylene adsorption on $Zr(BH_4)_4/Al_2O_3$ might consist of relatively short or highly branched chains, or might have a double bond: single bond ratio less than one (i.e., imperfections in the conjugated skeletal structure). Such situations could lead to a non-negligible population of $-CH_2-$ and/or $=CH_2$ groups which would also contribute to the observed spectra. (Formation of CH_3 groups is unlikely as they would require a significant source of hydrogen.) The presence of some unconjugated C=C bonds is indicated by a possible, weak feature at 1597 cm^{-1} (C=C stretch). The conjugated polymer chain has been shown to have a carbon-carbon stretching feature near 1370 cm^{-1}, indicative of an interaction intermediate between that of a single bond (900 - 1000 cm^{-1}) and that of a double bond (1600 - 1700 cm^{-1}) (22). A feature appearing in our acetylene spectra at 1380 cm^{-1} can thus be assigned to a carbon-carbon stretching mode of polyacetylene. The observed C-H stretching peaks also exhibit some degree of unsaturation, being higher in energy than saturated species, but lower than for pure C=C or C≡C bonded molecules. Polymer chains have been observed to have skeletal deformation modes between 400 and 600 cm^{-1}, these modes being particularly evident if unsaturated linkages occur within the chain (19). Spectra of adsorbed acetylene show two well-resolved peaks at 485 and 573 cm^{-1}. This is in marked contrast to the low intensity, unresolved structure appearing in the 480 - 580 cm^{-1} region due to Zr-O and $Zr-BH_4$ modes. These observations are consistent

with the identification of acetylene polymer.

An examination of Fig. 5 reveals perturbations of B-H_t stretching modes caused by hydrocarbon adsorption. Ethylene adsorption appears to reduce intensity around 2490 cm^{-1}, while having less effect on other features in the 2400 - 2500 cm^{-1} region. Acetylene and, to a lesser extent propylene, have just the opposite effect on B-H_t stretching modes: their adsorption greatly strengthens structure at 2500 cm^{-1}. The basis for these varying effects on B-H_t vibrations is as yet unclear. It is also of interest to note that in the case of acetylene a high surface concentration of hydrocarbon can accumulate with very little (if any) accompanying loss of BH groups (compare Figs. 3 and 4). This is consistent with the view that polymer formation at a few active centers (probably Zr-H) is the mechanism for incorporating additional acetylene molecules into the surface phase.

Conclusions

Various aspects concerning the interactions of unsaturated hydrocarbons with supported zirconium complexes are revealed in the vibrational spectra of $Zr(BH_4)_4/Al_2O_3$ samples exposed to ethylene, propylene and acetylene.

By analyzing both the positions and shapes of features in the C-H stretching region (2850 - 3000 cm^{-1}), it is observed that ethylene and propylene both saturate upon adsorption, forming surface species with similar types of $-CH_3$ and $-CH_2-$ groups. Surface acetylene structures are somewhat different, probably consisting mainly of -CH- and $-CH_2$ groups

while retaining some characteristics of unsaturated carbon-carbon bonds. Ethylene and propylene readily saturate the surface with no indication of polymer formation under the conditions studied here. Only slight increases in surface concentration occur with temperature up to 575 K. Acetylene, however, does appear to polymerize on the surface. Saturation coverages are apparently not obtained within the observed temperature and exposure ranges. High concentrations of surface hydrocarbons are obtained with little or no effect on the concentration of BH species, since acetylene apparently forms long polymer complexes from a small number of active centers (probably Zr-H) without displacing existing ligands. The identification of acetylene polymer is supported by two well-defined peaks at 485 and 573 cm^{-1} characteristic of polymer skeletal deformations. A peak at 1380 cm^{-1} can be assigned to a C-C stretch whose bond strength is intermediate between that of a single and of a double carbon-carbon bond, as observed in an IR study of bulk polyacetylene (22). This study of hydrocarbons interacting with supported zirconium complexes further demonstrates the versatility and value of IETS by providing important, new data on a unique catalytic system of significant industrial as well as fundamental importance.

Acknowledgments

We wish to thank Drs. F. N. Tebbe and L. E. Firment for providing both helpful suggestions and useful information, in addition to supplying the $Zr(BH_4)_4$. We express appreciation to Professor R. H. Grubbs for contributing also valuable ideas and discussions. This research was supported by

the National Science Foundation under Grant Number ENG78-16927. Additional support from the Camille and Henry Dreyfus Foundation in the form of a Teacher-Scholar award to WHW is also greatly appreciated.

References

1. Evans, H. E.; Weinberg, W. H. J. Am. Chem. Soc. (submitted).
2. Evans, H. E.; Weinberg, W. H. J. Am. Chem. Soc. (submitted).
3. E.g., Marks, T. J.; Kolb, J. R. Chem. Rev. 1977, 77, 263-293.
4. Zakharov, V. A.; Yermakov, Yu. I. Catal. Rev.-Sci. Eng. 1979, 19, 67-103.
5. Ballard, D. G. H. J. Polymer Sci. 1975, 13, 2191-2212.
6. Basset, J. M.; Norton, J. in "Fundamental Research in Homogeneous Catalysis" (M. Tsutsui and R. Ugo, ed.); Plenum Press: New York, N.Y.; pp. 215-224.
7. Michalska, Z. M.; Webster, D. E. Chemtech 1975, February, 117-122.
8. Basset, J. M.; Smith, A. K. in "Fundamental Research in Homogeneous Catalysis" (M. Tsutsui and R. Ugo, ed.); Plenum Press: New York, N.Y., 1977; pp. 69-98.
9. Lambe, J.; Jaklevic, R. C. Phys. Rev. 1968, 165, 821-832.
10. Bowser, W. M.; Weinberg, W. H. Rev. Sci. Instrum. 1976, 47, 583-586.
11. Weinberg, W. H. Ann. Rev. Phys. Chem. 1978, 29, 115-139.
12. Matsuda, T.; Kawashima, H. J. Catal. 1977, 49, 141-149.
13. Marks, T. J.; Kolb, J. R. J. Am. Chem. Soc. 1975, 97, 3397-3401.
14. Alpert, N. L.; Keiser, W. E.; Szymanski, H. A. "Theory and Practice of Infrared Spectroscopy"; Plenum Press: New York, N. Y., 1970; pp. 184-302.
15. Conley, R. T. "Infrared Spectroscopy"; Allyn and Bacon: Boston, 1972: pp. 92-188.
16. Krimm, S.; Liang, C. Y.; Sutherland, G. B. B. M. J. Chem. Phys. 1956, 25, 549-562.

17. Nielsen, J. R.; Woollett, A. H. J. Chem. Phys. 1957, 26, 1391-1400.

18. Wood, D. L.; Luongo, J. P. Modern Plastics 1961, March, 132-144, 201-208.

19. Hummel, D. O. Polymer Rev. 1966, 14, 8-97.

20. Abe, K.; Yanagisawa, K. J. Polymer Sci. 1959, 36, 536-539.

21. Luongo, J. P. J. Appl. Polymer Sci. 1960, 3, 302-309.

22. Fincher, C. R.; Ozaki, M.; Heeger, A. J.; MacDiarmid, A. G. Phys. Rev. B 1979, 19, 4140-4148.

23. Su, W. P.; Schrieffer, J. R.; Heeger, A. J. Phys. Rev. Letters 1979, 42, 1698-1701.

24. Chiang, C. K.; Druy, M. A.; Gau, S. C.; Heeger, A. J.; Louis, E. J.; MacDiarmid, A. G.; Park, Y. W.; Shirakawa, H. J. Am. Chem. Soc. 1978, 100, 1013-1015.

Table 1. Peak Positions (in cm^{-1}) for C_2H_2, C_2H_4 and C_3H_6 on Alumina-Supported $Zr(BH_4)_4$.

C_2H_2		C_2H_4		C_3H_6		Assignments
300 K	400 K	300 K	525 K	300 K	525 K	
264	264	264	264	264	264	BH_4-Zr-BH_4 bend or Zr-BH_4 torsion
299	299	299	299	299	299	Al phonon
323	323	323	323	323	323	Metal oxide mode or Zr-BH_4 torsion
485	485	∿480	∿480	490	490	Zr-BH_4 stretch, Zr-O modes and (acetylene only) polymer skeletal deformations
		to	to	to	to	
573	573	580	580	580	580	
690	690	693	693	693	693	Zr-O stretch
910	910	910	910	910	910	Zr-O stretch
945	945	945	945	945	945	Al-O (bulk) stretch
1027	1027	1044?	1040?	1027	1027	CH modes
1071	1071					
1106	1106	1106	1106	1102	1102	BH deformations
1130	1130	1130	1130			
1173	1173	1169		1165		
1220	1220	1218		1213		
1260	1260	1256	1244	1258	1258	BH or B-O mode
1351	1351	1302	1302	1342	1342	C-C stretch (C_2H_2 only),
1380	1380	1383	1380	1378	1378	CH deformations and
1452	1452	1455	1455	1449	1449	B-O modes
1597	1597					C=C stretch?
1870	1870	1870	1874	1870	1876	Harmonic of 945 cm^{-1}
2150	2150	2142		2134		Bridging BH stretch
2181	2177	2177		2177		
2236	2233	2229		2229		
2258	2250	2256		2252		
2410	2410	2406	T	2410	2410	Terminal BH stretch
2434	2434	2435	2440	2427	2427	
			(broad)			
2484	2492	2486	I	2473	2473	
2505				2501	2490	
2871	2871	2879	2879	2863	2867	CH stretch
		2913	2920	2903	2899	
2935	2922	2930	2938	2930	2930	
2981	2960	2960	2958	2952	2950	
3677	3677	3677	3641	3669	3625	OH stretch

Figure Captions

Fig. 1: IET spectra (240 - 4000 cm^{-1}) for saturation coverages of ethylene on $Zr(BH_4)_4/Al_2O_3$ at 300, 400, 450 and 575 K.

Fig. 2: IET spectra for saturation coverages of propylene on $Zr(BH_4)_4/Al_2O_3$ at 300, 400 and 575 K.

Fig. 3: IET spectra of acetylene (300 torr-sec exposure) on $Zr(BH_4)_4/Al_2O_3$ at 300 and 400 K.

Fig. 4: IET spectra of $Zr(BH_4)_4$ adsorbed on Al_2O_3 over the spectral ranges (a) 240 - 2000 cm^{-1}, and (b) 2000 - 4000 cm^{-1}.

Fig. 5: Comparative view of the BH (2000 - 2500 cm^{-1}) and CH (2850 - 3000 cm^{-1}) stretching features in the IET spectra for ethylene, acetylene and propylene on $Zr(BH_4)_4/Al_2O_3$ at 300 K.

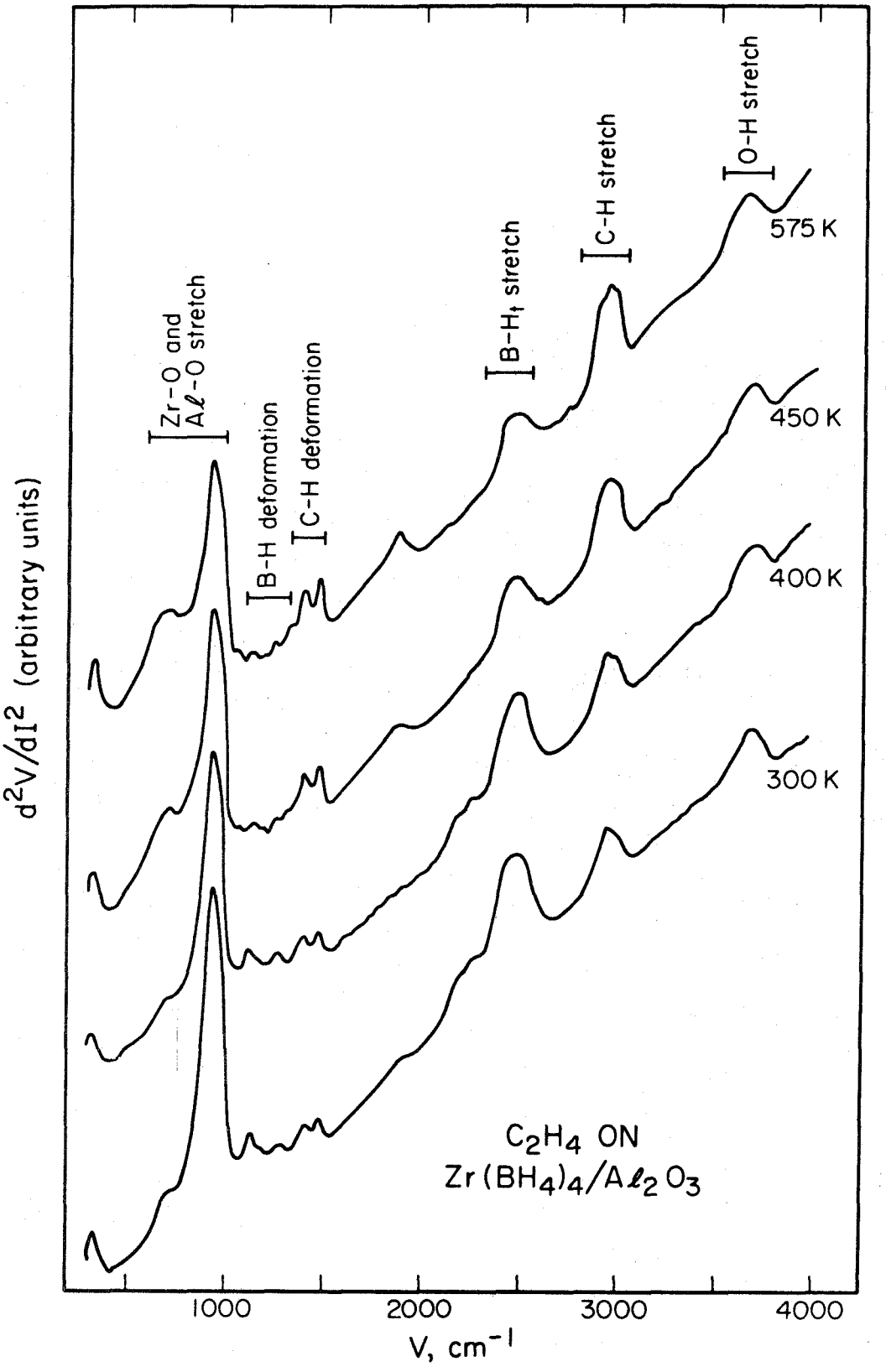
Zr-O and
Aℓ-O stretch
B-H deformation
C-H deformation
B-H$_t$ stretch
C-H stretch
O-H stretch
575 K
450 K
400 K
300 K
C_2H_4 ON
$Zr(BH_4)_4/A\ell_2O_3$
d^2V/dI^2 (arbitrary units)
1000
2000
3000
4000
V, cm^{-1}

Figure 1

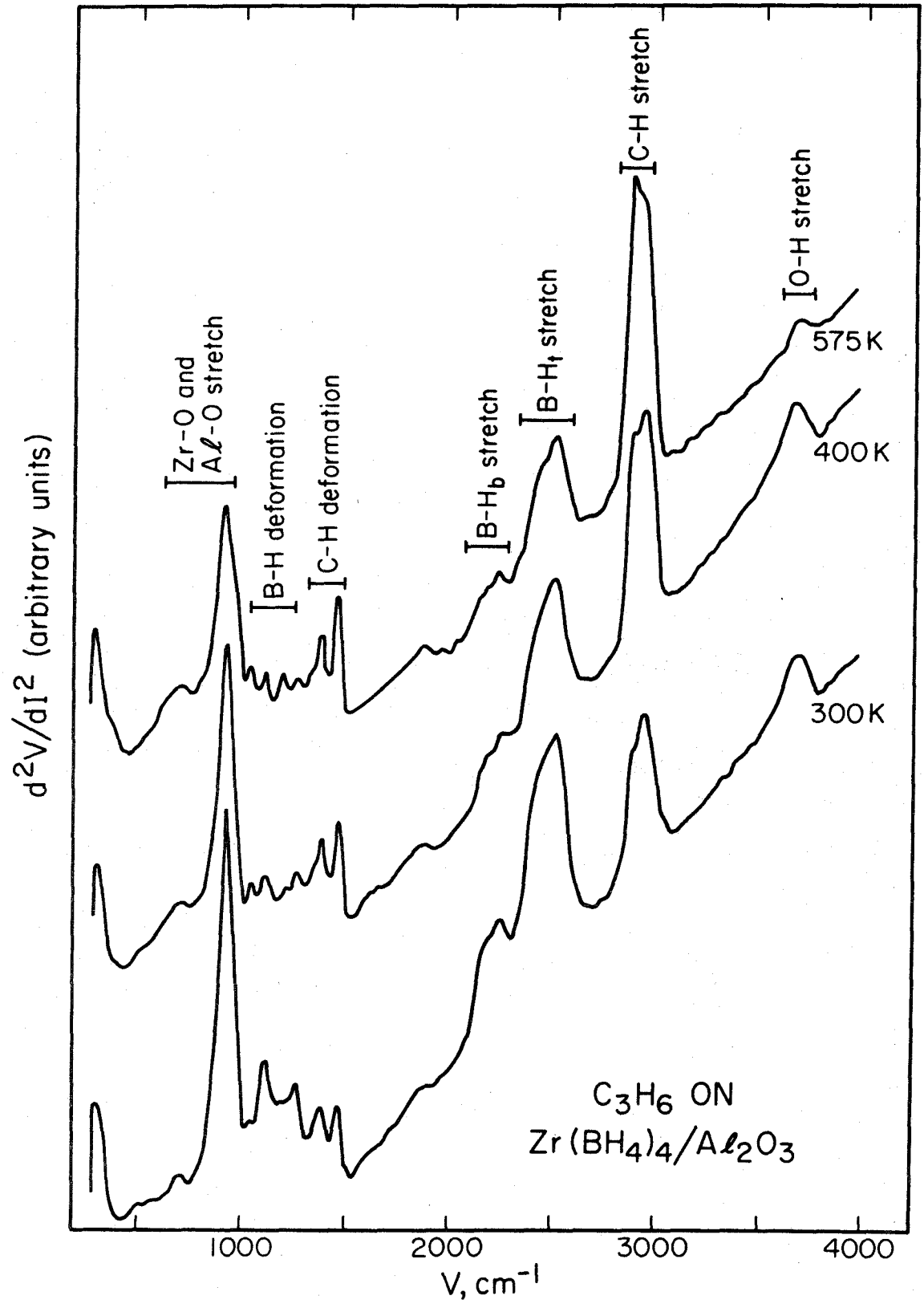
Zr-O and
Aℓ-O stretch
B-H deformation
C-H deformation
B-Hb stretch
Bt-Ht stretch
C-H stretch
O-H stretch
575K
400K
300K
C3H6 ON
Zr(BH4)4/Aℓ2O3
d2V/dI2 (arbitrary units)
1000
2000
3000
4000
V, cm-1

Figure 2

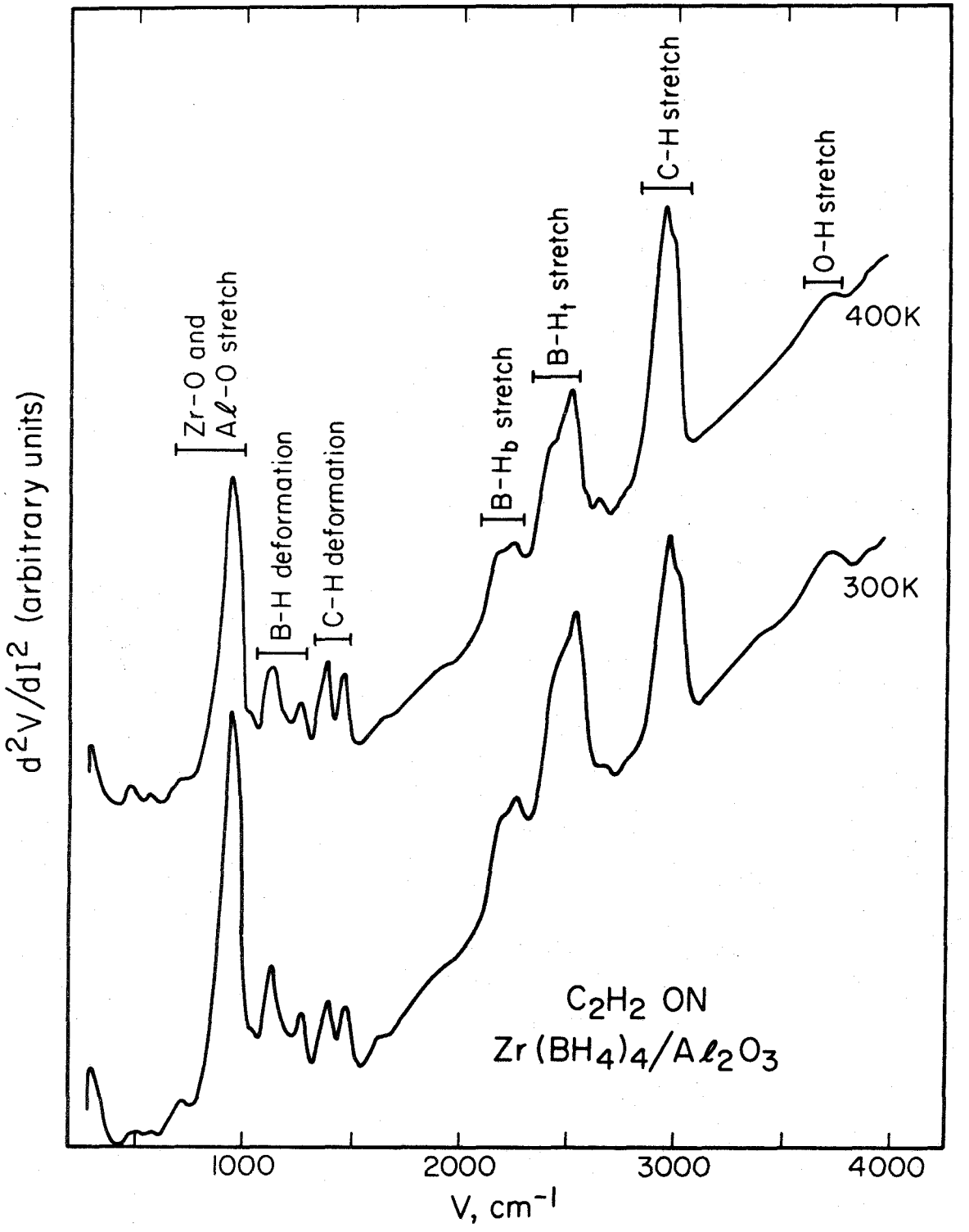
Zr-O and
Aℓ-O stretch
B-H deformation
C-H deformation
B-Hb stretch
Bt-Ht stretch
C-H stretch
O-H stretch
400K
300K
C2H2 ON
Zr(BH4)4/Aℓ2O3
d2V/dI2 (arbitrary units)
1000
2000
3000
4000
V, cm-1

Figure 3

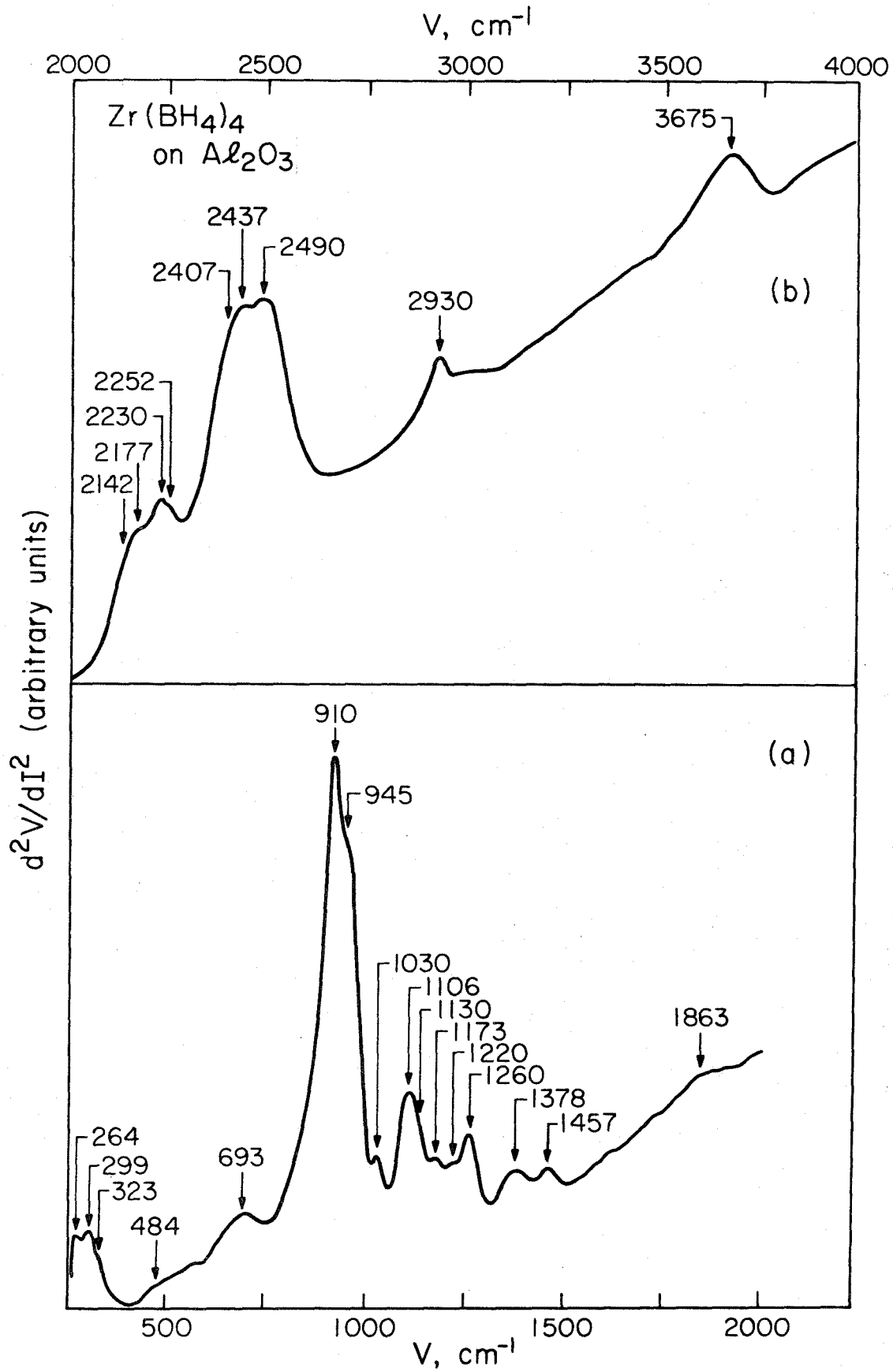
V, cm⁻¹
2000
2500
3000
3500
4000
Zr(BH4)4
on Aℓ2O3
3675
2437
2490
2407
2930
(b)
2252
2230
2177
2142
d²V/dI² (arbitrary units)
910
(a)
945
1030
1106
1130
1173
1220
1260
1378
1457
1863
264
299
323
484
693
500
1000
1500
2000
V, cm⁻¹

Figure 4

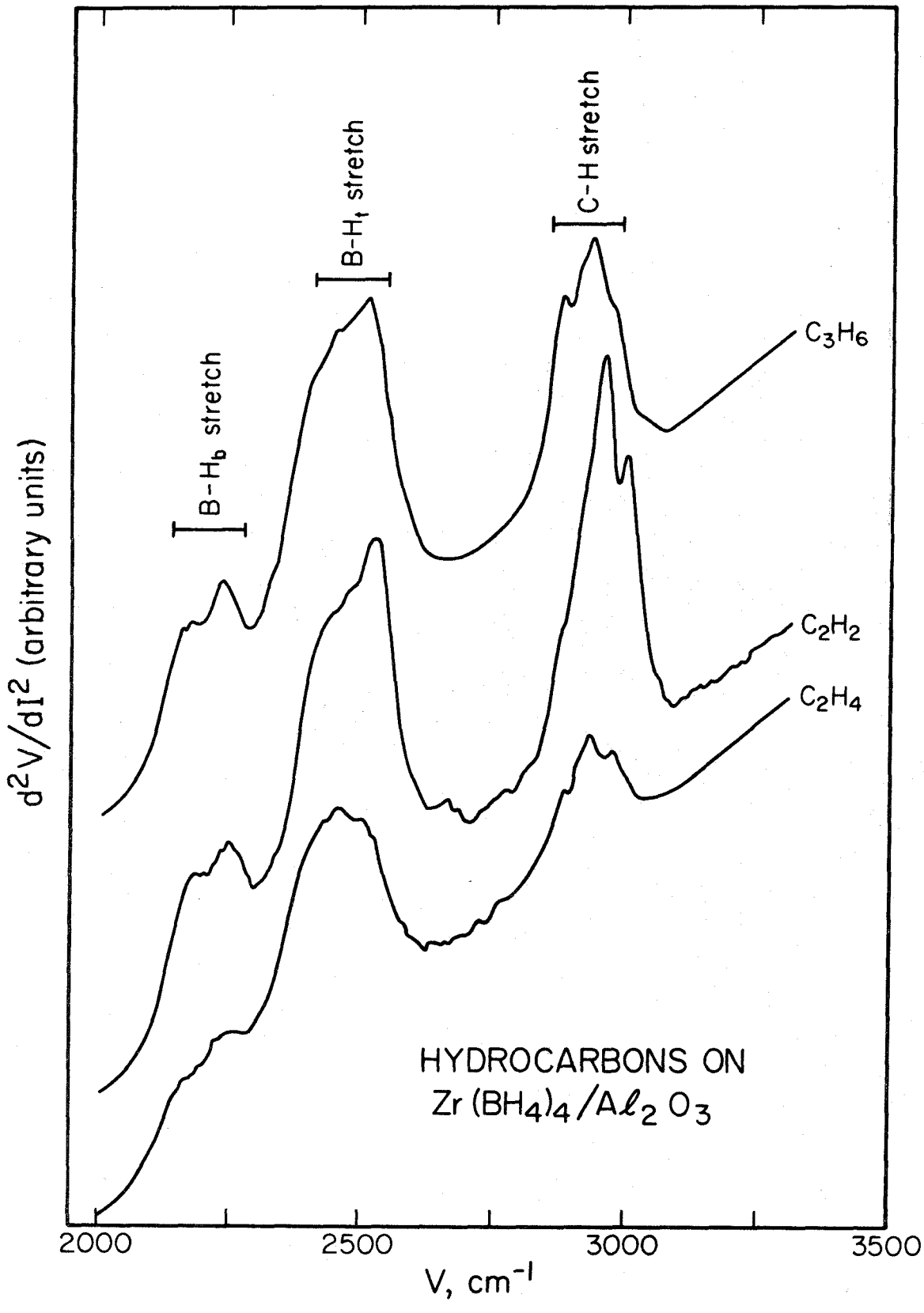
B-Hb stretch
B-Ht stretch
C-H stretch
C3H6
C2H2
C2H4
HYDROCARBONS ON
Zr (BH4)4 /Aℓ2 O3
d2V/dI2 (arbitrary units)
2000
2500
3000
3500
V, cm-1

Figure 5

Chapter IX

Conclusions

The objectives of research presented in this thesis have been to develop inelastic electron tunneling spectroscopy (IETS) into a technique that can be utilized as a valuable probe in catalytic research and to demonstrate its flexibility and effectiveness by providing new information on catalytic systems of industrial importance.

In order to meet these objectives, the following steps were outlined:

(1) Provide for the characterization of IET oxide films relative to commercial aluminas;

(2) Demonstrate the capability of IETS for following surface reactions;

(3) Demonstrate the capability of IETS for distinguishing between even very similar surface structures; and

(4) Expand the range of systems to which IETS can be applied by utilizing the technique to probe details in the important areas of catalysis by supported metals and supported complexes.

X-ray photoelectron spectroscopy was utilized to obtain characteristic information for a number of thin film systems. Differentiation among films oxidized in liquid water, by heating in oxygen, or by exposure to plasma discharges of oxygen or water vapor can readily be accomplished via analysis of XPS peak positions. Peak intensities were used to obtain

aluminum-to-oxygen concentration ratios for the various samples, providing a means of assessing relative degrees of bulk hydration. Peak widths were observed to determine relative chemical state distributions. Although the distribution of Al states remained rather constant with heating or halogenation, the distribution of oxygen states was sharpened considerably by heating and significantly broadened by halogenation of the surface. The XPS data provide a means of distinguishing among the various films, as well as presenting information in a form which can be compared directly to corresponding results for commercial, bulk aluminas.

For ethanol adsorption on alumina, the ethoxide $\rightarrow$ acetate surface reaction at approximately 470K was clearly observed via IETS. The loss of ethoxide CH_2 modes and the appearance of OCO stretching and deformation features characteristic of acetate structures established decisively the transformation from the ethoxide.

Comparison of the acetate structure formed at higher temperatures by ethanol adsorption, with structures of adsorbed acetaldehyde and acetic acid has also been accomplished via IETS. By accurately assigning the spectral features corresponding to OCO symmetric and asymmetric stretching modes it was determined that acetic acid and acetaldehyde form almost identical bidentate symmetrical bridging structures. Acetate formed from ethanol is also of the bidentate bridging form,

but the OCO bonding is less symmetrical than in the other two species. The observed temperature dependence of surface concentrations was related to the nature of binding sites available on the surface, as well as to the initial mechanisms of adsorption for the three hydrocarbon species. IETS not only provided for unique characterizations of three very similar surface structures, but also furnished insights into surface composition and adsorption mechanisms.

In a more complicated case requiring differentiation between two similar species occurring together on the same surface, IETS was shown to have resolution fine enough to distinguish between Al-ethoxide and Ag-ethoxide species on supported silver catalysts. Observation of the Ag species extended the range of IETS uses to include a broader spectrum of supported metal systems than had been indicated previously.

The most significant aspect of this work is perhaps the use of IETS to study $Zr(BH_4)_4$ supported on alumina. At least two distinct types of surface zirconium complexes were identified due to the appearance of both bulk-like Zr-O stretching modes and modes indicative of Zr atoms less highly coordinated to surface oxygens. The migration of displaced ligands onto the surface to form $Al\text{-}BH_4$ and $O\text{-}BH_2$ groups was also observed. The nature of $Zr\text{-}BH_4$ bonds was determined to be bidentate for the supported complex as opposed to tridentate as observed for pure $Zr(BH_4)_4$. Interpretations of the various spectral

features were facilitated by studying the interactions of $Zr(BH_4)_4/Al_2O_3$ with H_2O, D_2O and D_2 as a function of temperature.

After characterizing the supported complex, reactions were studied with ethylene, propylene and acetylene. Acetylene was observed to polymerize on the surface as judged by its failure to attain saturation coverage, whereas ethylene and propylene both readily saturated the surface. Spectral features of adsorbed acetylene are consistent with the formation of polyacetylene, retaining some characteristics of unsaturated carbon-carbon bonds; whereas features for ethylene and propylene indicate no remaining unsaturation and provide no evidence of polymer formation. In addition to extending the use of IETS to include (for the first time) the study of supported complexes, significant new structural information has been obtained on an industrially important type of catalytic system.

The results obtained during the course of this thesis research have fulfilled the original objectives of contributing new information on catalytic systems of significant interest and importance while concurrently demonstrating the utility and versatility of IETS as an experimental technique of considerable value in catalytic research. Hopefully, demonstrations of the effectiveness of IETS presented here, coupled with the continuing efforts of other researchers in this field, will enable IETS to be moved from a phase of exploration of its

capabilities to a phase where its capabilities can be exploited in catalytic research. Furthermore, it is hoped that in addition to providing for an increased understanding of the catalytic phenomena examined here, the results and ideas contained in this thesis will serve both as a stimulus and as a guide for continued effort in this field of research.

APPENDIX A

Details and Specifications of IETS Experimental Procedures

A general outline of our IETS experiments has been presented in an earlier section. This Appendix represents a more detailed description of the equipment and procedures utilized in these experiments. The tunneling experiment consists of two parts: junction fabrication (sample preparation) and spectral measurements. The electronic equipment utilized in tunneling measurements is documented thoroughly elsewhere (1). Accordingly, this Appendix will be restricted to, first, documentation of the equipment employed in preparing the tunneling samples and, second, presentation of a detailed outline of the basic procedures involved in sample preparation. This second part will be accompanied by a brief section dealing with some of the general procedures followed in making IETS measurements. A third, and final, section will describe a few specialized procedures developed for particular experiments. These specialized techniques are included here to serve as a guide for any researchers engaging in similar studies.

I. Sample Preparation Equipment

A. Vacuum System

The vacuum system employed in preparing IETS samples, shown schematically in Fig. 1, includes an 18" Pyrex bell jar (approximately 120 liters in volume). The primary source of pumping is a CVC 4" water-cooled oil diffusion pump. This pump is separated from the bell jar by a large gate valve, a LN_2-cooled baffle, and a Chevron-type baffle. Only Dow Corning 705 Silicon Diffusion Pump Fluid or a similarly high quality oil is used in the diffusion pump in order to maximize pumping effectiveness and

minimize pump oil contamination in the bell jar. As a further guard against contamination, the LN_2 baffle is always kept cold whenever the gate valve is open. Under routine use the entire pumping stack (including diffusion pump, baffles and gate valve) is dismantled and thoroughly cleaned on a yearly basis, at which time the pump oil should also be replaced.

The diffusion pump is backed by a mechanical forepump. The one currently being utilized is a Welch Duo-Seal #1397 vacuum pump with 500 liters per minute pumping capacity. This pump doubles as a roughing pump, and is separated from any vacuum lines by a bakable trap filled with Linde Type 13X molecular sieve to prevent backstreaming of oil or other contaminants. This pump is also routinely cleaned and supplied with a fresh change of oil on a yearly basis. The trap can also receive fresh sieve at this time. The absorbancy of the molecular sieve can be regenerated throughout the year by baking the trap. Temperatures should be low enough, however, so as not to endanger the integrity of any solder joints. The exhaust of the mechanical pump is fed through copper tubing directly into the fumehood, thus preventing the chemicals used in any experiments from being exhausted directly into the laboratory.

Evacuation of the bell jar from atmospheric pressure can be accomplished by first isolating the diffusion pump by closing valve V2 (see Fig. 1). The gate valve is, of course, already closed. The bell jar can then be roughed out by opening valve V1. Evacuation should proceed via the roughing pump until the pressure in the bell jar falls below approximately 1 or 2×10^{-1} torr. Pressures in this range can be monitored via the alphatron gauge (range from 760 to 10^{-4} torr) or the thermocouple gauge TC1 (range from 760 torr to a few microns). V1 is then closed and V2 reopened.

Caution should always be taken to insure that pressure in the foreline never rises above approximately 200 microns, as this can force oil in the diffusion pump up into the baffles and gate valve. Foreline pressure can be monitored with the thermocouple gauge TC2. The gate valve is then opened slowly, the rate of opening being determined by the foreline pressure. Once the gate valve is fully opened, the ionization gauge (Varian #0563-K2466-302) can be turned on and used to monitor pressures in the bell jar from 10^{-3} to 10^{-10} torr. (Both thermocouple gauges and the ionization gauge are connected to an NRC 763R ultrahigh vacuum gauge control unit.) Care should be exercised in guaranteeing that the diffusion pump is supplied with a constant stream of cooling water, that the LN_2 reservoir is filled as long as the diffusion pump is open, and that the foreline pressure is maintained within allowable limits.

The bell jar can be brought up to atmosphere by turning off the ion gauge, closing the gate valve and filling the bell jar with N_2 through the manifold line. When it becomes necessary to bring the diffusion pump up to atmospheric pressure, the pump heater should first be turned off and the oil allowed to cool (usually around 2 - 3 hours). The cooling water and the mechanical pump can then be turned off and the pumps brought up to atmosphere by opening the vent valve, V3. The bell jar can be maintained under vacuum if both V1 and the gate valve remain closed. Similarly, the diffusion pump can be maintained under vacuum if it becomes necessary to vent the mechanical pump by closing both V1 and V2 before turning off the mechanical pump and opening V3. The gate valve should never be open if V2 is closed. V1 and V2 should never be open simultaneously, and the foreline pressure must be monitored closely whenever V2 is closed.

The bell jar has been fitted with a large Pyrex flange which permits the use of an auxiliary, custom-built titanium sublimation pump, also shown schematically in Fig. 1. The sublimation pump is basically a double-walled vessel, with nozzles permitting the space between the walls to be filled with LN_2. A titanium wire filament supported on a ceramic rod between 0.1" diameter W wire leads can be inserted along the center of the pump through a port on the end opposite the bell jar. Titanium is evaporated on the inner wall of the pump by passing a current through the W leads utilizing a Kepco #KO 45-30M regulated DC power supply. The standard procedure is to turn the voltage adjust to its highest setting, then slowly raise the current until evaporation begins. Usual parameters are approximately 40 volts and 17 amps. Evaporation causes an immediate pressure decrease in the bell jar. One freshly evaporated titanium layer maintains its full pumping efficiency for up to forty minutes, with some residual pumping effects being continued for over one hour. When the sublimation pump is not required, the flange on the belljar is blanked off with an aluminum or glass flat circular plate. The sublimation pump is wrapped with insulation and enclosed in a perforated-metal cage to prevent breakage.

The diffusion pump is capable of bringing the belljar into the low 10^{-7} torr range from atmosphere within a few hours. Utilization of the titanium sublimation pump can decrease this base pressure by more than an order of magnitude.

B. Manifold

Tunneling experiments require the use of a wide range of gases and vapors. Therefore, an extensive and versatile manifold system has been

constructed and attached to the bell jar. It is illustrated schematically in Fig. 2.

The manifold is isolated from the bell jar by the valves M1 and B1. M1 is a Nupro 4BMG metering valve. Equipped with a micrometer handle, it is used for fine regulation of gas and vapor streams into the bell jar. Since it is not recommended for positive shut-off (i.e., even when closed it still permits flow up to 5 Std. cc/min through the valve), it is backed by valve H1. When the manifold is evacuated, the flow through M1 has a negligible effect upon pressure in the bell jar, and H1 can usually be left open. All of the "H" valves are Nupro 4H bellows sealed valves, and are capable of providing positive leak-tight seals. B1 is a Nupro 4B bellows sealed valve also capable of providing positive shut-off, but is more reliable at high pressures and has better regulating properties than the H models. All of the valves, tubing and fittings are of stainless steel.

A Welch Duo Seal #1376 vacuum pump (300 liters per minute capacity) is used to evacuate the manifold, a molecular sieve trap similar to that described above being utilized to prevent pump oil contamination. H11 and H12 are used to isolate the manifold from the pump. The exhaust from this pump is also fed directly into the fume hood. If desirable, evacuation can also proceed through the bell jar by opening H1 and M1. Either means of evacuation yields a base pressure of a few microns. Pressures in the manifold are monitored by a Matheson #63-5601 stainless steel test gauge (range from 0 to 770 mm Hg) and a thermocouple gauge (Varian #801, range from 1 micron to 1 atmosphere). The gauges should not be exposed to pressures higher than atmospheric.

Oxygen and nitrogen are consistently utilized in sample preparation and thus are always attached to the manifold. Matheson Research Purity oxygen in size 7B cylinders is used for oxidizing the Al films, and is connected to the manifold through H15. Prepurified grade N_2 is obtained from the Caltech central warehouse in large (size 1A) cylinders. Nitrogen is used to bring the bell jar up to atmospheric pressure (by opening B1 once the ionization gauge is turned off and the gate valve is closed). A steady stream of N_2 is also commonly used for drying; such a stream can be created by first closing H12 and H16, then opening H14 and H13. The resultant N_2 stream can be easily directed through use of a glass nozzle connected to H13 by a length of flexible rubber tubing.

Other gas cylinders (generally lecture bottles) can be attached through H9 and H10. Gases utilized in various experiments have included NO_2, NO, Cl_2, HCl, DCl, CO, C_2H_4, C_3H_6, H_2 and Ar. All gas cylinders are fitted with an appropriate regulator before being connected to the manifold.

Vapors from liquids are also commonly used in IETS experiments, and provisions for handling liquids are thus included in the manifold design. Two 100 ml flasks, shielded from accidental breakage by sheets of aluminum, are connected with Swagelok Ultra Torr fittings to H8 and H17. These particular fittings allow for repeated easy removal or connection of the flasks to the manifold. The flasks can additionally be heated by means of a variac-controlled heating mantle which is permanently in place on the manifold. Liquids which have been used include H_2O, D_2O, ethanol, acetic acid, acetaldehyde, cumene, pyridene, cyanoacetic acid and benzene.

H7 was designed to accommodate high purity gases obtained in glass flasks as opposed to cylinders, the area being shielded with aluminum

sheets. Isotopic gases can be fed through H2 (H1 should be closed), thus eliminating any excessive waste of rare or explosive gases arising from filling the entire manifold.

The manifold is also equipped with a pair of 500 ml mixing flasks (enclosed in perforated-metal cages), isolated from the main line by H3 and H5, and from each other by H4. These have been used, for example, to prepare a reservoir of a 50% CO-50% NO mixture for studies of co-adsorption of these gases on supported Ni.

It should be noted that one half of the manifold can be isolated from the other by appropriate use of H6, H11, H12 and H16. Thus, one side can be evacuated while the other is being utilized for gas transfer. The manifold can be baked out by means of heating tape which is wrapped around all of the stainless steel tubing and fittings. The heating tape is controlled by a variac, the typical setting for bakeout being between 90 - 100 (on a 0 - 130 scale). Bakeout is done routinely for $\sim$ 30 minutes following the use of water vapor or any organic compounds.

C. Bell Jar Interior Assemblage

The Pyrex bell jar and its protective metal screen can readily be raised and lowered by means of a pulley/counterweight system, thus providing for straightforward access to any part of the interior assemblage. Two aluminum guide rods prevent the bell jar from swinging or twisting. When raised, a clamp is placed on one of the rods to prevent the bell jar from lowering accidentally. The bell jar interior is pictured in Fig. 3. The actual design details of many of the interior components is described elsewhere (1), and thus only a general description of their function and

use will be presented here.

There are three sample holders (a) in the bell jar, to allow for making three sets of junctions simultaneously. Each sample holder consists of a 6 mm x 16 mm x 38 mm copper block, one face of which has been milled out to accommodate a 12 mm x 25 mm glass slide. Machinable ceramic blocks 6 mm x 6 mm x 38 mm are attached along the two long sides of the copper block. These insulators are used to support electrical leads to each sample, which will be discussed in detail later. The electrical leads, attached to the glass slide with 50%In/50%Sn solder, are sufficient to hold the glass slide in place on the copper sample-support block. Each glass slide-ceramic-copper block assembly can then be clamped tightly to a similarly sized copper block permanently mounted on a support table (n) inside the vacuum system. There is a 0.25 inch O.D. stainless steel cooling line (m) silver-soldered to each permanent block. Water, liquid nitrogen and air have all been used as coolants in various applications. Flow to each of the samples can be regulated by valves located external to the bell jar. After passing by the samples, all coolant is fed into a common 0.5 inch O.D. stainless steel return line. A recirculation pump and reservoir system is available when needed, although it is not utilized generally.

Electrical leads in the bell jar are soldered to an array of gold pins supported on blocks of machinable ceramic (h), which are also permanently mounted to the support table. Wires soldered to the glass slide samples are equipped with gold sockets, thus allowing for rapid connections to be made or broken whenever sample holders are mounted or removed.

The metal evaporation sources (g) are located a vertical distance of 16 inches below the samples. Sources for evaporating up to four different metals are available, but only three are currently installed. Each source consists of a filament, boat or basket clamped with stainless steel bolts and washers between 0.5 inch diameter copper posts, which in turn are connected to an external variac-controlled high-current transformer (7.5 V, 3kVA). Only one evaporation source may be utilized at a time, since they all have one side in common. The selection of evaporation sources is controlled via an external switch box. The evaporation sources are shielded from each other and from most of the bell jar interior by a stainless steel box with dividing panels which fits around the sources. Only a line-of-sight path to the samples is left unshielded. An additional shield (k) is used to insure that there is at least one area of the bell jar uncoated by metal evaporants to provide for viewing the samples during preparation. The amount and rate of metal evaporations are monitored by a quartz crystal oscillator-based deposition monitoring system with two sensor heads (e and f), one located at the level of the samples and the other approximately 5 inches above the evaporation sources. The function and use of this monitoring system is detailed below.

Evaporation of Pb and Al strips onto the glass slides requires the use of different masks. A circular mask assembly (b) is divided into four sections, these being a section consisting of three Al masks, one with three Pb masks, one open section and one solid blank section. A shutter, shielding the masks and samples, is also part of this assembly. The mask and shutter rotate on concentric shafts and are coupled to a single rotary-linear feedthrough through a gear box, or transmission (c), two universal

joints (p and q), and an expandable drive shaft (d). The mask and shutter can be operated independently, the linear motion of the feedthrough being responsible for engaging the appropriate gear. Selection of the gear operating the mask also results in increasing the distance between the mask and the samples by approximately 0.5 inch. This is to prevent the mask from scratching the samples as it is being rotated. A spring provides the restoring force to reposition the mask close to the samples once the mask has been maneuvered into place. Operation of the shutter causes no such displacement. Accurate positioning of the mask assembly relative to the samples is accomplished by aligning a fixed pin with corresponding holes in the mask.

Provisions for maintaining a glow discharge inside the bell jar include an aluminum electrode (j). This electrode, 100 mm of 2 mm diameter rod, is crimped to three intertwined lengths of 18 gauge solid copper wire leading to a high voltage power supply (Fluke #412 B). External to the bell jar, the line to the high voltage source includes three 2.5 kΩ resistors in series. These resistors were inserted to stabilize the discharge current. Discharge parameters are observed in part by monitoring the voltage drop across one of the resistors. The entire length of the copper line interior to the bell jar is enclosed in glass tubing, thus allowing the discharge to occur only along the aluminum electrode.

The interior assemblage is supported on a 22 mm thick stainless steel baseplate (r). The bell jar is sealed to the baseplate by means of a Viton gasket, which must be kept clean and supplied with a thin coat of vacuum grease (Dow Corning #970 V). Regreasing need only be done once for each 7 - 10 times that the bell jar is opened. Feedthroughs are attached

through holes drilled in the baseplate, and most are sealed with Viton O-rings which also have a thin coat of grease (Apiezon L). Arrangement of the various feedthroughs currently in use is schematically diagramed in Fig. 4. Holes for the thermocouple gauge and manifold inlet are tapped to provide pipe-thread seals. In order to prevent leakage, threads are first wrapped with Teflon tape and the outside is sealed with Varian's Torr-Seal vacuum sealant.

The high current feedthroughs are NRC #1332 and are rated for currents up to 400 amps. The high voltage feedthrough for the glow discharge line is Ultek #281-3000, rated for up to 12 kilovolts and 5 amps. The linear-rotary feedthrough used for manipulating the mask and shutter system is NRC #1371. It employs a combination of O-rings and vacuum grease seals to function at pressures down to 10^{-8} torr. However, we have achieved a significantly lower leak rate by omitting most of the vacuum grease (only modestly greasing the shaft with Apiezon L vacuum grease), then differentially pumping on the reservoir where excess grease would have been stored with a molecular sieve-trapped mechanical pump.

Port A has been utilized to accommodate either a high current feedthrough (which provides for the 4th evaporation source), or a rotary-linear feedthrough which facilitates handling low vapor pressure compounds used in some IETS studies (2). Port B has also been adapted for working with low vapor pressure materials which cannot be fed in through the manifold lines. It has additionally been utilized to connect a helium leak detector when leak checking is being done.

The feedthrough for cooling fluids employs three stainless steel ¼" input lines (one for each sample holder) and a ½" common output line, all

welded to a stainless steel flange. This construction was accomplished on campus. Connections inside the bell jar have been made with standard stainless steel Swaglok fittings, and both experience and helium leak checking have shown these to be quite leak free. The electrical feedthrough, also constructed on campus, has provisions for up to 44 separate electrical lines running into the bell jar. Specific electrical connections and usage will be discussed in a later section.

D. Calibrating and Monitoring Metal Depositions

Two sensor heads (Sloan #900010), positioned in the bell jar as described above, are employed in monitoring the rate and total amount of metal depositions. Each sensor head contains one silver-coated, 0.5 inch diameter quartz crystal (Sloan #000064). When driven with a 5 volt dc power supply (Analog Devices #902, located external to the bell jar), these quartz crystals oscillate with a frequency near 5 MHz. The precise frequency of oscillation is monitored with a Data Precision #5740 frequency counter. As metal is deposited on the crystal, the change in weight alters the oscillation frequency. The frequency change experienced during the course of an evaporation can therefore be directly related to the amount of material deposited.

In order to understand the relationship between frequency and the amount of metal deposited, calibration tests were run. The usual samples and sample holders were replaced with #2 glass cover slips (22 mm x 40 mm) suspended on two #30 copper wires, the weight of the cover slips having previously been determined on the precision Mettler balance in the analytical services section of the chemistry department at Caltech. Repeated

weighings of the same slides, even after several days, showed the weights to be accurate to within $\pm 1 \times 10^{-3}$ milligram. The total weight of one cover slip is on the order of 500 milligrams.

After being weighed and placed in the bell jar, the initial frequency of the oscillator was noted and large amounts of either Pb or Al were deposited on the cover slips and quartz crystal. After noting the final oscillator frequency, the samples were removed from the vacuum system and reweighed to determine the amount of material deposited, which was commonly on the order of 5 - 8 milligrams. The change in frequency per one statistical $\mathring{A}$ of metal deposited, $\frac{\Delta Hz}{\mathring{A}}$, was determined via the relation

$$\frac{\Delta(Hz)}{\mathring{A}} = \frac{A\rho\Delta f}{\Delta w} \quad ,$$

where A is the area of the cover slips exposed to evaporation, ρ is the bulk density of the metal being deposited, Δf is the noted change in the oscillator frequency, and Δw is the weight of metal deposited on the cover slip. The assumption of the bulk value for the density is the only approximation. Averaging several runs indicated a frequency response of approximately 4.2 $Hz/\mathring{A}$ for Pb, and 1.0 $Hz/\mathring{A}$ for Al. It should be noted that multiplying 4.2 by the ratio $\rho Al/\rho Pb$ also gives a value of 1.0, which serves as further verification of the accuracy of these numbers. Thus, the frequency response of the oscillator, R, might also be expressed as

$$R = 0.365\rho \quad Hz/\mathring{A} \quad ,$$

where ρ is the metal bulk density expressed in g/cm^3.

Two sensor heads are employed in the monitoring system. The one

located near the sample holders, approximately 16 inches above the evaporator source, is used for monitoring Al and Pb evaporations, where accuracy of plus or minus a few tens of Angstroms for Al or a few hundreds of Angstroms for Pb is acceptable. Accuracy is much better than this, generally being ± a few Hz independent of what metal is being used. For experiments in which we have attempted to model supported metal catalysts, however, greater accuracy is required. In studies of ethanol adsorption on Ag/Al_2O_3, for example, silver coverages of only a few statistical angstroms were utilized, and thus had to be determined with greater accuracy and precision than afforded by the first sensor head (3). A second sensor head was therefore installed approximately 5 inches above the evaporation sources.

The thickness of a film deposited by evaporation onto a substrate is proportional to

$$\frac{h^2}{(h^2 + \delta^2)^2} \quad ,$$

where h is the horizontal distance from the source to the substrate and δ is the vertical distance (4). In our case, h is sufficiently greater than δ so that ignoring δ in the above relation results in errors of less than 3 percent. The relationship between the thickness of a film at the sample height, h_1, compared to the thickness monitored by the second sensor head, at height h_2, is therefore approximately equal to

$$\frac{h_2^2}{h_1^2} = \frac{5^2}{16^2} \approx 0.1 \ .$$

Or, in other words, measurements of metal depositions can be effected ten times more accurately by utilizing the lower sensor head. This accuracy is only required for the supported metal work. The selection between sensor heads is determined by switching a BNC cable between two BNC re-cepticles located exterior to and behind the bell jar.

E. Sample Heating and Electrical Connections

There are two independent means whereby tunneling samples may be heated while being prepared inside the vacuum system. The first, and most straightforward, way involves utilizing a compact heating element attached to the copper sample holder on the side opposite the glass slide. The temperature is monitored with a thermocouple soldered directly to the glass slide. The second method of sample heating makes use of a technique devised by Bowser and Weinberg (5) where a four point-probe geometry provides for resistively heating the Al strip while simultaneously measuring its temperature. Although this method is more complicated than the first, it is used more often in practice. The reasons for this will be discussed below along with a more detailed outline and analysis of these two heating techniques.

Each sample holder (i.e., copper support block) has been custom-fitted with a coiled length of heating wire. These compact heating elements were obtained from Thermometrics Company (Northridge, California). The heating wire consists basically of a thin nickel alloy wire insulated from an outer stainless steel covering by a layer of magnesium oxide. Coiled inside an area milled out on the back of the copper sample holders, the heating elements are silver soldered to the blocks to provide excellent thermal

contact. A large heat sink, also stainless steel and magnesium oxide, is attached to the heating wire right at the edge of the copper block in order to eliminate any hot spots at areas where thermal transport away from the heating wire is slow.

These heaters can be independently controlled by variacs mounted on the sample heating power supply panels located in the instrument rack (see Fig. 5a). The heaters are designed for a maximum voltage of 30 - 40 volts. They have been used for heating samples to > 800 K. Heating by this means is a relatively slow process, but once an equilibrium temperature has been established it is remarkably stable with respect to time, small pressure fluctuations, etc. Other disadvantages include the long cooling times required and the fact that large masses near the samples are heated also to high temperatures, thus desorbing molecules which can possibly adsorb as contaminants on the samples.

The second method selectively heats the Al strip without excessive heating of other areas near the samples. The temperature is determined according to the relation

$$T = T_i + \frac{1 + \alpha T_i}{\alpha} \left(\frac{R - R_i}{R_i} \right) ,$$

where R is the resistance of the Al strip at temperature T, R_i is the initial resistance at the initial temperature T_i, and α is the temperature coefficient of resistance (6). After the method of Bowser and Weinberg (5), T_i and R_i are measured initially, and R is calculated during heating by the relation

$$R = \frac{V_s}{I_s}$$

where V_s and I_s are the voltage and current, respectively, across the Al strip. V_s is measured directly, and I_s determined by measuring the voltage drop (V_R) across a precision resistor with known resistance (R_R) in series with the Al strip. Heating currents are provided to each of the samples by separate Hewlitt-Packard 6201B power supplies (0 - 20 volts, 0 - 1.5 amps) mounted on the sample heating power supply panels.

Since the room temperature in our laboratory is carefully regulated, T_i is very nearly a constant. Values for $\frac{1 + \alpha T_i}{\alpha}$ were determined experimentally (also according to the method presented previously) by utilizing the sample heaters described above, a thermocouple to monitor T, and a low power ohmmeter to obtain values for R at given values of T. Data from twenty separate samples were averaged together to yield an observed value of

$$\frac{1 + \alpha T_i}{\alpha} = 558.66 ,$$

with a maximum variance less than ± 8%. All of the above temperatures are in degrees Centigrade.

The necessary voltage, resistance and temperature readings are accomplished through use of electrical circuits as diagramed in Fig. 6, a switching panel (Fig. 5b), and a Hewlitt-Packard 3455A digital voltmeter. There are currently twelve electrical lines associated with each of the three samples (see Fig. 6). Lines #1 through #6 are attached directly with In/Sn solder to the Al strip as shown in the diagram. Lines #7 and #8 represent an iron/constantan thermocouple which is soldered to the glass slide. Each thermocouple line is equipped with an ice point reference junction exterior to the bell jar as shown. Line #7 is the iron wire.

Lines #9 and #10 are totally exterior to the bell jar, and are used to measure voltage drops across, and the resistance of, the precision series resistor in the junction resistive heating circuit. Three "resistor select" toggle switches on the switching panel (Fig. 5b), one for each sample, can be used to select either a 1Ω or a 10Ω value for this in-line resistance. The value is selected to match most closely the resistance of the Al strip, which is typically closer to 10Ω. Lines #11 and #12 are connected directly to a variac and used to power the sample heaters attached to the back of the copper blocks as described previously. Lines #5 and #6 can be used as part of the resistive heating circuit or for the 4 wire resistance measurement of the Al strip. Their function is determined by the "OHMS/HEATING" select switch on the switching panel. When switched to the heating setting, resistive heating circuits for all three samples are connected.

On the switching panel, the "SAMPLE SELECT" switch is used to choose between all lines #1 through #9 from either sample 1, sample 2 or sample 3. The "LINE SELECT" multiple station pushbutton switch is used to select two of the nine lines as input to the DVM. The buttons labeled $_1V_2$, $_2V_3$, $_3V_4$ and $_1V_4$ are used to read voltages or resistance between points 1 and 2, 2 and 3, 3 and 4, and 1 and 4, respectively, along the Al strip (see Fig. 5b). When measuring resistance, the "OHMS/HEATING" switch should be set at ohms and the DVM function should be at the 4 wire kΩ setting. (Although provisions have thus been made for monitoring the temperature of three separate sections along the strip, in practice only the average temperature of the whole strip, i.e., between points 1 and 4, is generally measured.) The button labeled T selects the thermocouple lines, while the one labeled

R selects those lines connected across the series resistor. When measuring this resistance, the "OHMS/HEATING" switch should be set on heating, and the DVM function set for 2 wire kΩ.

The two lines (one blue, one black) leading from the LINE SELECT switch are connected to a dual banana plug which can be connected to the rear terminals on the DVM from the back of the instrument rack. The 4 wire resistance measurement lines (#5 and #6), both white, are similarly connected. When using this configuration the "REAR TERMINAL" select switch on the back of the DVM must be set.

Wires connecting the switching panel to lines from the electrical feedthrough are red for all lines from sample 1, white for lines from sample 2, and either blue or green for lines from sample 3. Wires attached directly to the electrical feedthrough, both inside and outside the bell jar, are color-coded in the following manner:

Sample #	Line #1 (after Fig. 5b)	Color
1, 2 and 3	1	orange
	2	yellow
	3	green
	4	blue
	5	violet
	6	red
	7	brown
	8	black
1	11	red
	12	orange
2	11	yellow
	12	green
3	11	blue
	12	violet

Lines from the electrical feedthrough inside the bell jar are terminated with gold plated pins secured in ceramic blocks fixed permanently to the main support table (see Fig. 3). There are three ceramic blocks, each accommodating lines #1 through #8 from one of the samples. Lines #11 and #12 from all three samples are attached to the block for sample 3. Wires connected directly to the samples are easily joined to the feedthrough wires by being fitted with matching gold plated sockets as described above.

Although the resistive heating technique is less stable with respect to time, pressure changes and small power fluctuations than are the heating elements, it is more frequently employed during junction preparation. Its advantages include the following: (1) more rapid heating and cooling rates, (2) less time required to establish an equilibrium temperature, and (3) fewer contaminants desorbed from nearby areas.

II. Basic Sample Preparation Procedures

The following is presented in the form of a list of steps required for preparing tunnel junctions.

1. Cut and clean glass supports. These are cut to be 12 x 25 mm using a diamond-tipped scribe from precleaned plain 25 x 75 mm microslides. They are washed and rinsed individually with soap and tap water, then collectively placed in a small beaker and rinsed for several minutes in a strong flow of distilled water. Repeated washings and rinsings in an ultrasonic cleaner are recommended. Clean slides can be stored in distilled water, and dried when needed using a dry nitrogen stream from the manifold.

2. Mount glass slides on sample holders. When utilizing In or In alloy solders, a setting of 65 (on a 0 - 100 scale) for a variac-controlled soldering iron has been found to be most effective.
3. Mount slides and sample holders in the bell jar and connect the gold pin and socket electrical leads.
4. Clean the discharge shield. Remove the shield carefully so as not to damage the discharge electrode, sand it with a fine grade of emory cloth, rinse with acetone and replace the shield in its original position. Repositioning either the electrode or the shield can affect the rate of oxidation, so any displacements should be minimized in order to insure reproducibility.
5. Position the mask and shutter for Al evaporation. Although this can be accomplished even after the bell jar is closed, it is easier at this point.
6. Resupply the evaporation sources. Aluminum is evaporated from a coiled tungsten filament (R. D. Mathis Co. #F4-3X.030W). Four 15 mm lengths of 2 mm Al rods (Balzers #261549, 99.9%) are bent into U-shapes, then hung on separate coils of the filament. Lead (Pb) shot (Balzers #261582, 99.9995%) is placed into a tungsten boat (Mathis #S8A-.005W) for evaporation.
7. Clean the baseplate. Wipe off any dust or dirty grease, especially from the area which will contact the Viton gasket on the bell jar.
8. Check Viton gasket for cleanliness and insure that it is properly greased.
9. Lower the bell jar, attach Ti sublimation pump (if being used), and open the roughing pump. Follow carefully the procedures outlined

in Section I.

10. Fill trap supply reservoir with LN_2.
11. When appropriate, close roughing line, open system to the diffusion pump, and turn on ion gauge.
12. Melt the Pb. This is done at low pressure ($< 1 \times 10^{-5}$ torr) before beginning to fabricate the tunnel junctions in order to desorb contaminants. A variac setting of 10 - 12 is sufficient (this produces approximately 60 amps), and the melting point can be determined by either a rapid pressure rise or initial indications of evaporation on the deposition monitor. Following melting the Pb, the switch can then be set for the Al evaporation source.
13. Evaporate the Al. After the desired pressure has been reached (generally on the order of 5×10^{-7} torr), current through the filament should be increased slowly to allow for uniform heating of the aluminum. Rapid, uneven heating often results in the bulk of the aluminum not wetting the tungsten filament properly and falling off. An increase in the variac setting of 5 per every 15 - 20 second period is sufficient. A variac setting of 40 will melt the aluminum. As it melts, the current jumps from approximately 45 amps to over 60 amps. The shutter can be opened at this point, and the current adjusted to produce a deposition rate of 8 - 12 Hz/sec. A slow decrease in current accompanies continued evaporation, the current returning to a value of 45 amps by the time all aluminum has been evaporated. Film thicknesses from 800 to 1000 Å are preferred, but films as thin as 400 Å have produced adequate tunnel junctions. These thinner films might, however, have a different temperature

coefficient of resistance and therefore would require further calibration experiments before being utilized in the resistive heating scheme. Since aluminum alloys with tungsten, the electrical and mechanical properties of the evaporation filament change with each evaporation. This results in slight changes in the current required for evaporation as a function of use, and also leads to weakening and embrittlement of the filament. Each filament can be cycled through from five to ten aluminum evaporations before requiring replacement. During evaporation, the pressure should not rise much above 1×10^{-5} torr. Higher pressures generally indicate large amounts of contaminants adsorbed on a build-up of porous aluminum inside the box used to shield the evaporation sources. This can be removed without damaging the box by soaking in a concentrated solution of NaOH, then washing and drying thoroughly. This cleaning is generally required every few months.

14. Oxidize the evaporated Al strip. The manifold is first filled with approximately 100 microns of H_2O, then 400 torr of O_2. Traces of water vapor seem to favor the formation of more uniform and stable oxide layers. The usual discharge voltage is -1300 V, with a current of approximately 22 milliamps. This current is equivalent to a 55 volt voltage drop across one of the series resistors. The current is a function of the O_2 pressure. An initial pressure of 120μ of O_2 is admitted to the bell jar, and the discharge initiated at -1000 V. The voltage is increased up to -1300 V as the current falls below 22 ma. After 30 seconds, the discharge has stabilized and the shutter is opened. The O_2 pressure must be continuously

increased throughout the duration of the discharge to maintain constant current, generally resulting in a final O_2 pressure of 160 μ. Oxidation times range from 10 to 20 minutes depending on the desired junction resistances and the nature of molecular adsorbates to be studied. The high voltage power supply is turned off and oxygen pumped from the system through the diffusion pump at the conclusion of the oxidation period. More details of plasma oxidation techniques are available in the literature (7).

15. Introduce reactants into the system and adjust to desired temperatures. Resistive heating is best accomplished prior to exposures for pressures below 10^{-3} torr. At higher pressures, it is most effective to first fill the bell jar with reactants before initiating the sample heating. Also, when utilizing the resistive heating technique, heating should be discontinued before evacuating the bell jar as a drop in pressure can cause extremely rapid increases in temperature. The heating elements are, of course, affected to a much lesser extent by pressure.

16. Deposit the Pb top electrodes. The system is evacuated to $< 1 \times 10^{-5}$ torr, the mask is set for cross strip evaporation, and on the order of 2500 Å of Pb is deposited. (This corresponds approximately to a 10,000 Hz frequency change for the oscillator.) Slow heating is not as important as with the aluminum. A variac setting of 15, resulting in a current of 60 - 65 amps, is routinely used to obtain deposition rates on the order of 20 Å/sec.

17. Remove the completed samples. After allowing a few minutes for the Pb evaporation source to cool, the diffusion pump is closed and the

bell jar filled with N_2 up to atmospheric pressure. The bell jar can then be raised and the sample holders removed. At this time the ports to the diffusion pump and ionization gauge are generally covered with aluminum foil to prevent small nuts or screws from being dropped into them. The foil is removed again just before pumpdown.

* * * * *

After being removed from the bell jar, the three glass sample slides are mounted on a 10 x 40 mm strip of circuit board, held in place by electrical leads attached with In alloy solder at both ends of the Al strip and of each Pb cross strip. The circuit board can be attached to the end of a phenolic rod and inserted directly into a LHe dewar where measurements can be done. If the samples are not to be measured immediately, they are placed in a LN_2 storage dewar where they apparently can be stored indefinitely without changing characteristics (8). While a more extensive description of the measurement sample holders and measurement technique are recorded elsewhere (1), just a few of the characteristic measurement procedures will be mentioned here.

First, a wide spectral scan is taken for each junction to determine the noise level, check for contamination and establish the appearance of desired surface species. (Initially, exposures required to produce a sufficient surface coverage of a particular adsorbate are possibly unknown, and the wide scan gives a general indication of the surface coverage.) The modulation level is set for 2 mV. The sensitivity level of the lock-in amplifier is set to produce a deflection as close to full scale as possible when going from 30 to 500 mV bias voltage. The phase is set so as to

maximize the deflection at a bias voltage of 250 mV. The time constant, generally set at 300 msec while adjustments are being made to allow a fast response time, is then set at 1 sec and the spectral measurement initiated. A wide scan usually entails measuring from 30 to 500 mV in 1 mV steps, counting for 2 seconds at each step. For samples where greater resolution is desired, more detailed scans can then be taken. This is often accomplished by reducing the modulation voltage to 1.0 mV and resetting the sensitivity and phase (the deflection again being maximized at the midpoint of the energy range to be investigated). Measurements can be taken at smaller increments of the bias voltage, 0.5 mV being a typical value, and multiple sweeps through the spectral range also enhance resolution by allowing larger total measurement times at each point without introducing variations across the spectral range due to slow drift in any of the electronic components. After measurements, samples can be discarded or returned to the storage dewar. Again, these procedures are presented in more detail elsewhere (1).

III. Adaptations and Special Procedures for Particular Experiments

A. Electron Microscope Samples

Electron microscopy can contribute to the characterization of certain surfaces used in IETS studies. This has been demonstrated previously in an investigation of ethanol adsorption on Ag particles supported on Al_2O_3 (3), the Ag being deposited on the surface via typical evaporation techniques. Electron microscopy was employed to monitor the size and shape of Ag particles as a function of amount deposited onto the surface.

Samples were prepared for use in a transmission electron microscope

(a microscope is available in the Biology Department at Caltech for limited studies) according to standard procedures under the direction of Mr. Pat Koen.

Carbon is first evaporated in a vacuum system onto freshly cleaved mica substrates. A piece of this carbon-coated mica, approximately 1 cm^2, is cut off and the carbon film separated from the mica by flotation in a beaker of distilled water. Using tweezers, a 400 mesh copper grid (Pelco #1GC400, approximately 3 mm in diameter) is immersed directly below the floating carbon film, and using one continuous motion the grid is brought up from the water through the film so as to have a uniform carbon coating on one side. Since the carbon film is very thin, extreme care must be taken so as not to endanger its integrity. For example, coated grids should be placed only on clean filter paper, as tissues (such as Kimwipes) have fibers which can penetrate the carbon layer. When dry, these coated grids act as substrates for the TEM samples. They are then placed, coated side down, on 1 x 2 mm Cu screens suspended in the IETS sample preparation chamber in the same position as the IET sample holders. Aluminum is next deposited in the usual manner, except that a thickness of only 100 Å or less is used as thicker Al layers might significantly retard electron transmission. Oxidation is also carried out in the usual manner. This surface can then be treated in the desired manner, e.g., by evaporating small quantities of another metal in order to model supported metal catalysts, or by exposing the surface to particular adsorbates. Samples can then be removed from the vacuum system, carefully placed coated side up on clean filter paper in a glass Petri dish, and transported to the microscope for examination.

B. Use of $Zr(BH_4)_4$

The use of $Zr(BH_4)_4$ presents certain hazards which require that special handling procedures be followed in order to avoid fire and/or explosion. In air, rapid hydrolysis of $Zr(BH_4)_4$ produces hydrogen and a temperature rise sufficient to ignite the hydrogen explosively. Contact of $Zr(BH_4)_4$ with air, water or oxygenated or halogenated solvents should thus be specifically avoided.

The $Zr(BH_4)_4$ used in our studies was prepared at du Pont and shipped in double valved Hoke cylinders. A cylinder was connected to the vacuum system through the needle valve and the connection checked carefully for leaks. The space between the two valves was then leak checked also. When putting $Zr(BH_4)_4$ into the bell jar, the cylinder is first cooled in liquid nitrogen (LN_2), and then both the ball valve and needle valve are opened so that gases can be pumped from the cold cylinder. [$Zr(BH_4)_4$ decomposes slowly at room temperature.] Both valves are then closed and the cylinder allowed to warm to room temperature. The ball valve is reopened, and material may then be bled into the system through the needle valve. When exposure to the zirconium complex is complete the cylinder is recooled in LN_2 and all volatiles evacuated from the cold cylinder as well as from the bell jar through a specially designed trap line.

The trap line is shown in Fig. 7, and is intended to be used in evacuating the experimental chamber and collecting unused $Zr(BH_4)_4$. The line itself serves as a connection between the experimental chamber and a mechanical pump as illustrated. The trap portion of the line is to be immersed in LN_2 during use, and is isolable by means of two Varian valves. Any trapped volatile species can be isolated, then transferred via the

side arm into an empty collection cylinder. The thermocouple gauge is included only for checking the vacuum integrity of the trap line. It should not be used during actual exposure to $Zr(BH_4)_4$, as the complex will immediately decompose on the hot filament in the gauge tube. The entire trap line, side arm and collection cylinder were leak checked thoroughly after connection to the vacuum system.

To trap $Zr(BH_4)_4$, the chamber is evacuated through the LN_2 cooled trap. After evacuation (usually to pressures below 5×10^{-3} torr), the trap section is isolated by closing the Varian valves. The bell jar can then be opened to the diffusion pump. On the trap line the collection cylinder is cooled in LN_2, the Nupro ¼" valve is opened and the trap is allowed to warm to room temperature. Approximately one hour is allowed for the trap to warm and for the $Zr(BH_4)_4$ to recondense in the collection cylinder. After evacuating both the supply and collection cylinders while cooled in LN_2, all valves on the cylinders are closed and both are allowed to warm to room temperature. This procedure has proved effective as a safe and reliable means of handling $Zr(BH_4)_4$, and should be followed carefully whenever this hazardous complex is used.

References

1. W. M. Bowser, Ph.D. Thesis, California Institute of Technology.

2. W. M. Bowser and W. H. Weinberg, in preparation.

3. H. E. Evans, W. M. Bowser and W. H. Weinberg, to be published in Surface Sci.

4. L. Holland, Vacuum Deposition of Thin Films, p. 141, (Wiley, N.Y., 1956).

5. W. M. Bowser and W. H. Weinberg, Rev. Sci. Instrum. 47, 583 (1976).

6. R. C. Weast, Handbook of Chemistry and Physics, (The Chemical Rubber Co., Cleveland, Ohio, 1971), 52nd edition.

7. J. L. Moles and P. H. Smith, J. Electrochem. Soc. 110, 1240 (1963).

8. O. I. Shklyarevskii, A. A. Lysykh and I. K. Yanson, Sov. J. Low Temp. Phys. 2, 328 (1976).

Figure Captions

Fig. 1: Schematic representation of the vacuum system utilized in preparing IETS samples.

Fig. 2: Schematic of manifold system for handling various gases and vapors used in IETS experiments.

Fig. 3: Photographs of the interior of the IETS sample preparation chamber and its component parts: (a) Sample holders, (b) mask and shutter assembly, (c) gear box controlling mask and shutter, (d) coupling shaft from feedthrough to gear box, (e) and (f) deposition monitor sensor heads, (g) evaporation sources, (h) electrical lead connectors, (j) HV electrode for plasma discharge, (k) evaporation shield, (m) cooling lines, (n) support table, (p) and (q) universal joints, and (r) baseplate.

Fig. 4: Diagram of the location of the various ports and feedthroughs on the baseplate of the IETS sample preparation system.

Fig. 5: Representations of (a) a sample heating power supply panel, and (b) the switching panel used to control and monitor sample temperatures.

Fig. 6: Schematic drawing of the electrical circuits constructed to heat the IETS samples and simultaneously monitor their temperatures.

Fig. 7: Schematic of trap line used for recovery of $Zr(BH_4)_4$ from the sample preparation area.

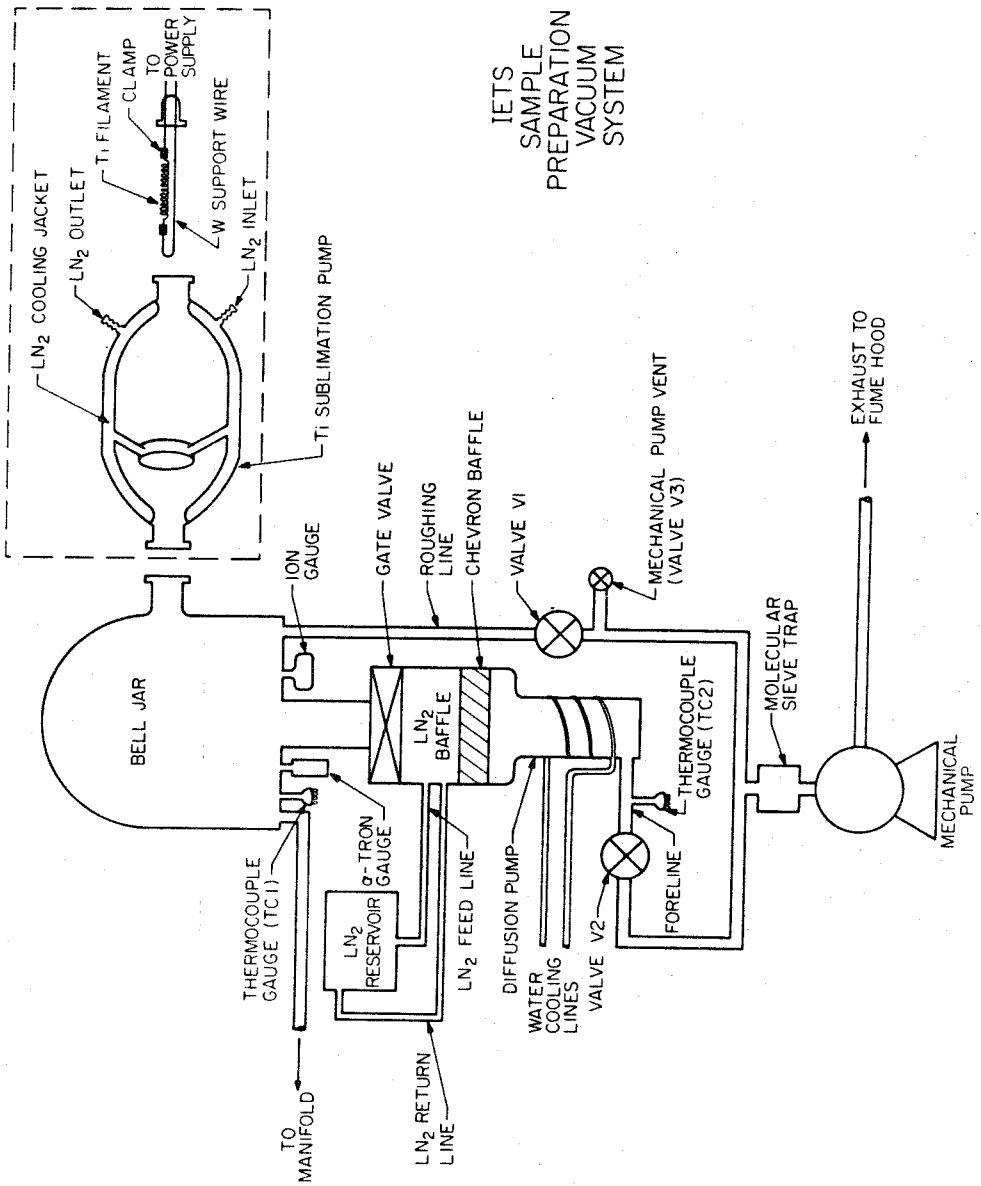
IETS
SAMPLE
PREPARATION
VACUUM
SYSTEM
LN2 COOLING JACKET
LN2 OUTLET
Ti FILAMENT
CLAMP
TO
POWER
SUPPLY
W SUPPORT WIRE
LN2 INLET
Ti SUBLIMATION PUMP
ION
GAUGE
GATE VALVE
ROUGHING
LINE
CHEVRON BAFFLE
VALVE VI
MECHANICAL PUMP VENT
(VALVE V3)
EXHAUST TO
FUME HOOD
BELL JAR
LN2
BAFFLE
MOLECULAR
SIEVE TRAP
THERMOCOUPLE
GAUGE (TC2)
MECHANICAL
PUMP
THERMOCOUPLE
GAUGE (TC1)
α-TRON
GAUGE
LN2
RESERVOIR
LN2 FEED LINE
DIFFUSION PUMP
FORELINE
WATER
COOLING
LINES
VALVE V2
TO
MANIFOLD
LN2 RETURN
LINE

Fig. 1

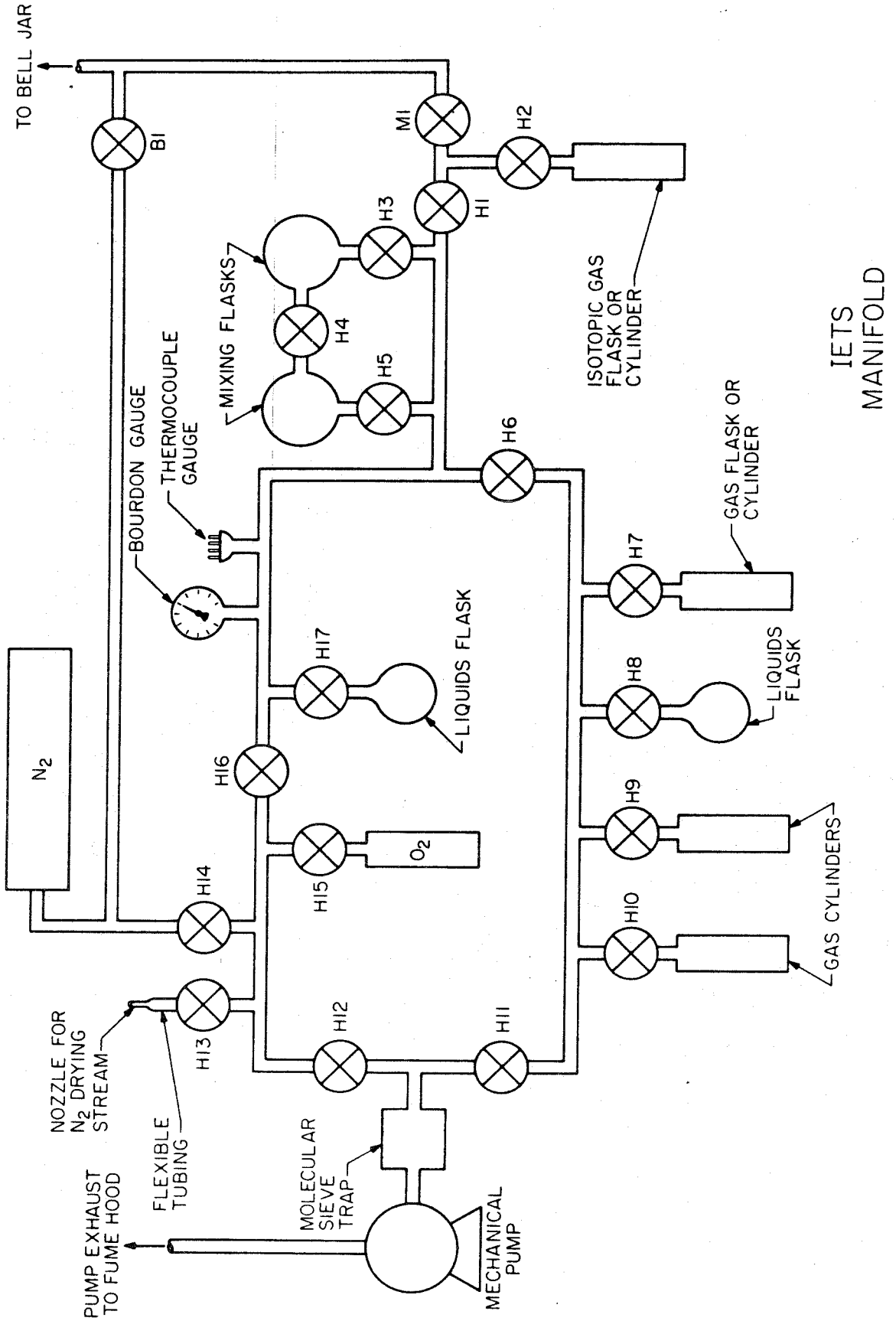
TO BELL JAR
B1
M1
H2
H1
H3
MIXING FLASKS
H4
H5
ISOTOPIC GAS FLASK OR CYLINDER
BOURDON GAUGE
THERMOCOUPLE GAUGE
H6
GAS FLASK OR CYLINDER
H7
IETS MANIFOLD
H17
LIQUIDS FLASK
H8
LIQUIDS FLASK
N_2
H16
H9
O_2
H15
H14
H10
GAS CYLINDERS
NOZZLE FOR N_2 DRYING STREAM
H13
H12
H11
FLEXIBLE TUBING
MOLECULAR SIEVE TRAP
PUMP EXHAUST TO FUME HOOD
MECHANICAL PUMP

Fig. 2

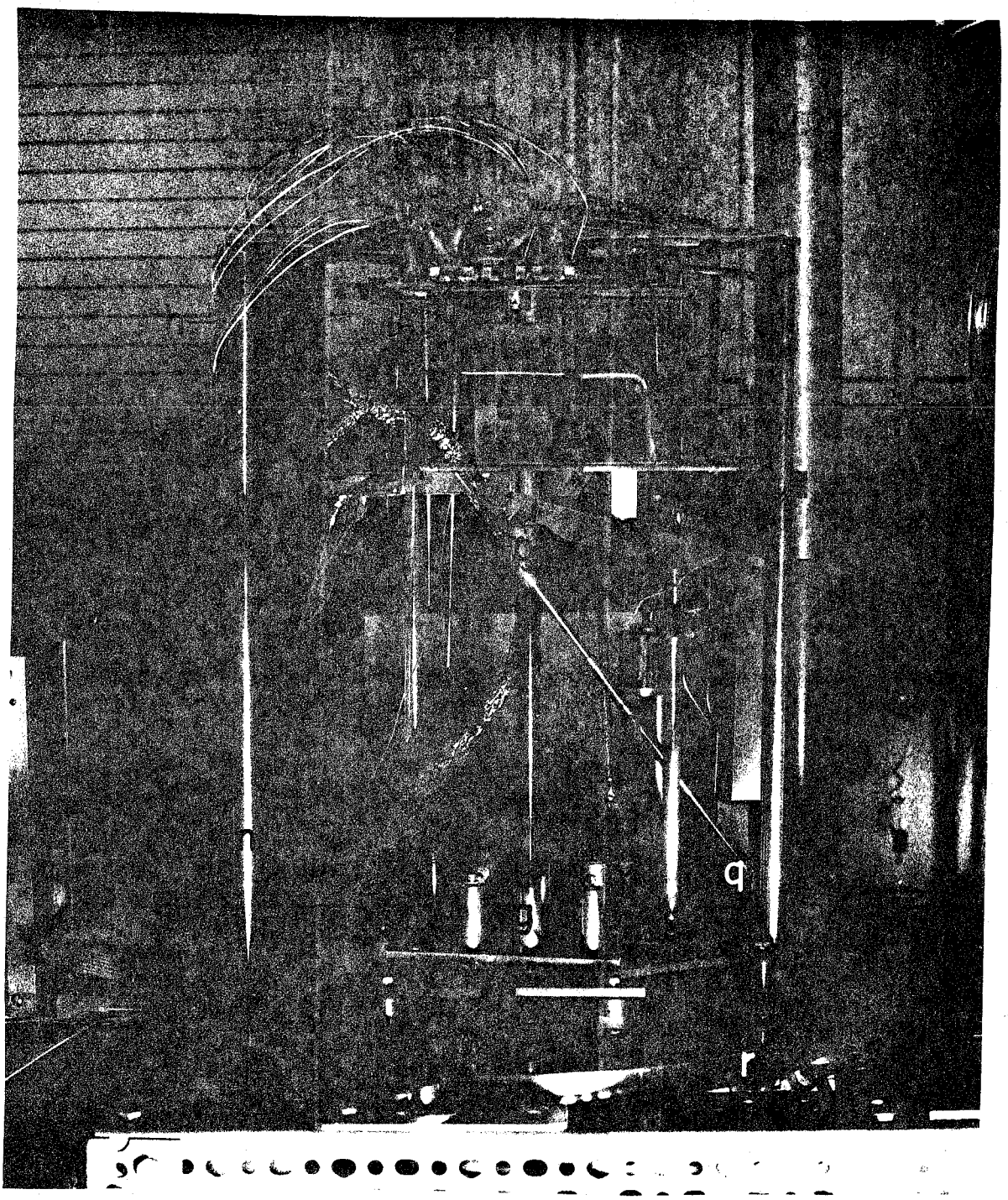

Fig. 3

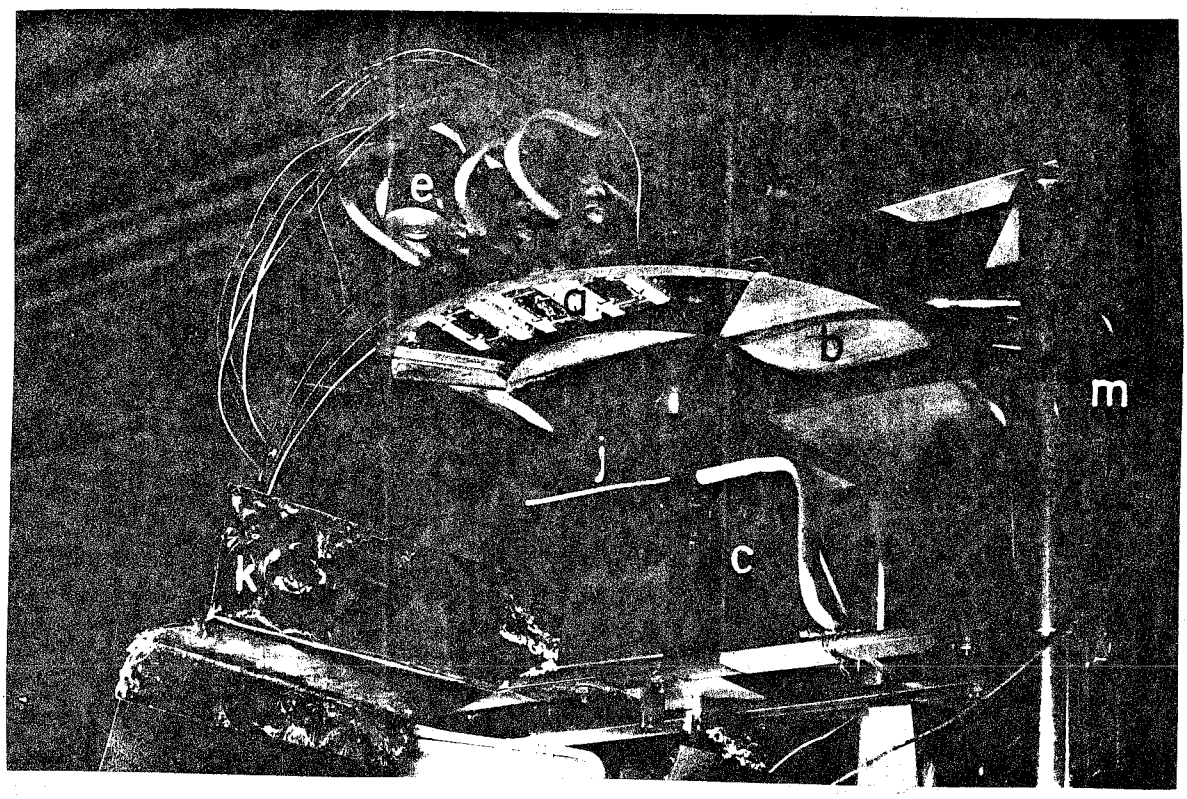

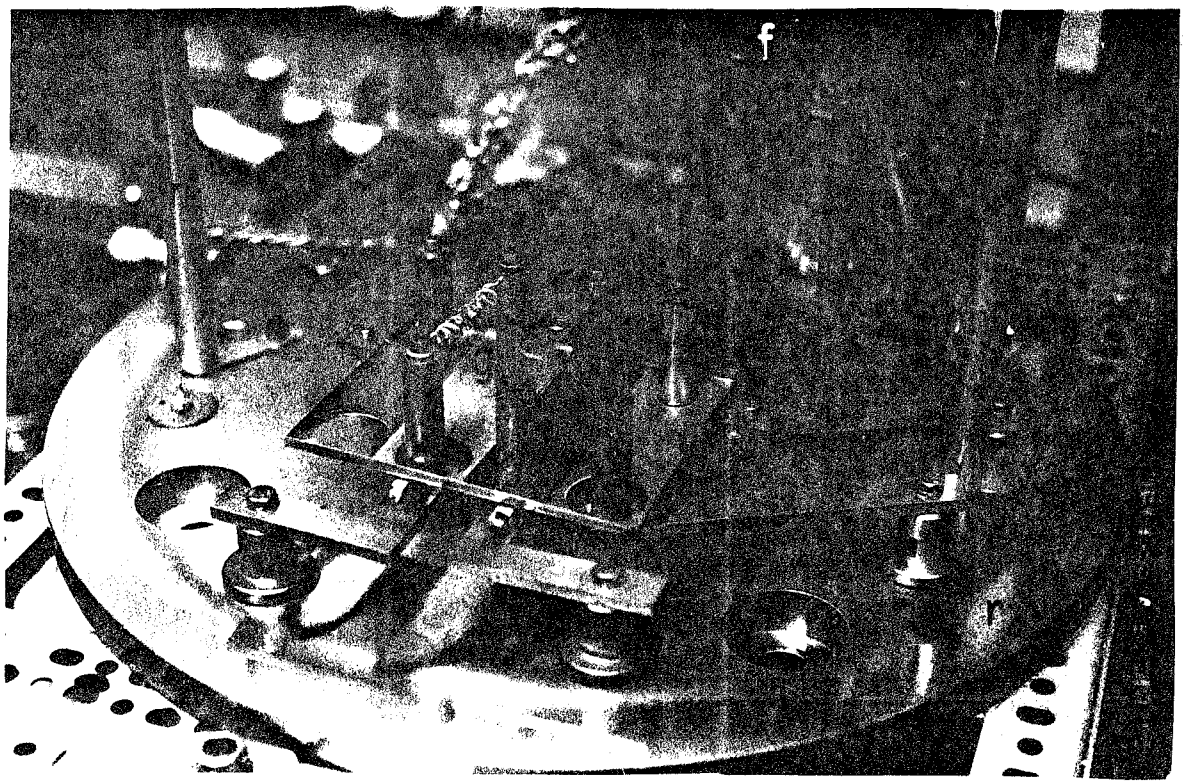

Fig. 3
(cont.)

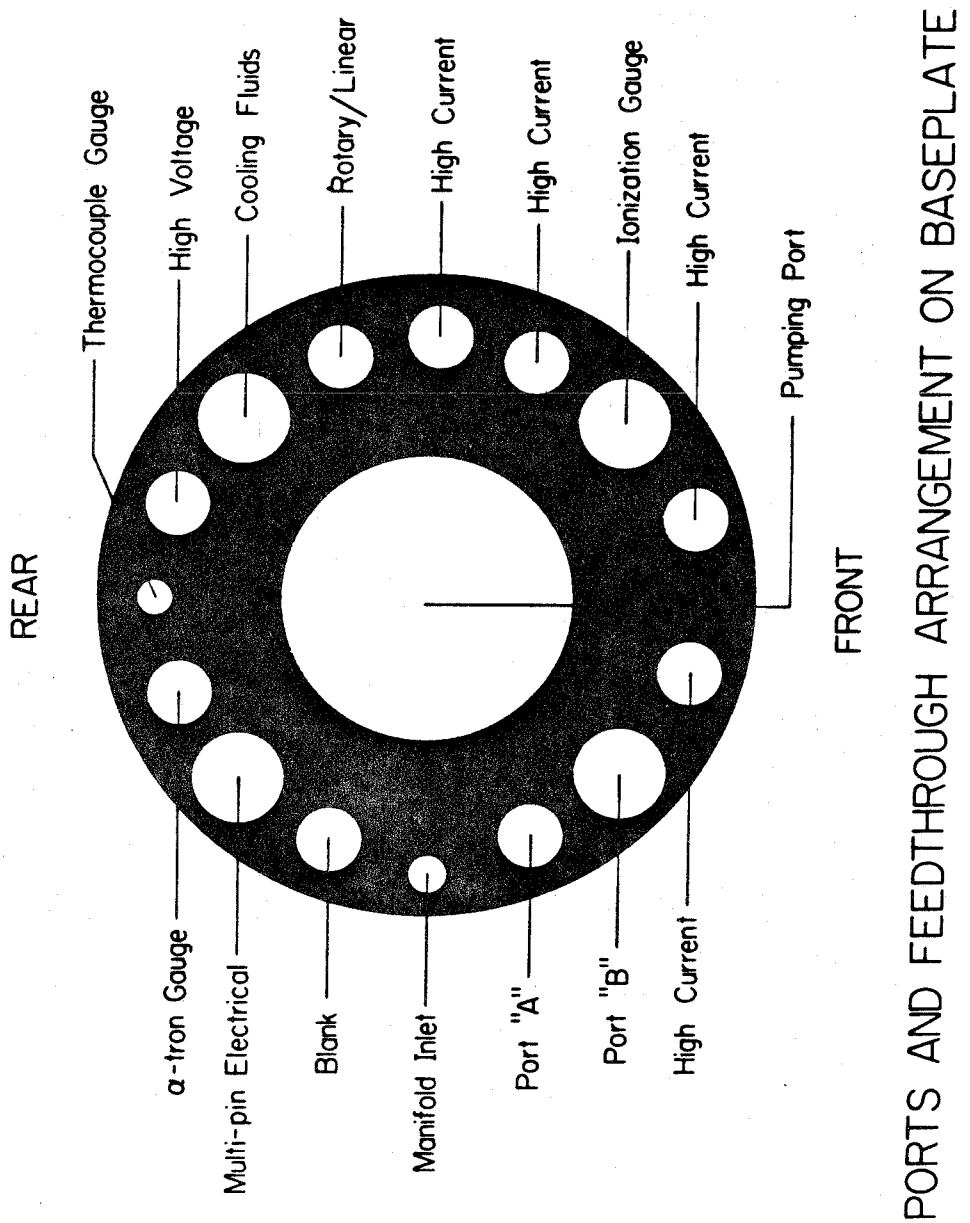

PORTS AND FEEDTHROUGH ARRANGEMENT ON BASEPLATE

Fig. 4

(a)

SAMPLE HEATING POWER SUPPLY PANEL

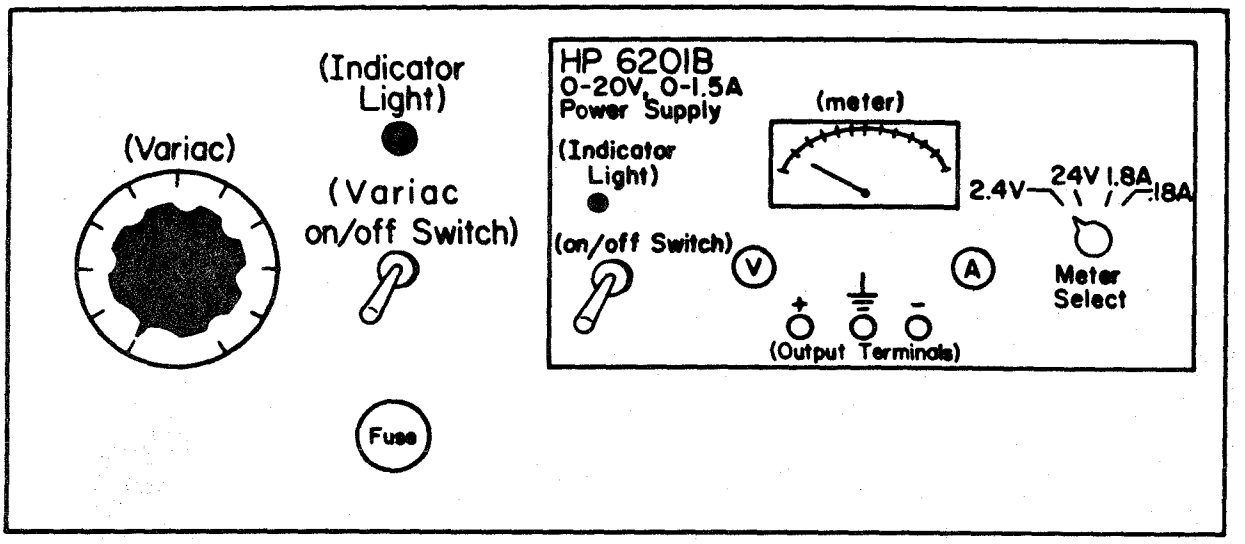

(b)

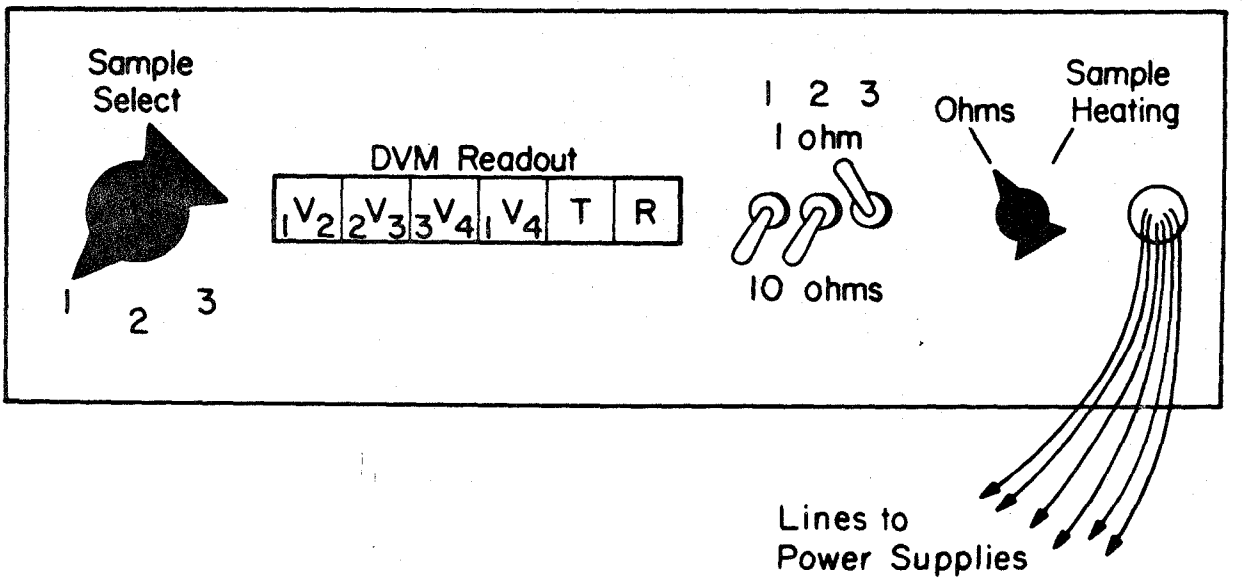

SWITCHING PANEL

Fig. 5

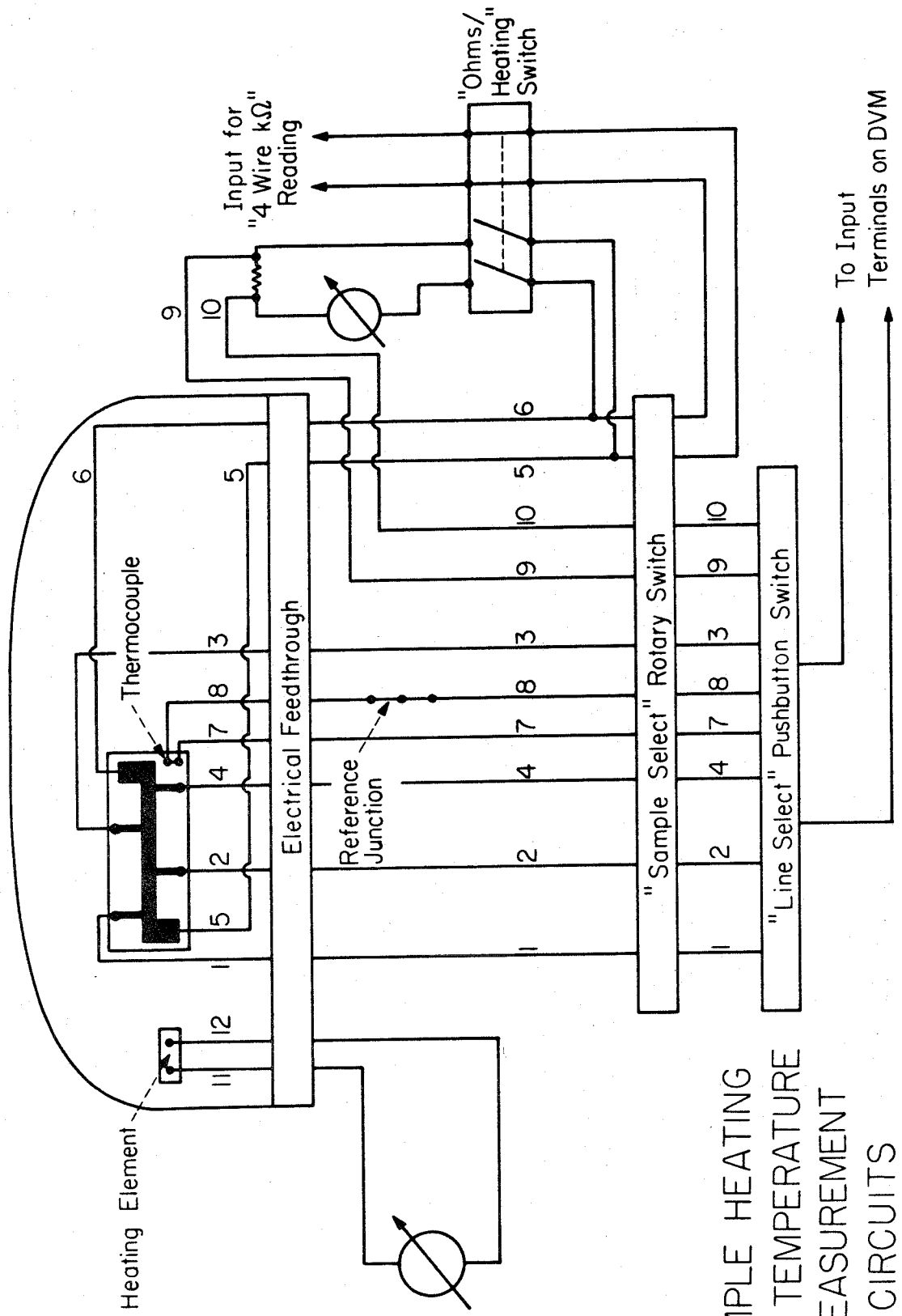
Heating Element
Thermocouple
Electrical Feedthrough
Reference Junction
"Sample Select" Rotary Switch
"Line Select" Pushbutton Switch
"Ohms/ Heating" Switch
Input for "4 Wire kΩ" Reading
To Input Terminals on DVM
SAMPLE HEATING AND TEMPERATURE MEASUREMENT CIRCUITS

Fig. 6

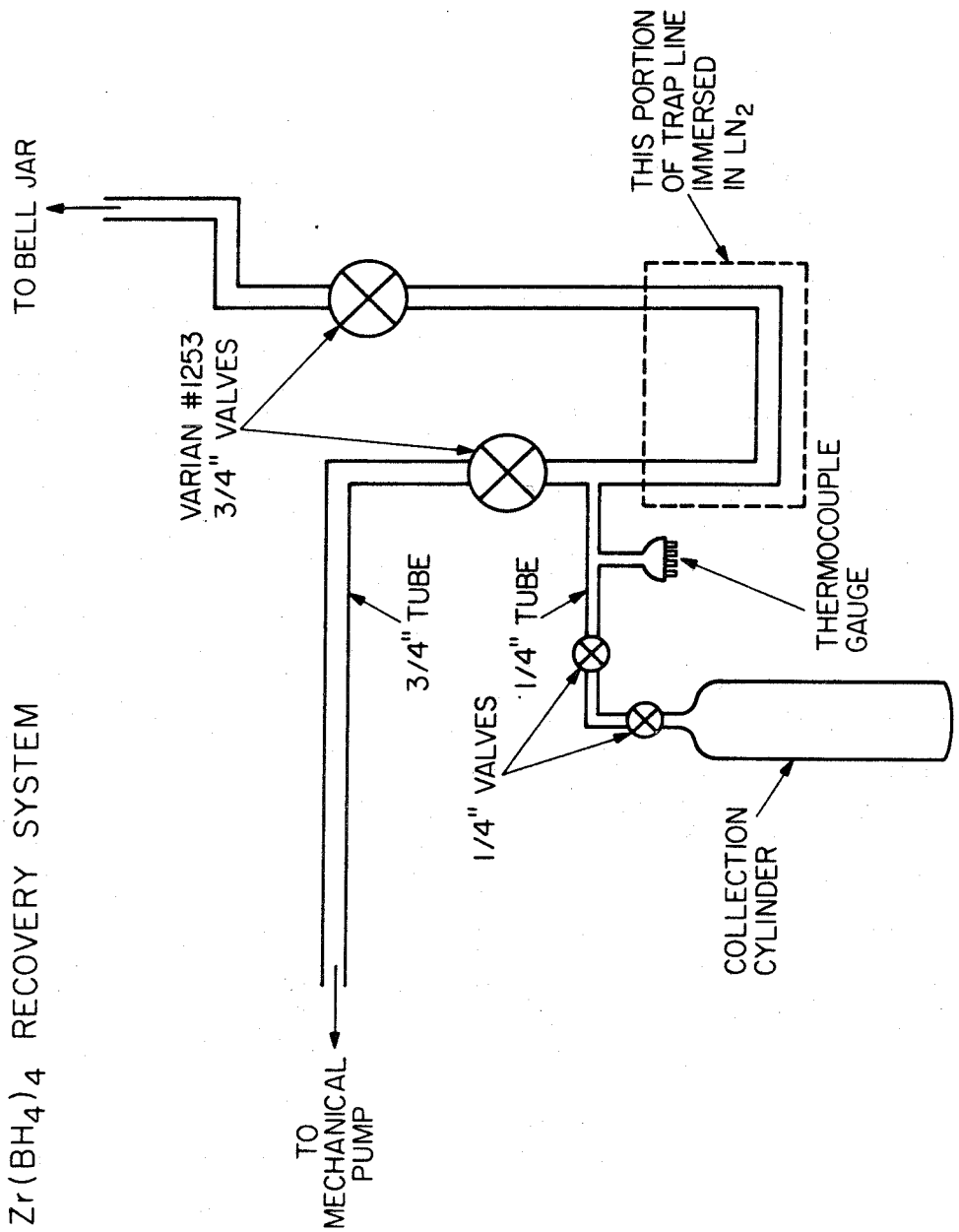
$Zr(BH_4)_4$ RECOVERY SYSTEM
TO BELL JAR
VARIAN #1253
3/4" VALVES
THIS PORTION
OF TRAP LINE
IMMERSED
IN LN_2
3/4" TUBE
1/4" TUBE
THERMOCOUPLE
GAUGE
1/4" VALVES
COLLECTION
CYLINDER
TO
MECHANICAL
PUMP

Fig. 7

APPENDIX B

A Method for Extracting Information from Floppy Disks with the IBM 370/3032 System

The potential capabilities of our current PDP-11/10 computer-based data acquisition system would be significantly enhanced if it were possible to operate conveniently on our data (stored on floppy disks) with the IBM 370/3032 system. One method of accomplishing this is presented here. This method involves reading the floppy disk information onto a magnetic tape, operating on this tape with the program TRANSFER (which creates a second tape with a useful directory and logically ordered data sets), then locating any desired data sets with the subroutine GETDTA and reading them into the memory of the IBM 370/3032 system (where the data can be processed and analyzed further). This can be illustrated schematically as

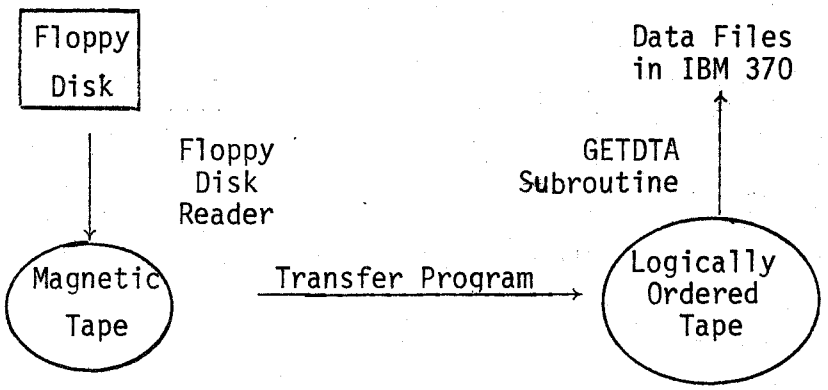

The details of this method and the programs involved are documented in the following discussion.

A newly installed floppy disk system in the computer center is capable of reading or writing PDP-11 compatible disks. This system will copy the information contained on one standard disk directly onto a magnetic tape. The disk should merely be submitted along with a green job request card and the specified magnetic tape. Processing will usually be completed the

following morning before 8:00 a.m. The resultant magnetic tape will consist of only one file containing one record per track. These units will be discussed more thoroughly below. The DCB characteristics for this tape will be RECFM = F, LRECL = 3328, BLKSIZE = 3328. Information transferred from a floppy disk onto a magnetic tape in this manner can be accessed using the IBM 370/3032 system, although significant reordering and processing is required before data can be retrieved.

The information on a disk is organized into physical "tracks" (also called "records"), most generally with 76 or 77 tracks/disk. A track is divided into 6.5 "blocks", or $\frac{6.5}{2}$ "segments", each block being made up of 4 "sectors" which in turn are individually composed of 128 8-bit bytes. (Thus, one track = 26 sectors = 3328 bytes.) Information, however, is not stored in sequential physical locations on the disk. Our disk programs place data on alternate sectors within each track (except between the 13th and 14th sectors, where there is a two-sector gap) until the track is full. Also, the sector where this procedure is initiated varies from track to track. Writing begins in sector 1 for the first track, sector 7 for the second track and sector 13 for the third track, with the starting sector for the Nth track, designated as S(N), given according to the recursion relation S(N) = S(N - 1) + 6. Since the information is transferred sequentially from disk onto the magnetic tape, it is NOT in the proper logical order on tape. This can be illustrated as shown below:

Physical Order of RT Sectors within a Track (order in which sectors appear initially on tape).	LOGICAL ORDER OF RT SECTORS FOR THE FIRST 6 TRACKS					
	1	2	3	4	5	6
1	1	11	8	5	2	12
2	14	24	21	18	15	25
3	2	12	9	6	3	13
4	15	25	22	19	16	26
5	3	13	10	7	4	1
6	16	26	23	20	17	14
7	4	1	11	8	5	2
8	17	14	24	21	18	15
9	5	2	12	9	6	3
10	18	15	25	22	19	16
11	6	3	13	10	7	4
12	19	16	26	23	20	17
13	7	4	1	11	8	5
14	20	17	14	24	21	18
15	8	5	2	12	9	6
16	21	8	15	25	22	19
17	9	6	3	13	10	7
18	22	9	16	26	23	20
19	10	7	4	1	11	8
20	23	20	17	14	24	21
21	11	8	5	2	12	9
22	24	21	18	15	25	22
23	12	9	6	3	13	10
24	25	22	19	16	26	13
25	13	10	7	4	1	11
26	26	23	20	17	14	24

It is important, therefore, that the sectors in any one track on the tape be rearranged into their logical order before information in that track can be utilized. This can be accomplished through use of a short Fortran program. The one used here has been written in the form of a subroutine called RDRREC (for "reorder record"). The RDRREC subroutine requires three parameters, (A1, A2, NR). A1 and A2 are arrays which should be dimensioned for 1664 INTEGER*2 words (i.e., 2-byte words). The DEC/RT-11 system uses words comprised of two 8-bit bytes. A1 contains the unordered information in one 3328-byte track from the tape being used as input to RDRREC. A2, the output of RDRREC, contains the same track of information but with all the sectors arranged in their proper logical order. NR, an integer, is the number of the track. The track numbers used for RDRREC begin with 2 for historical reasons. The RDRREC subroutine is listed below:

```
      SUBROUTINE RDRREC(A1,A2,NR)
      INTEGER*2 A1(1664), A2(1664)
      C=(NR-2.)*2.
      C1=C/26.
      IC1=C1
      IC=IC1*26
      D=(C-IC)*3.+1.
      D1=D/26.
      ID1=D1
      ID=ID1*26
      E=D-ID
      IF(E.NE.0) GO TO 77
      WRITE(6,57) NR
   57 FORMAT(' E=0 FOR NR=',I3)
   77 CONTINUE
      IE=E
      DIFFE=E-IE
      IF(DIFFE.EQ.0) GO TO 3
      WRITE(6,27) NR
   27 FORMAT('E IS NOT AN INTEGER FOR NR=',I3)
    3 CONTINUE
      DO 10 LB=1,13
      L=LB-1
      DO 9 K=1,64
      A11=64.*(E-1.)+K+2.*L*64.
      A111=A11/1664.
      IA111=A111
      IA11=IA111*1664
      A12=A11+64.
      A122=A12/1664.
      IA122=A122
      IA12=IA122*1664
      J=K+L*64
      JA=A11-IA11
      IF(JA.NE.0) GO TO 151
      JA=1664
  151 CONTINUE
      JB=J+832
      JC=A12-IA12
      IF(JC.NE.0) GO TO 152
      JC=1664
  152 CONTINUE
      A2(J)= A1(JA)
      A2(JB)= A1(JC)
    9 CONTINUE
   10 CONTINUE
      RETURN
      END
```

Information transferred from a floppy disk to magnetic tape consists not only of data sets, but also includes the directory information required by the DEC system to keep track of where different data sets are physically located on disk. Some of this directory information can also be utilized to facilitate locating various sets of data on the magnetic tape.

Directory information occupies thirty-two physical sectors, or four segments, including the last two sectors of the first track, all twenty-six sectors of the second track, and the first four sectors of the third track. Not all of the information in the directory is useful insofar as assisting in the location of data sets on the tape. The first five words of each directory segment are for header words, the contents of which are as follows:

(1) The number of segments available for entries;

(2) Segment number of the next logical directory segment;

(3) The highest segment currently open;

(4) The number of extra bytes per directory entry; and

(5) Block number where files in this segment begin.

After these five header words, the remainder of the segment is filled with directory entries. An entry has the following format:

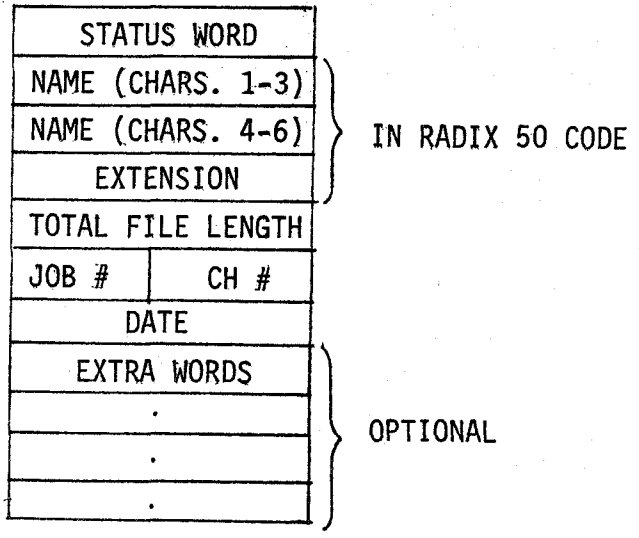

For our current system, there are no extra words used in a directory entry. If the system is modified or if a different system is being used, the number of extra words can be determined by checking the fourth header word. Dates are not entered on our current system, and this word is zero for all entries. The extension, job number and channel number are features utilized by the RT-11 system for managing storage on disk and are not employed in any way in this scheme for organizing and cataloging data transferred onto magnetic tape. Every data set is characterized by a 6-character name, the first three of which are alphabetic and the last three numeric. This is explained more fully in our POL User's Manual. Each 3-character set is stored in Radix-50 code, and therefore must always be accessed in this code. Radix-50 represents the letters A-Z by integers 1-26, and the numbers 0-9 by integers 30-39. These assignments are for base 10. Any 3-character set (represented, for example, by K1, K2 and K3) can be converted into a Radix-50 number through the following formula:

Radix-50 entry = 1600*K1 + 40*K2 + K3.

This formula becomes useful when attempting to identify the names of various data sets in the directory. The total file length represents the number of blocks (in integral increments only) assigned to each data set. This entry, along with the 2 name words, are essential in cataloging data sets properly on the tape. The status word is also important. For its own convenience, the RT-11 system duplicates parts of the directory in different physical areas on disk. This duplication is then transferred to the magnetic tape, thus making the exact ordering of data sets unclear. The status word is always 1024 except for entries marking the beginning and ending of duplicated sections, in which case it is 2048. By checking

the status word we can, therefore, skip over duplicated sections of the directory.

A program, called TRANSFER, has been written in Fortran to facilitate the use of information copied from disk to tape. It first extracts all directory segments from the tape and properly orders their sectors with the subroutine RDRREC. It then creates a new directory by selecting the names and file lengths of all data files in the order that they occur physically on the tape. This is accomplished by omitting duplicated portions of the directory as described above. This new directory is divided into 4 parts, each 288 words long. (Although much of this space designated for the new directory will most often be unused, it represents the corresponding maximum amount of directory space that is set aside on the floppy disks.) The first part lists, in sequential order according to the physical location of data files on tape, the first half of each file name; while the second part of the new directory lists the corresponding second half of the file names. The fourth part lists the length, in blocks, of each data file. The third part keeps track of which block on the magnetic tape each data set begins by summing the file lengths for all preceding directory entries. This new directory, 1152 words in length, is then written on a second tape. The TRANSFER program then takes each remaining track (all of which contain data files), orders the sectors logically using RDRREC, and writes the ordered data information onto the second tape. Reading and writing information on the magnetic tapes is accomplished through use of the standard available subroutines READRC and WRTREC, respectively. It is this second tape, which contains a useful directory and logically ordered data sets, that can be properly accessed and operated on for further data analysis with the IBM 370/3032. The TRANSFER program is listed below:

```
//TRANSFER JOB (98052,WHW,CHE),'HOWARD EVANS',TIME=(00,30)
/*JOBPARM TAPES=(0,0,2)
//  EXEC  FORTG
//SYSLIB  DD
//        DD
//        DD  DSN=SSS.EXTRA.CITLIB,UNIT=SYSDA,DISP=SHR,VOL=SER=CITSL1
//FORT    DD  *
C      READ DIR FROM TAPE INTO I1 AS INT*2 WORDS; A STNDRD DIR OF 8
C      BLOCKS BEGINNING AT RT BLOCK #6 IS ASSUMED
C      READ FIRST 2 SECTORS OF DIR, REORDER, AND PUT IN I3
       INTEGER*2 I1(1664), I2(1664), I3(3500), I4(1152), I5(3328),I6(256)
       ICOUNT=0
       CALL READRC(I1,3328)
       CALL RDRREC(I1,I2,2)
       DO 10 J1=1,64
       J1A=J1+1536
       J1B = J1 + 64
       J1C = J1 + 1600
       I3(J1) = I2(J1A)
       I3(J1B) = I2(J1C)
   10  CONTINUE
C      READ, REORDER, AND PUT IN I3 SECTORS 3-32 OF DIR; 03-28 ARE IN
C      REC 3, AND 29-32 ARE IN REC 4 ALONG WITH SOME DATA
       DO 20 M1 = 3,4
       CALL READRC(I1,3328)
       CALL RDRREC(I1,I2,M1)
       DO 20 J2 = 129,1792
       J2A = J2 + (M1-3)*1664
       J2B=J2-128
       I3(J2A) = I2(J2B)
   20  CONTINUE
```

```
C      MAKE A NEW DIR : 1ST 1/4=1ST 1/2 OF FILE NAME
C                       2ND 1/4=2ND 1/2 OF FILE NAME
C                       3RD 1/4= START BLOCK OF EACH FILE
C                       4TH 1/4= LENGTH (IN BLOCKS) OF EACH FILE
      MBLS=2
      LH=0
      KHA=0
  150 LH=LH+1
      IF(LH.GT.4) GO TO 160
      KH=0
  155 KH=KH+1
      IF(KH.GT.69) GO TO 150
      KH1=6+(KH-1)*7+(LH-1)*512
      IF(I3(KH1).EQ.2048) GO TO 150
      KH2=KH*7+(LH-1)*512
      KH3=KH2+1
      KH4=KH2+3
      KHA=KHA+1
      KHB=KHA+288
      KHC=KHA+576
      KHD=KHA+864
      I4(KHA)=I3(KH2)
      I4(KHB)=I3(KH3)
      I4(KHC)=MBLS
      I4(KHD)=I3(KH4)
      MBLS=MBLS+I4(KHD)
      GO TO 155
```

```
  160 CONTINUE
C     WRITE THE NEW "DIR" (I4) ON NEW TAPE
      CALL WRTREC(I4,2304)
      WRITE(6,11)
   11 FORMAT(' DIRECTORY TRANSFER COMPLETED')
C     READ DATA IN RECORDS 4 AND 5, REORDER SECTORS, AND WRITE IN BLOCKS
      DO 60 J5=1,1408
      J5A=J5+2048
      I5(J5)=I3(J5A)
   60 CONTINUE
      CALL READRC(I1,3328)
      CALL RDRREC(I1,I2,5)
      DO 70 J6=1,1664
      J6A=J6+1408
      I5(J6A)=I2(J6)
   70 CONTINUE
      DO 75 M4=1,12
      DO 80 M5=1,256
      M5A=M5+256*(M4-1)
      I6(M5)=I5(M5A)
   80 CONTINUE
      CALL WRTREC(I6,512)
      ICOUNT=ICOUNT+1
   75 CONTINUE
```

```
C      READ DATA IN RECORDS 6-76 (2 AT A TIME), REORDER SECTORS,
C       AND WRITE IN 256 WORD BLOCKS
       DO 85 K=1,35
       DO 90 L=1,2
       KL=3+2*K+L
   95  CALL READRC(I1,3328)
       CALL RDRREC(I1,I2,KL)
       DO 90 K1=1,1664
       K1A=K1+(L-1)*1664
       I5(K1A)=I2(K1)
   90  CONTINUE
       DO 85 M6=1,13
       DO 105 M7=1,256
       M7A=M7+256*(M6-1)
       I6(M7)=I5(M7A)
  105  CONTINUE
       CALL WRTREC(I6,512)
       ICOUNT=ICOUNT+1
   85  CONTINUE
C      READ DATA IN RECORD 76, REORDER, AND WRITE IN BLOCKS
       CALL READRC(I1,3328)
       CALL RDRREC(I1,I2,76)
       DO 110 M8=1,6
       DO 115 M9=1,256
       M9A=M9+(M8-1)*256
       I6(M9)=I2(M9A)
  115  CONTINUE
       CALL WRTREC(I6,512)
       ICOUNT=ICOUNT+1
  110  CONTINUE
       DO 120 K1=1,128
       K2=1536+K1
       I6(K1)=I2(K2)
  120  CONTINUE
```

```
      DO 125 K2=129,256
      I6(K2)=0
  125 CONTINUE
      CALL WRTREC(I6,512)
      ICOUNT=ICOUNT+1
      WRITE(6,21)ICOUNT
   21 FORMAT(' COMPLETED TRANSFER OF',I4,1X,'BLOCKS')
      STOP
      END
//READRC01  DD UNIT=TAPE16,LABEL=(1,BLP,,IN),DISP=OLD,
//         VOL=SER=CIT157,DCB=(RECFM=F,LRECL=3328,BLKSIZE=3328)
//WRTREC01  DD UNIT=TAPE16,LABEL=(1,BLP),DISP=NEW,
//           VOL=SER=IET001,
//           DCB=(RECFM=U,BLKSIZE=2304)
//
```

The only changes to be made by different users of TRANSFER are the initial JOB card, and the names of the magnetic tapes specified in the VOL = SER = (tape ID) portions of the DD cards for READRC and WRTREC located at the end of the program. The names of the tapes to be used for reading and writing should also be specified on a green job request card submitted along with the TRANSFER program.

Once TRANSFER has created a logically ordered tape with a directory, the subroutine GETDTA can be used to locate and enter into core any data files the user wishes to operate on for display or data manipulation purposes. This subroutine is listed below:

```
C      GETDTA (N,K,DATA)
C                  N=NUMBER OF FILES TO BE LOCATED AND RETURNED TO
C                    MAIN PROGRAM
C                  K=20 BY 6 MATRIX OF FILE NAMES IN RADIX 50 CODE
C                  DATA=20 BY 512 MATRIX OF DATA FILES IN ORDER REQUESTED
       SUBROUTINE GETDTA (N,K,DATA)
       INTEGER*2 J1(1200),J2(260),J3(1025),J12(2)
       INTEGER Q,K(20,6),IS(20),IL(20),INDX(20)
       REAL*4 DATA(20,512)
       INTEGER*4 J14,L1,L2
       EQUIVALENCE (J14,J12)
       J14=0
       DO 111 II=1,20
       LJ=520-II
       IS(II)=LJ
  111  CONTINUE
C      READ IN DIRECTORY AND DETERMINE LOCATION OF ALL DESIRED FILES
       CALL READRC (J1,2304)
       DO 5 I=1,N
       L1=K(I,1)*1600+K(I,2)*40+K(I,3)
       L2=K(I,4)*1600+K(I,5)*40+K(I,6)
       DO 10 M=1,288
       J12(2)=J1(M)
       IF(L1.NE.J14) GO TO 10
       WRITE(6,601)
  601  FORMAT('1ST 1/2 OF FILENAME LOCATED OK')
       MA=M+288
       J12(2)=J1(MA)
       IF(L2.EQ.J14) GO TO 15
   10  CONTINUE
       WRITE (6,13)
```

```
   15 MB=MA+288
      MC=MB+288
      J12(2)=J1(MB)
      IS(I)=J14
      J12(2)=J1(MC)
      IL(I)=J14
    5 CONTINUE
C     SORT FILES ACCORDING TO STARTING BLOCK LOCATION
      Q=20
      CALL SORTI1 (IS,Q,INDX)
      I1=IS(1)
      IF (I1.EQ.2) GO TO 20
      DO 25 I=3,I1
      CALL READRC(J2,512)
   25 CONTINUE
C     LOCATE EACH FILE AND STORE IN "DATA"
   20 MOVE=0
      DO 30 I=1,N
      M=INDX(I)
      L=IL(M)
      IF (MOVE.EQ.0) GO TO 35
      DO 40 J=1,MOVE
      CALL READRC (J2,512)
   40 CONTINUE
   35 DO 45 JJ=1,L
      CALL READRC(J2,512)
      DO 45 JA=1,256
```

```
      JB=JA+(JJ-1)*256
      J3(JB)=J2(JA)
   45 CONTINUE
      DO 50 JK=1,500
      JC=4+2*JK
      JD=JC+1
      DATA(M,JK)=J3(JC)*6.25/256.+J3(JD)*1600.
   50 CONTINUE
      IN=I+1
      MOVE=IS(IN)-IS(I)-L
   30 CONTINUE
   13 FORMAT(' FILE NOT FOUND')
      RETURN
      END
```

GETDTA requires three parameters, (N,K,DATA). N indicates the number of data files to be retrieved from tape at that particular time. K is an M by 6 matrix (where $M \geq N$) containing the Radix-50 equivalents for the 6 characters of each desired file name. This information for each file name needs to be fed in on data cards with format 6I3. DATA is an M by M' matrix where data files are stored as they are located and read off of the tape. In the above listing of GETDTA, M = 20 and M' = 512, meaning that we can locate in any given run a maximum of 20 data files, the largest of which cannot exceed 512 words. These parameters can easily be changed according to the particular user, yet care should be taken also to adjust the dimensions of IS, IL and INDX; the value of Q which is required in the SORTI1 subroutine; and the limits on the DO LOOPs numbered 111 and 50.

Before explaining the functional details of GETDTA, it is important to note a few of the features of data files as stored by RT-11 and our own POL operating systems. First, each data point is represented by two 2-byte words, the least significant word being first in physical order. Also, the beginning five words of each data file are set aside for information required by the POL software.

The GETDTA subroutine begins by reading in the directory information previously sorted by TRANSFER. Then it reads in (from a data card) the name of the first data file, finds the 2 Radix-50 numbers equivalent to the 6-character name, and searches the first ¼ of the directory for the appropriate file. When it locates the first half of the file name, it checks the corresponding position in the second ¼ of the directory for the second half of the file name. If this doesn't match, it continues searching in the first part of the directory until all entries here are exhausted.

Often a Radix 50 equivalent to a 3-character name will exceed 32768, the largest number that can be stored in 15 bits, and use will be made of the 16th bit. However, when dealing with 16-bit words, the 16th bit is recognized only as a parity check. Any problems that might arise here are taken care of by an initial EQUIVALENCE statement, allocating the same core space to a 4-byte (IBM) word, J14, and two 2-byte (DEC) words, J12 (1 and 2). During the file name search, the entries in the directory are examined by first putting them into J12(2) and then matching J14 against the calculated Radix 50-coded file name.

Once the Ith file name has been located, the corresponding points in the 3rd ¼ and 4th ¼ of the directory are checked to obtain the starting block and file length of that data set. These values are then stored in IS(I) and IL(I), respectively. This procedure is repeated until directory information on each of the requested files has been located. Data sets can only be read off of the magnetic tape in the order that they physically appear on the tape. Since the order in which a given set of data file names is requested might not correspond to their order on the tape, the SORTI1 subroutine is used to sort the file starting block locations (stored in IS) into ascending order. This is then the order that data files are located. GETDTA moves the tape to the appropriate starting block location for each file, then reads off the number of blocks as specified in the directory as belonging to that file. The first 5 words in each data file are omitted as these do not contain actual data points. The remaining words are taken two at a time (2 words per data point), and combined into one 4-byte (IBM) word according to the relation

one data point = one IBM word = $\frac{6.25}{256}$ * first DEC word + 1600* second DEC word.

A complete data file is stored in one row of the DATA array. Its position in that array is determined by the order in which the file names were requested by the user and not the order in which they were arranged and located on the magnetic tape. Thus, at the end of the GETDTA subroutine the user has available in core the desired data sets, where they can be operated on with any other Fortran programs.

Finally, in addition to data cards specifying the number of files desired with the appropriate file names and changes in the dimensions for some of the arrays and DO LOOPs, it should also be noted that any use of the GETDTA subroutine requires the appropriate DD cards for use of SORTI1 and READRC.

References

RT-11 Software Support Manual, p. 3-1, Digital Equipment Corporation.

RT-11 System Reference Manual, p. H-13 and 5-44, DEC.

The following CIT "How to" Write-Ups:

CIT Deck Setup for IBM 370/3032,

Fortran IV User's Guide to Using Magnetic Tapes on 370/3032,

The DD Statement.

Write-Ups on the Following CIT Subroutines:

READRC,

WRTREC,

SORTI1